

Experimental and Numerical Studies of Concrete-Filled Double Steel Tubular Columns

by

Mizan Ahmed



Thesis submitted in fulfillment of the requirement for the Degree of

Doctor of Philosophy

Institute for Sustainable Industries and Liveable Cities, Victoria University
Melbourne, Australia

January 2020

ABSTRACT

Concrete-filled double steel tubular (CFDST) columns are high-performance composite columns, which have increasingly been used in high-rise composite buildings and bridges as well as in strengthening conventional concrete-filled steel tubular (CFST) columns. The additional confinement provided by the inner circular tube in CFDST columns considerably improves their strength and ductility compared to CFST columns. However, research studies on the behavior of CFDST columns have been very limited and no design rules are given in current design codes. This thesis presents experimental and numerical studies on the fundamental behavior of circular and rectangular CFDST short and slender columns subjected to axial compression, combined axial load and bending, and preloads.

Experiments on the behavior of square CFDST short columns with circular inner tube, circular CFDST short columns with circular inner tube and rectangular CFDST short columns composed of inner rectangular tube loaded concentrically and eccentrically are undertaken. Fiber-based mathematical models are developed for predicting the structural responses of CFDST short and slender columns under various loading conditions. The formulations of the mathematical models consider the influences of concrete confinement, geometric and material nonlinearities, and local buckling. New confining pressure models are proposed based on test results for ascertaining the compressive and residual strengths of confined concrete in CFDST columns, and incorporated in the mathematical models. The highly dynamic nonlinear equilibrium equations of CFDST columns under eccentric loading are solved by the efficient computer solution algorithms, which are developed based on the inverse quadratic method. The validations of the

numerical models are made by comparisons with experimental results. The influences of various geometric and material parameters on the behavior of CFDST columns are examined. The results obtained from experimental and numerical studies are used to propose design equations.

This research makes significant contributions to the knowledge by adding new test results on CFDST short columns to the database. The numerical models developed provide researchers and structural designers with accurate and efficient computer simulation and design tools, which lead to safer and more economical designs of composite structures. The design equations proposed can be utilized to design CFDST short and slender columns under various loading conditions.

DECLARATION

I, Mizan Ahmed, declare that the PhD thesis by publication entitled *Experimental and Numerical Studies of Concrete-Filled Double Steel Tubular Columns* is no more than 100,000 words in length including quotes and exclusive of tables, figures, appendices, bibliography, references, and footnotes. This thesis contains no material that has been submitted previously, in whole or in part, for the award of any other academic degree or diploma. Except where otherwise indicated, this thesis is my own work.

Signature: Mizan Ahmed  Digitally signed by Mizan Ahmed
Date: 2020.04.22 20:19:03 +10'00'

Date: 22-04-2020

ACKNOWLEDGMENTS

First and foremost, all glory to the almighty for granting me this research opportunity which has been a great privilege. I would like to then express my sincere gratitude to my principal supervisor Associate Professor Qing Quan Liang of Victoria University, Melbourne for his time, support and invaluable suggestions throughout my doctoral study. I would also like to thank my associate supervisors Associate Professor Muhammad N. S. Hadi of the University of Wollongong, NSW and Dr. Vipulkumar Ishvarbhai Patel of La Trobe University, Bendigo for their discussions and suggestions.

The research project was supported by the Research Training Scheme and a College of Engineering and Science scholarship at Victoria University, Melbourne, Australia. The experimental work conducted as part of this research project was supported by the grants provided by La Trobe University, Bendigo and Victoria University, Melbourne, Australia. The financial support is gratefully acknowledged.

I would like to acknowledge the patience, support and constant care of my wife given during the completion of this research degree. I am also grateful to my parents and parents-in-law for their endless love, prayer, and support towards me. I really appreciate their time to visit me in Australia and accompanying my wife and children during my study. Heartfelt thanks to all of you. Last, but not least, I would like to dedicate this thesis to my beloved children Muhammad Bin Ahmed and Fatimah Al Zahra Ahmed.

LIST OF PUBLICATIONS

Based on this research, the following papers have been either published or submitted for publication in international journals and conference proceedings.

Journal Articles

1. **Ahmed, M.**, Liang, Q. Q., Patel, V. I. and Hadi, M. N. S. (2018). Nonlinear analysis of rectangular concrete-filled double steel tubular short columns incorporating local buckling. *Engineering Structures*, 175: 13-26.
2. **Ahmed, M.**, Liang, Q. Q., Patel, V. I. and Hadi, M. N. S. (2019). Numerical analysis of axially loaded circular high strength concrete-filled double steel tubular short columns. *Thin-Walled Structures*, 138: 105-116.
3. **Ahmed, M.**, Liang, Q. Q., Patel, V. I. and Hadi, M. N. S. (2019). Local-global interaction buckling of square high strength concrete-filled double steel tubular slender beam-columns. *Thin-Walled Structures*, 143, 106244.
4. **Ahmed, M.**, Liang, Q. Q., Patel, V. I. and Hadi, M. N. S. (2019). Experimental and numerical studies of square concrete-filled double steel tubular short columns under eccentric loading. *Engineering Structures*, 197, 109419.
5. **Ahmed, M.**, Liang, Q. Q., Patel, V. I. and Hadi, M. N. S. (2019). Behavior of eccentrically loaded double circular steel tubular short columns filled with concrete. *Engineering Structures*, 201, 109790.
6. **Ahmed, M.**, Liang, Q. Q., Patel, V. I. and Hadi, M. N. S. (2020). Experimental and numerical investigations of eccentrically loaded rectangular concrete-filled double steel tubular columns. *Journal of Constructional Steel Research*, 167, 105949.

7. **Ahmed, M.**, Liang, Q. Q., Patel, V. I. and Hadi, M. N. S. (2020). Computational simulation of eccentrically-loaded circular thin-walled concrete-filled double steel tubular slender columns. *Engineering Structures*, 213, 110571.
8. **Ahmed, M.**, Liang, Q. Q., Patel, V. I. and Hadi, M. N. S. (2020). Nonlinear analysis of square concrete-filled double steel tubular slender columns incorporating preload effects. *Engineering Structures*, 207, 110272.
9. **Ahmed, M.**, Liang, Q. Q., Patel, V. I. and Hadi, M. N. S. (2020). Behavior of circular concrete-filled double steel tubular slender beam-columns including preload effects. *Engineering Structures*, (currently under review).

Refereed Conference Papers

1. **Ahmed, M.**, Liang, Q. Q., Patel, V. I. and Hadi, M. N. S. (2018). Numerical modelling of axially loaded circular concrete-filled double steel tubular short columns, Part I: Formulation. *Proceedings of the 13th International Conference on Steel, Space and Composite Structures*, Perth, Australia, 2018.
2. **Ahmed, M.**, Liang, Q. Q., Patel, V. I. and Hadi, M. N. S. (2018). Numerical modelling of axially loaded circular concrete-filled double steel tubular short columns, Part II: Parametric study. *Proceedings of the 13th International Conference on Steel, Space and Composite Structures*, Perth, Australia, 2018.
3. **Ahmed, M.**, Liang, Q. Q., Patel, V. I. and Hadi, M. N. S. (2019). Nonlinear inelastic analysis of high-strength square concrete-filled double steel tubular slender columns. *Proceedings of the 4th Australasian Conference on Computational Mechanics*, Tasmania, Australia, 2019.

PART A:

DETAILS OF INCLUDED PAPERS: THESIS BY PUBLICATION

Please list details of each Paper included in the thesis submission. Copies of published Papers and submitted and/or final draft Paper manuscripts should also be included in the thesis submission.

Item/ Chapter No.	Paper Title	Publication Status (e.g. published, accepted for publication, to be revised and resubmitted, currently under review, unsubmitted but proposed to be submitted)	Publication Title and Details (e.g. date published, impact factor etc.)
3	Nonlinear analysis of rectangular concrete-filled double steel tubular short columns incorporating local buckling.	Published	<i>Engineering Structures</i> , 2018, 175, 13-26. SCImago Journal Rank: Q1 Impact Factor: 3.084 (Year of 2018)
	Experimental and numerical studies of square concrete-filled double steel tubular short columns under eccentric loading.	Published	<i>Engineering Structures</i> , 2019; 197: 109419. SCImago Journal Rank: Q1 Impact Factor: 3.084 (Year of 2018)
	Experimental and numerical investigations of eccentrically-loaded rectangular concrete-filled double steel tubular columns.	Published on April 2020	<i>Journal of Constructional Steel Research</i> , SCImago Journal Rank: Q1 Impact Factor: 2.650 (Year of 2018)
4	Numerical analysis of axially loaded circular high strength concrete-filled double steel tubular short columns.	Published	<i>Thin-Walled Structures</i> , 2019, 138,105-116. SCImago Journal Rank: Q1 Impact Factor: 3.488 (Year of 2018)

	Behavior of eccentrically loaded double circular steel tubular short columns filled with concrete.	Published	<i>Engineering Structures</i> , 2019, 201, 109790. SCImago Journal Rank: Q1 Impact Factor: 3.084 (Year of 2018)
5	Local-global interaction buckling of square high strength concrete-filled double steel tubular slender beam-columns.	Published	<i>Thin-Walled Structures</i> , 2019, 143, 106244. SCImago Journal Rank: Q1 Impact Factor: 3.488 (Year of 2018)
6	Computational simulation of eccentrically-loaded circular thin-walled concrete-filled double steel tubular slender columns.	Published on 15 th June 2020	<i>Engineering Structures</i> , SCImago Journal Rank: Q1 Impact Factor: 3.084 (Year of 2018)
7	Nonlinear analysis of square concrete-filled double steel tubular slender columns incorporating preload effects.	Published on 15 th March 2020	<i>Engineering Structures</i> , SCImago Journal Rank: Q1 Impact Factor: 3.084 (Year of 2018)
	Behavior of circular concrete-filled double steel tubular slender beam-columns including preload effects	Under review	<i>Engineering Structures</i> , SCImago Journal Rank: Q1 Impact Factor: 3.084 (Year of 2018)

Declaration by [candidate name]:

Signature:

Date:

Mizan Ahmed

Mizan Ahmed Digitally signed by Mizan Ahmed
Date: 2020.04.22 20:20:20 +10'00'

22-04-2020

CONTENTS

	Page No.
Title	i
Abstract	ii
Declaration	iv
Acknowledgements	v
List of Publications	vi
Details of Included Papers: Thesis by Publication	viii
Contents	x
Chapter 1 Introduction	1
1.1 Background.....	1
1.2 Research Significance.....	5
1.3 Aims of This Research.....	6
1.4 Thesis Layout.....	8
Chapter 2 Literature Review	12
2.1 Introduction.....	12
2.2 Local and Post Local Buckling of Steel Plates.....	13
2.3 Concrete-Filled Steel Tubular Columns.....	19
2.3.1 Experimental Studies.....	19
2.3.2 Numerical Studies.....	26
2.4 Double Skin CFST Columns.....	31
2.4.1 Experimental Studies.....	31
2.4.2 Numerical Studies.....	35
2.5 Concrete-Filled Double Steel Tubular Columns.....	38
2.5.1 Experimental Studies.....	38
2.5.2 Numerical Studies.....	42
2.6 Composite Columns With Preload Effects.....	45
2.6.1 Experimental studies.....	45

2.6.2	Numerical studies.....	47
2.7	Concluding Remarks.....	49
Chapter 3	Rectangular CFDST Short Columns.....	51
3.1	Introduction.....	51
3.2	Declarations.....	53
3.3	Nonlinear analysis of rectangular concrete-filled double steel tubular short columns incorporating local buckling.....	59
3.4	Experimental and numerical studies of square concrete-filled double steel tubular short columns under eccentric loading.....	73
3.5	Experimental and numerical investigations of eccentrically-loaded rectangular concrete-filled double steel tubular columns.....	90
3.6	Concluding Remarks.....	145
Chapter 4	Circular CFDST Short Columns.....	146
4.1	Introduction.....	146
4.2	Declarations.....	148
4.3	Numerical analysis of axially loaded circular high strength concrete-filled double steel tubular short columns.....	152
4.4	Behavior of eccentrically loaded double circular steel tubular short columns filled with concrete.....	164
4.5	Concluding Remarks.....	180
Chapter 5	Local-Global Interaction Buckling of Square CFDST Slender Columns.....	181
5.1	Introduction.....	181
5.2	Declarations.....	183
5.3	Local-global interaction buckling of square high strength concrete-filled double steel tubular slender beam-columns.....	185
5.4	Concluding Remarks.....	202

Chapter 6 Circular CFDST Slender Columns under Eccentric Loading	203
6.1 Introduction.....	203
6.2 Declarations.....	205
6.3 Computational simulation of eccentrically-loaded circular thin-walled concrete-filled double steel tubular slender columns.....	207
6.4 Concluding Remarks.....	260
Chapter 7 CFDST Slender Columns with Preload Effects	261
7.1 Introduction.....	261
7.2 Declarations.....	263
7.3 Nonlinear analysis of square concrete-filled double steel tubular slender columns incorporating preload effects.....	267
7.4 Behavior of circular concrete-filled double steel tubular slender beam-columns including preload effects.....	322
7.5 Concluding Remarks.....	367
Chapter 8 Conclusions	368
8.1 Summary.....	368
8.2 Achievements.....	369
8.3 Further Research.....	370
References	373

Chapter 1

INTRODUCTION

1.1 BACKGROUND

Steel-concrete composite columns have been extensively used in modern construction industry owing to their high performance in terms of ductility, strength, energy absorption capacity as well as good constructability in comparison with reinforced concrete columns.

In a concrete-filled steel tubular (CFST) column as depicted in Fig. 1, the filled concrete prevents the steel tube from the inward local-buckling and works compositely with the steel section. The steel tube acts as the permanent formwork for the concrete so that the construction cost and time can be greatly minimized. The concrete-filled double steel tubular (CFDST) column as shown in Fig. 2 is an innovative form of composite columns where the steel tubes are placed concentrically and filled with concrete.

The choice of the cross-section and geometry of a CFDST column for a specific project is dependent on the structural efficiency of the column, specific architecture or aesthetic criteria, material availability or the cost and method of construction. As an example, circular CFDST columns illustrated in Fig. 2 (a) have higher ductility and strength than rectangular CFDST columns, therefore, they can be used to carry large axial loads.

However, rectangular CFDST columns (Fig. 2(b)) offer ease of connection to the steel beams and can be used in the case where the large bending stiffness is essential.

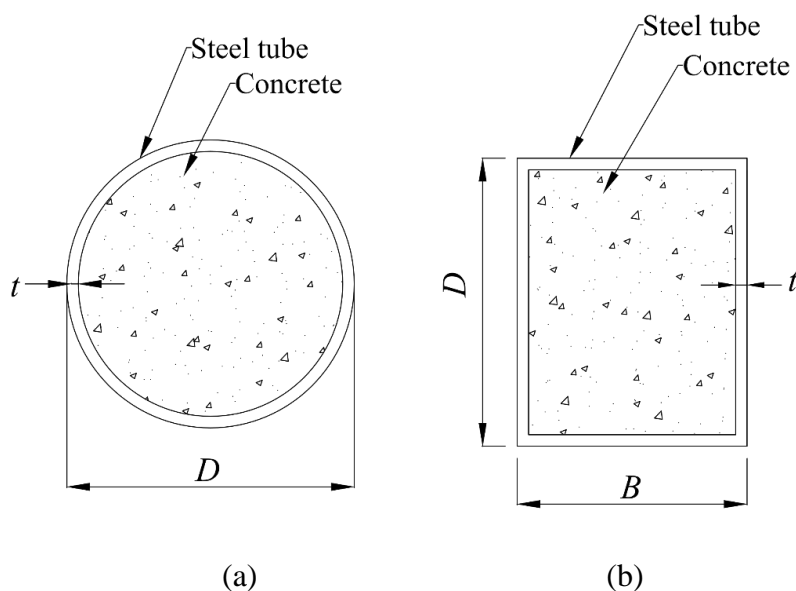


Fig. 1. Cross-sections of CFDST columns: (a) circular; (b) rectangular.

Square CFDST columns composed of an internal circular tube as illustrated in Fig. 2 (c) combine the benefits of both circular and square CFST columns. The presence of the internal circular tube improves the strength, ductility and fire-resistance of CFDST columns compared to CFST columns as well as double-skin concrete-filled tubular (DCFST) columns illustrated in Fig. 3 (Pei 2005; Romero et al. 2015; Ekmekyapar and Al-Eliwi 2017).

In addition to being used in new composite structures, a CFDST column can also be constructed by strengthening an existing CFST column with an external steel tube that is filled with concrete. Moreover, different strengths of materials can be used for the external and internal tubes of CFDST columns to achieve economic designs. Due to their

availability, high-strength materials are increasingly used to construct such composite columns. Nonetheless, high strength concrete is less ductile and therefore its effect on the ductility of CFDST composite columns must be properly evaluated and understood. Furthermore, rectangular CFDST columns with non-compact or slender sections are susceptible to local buckling which significantly affects the column performance. The steel tubular walls of a rectangular CFDST column under axial load combined with bending resulting from the eccentric loading may be subjected to either uniform stresses or stress gradients. The nonlinear analysis of local-global interaction buckling of slender rectangular CFDST columns is complicated and a challenging problem in structural engineering.

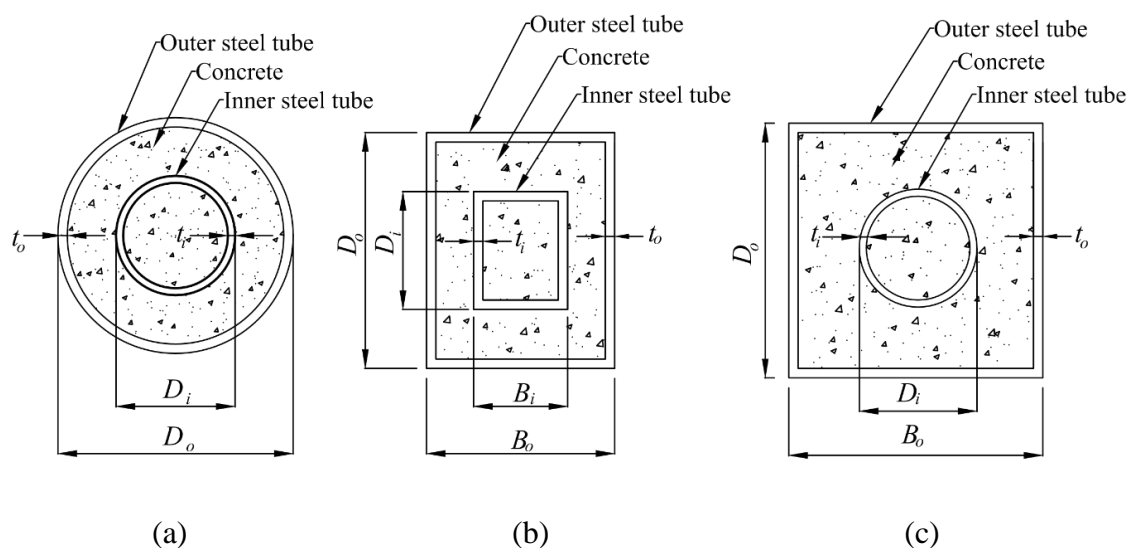


Fig. 2. Cross-sections of CFDST columns: (a) circular CFDST column; (b) rectangular CFDST columns; and (c) square CFDST columns composed of an internal circular tube.

There is a difference between the confinement mechanism in CFDST and other steel-concrete composite columns. The core-concrete of a circular CFDST column incorporating an internal circular steel section is confined by both steel tubes, which

improves the strength and ductility of CFDST columns in comparison with CFST ones. The concrete confinement in CFDST columns is related to the geometric and material properties of the columns. To accurately determine the behavior of CFDST columns, it is essential to develop accurate confinement models that recognize the effects of material and geometric properties of concrete and steel components in CFDST columns.

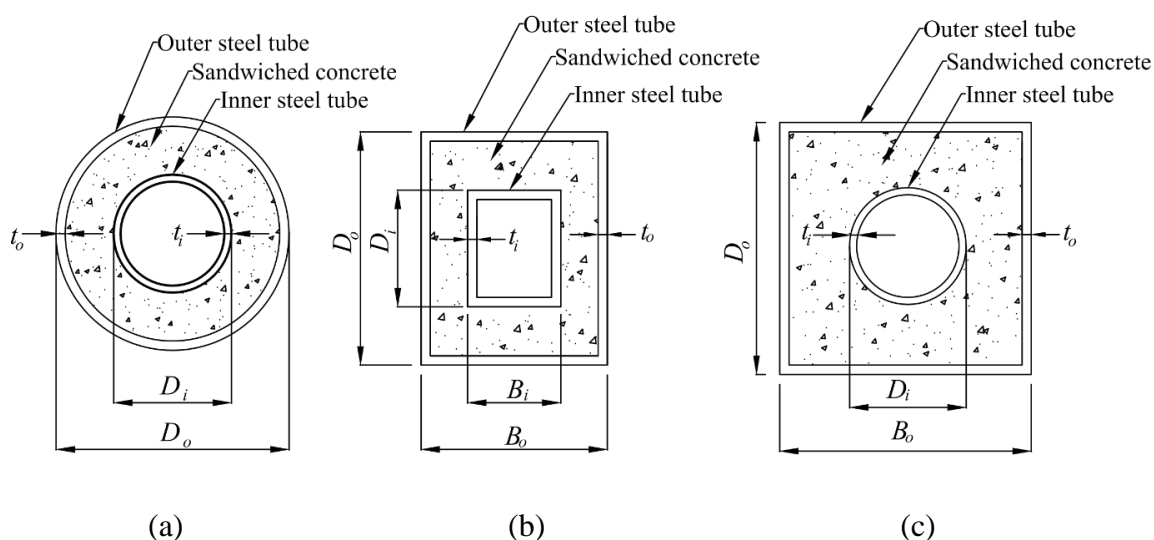


Fig. 3. Cross-sections of DCFST columns: (a) circular DCFST column; (b) rectangular DCFST columns; and (c) square DCFST columns with inner circular tube.

In the construction of composite buildings, the common practice is to erect both steel tubes of CFDST columns with composite floors several stories before the wet concrete is filled into the hollow steel tubes. The permanent and constructional loads of the upper stories induce deformations in addition to initial stresses in the steel tubes, which leads to reductions in the stiffness and strength of CFDST columns. Therefore, the influences of preloads on the structural responses of CFDST composite columns must be properly examined and included in the analysis and design of such composite columns.

The behavior of CFDST columns is influenced by their material and geometric properties, such as the concrete compressive strength, steel yield stress, the ratio of diameter-to-thickness, width-to-thickness ratio, loading eccentricity, and member slenderness. Although the influences of each of these variables on the responses of such columns can be examined experimentally, the experimental work is highly expensive and time-consuming. The computer simulation of CFDST columns is the most cost-effective alternative method that can be used to ascertain the responses of CFDST columns.

1.2 RESEARCH SIGNIFICANCE

Although CFDST columns are increasingly used in the construction of composite structures, little research has been performed to date to investigate their performance under different loading conditions so that their behavior has not been fully understood. Understanding the performance of CFDST composite columns subjected to various loading conditions as well as the effects of materials and geometry on their performance is vital in designing these columns safely and efficiently. The current design standards, such as Eurocode 4 (2004), AISC 360-16 (2016) and AS/NZS 2327:2017 (2017), have not provided design rules for designing CFDST composite columns. The existing design specifications for conventional CFST columns may not accurately predict the behavior of CFDST columns. Therefore, design models for CFDST columns under various loading conditions are much needed by design engineers when designing CFDST columns.

The accurate material constitutive relations implemented in numerical models are essential for accurately simulating the responses of CFDST columns. As discussed

earlier, CFDST columns have a different confinement mechanism from CFST columns. Therefore, accurate confinement models need to be developed for the concrete in CFDST columns to accurately predict the behavior of CFDST columns. The outer rectangular steel tube of a CFDST column may undergo local buckling, which affects the column performance significantly. However, no fiber-based numerical models have been formulated for accurately quantifying the responses of CFDST rectangular composite columns incorporating the effect of local-buckling.

This research makes significant contributions to the knowledge base of CFDST composite columns by adding new test data on short CFDST columns and developing computationally efficient numerical models for predicting the responses of CFDST columns with different loading conditions including axial compression, axial load combined with bending, and preloads. The proposed confinement models can accurately ascertain the confinement of confined concrete in such columns and incorporated in inelastic analysis procedures for CFDST columns. The fiber-based techniques developed in this research provide researchers and structural designers with accurate and efficient computer simulation and design tools, which lead to safer and more economical designs of composite structures. The design models proposed in this research can be included in design standards for the design of CFDST columns.

1.3 AIMS OF THIS RESEARCH

The main aim of this research is to examine the behavior of CFDST short columns experimentally and develop mathematical models for the simulations of structural

performance of short and slender CFDST columns under various loading conditions considering the influences of confinement, local buckling of thin-walled steel sections, and geometric and material nonlinearities. The specific aims are as follows:

1. To perform a series of tests on the responses of circular and rectangular CFDST short columns which are loaded axially and eccentrically.
2. To develop mathematical models for calculating the performance of short CFDST rectangular columns with either circular or rectangular inner tube incorporating local buckling.
3. To develop mathematical models for predicting the responses of short circular CFDST columns loaded concentrically and eccentrically.
4. To develop a mathematical model for circular slender CFDST columns subjected to eccentric loading.
5. To develop a mathematical model for simulating the interaction local-global buckling behavior of eccentrically loaded slender rectangular CFDST columns with inner circular tube.
6. To develop mathematical models for circular and rectangular CFDST slender columns with preload effects.
7. To verify the mathematical models developed by experimental results.
8. To assess the sensitivities of the structural behavior of CFDST columns with various design loads to key design parameters.
9. To propose design models for the design of CFDST columns subjected to various design loads.

1.4 THESIS LAYOUT

This thesis comprises of 8 chapters. An extensive literature review on the investigations of steel-concrete composite columns under different design loads is presented in **Chapter 2**. Firstly, research studies on the post-local buckling of plate elements in addition to initial local-buckling are studied. Experimental studies as well as numerical investigations on the behavior of concrete-filled steel composite columns under axial loading and combined axial load with bending are then reviewed. Finally, a review on the existing experimental and computational investigations of steel-concrete composite columns with preload effects is carried out.

In **Chapter 3**, the performance of short CFDST columns made of square and rectangular cross-sections is investigated that are loaded axially and eccentrically. Firstly, a computational model is proposed for the response analysis of square CFDST stub columns with an internal circular tube loaded concentrically, incorporating local buckling, concrete confinement, and geometric and material nonlinearities. New expressions are developed to quantify the lateral pressure and residual strength of the filled concrete in CFDST columns based on the available experimental results. The effects of crucial parameters on the responses of such columns that are loaded axially are examined by employing the numerical models developed. A simple design model is derived to estimate the column's ultimate axial capacity. Experiments are also undertaken to investigate the behavior of square CFDST short columns having an inner circular tube and double rectangular/square steel tubular short columns filled with concrete loaded either axially or eccentrically. The test setup and the test results are discussed. An efficient

mathematical model incorporating local buckling is further proposed that can simulate the strength envelopes and moment-curvature relationships of CFDST columns under eccentric loading. Effective solution algorithms implemented the inverse quadratic method are developed to solve the dynamic equilibrium function. The validation of the computational models is performed by comparing computations with experimental results. The influences of section geometry and material parameters on the structural responses of CFDST columns are examined using the computational model developed.

The axial responses of circular CFDST stub columns having an internal circular tube are investigated in **Chapter 4**. A mathematical model utilizing the fiber analysis method is developed for the response analysis of short columns that are axially loaded. Upon the interpretation of the existing test data, formulas for quantifying the lateral pressures on concrete and the strength degradation of the confined concrete are suggested. The new constitutive laws of concrete of CFDST columns are incorporated in the mathematical model formulated and verified by experiments. Design models are proposed that ascertain the ultimate loads of CFDST columns incorporating confinement and strain-hardening of steel tubes. Furthermore, a series of tests are performed to investigate the behavior of short circular CFDST columns that are loaded both axially and eccentrically. The test results and discussions provide crucial information on the behavior of such columns loaded eccentrically. A nonlinear mathematical model is also developed for simulating the responses of CFDST columns under eccentric loading. The influences of concrete confinement, section geometry, material properties and loading ratio on the moment capacity and interaction curves are investigated.

Chapter 5 presents a mathematical model for ascertaining the global buckling behavior of slender square CFDST beam-columns where the internal tube is circular. The model explicitly considers the interaction of local and global buckling, second-order effects, concrete confinement as well as geometric and material nonlinearities. The solution algorithms based on the inverse quadratic method are utilized to solve the highly dynamic equilibrium equations during the loading history. The mathematical modeling approach is verified against the independent test results and utilized to quantify the behavior of slender CFDST columns loaded eccentrically. Design formulas are derived to estimate the ultimate loads as well as strength curves of slender CFDST square columns.

In **Chapter 6**, a mathematical model is presented for the computational simulation of eccentrically-loaded slender CFDST circular columns with a circular inner tube. The model is formulated by using the concept of fiber analysis and considers the influences of concrete confinement, second-order effects, and geometric and material nonlinearities. The existing test results of high-strength slender CFDST columns are used to validate the mathematical model developed. The model is further validated against the test results of DCFST columns. Upon validation, the influences of material and geometric variables on the performance of slender CFDST columns are evaluated. Design equations are derived for the design of slender circular CFDST composite columns.

Fiber analysis models are developed in **Chapter 7** for ascertaining the structural performance of slender square CFDST columns with an internal circular tube and circular CFDST columns with an inner circular tube loaded eccentrically with the preload effects. The computational models explicitly take into consideration the effects of local buckling,

concrete confinement, second-order as well as geometric and material nonlinearities. The nonlinear equilibrium equations are solved using the inverse quadratic method. The validations of the mathematical models developed are undertaken. The influences of preload and important design parameters including the section geometry, local buckling, and concrete confinement on the behavior of CFDST columns are examined using the computational models developed. The effects of preload on the load distributions in the components of CFDST columns are also assessed. Finally, design models are suggested for the design of slender square CFDST columns with preload effects.

Chapter 8 provides conclusions on the experimental and computational investigations on the responses of rectangular, square and circular CFDST short and slender columns subjected to various design loads. Significant achievements are highlighted. Further research studies on this topic are recommended.

Chapter 2

LITERATURE REVIEW

2.1 INTRODUCTION

Research investigations on the structural performance of concrete-filled composite columns with various loading conditions have been an active area in the field of structural engineering. Experimental and numerical investigations provide useful insight into the performance of composite columns subjected to various loading conditions and the basis for developing design guidelines. Several books on steel-concrete composite structures have been published (Oehlers and Bradford 1999; Han 2007; Zhao et al. 2010a; Liang 2014; Patel et al. 2015a, 2018; Han et al. 2018). Although this thesis concerns with investigations on the performance of CFDST columns, existing studies on the behavior of CFST composite columns and double-skin CFST (DCFST) composite columns under various loading conditions are also reviewed. Firstly, the current knowledge on the critical local-buckling as well as post-local buckling of steel plates is discussed, followed by the extensive review of the published experimental and computational works on the responses of CFST and DCFST columns under axial loading as well as combined axial load with bending. Finally, existing investigations on the structural responses of concrete-filled composite columns where the steel tubes were preloaded are reviewed.

2.2 LOCAL AND POST-LOCAL BUCKLING OF STEEL PLATES

There have been numerous studies performed on the behavior of the local and post-local buckling of steel elements at both room and high temperatures (Bryan 1890, Lundquist and Stowell 1939, Lundquist et al. 1943, Chilver 1953, Maas 1954, Gerard and Becker 1957, Timoshenko and Gere 1961, Bulson 1969, Usami and Fukumoto 1982, Usami 1982, Usami and Fukumoto 1984, Azhari and Bradford 1991, Wright 1993, Wright 1995, Uy and Bradford 1995, Liang and Uy 1998, Liang and Uy 2000, Liang et al. 2004, Knobloch and Fontana 2006, Liang et al. 2007, Heidarpour and Bradford 2007, Heidarpour and Bradford 2008, Bedair 2009, Bedair 2010, Quiel and Garlock 2010, Couto et al. 2014). The very first work on the local buckling of rectangular steel plates was reported by Bryan (1890) who investigated the local-buckling behavior of rectangular steel plates under in-plane uniform compressive loads. Lundquist and Stowell (1939) performed instability analysis of plates that formed rectangular and channel sections subjected to uniform compression. Lundquist et al. (1943) utilized the method of moment distribution to study the instability of structures composed of flat steel plates in compression.

The differential equations of the deflection for the general section made of steel plates can be used for the instability analysis in which the lowest eigenvalue represents the buckling load. However, such differential equations are difficult to be developed for complex sections and therefore the Rayleigh-Ritz method developed by Ritz (1909) had been widely employed to quantify the critical stress of local-buckling for steel plate elements from 1950 to 1970 by a number of researchers, like Chilver (1953), Gerard and

Becker (1957) and Bulson (1969). However, with the development of the digital computer in the early 70s, using the matrix method including the finite element (FE) method became popular amongst the researchers for the buckling analysis of steel plates without difficulty. Some of the earlier researchers utilized the matrix method included Przemieniecki (1963, 1968), Kapur and Hartz (1966), Wittrick and Curzon (1968), and Williams and Wittrick (1969, 1972). Usami (1982) developed a theoretical method for studying the elastic post-local buckling of rectangular steel elements under combined compression and bending. Marguerre's compatibility equations (Marguerre 1938) with the energy method were used to obtain the solution in the theoretical investigation. Expressions for predicting the effective widths of plates in compression and bending were suggested based on the theoretical study.

Bradford and Hancock (1984) investigated the post-local buckling strengths of geometrically imperfect steel plate elements by means of utilizing the method of finite strip. The proposed computational method provided an alternative approach to Winter's concept of effective widths for the post-local buckling of beams that were simply supported. The interaction of local buckling and flexural-torsional buckling in beams with thin steel flanges was studied. Bradford (1985a) further extended the method of finite strip to the post-local buckling response analysis of rectangular box sections that were under transverse gradient stress and longitudinal stress. Design charts of elastic local buckling coefficients were provided, and expressions were proposed that estimated the post-buckling strength of rectangular box sections considering residual stresses.

The finite element (FE) model was formulated by Bradford (1985b) for studying the distortional buckling of fabricated mono-symmetric steel I-beams under moment gradients. The effects of the web slenderness of the I-beams on the buckling behavior were studied. Design equations were formulated for the determination of the distortional stress of steel I-beams under moment gradients. Bradford and Cuk (1988) further extended the FE modeling technique to the simulation of the flexural-torsional buckling of beam-columns made of non-prismatic tapered I-section. In computational modeling, the beam-column was represented by one-dimensional element. The stability matrices in addition to the stiffness matrices were derived for the flexural-torsional buckling analysis of the beam-columns. Bradford and Wong (1991) employed the semi-analytical method of finite strip to capture the local buckling responses of elastic composite box girders subjected to negative bending. The local buckling coefficients of composite box girders were derived, and the limits were given for classifying the compact and slender webs.

Wright (1995) described a method underlying the energy principles for investigating the local instability of the steel sections restrained by concrete. The theories of orthotropic plates and the flow of plasticity were used to derive the limits on the width-to-thickness (B/t) ratios of steel elements under axial compression and combined bending and shear. The suggested B/t ratios for steel elements restrained by the concrete were larger than those of the steel plates that were unrestrained by concrete. This showed the benefits of utilizing the concrete to fill the steel hollow sections.

Uy and Bradford (1995, 1996) used the method of finite strip to investigate the local buckling characteristics of elastic steel plate elements in steel-concrete composite

columns at ambient temperature as well as elevated temperatures. The influences of high temperatures on the properties of steel material namely the yield strength and Young's modulus were considered in the analysis method. The plate local-buckling of composite columns was found to be influenced by the material properties of steel exposed to elevated temperatures. Design equations were provided, which could be used to calculate the slenderness limits and the local-buckling stress of steel elements exposed to high temperatures.

The FE models were created by Liang and Uy (1998, 2000) by means of employing the finite element analysis system Strand6 to quantify the post-local buckling strength in addition to the critical local-buckling behavior of steel tubular walls in rectangular CFST columns under uniform compression. The edges of steel tubular walls in a box column filled with concrete were assumed to be clamped. The influences of initial geometric imperfection, material yielding, residual stresses, and the B/t ratio of the steel boxes on the behavior of local buckling of clamped steel plate elements were investigated. It was reported that owing to residual stresses and geometric imperfections, the steel elements could not attain their yield strengths. The formulas of effective widths were developed to predict the post-local buckling strengths of steel elements loaded concentrically and verified by available test results on short CFST columns.

Uy (2000, 2001) proposed a theoretical model underlying the method of finite strip for ascertaining the local-buckling behavior of CFST columns. The in-plane stresses of the steel elements were redistributed using the formulas of effective widths to consider the post-local buckling of non-compact steel boxes. It was discovered that the small B/t

ratio did not have a significant effect on the local buckling behavior of CFST columns. However, the local-buckling effect became significant when the steel section had a large B/t ratio.

The post-local buckling responses of steel elements in addition to their initial local-buckling in double-skin steel-concrete composite panels subjected to either biaxial compressive stresses or combined shear and biaxial compression load were investigated by Liang et al. (2003, 2004) utilizing the FE software Strand7. The single steel plate field between stud shear connectors was employed to simulate the local buckling in addition to the post-local buckling of steel-concrete composite panels. The edges of the steel plate field were identified to be hinged and its corners were restrained by stud shear connectors which were simulated by the shear-slip model. The FE models created accounted for the influences of the initial imperfection of the steel plate field, material nonlinearities and headed stud shear connectors. Several expressions were derived that calculated the critical stresses of local buckling of plates with various boundary conditions and the post-local buckling strengths of steel plate fields.

Liang et al. (2007) undertook numerical investigations into the behavior of local and post-local buckling of steel tubular walls in rectangular CFST columns loaded biaxially. The steel tubular walls of CFST columns loaded biaxially were under stress gradients and assumed to be clamped at their edges. The influences of geometric imperfection initially presented, material yielding and residual stresses were considered in the nonlinear analysis. It was found that there was no bifurcation point on the load-deflection relationships which could be identified for steel plates because of geometric

imperfections. In addition to this, the stiffness and ultimate strength of steel plate elements were found to decrease by increasing the ratio of B/t . Moreover, the steel plate that had a B/t ratio of 100 could attain only 61.4% of its ultimate load. A set of equations were derived based on the FE results for computing the critical stress of local-buckling and the strength of post-local buckling of steel tubular walls in rectangular CFST columns loaded biaxially. These equations could be implemented in nonlinear analysis programs to consider the influences of local and post-local buckling on the strength and ductility of CFST rectangular columns where the cross-sections are non-compact or slender (Liang 2009a, 2009b).

A model based on a semi-analytical approach was developed by Heidarpour and Bradford (2007) for the investigation of the local instability of steel flanges exposed to elevated temperatures. Based on the sensitivity analyses, the plasticity and yield slenderness limits on the steel plates were suggested. The critical temperature that caused the local buckling of flange outstands with either clamped or pinned supports was determined. Heidarpour and Bradford (2008) further examined the behavior of local buckling of steel webs and flanges in I-beams under axial loading in combination with bending and shear at elevated temperatures. The variation of the mechanical strains was considered in the computational modeling along with the web depth. The theoretical analysis showed that the elastic buckling coefficients and the web slenderness limits were affected by the thermal gradient, shear strain and the depth of the compression zone.

An inelastic stability model was presented by Ragheb (2015) to examine the influences of web-flange interaction on the local buckling of I-beams under bending. The numerical

results demonstrated that while the local instability of the flange was markedly influenced by both the ratio of depth-to-thickness of the web and the width-to-depth ratio of the section, only the width-to-depth ratio of the section influenced the local buckling of the web.

Yaghoubsahi et al. (2015) studied the post-local buckling of the flawed shear panel made of aluminum alloy and mild steel using the FE analysis. The initial crack induced in the panel was allowed to grow during the loading history and simulated using the Bonora damage model. The ultimate loads of the very thin shear panels were found to be influenced by the initial crack size. However, these effects became insignificant as the slenderness of the panels was reduced. Furthermore, the ultimate loads of the panels were affected by the boundary conditions.

The local instability of columns made of steel I-sections loaded concentrically exposed to high temperatures was investigated theoretically by Ragheb (2016). The reductions in the stiffness and the yield stress of steel under high temperatures were considered in the modeling. However, the effects of residual stresses resulting from the manufacturing process were ignored. It was found that the geometry of the web and flanges of the section greatly influenced the buckling load of the plate elements, and the steel yield strength had a negligible impact on the local buckling load.

2.3 CONCRETE-FILLED STEEL TUBULAR COLUMNS

2.3.1 Experimental Studies

The structural responses of CFST columns have been extensively studied by investigators since the early 1960s. Some of the earliest investigations into the behavior of CFST columns were performed by Kloppel and Goder (1957), Furlong (1967), Knowles and Park (1969, 1970), Bridge (1976) and Shakir-Khalil and Zeghiche (1989). The strength of square and circular short CFST columns were experimentally investigated by Furlong (1967). The effects of the B/t ratio of the steel section together with the confinement provided by the steel tube were examined. Test results showed that the confinement increased both the ductility and strength of the concrete in CFST columns with circular cross-sections, but only the improvement on the concrete ductility could be observed in square cross-sections. Knowles and Park (1969) studied the sensitivities of the concrete confinement of CFST beam-columns to the ratio of the member slenderness (L/r) and the ratio of the depth-to-thickness (D/t). The steel tubes of the tested columns had the D/t ratios ranged from 15 to 59. The confinement considerably improved the ductility as well as the strength of circular columns. However, increasing the L/r ratio reduced the confinement on the filled concrete.

Bridge (1976) designed a test program to assess the structural behavior of slender pin-ended CFST beam-columns made of square cross-sections that were loaded biaxially. All tested columns were made of compact steel sections with B/t ratios ranged from 20.5 to 23.5. The influences of loading eccentricity, member slenderness, and the loading angle on the structural responses of CFST columns were investigated. From the experiments, it could be found that there was no local buckling took place on the faces of the columns tested due to their small B/t ratios. The ultimate capacities of the CFST columns were shown to reduce remarkably as either the slenderness of the columns or the loading

eccentricity increased. However, the loading angle had an insignificant effect on the ultimate loads of the columns.

Experiments on the behavior of slender rectangular CFST beam-columns loaded eccentrically were undertaken by Shakir-Khalil and Zeghiche (1989). The column cross-sections, which were fabricated by cold-formed steel tubes, were compact. The concrete used to fill the hollow sections had the compressive strength up to 45 MPa. It was found that all column specimens failed by the overall buckling without any sign of local buckling. The ultimate loads of CFST columns obtained from experiments were compared against the FE results as well as the design ultimate strengths calculated by the method specified in BS 5400 (1979). Shakir-Khalil and Mouli (1990) carried out further tests to assess the sensitivities of the strength of slender CFST rectangular columns loaded concentrically to the cross-sectional size, the member L/r ratio, steel yield strength as well as concrete strength. The ratios of D/t were 24, 30 and 40. The local buckling of steel sections did not occur owing to small D/t ratios.

Schneider (1998) conducted experiments on fourteen short CFST columns made of either circular, rectangular or square cross-section where the D/t ratios varied up to 50. The steel tubes that had the yield stress up to 430 MPa and the concrete with a strength of 30 MPa were utilized to construct these specimens. The effects of the geometry and the ratio of D/t on the axial load-strain relationships of CFST columns were evaluated in the experimental program. The strain hardening behavior of all circular columns was observed. However, only rectangular and square cross-sections that had a D/t ratio less than 20 exhibited the strain-hardening behavior.

The influences of concrete infill on the responses of CFST rectangular short columns loaded axially were investigated by Bridge and O'Shea (1998) by means of conducting experiments on columns that had B/t ratios varied from 37 to 131. It was indicated that using a large B/t ratio remarkably reduced the strengths of the columns. O'Shea and Bridge (2000) further studied the performance of circular short CFST columns where the D/t ratios varied from 60 to 220. High-strength concrete that had the strength up to 120 MPa was employed to construct these columns. Design models for calculating the capacities of CFST columns with different loading conditions were given. The comparison between the ultimate strengths obtained by the tests and computed by the approach specified in Eurocode 4 (1994) was made. The comparison showed that the design code conservatively predicted the ultimate capacities of CFST columns constructed by normal strength concrete.

Uy (2000) reported the behavior of short square CFST columns loaded eccentrically through an experimental program. The B/t ratios of the square columns formed by welding four individual steel plates were 40, 50, 60, 80 and 100. These specimens had the steel yield stress up to 750 MPa. It was confirmed that the failure patterns of these columns were the outward local-buckling of the steel sections, concrete crushing and weld fracture. The ultimate load of CFST columns tested was observed to decrease as the ratio of B/t increased.

Experiments on twenty-four short CFST rectangular columns were performed by Han (2002) to ascertain the influences of the ratio of B/t and the confinement factor on the axial responses of CFST columns. The steel tubes of the columns, which had the B/t

ratios varied from 24.5 to 47, were formed by mild steel sheets with the steel yield stress varied from 194 MPa to 228 MPa. The average concrete cubic strength was measured as 59.3 MPa. It was evident that the CFST columns tested failed by local buckling, and increasing the confinement factor resulted in an improvement in the axial performance of CFST columns.

Mursi and Uy (2003, 2004) studied the structural performance of rectangular CFST columns which were slender. Their studies indicated that the slender columns failed by the global instability coupled with the tube local-buckling. The filled concrete significantly increased the capacities of CFST columns when compared to their hollow counterparts. However, increasing the eccentricity-to-width (e/B) ratio considerably reduced the strength and stiffness performance of CFST columns.

An experimental program comprised of 114 specimens was undertaken by Sakino et al. (2004) to evaluate the significance of high-strength materials on the performance of short circular and rectangular CFST columns. The range of the steel yield stress was between 277 MPa to 853 MPa and the strength of the filled concrete varied from 25.4 to 85.1 MPa. The experimental observations demonstrated that the confinement in circular cross-sections was more obvious than their rectangular counterparts. Increasing either the steel yield stress or concrete strength considerably led to an increase in the strength of the composite columns. Design equations for CFST columns loaded axially were presented.

Fujimoto et al. (2004) undertook experimental investigations on the structural behavior of eccentrically-loaded CFST short columns. The significance of the with-to-thickness

ratios of the steel sections and high-strength materials of concrete and steel on the performance of CFST columns was ascertained. The column specimens were constructed by the concrete with strength up to 80 MPa and steel sections with the maximum yield stress of 834 MPa. It was pointed out that the failure of square CFST columns was owing to the local-buckling of thin-walled steel sections and the effect of concrete confinement could be negligible. An analytical model was also presented that determined the moment-curvature responses of CFST columns and its accuracy was validated by experimental data.

Experimental work on fifteen short CFST circular columns loaded concentrically was reported by Giakoumelis and Lam (2004) who assessed the influences of the ratio of D/t , bond strength, and concrete confinement. Concrete compressive strength up to 100 MPa was used to construct these columns. It was demonstrated that the bond strength had a considerable influence on the performance of short CFST columns constructed by high-strength concrete. From the comparisons of test and design strengths determined by using Eurocode 4 (1994), ACI 318-02 (2002) and AS 3600 (1994), it was found that these codes underestimated the capacities of composite columns and the best estimation was obtained by Eurocode 4.

Lee et al. (2011) performed tests on eleven short CFST circular columns that were eccentrically loaded. The test variables included the material strength, the ratio of D/t , and loading eccentricity ratio (e/D). The steel tubes had the D/t ratios varied from 40 to 100. The steel yield stress was in the range from 468 MPa to 517 MPa while the concrete with different strengths of 31.5 MPa and 59 MPa were used to cast these

specimens. The columns were subjected to two different e/D ratios of 0.167 and 0.5. The test results indicated that for columns that had the D/t ratio greater than 40, there was no significant improvement in their ultimate resistances due to the confinement effect. Furthermore, CFST columns with lower strength concrete had better ductility. The design strength envelopes of CFST columns developed based on the specifications given in Eurocode 4 (1994), AISC 360-05 (2005), KBCS (2009) were compared against the test results. It was found that AISC 360-05 and KBCS provided strength estimations with reasonable accuracy compared to the test data while Eurocode 4 overestimated the strength envelopes of CFST columns.

The experimental results of thirty-seven slender circular CFST columns loaded eccentrically were described by Portolés et al. (2011). The significance of the D/t ratio, concrete strength, e/D ratio and L/r ratio on the responses of CFST columns was assessed. The tested columns had the diameters varied from 100 mm to 160.1 mm and the strengths of concrete varied from 32.7 MPa to 107.33 MPa. It was found that the longer the column, the better its ductility. Owing to the overall buckling, high-strength concrete was shown to have an insignificant effect on the capacities of slender CFST columns.

Uy et al. (2011) presented experimental results on the responses of concrete-filled stainless steel tubular (CFSST) slender and short columns that were loaded either concentrically or eccentrically. Austenitic stainless steel was utilized to construct these columns that had the D/t ratios ranged up to 101.6. From the experimental results, it could be found that the deflection performance of CFSST columns was affected by the

distinguished strain-hardening of stainless steel. The CFSST columns had higher ductility than CFST columns. The experimental ultimate loads of CFSST columns have been compared with those computed by AS 3600 (2009), Eurocode 4 (2004), AISC 360-05 (2005) and DBJ/T 13-51 (2010). It was discovered that these design codes generally provided conservative strength estimations because the strain-hardening of stainless steel was not accounted for in the design codes.

Recently, the experimental performance of CFST rectangular columns constructed by high-strength materials was discussed by Huang et al. (2019). The steel plates were cut into desired shapes and welded to form CFST columns where the B/t ratios varied from 18 to 68. The steel yield stress and the concrete strength varied up to 750 MPa and 50 MPa, respectively. The local buckling of the rectangular steel boxes that had large B/t ratios was observed. In addition, it was shown that increasing the B/t ratio markedly reduced the capacity and stiffness of CFST columns.

2.3.2 Numerical Studies

Vrcelj and Uy (2002) theoretically investigated the overall buckling responses of CFST rectangular columns which were slender. The influences of concrete strength, member slenderness ratio and the yield stress of steel on the load-carrying capacities of slender CFST columns were evaluated. An elastoplastic constitutive model was adopted for the structural steel while the material laws of concrete considered the strain softening were employed. The effective width formulas were adopted to quantify the post-local buckling strengths of steel tubular walls subjected to uniform edge compression. However, the

gradual post-local buckling of the steel boxes was not considered and the concrete material laws adopted ignored the tensile strength and shear deformation of concrete.

The nonlinear structural responses of CFST columns were analyzed by employing the FE program Abaqus by Hu et al. (2003). From the FE results, it was found that circular steel sections provided good confinement to the filled concrete, particularly for columns that had the D/t ratio smaller than 40. For square sections, the confinement effect on the axial capacity of columns where the ratio of B/t was greater than 30 was negligible. However, the confinement in square sections could be increased by using reinforcing ties spaced closely. Equations were proposed for quantifying the lateral confining stresses on the concrete infill in CFST columns of square and circular sections and square CFST columns with reinforcing ties. However, Liang and Fragomeni (2009) found that the model given by Hu et al. (2003) for the concrete in circular cross-sections overestimated the performance of circular CFST columns constructed with high-strength materials, particularly for columns where the ratio of D/t was less than 47.

Ellobody et al. (2006) simulated the inelastic responses of CFST columns using the FE software Abaqus. The numerical model accounted for the strain-hardening behavior of structural steel as well as the concrete confinement effect using the equations of confining pressures given by Hu et al. (2003). The correlation between numerical and experimental load-deflection curves was generally good. Parameter study showed that there was a remarkable improvement in the column capacity when the concrete and steel grades were increased. The acceptability of the design methods given by Eurocode 4 (2004), ACI 318-02 (2002), AISC 360-05 (2005) and AS 3600 (1994) was examined. It was found that AS

3600 and ACI 318-02 conservatively estimated the column strengths owing to the negligence of the effect of concrete confinement.

A numerical model utilizing the concept of fiber elements was proposed by Liang et al. (2006) that simulated the structural behavior of nonlinear CFST short columns of rectangular and square cross-sections loaded concentrically. The influence of the post-local buckling of thin-walled steel sections was incorporated in the mathematical model by means of employing the effective width equations of Liang and Uy (2000). The verified model was utilized to evaluate the significance of steel yield stress, concrete strength and B/t ratio of the steel section on the ultimate resistance of CFST columns.

Liang (2009a, 2009b) developed a method of performance-based analysis underlying the theory of fiber elements for the prediction of the performance of short rectangular CFST columns loaded biaxially. The stress-strain constitutive laws of structural steels recognizing confinement effects were given. Proposed were a coefficient of strength degradation for compressive concrete in the post-yield regime and a coefficient of strength reduction that was used to consider the effect of column size on the concrete strength. The effect of local and post-local buckling of steel tubular walls was included in the mathematical modeling method using the expressions given by Liang et al. (2007). An efficient computer program was specially developed to model the gradual local and post-local buckling of steel flanges and webs of CFST columns loaded biaxially. The in-plane fiber stresses were gradually redistributed from the area heavily buckled to the edge strips in the steel tube wall based on the concept of effective widths. Computational procedures were designed that calculated the load-axial strain as well as axial load-

moment-curvature responses of CFST columns including local buckling. The dynamic equilibrium equations were solved by employing efficient solution algorithms that were developed based on the secant method. The accuracy of the computational modeling method was established by means of comparing computer solutions with the experimentally measured responses of CFST columns.

The theoretical models of fiber approach for the response simulation of CFST circular columns loaded axially and eccentrically were formulated by Liang and Fragomeni (2009, 2010). A confining pressure model, which was expressed in terms of the steel yield stress and the D/t ratio, was proposed to ascertain the confinement effect on the concrete. An iterative mathematical modeling procedure was designed to obtain the moment-curvature relationships of CFST columns loaded eccentrically. The equilibrium condition was maintained during loading history by adjusting the neutral axis depth. An efficient solution algorithm implementing the secant method was developed to solve the nonlinear equilibrium functions. The fiber modeling approach proposed was shown to accurately capture the performance of CFST circular columns. Design models were proposed, which estimated the section ultimate load and pure moment capacity of CFST columns and verified against independent experimental results.

Liang (2011a, 2011b) developed a mathematical modeling scheme, which simulated the overall buckling behavior of slender high-strength CFST circular columns that were eccentrically loaded. The fiber-based mathematical model incorporated various important features, including the geometric imperfection, concrete confinement, and material nonlinearities. Computer modeling procedures for calculating the load-displacement and

axial load-moment interaction relations of CFST columns were presented. The secant method was implemented in the iterative computational procedures to calculate the true neutral axis depth as well as the curvature in the simulation of nonlinear slender CFST columns. The computational modeling method has been found to accurately predict the responses of CFST circular columns.

A multiscale computational model was formulated by Liang et al. (2012) for ascertaining the interaction behavior of local-global buckling of biaxially-loaded rectangular slender CFST columns with pin-ended supports. The multiscale modeling technique accounted for the local and post-local buckling of non-compact and slender steel sections that were subjected to stress gradients. Computational solution algorithms underlying Müller's method were programmed to solve the highly dynamic, nonlinear equilibrium functions generated in the iterative-incremental analysis of CFST columns. The validation of the mathematical model was presented by Patel et al. (2015b) by comparing computations against independent test data. The influences of material strengths and dimensions of the tubes on the steel and concrete contribution ratios and ultimate strengths of CFST columns under biaxial loads were assessed.

Patel et al. (2017a) employed a fiber method to predict the behavior of load-lateral displacement and the axial load-moment of slender circular CFSST columns composed of stainless steel tubes loaded eccentrically. The three-stage material constitutive laws provided by Quach et al. (2008) and Abdella et al. (2011) were included in the fiber model to model the behavior of stainless-steel. The effects of confinement, second-order, and material nonlinearities were considered in the mathematical modeling method. Computer

algorithms, which implemented Müller's method, were programmed to solve the highly dynamic equilibrium equations during the loading history. Patel et al. (2017b) further developed the fiber method for quantifying the structural responses of CFSST slender columns composed of rectangular cross-sections which were eccentrically loaded to failure. The behavior of local and post-local buckling of thin-walled steel tubular walls of CFSST columns was simulated by employing a set of expressions given by Liang et al. (2007) for carbon steel tubes. Computational investigations on the significance of various design variables on the ultimate loads, ultimate moments, deflection and interaction strengths of CFST columns were undertaken.

The computer simulations of the nonlinear behavior of short concrete-filled aluminum tubular (CFAT) circular columns concentrically loaded were presented by Patel et al. (2020). A new lateral pressure model was derived based on the existing experimental data to quantify the confinement effect on the concrete in CFAT columns. The validated model was used to ascertain the influences of important variables on the structural performance of CFAT columns.

2.4 DOUBLE-SKIN CFST COLUMNS

2.4.1 Experimental Studies

Wei et al. (1995) experimentally investigated the structural performance of DCFST short columns that were concentrically loaded to failure. Polyester-based polymer concrete of 60 MPa was employed in this study. The tubes, which had the D/t ratio up to 169 and

steel yield strength of 480 MPa, were utilized to construct these columns. The experimental observations indicated that the lateral pressure provided by the tubes increased the ductility and strength performance of the columns. It was evident that the hollow inner tube buckled outwardly, and the concrete crushed in the region where the local buckling took place.

The experimental behavior of eight square DCFST short columns with an inner circular tube was described by Elchalakani et al. (2002). The width-to-thickness ratios of the external tubes varied from 19 to 55 while the depth-to-thickness ratios of the internal tubes ranged from 20 to 26. The compressive strength of concrete in these columns was determined as 64 MPa. The experimental work demonstrated that the ductile failure was observed in all the tested columns without fracture. Columns with a larger slenderness ratio were less ductile but had a higher energy absorption capacity. The comparisons with calculations using the codified method given in European design code indicated that the design code generally overestimated the axial strength of DCFST columns so that the codified method was unsafe for design purposes.

Tao et al. (2004b) performed experiments on circular DCFST columns to examine the effects of several variables, which included the ratio of D/t , the hollow ratio, the loading eccentricity, and the member slenderness ratio, on the nonlinear responses of DCFST columns. The steel yield stress of the outer tubes ranged from 275 MPa to 294.5 MPa and the inner tubes had the yield stress varied from 320.5 MPa to 396.1 MPa. It was reported that the internal tube underwent local buckling, which was influenced by the tube depth-to-thickness ratio. For the tube that had a small D/t ratio, there was no local buckling

that could be detected. It was evident that the larger the D/t ratio, the lower the ductility of the column. Furthermore, the ductility of DCFST columns was insignificantly influenced by the hollow ratio of the column. However, the beam-columns with a large loading eccentricity displaced good ductility. A theoretical model for quantifying the responses of DCFST columns was proposed and validated by experimental data.

The experiments on the behavior of three rectangular DCFST stub columns, twenty-four DCFST beam-columns, and three DCFST beams were conducted by Tao and Han (2006). The loading eccentricity of the beam-columns varied from 0 to 60 mm. The length of all beam specimens was 1400 mm. The specimens had the internal tube cross-section of 45×75 mm and the external tube cross-section of 100×150 mm. The concrete of high strength was employed to construct these columns. For stub columns, the outward and inward folding failures were observed. For beams, the compression flange of the outer tube underwent local buckling, followed by a buckle at the compressed part of the web. There were fractures spotted on the specimens before failure. The mode of failure of the inner tubes was the unilateral local-buckling due to an inner void. A theoretical model and simplified formulas were proposed for analyzing and designing short DCFST columns.

Zhao et al. (2010b) described an experimental investigation into the responses of short DCFST circular columns. The columns were initially tested under only static load, and then the cyclic load at different stages and the constant axial load. The steel tubes had the D/t ratios varied from 19 to 96 and the yield stress ranged from 395 MPa to 454 MPa. The compressive strength of the filled concrete was estimated as 63.4 MPa. For columns

with smaller slenderness ratios, there was no obvious crack whereas multiple cracks were found on columns where slenderness ratio was large. It was found that the performance of DCFST short columns was largely affected by the depth-to-thickness ratio of the steel sections. The section slenderness ratio less than 82 did not have a significant effect on the deformation responses of DCFST columns. However, for DCFST columns, which had a section slenderness ratio higher than 110, their strength and stiffness were considerably influenced by their section slenderness ratio.

The nonlinear responses of fifty-four DCFST columns with an outer stainless-steel tube were investigated by Han et al. (2011) by means of conducting experiments. Different cross-sections of DCFST columns including circular, square, round-ended rectangular and elliptic sections were examined. The columns were subjected to either vertical loading or inclined loading at 9° or tapered with the tapered angle varied from 0 to 1° . High-strength concrete was employed to construct these columns. Due to the lack of restraint at the column ends, the elephant foot buckling occurred. The columns failed by the outward local-buckling of the outer tube as well as the outwardly local-buckling of the internal tube. The behavior and strength of DCFST columns were found to be remarkably influenced by the hollow ratio. The strength of DCFST columns decreased with increasing the hollow ratio. The inclined and tapered angle had remarkable effects on the ultimate loads of DCFST columns. A set of formulas for designing DCFST columns were suggested and comparisons with experimental values were made.

Li et al. (2014) presented experimental results on eighteen DCFST columns that were loaded by tensile forces to failure. The hollow ratio, the nominal steel ratio, and the

loading eccentricity were treated as test variables. The compressive strength of concrete cube was 60 MPa. The loading eccentricities varied from 35 mm to 140 mm were used. The tested columns exhibited good ductility. No obvious local buckling was observed. Several concrete cracks were found with a width of less than 0.1 mm after removing the outer skin. It was discovered from the test observations that the ultimate tensile strength of DCFST columns increased as the result of increasing the hollow ratio. However, this had an insignificant effect on the column ultimate tensile strength under combined actions. Simplified equations were provided for estimating the ultimate tensile resistance of DCFST columns.

2.4.2 Numerical Studies

The responses of square and circular DCFST columns under concentric loads were investigated using the FE software Abaqus by Huang et al. (2010). A five-stage stress-strain curve and damage plastic model were adopted to describe the material behavior of steel and concrete materials, respectively. The inner and outer tubes were modeled by the shell elements with reduced integrations. The 8-node brick elements were employed to discretize the concrete and endplates. However, the concrete in tension was not included in the numerical analysis of DCFST columns. There were discrepancies between the test and predicted load-strain and load-displacement responses. It was reported that increasing the hollow ratio and concrete strength led to a decrease in the concrete confinement.

Hu and Su (2011) carried out the FE analysis on short DCFST circular columns that were concentrically loaded by using the FE software Abaqus. Investigations of the lateral

stresses on the sandwiched-concrete were performed. Based on the test and FE results, confining pressure models for estimating the lateral stresses on the concrete sandwiched by both outer and inner steel tubes were proposed as a function of the ratios of the depth-to-thickness of the steel sections and steel yield stress. A strength degradation parameter was given to quantify the concrete post-peak strength based on regression analyses.

The FE models of axially loaded DCFST columns were created by using Abaqus by Hassanein et al. (2013b) and Hassanein and Kharoob (2014), respectively. The external tube was made of either carbon steel or lean duplex stainless steel. The model given by Liang and Fragomeni (2009) for the filled concrete in CFST circular columns was employed to estimate the confining stresses on the concrete sandwiched by both tubes. The validations of the FE models were undertaken by means of comparing computations with independent test results reported by Tao et al. (2004a) and Uenaka et al. (2010). The parameter studies showed that using higher strength material of either concrete or the outer tube improved the resistance of the DCFST columns. However, the effect of either the thickness (t_i / t_o) ratio or the yield stress of the internal tube on the strength of DCFST columns was insignificant. Hassanein et al. (2015, 2018) undertook finite element analyses on the behavior of square DCFST columns by means of utilizing Abaqus. The significance of the member slenderness ratio in addition to material and geometric variables on the structural responses of DCFST columns was ascertained. The FE results demonstrated that the resistance of DCFST columns was reduced by increasing either the member slenderness ratio or the hollow ratio.

The responses of short DCFST columns to axial loads were investigated by Pagoulatou et al. (2014) by using the FE models which were created by Abaqus. The lateral pressure model of Hu and Su (2011) was employed to quantify the lateral compressive stresses on the sandwiched-concrete of DCFST columns. From the comparative studies, it could be observed that the FE models yielded conservative solutions to the experimentally measured resistances of DCFST columns. The significance of the D/t ratio and material strengths on the load-displacement relationships of DCFST columns was studied. The applicability of the rules for CFST columns given by Eurocode 4 (2004) to the design of DCFST circular columns was examined.

Liang (2017) developed a numerical model of fiber elements for quantifying the behavior of short DCFST columns of circular cross-sections loaded concentrically. The confinement exerted by both the inner and outer steel tubes on the concrete was incorporated in the fiber model. The models for computing confining stresses on concrete presented by Hu and Su (2011) were evaluated and the corrected model was identified and implemented in the computer model. The strength degradation coefficient and concrete strain were given that quantified the post-peak stress-strain curve for the sandwiched concrete. The developed modeling method was found to accurately capture the responses of DCFST short columns. Simple design formulas were derived for designing short DCFST columns loaded axially. Liang (2018) extended the fiber-based model to the determination of the load-deflection relationships of slender DCFST circular columns, incorporated the strain hardening of structural steel, concrete confinement, second-order effects, and geometric and material nonlinearities. Müller's method has been programmed that solved the dynamic nonlinear equilibrium functions created in the

incremental-iterative analysis of slender columns. Steel and concrete contribution factors were defined and employed to assess the contributions of steel and concrete components to the capacity of DCFST columns. The computer modeling procedures proposed not only captured well the experimentally measured behavior of DCFST columns but also could monitor the distributions of loads during the loading history. The effects of key geometric and material variables on the column strength curves and load-displacement responses of DCFST columns were investigated.

2.5 CONCRETE-FILLED DOUBLE STEEL TUBULAR COLUMNS

2.5.1 Experimental Studies

Pei (2005) performed experiments to ascertain the structural behavior of CFDST square columns composed of an internal circular tube under eccentric loads. The cross-section of the external tube of the specimens was 120×120 mm had the steel yield stress of 407.5 MPa. The diameters of the internal circular tube varied from 58.5 mm to 83 mm and the steel yield stress ranged from 352.5 MPa to 680 MPa. The loading with eccentricity ratios (e / B_o) varied from 0.17 and 0.25 was applied to the column ends. It was reported that CFDST columns had higher capacities than DCFST columns. The strength of CFDST columns was found to improve by using a larger cross-section of the internal tube. However, the performance of CFDST columns in terms of ductility and strength was reduced by increasing the eccentricity ratio.

Experimental works on the strength of short CFDST circular columns consisted of an internal circular tube loaded concentrically were undertaken by Peng et al. (2011). The outer steel tube of the tested columns had the D_o/t_o ratios varied up to 65. These specimens were constructed by high-strength concrete that had a maximum cube strength of 102 MPa. Because of the utilization of the internal tube, the ductility and strength of CFDST columns were shown to improve significantly. Moreover, increasing the steel ratio and concrete grades significantly improved the resistances of CFDST columns. However, the column ductility was reduced by employing high-strength concrete. Design equations considering the confinement effects of both outer and inner tubes were given.

Qian et al. (2011) performed tests to ascertain the strength of square short CFDST columns where the inner steel tube was circular. The outer square tubes had an identical cross-section of 180×180 mm. The outer tubes had varying B_o/t_o ratios due to the changes in their thickness. The diameter of internal circular tubes varied from 89 mm to 140 mm. The core-concrete had a different strength from that of the sandwiched concrete in the inner tube. The filled concrete had the compressive strengths which were varied from 87.5 MPa to 103 MPa. The yield stress of the external tubes with a thickness of 3.62 mm was 348 MPa while it was 338 MPa when the thickness was 5.4 mm. For the inner tubes, the steel yield stress varied from 308 MPa to 345 MPa. It was found that all columns tested failed by the local-buckling of the external steel tube together with the crushing of the sandwiched concrete. The specimens could attain the longitudinal strains up to 0.9-0.11, and residual strength up to 70% of their ultimate loads. The column ultimate load increased with an increase in the steel ratios.

The cyclic performance of short square CFDST columns composed of a circular internal tube was assessed experimentally by Qian et al. (2014). The test specimens were designed as the columns for the lower story of a high rise building by using a base footing. The cross-section used for the outer tube was 300×300 mm with B_o/t_o ratios varied from 24.5 to 50.1 which were obtained by varying the tube thickness. The inner tube was circular with a diameter of 219 mm. The concrete employed to fill these columns had the compressive strength up to 80.9 MPa. The ratios of the axial force applied to the columns ranged from 0.35 to 0.46. The failure of columns tested was due to the significant local-buckling of the external square tube, the crushing of the sandwiched concrete, and the slight local-buckling of the internal tube. From the lateral force-deformation curves, it could be seen that the hysteresis loops were plump and stable. This indicated that CFDST columns had a large energy dissipation capacity. Increasing the D_i/t_i ratio of the inner tube or decreasing the B_o/t_o ratio of the external tube increased the flexural strength of CFDST columns.

Romero et al. (2015) reported the test results of slender circular CFDST and DCFST columns exposed to ambient and elevated temperatures. Different combinations of concrete strength and the thickness of internal and external tubes were examined. Ultra-high-strength (UHS) concrete with strength up to 150 MPa was employed in the specimens. It was indicated that the maximum strength of columns that had thick outer tube at room temperature increased due to the reduction in the effect of second order. The improvement in the ultimate strength owing to the utilization of UHS concrete in the inner tube was insignificant. However, the use of UHS concrete in the internal tube under fire exposure improved the fire resistance and strength of the CFDST column compared to

the one filled with normal strength concrete. The measurements were compared against the calculations using the provisions in Eurocode 4 (2004). The comparison indicated that Eurocode 4 significantly underestimated the axial resistance of CFDST columns.

The experiments on the structural responses of CFDST circular columns composed of a circular inner tube were described by Wan and Zha (2016). The external tube of the short columns had a diameter of 426 mm with varying thickness. The D_i / t_i ratio of the internal tubes varied from 20 to 42. It was demonstrated that CFDST columns had good ductility. The outer steel tube buckled outwardly while the inner tube failed by shear and concrete crushing at places where the local buckling took place. The larger the steel ratio, the higher the ductility and strength of the CFDST column. Furthermore, for the columns with the same steel ratio, using high strength steel markedly improved the resistance of the columns.

Ekmekyapar and Al-Eliwi (2017) conducted a series of experiments on short circular CFDST columns composed of a circular section, which were loaded concentrically to failure. To evaluate the applicability of CFDST columns in strengthening deformed CFST columns, eight deformed CFST columns were also converted to CFDST columns by placing an external tube which was filled with concrete. The test variables under investigations included the D_o / t_o ratio of the outer tube, and the compressive strength of concrete. The premature failure of the column ends was observed because the column ends were not stiffened. It was shown that the performance of CFDST columns and the retrofitted CFST columns was almost identical in terms of ductility, strength and failure

modes. The composite actions between the internal tube and core concrete remarkably improved the strength of CFDST columns when compared to CFST ones.

The performance of square CFDST columns consisted of a circular inner tube under axial loading was examined by Wang et al. (2017). The outer square tube of these specimens had a cross-section of 200×250 mm and a thickness of 2.01 mm. The internal tubes had the D_i / t_i ratios varied from 29.2 to 70 with the steel yield stress ranged from 322 MPa to 492 MPa. The concrete with cube strength of either 42.1 MPa or 69.8 MPa was employed to fill the hollow tubes. From the experimental observations, it was discovered that the failure modes of the CFDST columns included the local-buckling of the outer steel tube walls, concrete crushing and shear failure for some columns. The stiffeners welded to the inner face of the external tube buckled locally. The inner tube confined the core concrete and no damage to the core concrete could be observed. The resistance of CFDST columns was improved by increasing either the steel ratio of inner tubes or concrete strength.

2.5.2 Numerical Studies

Qian et al. (2011) presented a FE model created using Abaqus for analyzing axially loaded nonlinear short square CFDST columns consisted of an inner circular tube. The material constitutive laws of concrete in CFST columns given by Han et al. (2001) were adopted to model the behavior of concrete in CFDST columns. However, the local and post-local buckling of the outer square tubes was not included in the model. The test results reported by the authors were employed to establish the accuracy of the numerical modeling

method. The experimentally measured strengths of CFDST columns were slightly overestimated by the FE model.

The behavior of CFDST short columns composed of an outer circular stainless-steel tube and an inner circular carbon-steel tube was examined numerically using the FE software Abaqus by Chang et al. (2013) and Hassanein et al. (2013a). The double confinement on the core-concrete was considered by adding the lateral stresses on the sandwiched-concrete and core-concrete estimated by the confinement models of concrete in CFST circular columns. The model formulated by Liang and Fragomeni (2009) for concrete in CFST columns of circular sections was employed by Hassanein et al. (2013a) to quantify the lateral stresses on the concrete in CFDST columns. The numerical results were compared against experimental data reported by Chang et al. (2013). Parameter studies conducted by Hassanein et al. (2013a) showed that increasing the thickness of either the outer or internal steel tube improved the performance of CFDST columns. The column capacity was improved by using high-strength materials of concrete and steel. Design recommendations were suggested and compared against the design provisions given by ACI 318-05 (2005).

Wan and Zha (2016) investigated the axial responses of CFDST columns in which both the inner and outer tubes were circular using the FE program Abaqus. The FE model used a bilinear elastic-plastic law for steel material. A confining pressure model incorporated a confinement factor and a strength degradation parameter were developed based on the test results for concrete in CFDST columns. However, there was a significant discrepancy

between finite element results and measurements. This could be attributed to the inaccuracy of the confinement model proposed by Wan and Zha (2016).

The FE models of concentrically loaded short CFDST columns fabricated by an external square tube and an internal circular tube were created using the FE software Abaqus by Wang et al. (2017). The strain hardening of steel material was considered for the inner steel tube while the elastic-perfectly plastic relationship was utilized for the external square tube of CFDST columns. The concrete model given by Tao et al. (2013) for circular conventional CFST columns was employed to simulate the core-concrete behavior. However, the effect of the local-buckling of the external square steel tubes was not accounted for in the FE modeling of CFDST square columns. Consequently, the FE modeling technique considerably overestimated the axial resistance of CFDST short columns.

Zheng and Tao (2019) evaluated the ductility, strength, and stiffness of circular CFDST columns composed of an inner circular tube by means of utilizing the FE software Abaqus. The eight-node brick element (C3D8R) element was employed to discretize the concrete whereas the steel tubes were meshed by the four-node shell element (S4R). The strain hardening of steel material was incorporated in the FE models only for circular CFDST columns using the material laws for steel proposed by Katwal et al. (2017). The confinement for the confined concrete of circular CFDST columns was estimated. It was indicated that a good correlation between experimental and numerical results was obtained. Equations for estimating the stiffness, ultimate strain and ultimate load of CFDST columns were given.

2.6 COMPOSITE COLUMNS WITH PRELOAD EFFECTS

2.6.1 Experimental Studies

The influences of preloads on the performance of nonlinear circular CFST columns were ascertained by Zhang et al. (1997) by conducting experiments. The circular section had a diameter of 133 mm and a thickness of 4.5 mm. The steel yield strength and the concrete cube strength were measured as 325 MPa and 42.2 MPa, respectively. The columns tested had the lengths varied from 465 mm to 2730 mm. The columns were subjected to a wide range of preload ratios which varied from 0.0 to 0.82. The e/D ratio of the loading was either 0.38 or 0.45. It was observed that the small preload ratio had an insignificant influence on the column strength. However, the preload with a ratio greater than 0.4 could reduce the column ultimate load by more than 5%.

Han and Yao (2003) conducted tests on nineteen concentrically and eccentrically loaded square CFST columns where the steel tubes were preloaded before the concrete was filled. The slenderness ratio of the columns ranged up to 40 while the ratio of preload varied from 0.0 to 0.7. The column specimens were constructed by mild steel tubes, which were initially stressed by prestressing bars and filled with normal strength concrete. Their study indicated that all specimens exhibited a ductile behavior. It was found that increasing the preload ratio reduced the strength and axial stiffness of CFST columns. The maximum strength reduction was about 20% of the capacity of the slender CFST column. However, the preload with a ratio less than 0.3 caused an insignificant reduction in the column capacity and its effect on short columns could be ignored.

Experimental studies were conducted by Liew and Xiong (2009) to assess the performance of eleven CFST circular columns of which eight columns were subjected to preloads. The steel tubes of the tested columns had a diameter of 219 mm and a thickness of 6.3 mm. Steel tubes were preloaded by prestressing strands anchored on two steel end plates prior to filling concrete. The variables chosen for the study were the column relative slenderness, concrete compressive strength and preload ratio. It was observed that short columns failed by squashing while columns with intermediate and slender columns failed by the overall buckling. The local buckling of a few columns was detected after their ultimate strengths were attained. The preload was found to have an insignificant influence on the behavior of short columns and could be neglected for a preload ratio of less than 0.2. However, the preload had a considerable influence on intermediate and slender columns and could reduce the column ultimate strength by about 20%.

Huang et al. (2016) undertook experiments on preloaded circular CFST slender columns where the steel sections had a dimension of 108×4 mm. The steel yield strength and concrete cube strength were measured as 336 MPa and 54.9 MPa, respectively. The slenderness of the column varied from 12 to 72. The preload on the steel tube was applied using four bars welded to the end-plates prior to filling concrete. The ratio of the preload ranged from 0.0 to 0.54. It was reported that the failure of the intermediate and long columns was due to global buckling without significant plastic deformation whereas short columns failed due to the local-buckling at the mid-height of the columns. It was found that when the ratio of preload was 0.25, the reduction in the strength was only about 3%. However, as the ratio of preload increased to 0.5, the reduction in the ultimate load of the long column was calculated as 9.8%. It was confirmed that the influence of preload on

the resistance of short columns was insignificant and could be negligible in the practical design of short CFST columns.

The effects of long-term sustained load and preload on the behavior of circular concrete-encased CFST columns were examined by Li et al. (2019). The steel tubes had the D/t ratios varied from 32.5 to 44. All the tested columns had the same length of 600 mm. The preload on the steel hollow tube was applied by tightening the steel tie rods until the predetermined preload ratio was attained. The ratio of the preload on the steel hollow column was designed to be 0.3 and 0.6. After 28 days of casting concrete, the columns were under the long-term sustained load for 365 days before they were tested. The longitudinal strains of CFST columns increased with time under preload in addition to the long-term sustained load. However, within the first 40 days of the sustained load, the columns reached 70% of the final strain, and the remaining strain increased slowly and became stable after 100 days. It was discovered that the column ultimate load was reduced by about 8.7% due to the combined actions of long-term sustained load and preload. The columns with a smaller preload ratio had a larger creep coefficient. The ductility of the columns increased with either increasing the loading age or decreasing the preload ratio.

2.6.2 Numerical Studies

Han and Yao (2003) presented a fiber model for studying the influences of preload on the structural performance of CFST circular columns. The structural steel model suggested by Han et al. (2001) and the concrete constitutive laws proposed by Han and Huo (2003) were used in the fiber modeling technique. A strength indicator was defined for the

strength estimation of CFST columns accounting for the influences of preload, member slenderness ratio, and loading eccentricity.

The FE analysis model incorporating preload effects was developed for circular slender CFST columns by Liew and Xiong (2009) using the FE software Abaqus. The concrete and steel tube of CFST columns were meshed using solid element C3D8R and shell element S4R, respectively. The FE analysis assumed the perfect bond between steel and concrete elements of CFST columns. The accuracy of the FE results was validated against the independent experimental data. Based on the design specifications in Eurocode 4 (2004), design models were proposed that could be used to design slender circular CFST columns where the steel tubes were preloaded.

Li et al. (2012) conducted numerical investigations on the effects of preload on the responses of square and circular DCFST columns by means of using the FE software Abaqus. The damage plasticity relationships were used to simulate the concrete material. It was confirmed that the preload remarkably decreased the strength of such composite columns. Formulas were proposed for determining the strength indicator of DCFST columns in which the steel tubes were preloaded.

Patel et al. (2013, 2014) developed fiber models, which could predict the structural performance of slender circular and rectangular CFST columns that were preloaded. The load-control approach was used to quantify the lateral displacement of the steel hollow tube under preloads, which was incorporated in the simulation of nonlinear slender CFST column as an additional imperfection. The mathematical models developed considered

the interaction of local-global buckling, concrete confinement, second-order effects as well as geometric and material nonlinearities. The established experimental results were employed to verify the proposed fiber models. Parameters chosen for the study included preload ratio, column slenderness, depth-to-thickness ratio of the steel section, loading eccentricity, and material strength.

2.7 CONCLUDING REMARKS

An extensive literature review on the published works related to the present research project has been presented in this chapter. These have included publications on the local and post-local buckling of steel plates, experimental and numerical investigations on various concrete-filled composite columns that were under axial compression, combined bending and axial compression, and preloads. The following research gaps in the current knowledge have been identified:

1. Fiber-based computational models for the load-strain response analysis of short circular and rectangular CFDST columns have not been developed, considering the influences of confinement and local buckling.
2. The local-global interaction buckling of slender square CFDST columns composed of an inner circular tube has not been included in the fiber-based computational modeling method.
3. No accurate confining model has been proposed that simulates the responses of core concrete in circular CFDST columns based on the available test data.

4. Experiments on the behavior of square, circular and rectangular CFDST stub columns subjected to eccentric loading have rarely been reported.
5. Computational models underlying the fiber approach have not been developed, which can simulate the axial load-moment and moment-curvature curves of short CFDST columns with square, circular and rectangular sections loaded eccentrically.
6. A computational model employing the fiber analysis technique for the analysis of the overall buckling of slender CFDST columns of circular cross-sections has not been formulated.
7. The influences of preload on the behavior of slender CFDST columns of circular and square sections loaded eccentrically have not been investigated using the computational model.
8. Existing design models for conventional CFST columns can not accurately predict the performance of CFDST columns composed of circular and rectangular cross-section under different loading conditions.

Chapter 3

RECTANGULAR CFDST SHORT COLUMNS

3.1 INTRODUCTION

The square or rectangular outer steel tube of a CFDST short column under the increasing compressive load may undergo the progressive outward local-buckling, which leads to a reduction in the performance of the column. This progressive local instability problem is so complicated that it has not been taken into account in any fiber-based modeling procedures for the inelastic response simulation of square CFDST columns.

This chapter presents computational and experimental studies on the performance of axially and eccentrically loaded rectangular and square CFDST stub columns composed of either a circular internal tube or a rectangular/square inner tube. New expressions are proposed based on the existing test results to quantify the concrete post-peak characteristics and incorporated in the numerical modeling method for simulating the responses of CFDST rectangular columns having a circular inner tube. The local buckling of the outer steel section and the confinement offered by the circular inner tube are considered. The numerical simulation technique is validated by means of comparisons with independent test results. Parameter study is performed and simple design equations are suggested to quantify the axial resistance of CFDST short columns.

Experimental studies on eccentrically and concentrically loaded square CFDST short columns composed of a circular internal tube and rectangular short CFDST columns with a rectangular internal tube are described. Mathematical modeling techniques are also developed to ascertain the strength envelopes and moment-curvature relationships of CFDST stub columns incorporating the effects of local buckling. New computational solution programs underlying the inverse quadratic method are designed to solve the nonlinear equilibrium equations of short CFDST columns that are eccentrically loaded. The experimental data are utilized to validate the accuracy of the computational modeling methods proposed.

This chapter includes the following papers:

1. **Ahmed, M.**, Liang, Q. Q., Patel, V. I. and Hadi, M. N. S. (2018). Nonlinear analysis of rectangular concrete-filled double steel tubular short columns incorporating local buckling. *Engineering Structures*, 175, 13-26.
2. **Ahmed, M.**, Liang, Q. Q., Patel, V. I. and Hadi, M. N. S. (2019). Experimental and numerical studies of square concrete-filled double steel tubular short columns under eccentric loading. *Engineering Structures*, 197, 109419.
3. **Ahmed, M.**, Liang, Q. Q., Patel, V. I. and Hadi, M. N. S. (2020). Experimental and numerical investigations of eccentrically-loaded rectangular concrete-filled double steel tubular columns. *Journal of Constructional Steel Research*, 167, 105949 (published on April 2020).

OFFICE FOR RESEARCH TRAINING, QUALITY AND INTEGRITY

DECLARATION OF CO-AUTHORSHIP AND CO-CONTRIBUTION: PAPERS INCORPORATED IN THESIS

This declaration is to be completed for each conjointly authored publication and placed at the beginning of the thesis chapter in which the publication appears.

Title of
Paper/Journal/Book:

Ahmed, M., Liang, Q. Q., Patel, V. I. and Hadi, M. N. S. (2018). Nonlinear analysis of rectangular concrete-filled double steel tubular short columns incorporating local buckling. *Engineering Structures*, 175: 13-26.

Surname:

First
name:

Institute:

Candidate's Contribution (%):

Status:

Accepted and in press:

Date:

Published:

Date:

2. CANDIDATE DECLARATION

I declare that the publication above meets the requirements to be included in the thesis as outlined in the HDR Policy and related Procedures – policy.vu.edu.au.

Mizan Ahmed Digitally signed by Mizan Ahmed
Date: 2019.12.18 12:51:13 +11'00'

18-12-2019

Signature

Date

3. CO-AUTHOR(S) DECLARATION

In the case of the above publication, the following authors contributed to the work as follows:

The undersigned certify that:

1. They meet criteria for authorship in that they have participated in the conception, execution or interpretation of at least that part of the publication in their field of expertise;
2. They take public responsibility for their part of the publication, except for the responsible author who accepts overall responsibility for the publication;

3. There are no other authors of the publication according to these criteria;
4. Potential conflicts of interest have been disclosed to a) granting bodies, b) the editor or publisher of journals or other publications, and c) the head of the responsible academic unit; and
5. The original data will be held for at least five years from the date indicated below and is stored at the following **location(s)**:

R:\CFDST Columns

Name(s) of Co-Author(s)	Contribution (%)	Nature of Contribution	Signature	Date
Mizan Ahmed	60	Methodology, Software, Validation, Formal analysis, Investigation, Data curation, Writing–Original draft, Visualization.	Mizan Ahmed Digitally signed by Mizan Ahmed Date: 2019.12.18 12:51:30 +11'00'	18-12-2019
Qing Quan Liang	20	Conceptualization, Methodology, Software, Validation, Writing–Review and Editing, Supervision, Project administration.	Qing Quan Liang Digitally signed by Qing Quan Liang Date: 2019.12.18 13:10:15 +11'00'	18-12-2019
Vipulkumar I. Patel	10	Validation, Writing–Review and Editing, Supervision.	Vipul Patel Digitally signed by Vipul Patel Date: 2019.12.18 13:31:16 +11'00'	18-12-2019
Muhammad N.S. Hadi	10	Validation, Writing–Review and Editing, Supervision.	Muhammad Hadi Digitally signed by Muhammad Hadi DN: cn=Muhammad Hadi, o=University of Wollongong, ou=School of CME, email=mhadi@uow.edu.au, c=AU Date: 2019.12.18 14:48:25 +11'00'	18-12-2019

OFFICE FOR RESEARCH TRAINING, QUALITY AND INTEGRITY

DECLARATION OF CO-AUTHORSHIP AND CO-CONTRIBUTION: PAPERS INCORPORATED IN THESIS

This declaration is to be completed for each conjointly authored publication and placed at the beginning of the thesis chapter in which the publication appears.

Title of
Paper/Journal/Book:

Ahmed, M., Liang, Q. Q., Patel, V. I. and Hadi, M. N. S. (2019).
Experimental and numerical studies of square concrete-filled double steel
tubular short columns under eccentric loading. Engineering Structures,
197, 109419.

Surname: Ahmed

First
name: Mizan

Institute: Institute for Sustainable Industries and Liveable Cities

Candidate's Contribution (%): 60

Status:

Accepted and in press:

Date:

Published:

Date: 15-10-2019

2. CANDIDATE DECLARATION

I declare that the publication above meets the requirements to be included in the thesis as outlined in the HDR Policy and related Procedures – policy.vu.edu.au.

Mizan Ahmed

Digitally signed by Mizan Ahmed
Date: 2019.12.18 12:55:10
+11'00'

18-12-2019

Signature

Date

3. CO-AUTHOR(S) DECLARATION

In the case of the above publication, the following authors contributed to the work as follows:

The undersigned certify that:

1. They meet criteria for authorship in that they have participated in the conception, execution or interpretation of at least that part of the publication in their field of expertise;
2. They take public responsibility for their part of the publication, except for the responsible author who accepts overall responsibility for the publication;

3. There are no other authors of the publication according to these criteria;
4. Potential conflicts of interest have been disclosed to a) granting bodies, b) the editor or publisher of journals or other publications, and c) the head of the responsible academic unit; and
5. The original data will be held for at least five years from the date indicated below and is stored at the following **location(s)**:

R:\CFDST Columns

Name(s) of Co-Author(s)	Contribution (%)	Nature of Contribution	Signature	Date
Mizan Ahmed	60	Methodology, Software, Validation, Formal analysis, Investigation, Data curation, Writing–Original draft, Visualization.	Mizan Ahmed Digitally signed by Mizan Ahmed Date: 2019.12.18 12:55:22 +11'00'	18-12-2019
Qing Quan Liang	20	Conceptualization, Methodology, Software, Validation, Writing–Review and Editing, Supervision, Project administration, Funding acquisition.	Qing Quan Liang Digitally signed by Qing Quan Liang Date: 2019.12.18 13:20:00 +11'00'	18-12-2019
Vipulkumar I. Patel	10	Validation, Writing–Review and Editing, Supervision, Funding acquisition.	Vipul Patel Digitally signed by Vipul Patel Date: 2019.12.18 13:39:35 +11'00'	18-12-2019
Muhammad N.S. Hadi	10	Validation, Investigation, Writing–Review and Editing, Supervision.	Muhammad Hadi Digitally signed by Muhammad Hadi DN: cn=Mohammad Hadi, o=University of Wollongong, ou=School of CME, email=mhadi@uow.edu.au, c=AU Date: 2019.12.18 14:52:33 +11'00'	18-12-2019

OFFICE FOR RESEARCH TRAINING, QUALITY AND INTEGRITY

DECLARATION OF CO-AUTHORSHIP AND CO-CONTRIBUTION: PAPERS INCORPORATED IN THESIS

This declaration is to be completed for each conjointly authored publication and placed at the beginning of the thesis chapter in which the publication appears.

Title of
Paper/Journal/Book:

Ahmed, M., Liang, Q. Q., Patel, V. I. and Hadi, M. N. S. (2020).
Experimental and numerical investigations of eccentrically loaded
rectangular concrete-filled double steel tubular columns. Journal of
Constructional Steel Research, (accepted).

Surname:

First
name:

Institute:

Candidate's Contribution (%):

Status:

Accepted and in press:

Date:

Published:

Date:

2. CANDIDATE DECLARATION

I declare that the publication above meets the requirements to be included in the thesis as outlined in the HDR Policy and related Procedures – policy.vu.edu.au.

Mizan Ahmed Digitally signed by Mizan Ahmed
Date: 2020.01.16 09:18:05 +11'00'

16-01-2020

Signature

Date

3. CO-AUTHOR(S) DECLARATION

In the case of the above publication, the following authors contributed to the work as follows:

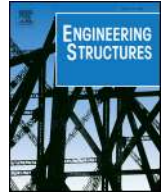
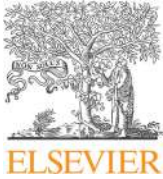
The undersigned certify that:

1. They meet criteria for authorship in that they have participated in the conception, execution or interpretation of at least that part of the publication in their field of expertise;
2. They take public responsibility for their part of the publication, except for the responsible author who accepts overall responsibility for the publication;

3. There are no other authors of the publication according to these criteria;
4. Potential conflicts of interest have been disclosed to a) granting bodies, b) the editor or publisher of journals or other publications, and c) the head of the responsible academic unit; and
5. The original data will be held for at least five years from the date indicated below and is stored at the following **location(s)**:

R:\CFDST Columns

Name(s) of Co-Author(s)	Contribution (%)	Nature of Contribution	Signature	Date
Mizan Ahmed	60	Methodology, Software, Validation, Formal analysis, Investigation, Data curation, Writing–Original draft, Visualization.	Mizan Ahmed Digitally signed by Mizan Ahmed Date: 2020.01.16 09:18:22 +11'00'	16-01-2020
Qing Quan Liang	20	Conceptualization, Methodology, Software, Validation, Writing–Review and Editing, Supervision, Project administration, Funding acquisition.	Qing Quan Liang Digitally signed by Qing Quan Liang Date: 2020.01.16 09:42:58 +11'00'	16-01-2020
Vipulkumar I. Patel	10	Validation, Writing–Review and Editing, Supervision, Funding acquisition.	Vipul Patel Digitally signed by Vipul Patel Date: 2020.01.16 09:48:39 +11'00'	16-01-2020
Muhammad N.S. Hadi	10	Validation, Investigation, Writing–Review and Editing, Supervision.	Muhammad Hadi Digitally signed by Muhammad Hadi DN: cn=Mohammad Hadi, o=University of Wollongong, ou=School of CME, email=mhadi@uow.edu.au, c=AU Date: 2020.01.16 13:52:12 +11'00'	16-01-2020



Nonlinear analysis of rectangular concrete-filled double steel tubular short columns incorporating local buckling

Mizan Ahmed^a, Qing Quan Liang^{a,*}, Vipulkumar Ishvarbhai Patel^b, Muhammad N.S. Hadi^c

^a College of Engineering and Science, Victoria University, PO Box 14428, Melbourne, VIC 8001, Australia

^b School of Engineering and Mathematical Sciences, La Trobe University, Bendigo, VIC 3552, Australia

^c School of Civil, Mining and Environmental Engineering, University of Wollongong, Wollongong, NSW 2522, Australia

ARTICLE INFO

Keywords:

Concrete-filled double steel tubes
Nonlinear analysis
Local buckling
Post-local buckling

ABSTRACT

Rectangular concrete-filled double steel tubular (CFDST) columns with inner circular steel tube possess higher structural performance than conventional concrete-filled steel tubular (CFST) columns. However, the local buckling of the outer steel tube of thin-walled rectangular CFDST columns has not been accounted for in the existing fiber element models and design codes that may overestimate the column ultimate axial strengths. This paper describes a computationally efficient fiber-based modeling technique developed for determining the behavior of concentrically-loaded rectangular CFDST short columns including the local buckling effects of the external steel tube and the confinement offered by the internal circular steel tube. The effective width concept is used to simulate the post-local buckling of the outer steel tube. Comparative studies are undertaken to verify the fiber-based model with the relevant test results. The computational model is then employed to investigate the axial load–strain responses of rectangular CFDST short columns with various key design variables. A design equation is developed for computing the ultimate axial loads of short rectangular CFDST columns and compared with design methods given in several international design codes. It is shown that the fiber-based modeling technique and the proposed design model predict well the structural performance of short CFDST columns.

1. Introduction

The rectangular concrete-filled double steel tubular (CFDST) column is a high performance composite column, which is constructed by an outer rectangular steel tube and an inner circular steel tube filled with concrete as depicted in Fig. 1. Experiments conducted by Knowles and Park [1], Tomii et al. [2], Schneider [3] and Sakino et al. [4] indicated that the rectangular or square steel tube provided little confinement to the filled concrete while the circular steel tube offered a significant confinement to the concrete infill. The addition of a circular steel tube to the rectangular concrete-filled steel tubular (CFST) column remarkably improves the column structural performance. The circular steel tube provides confinement to the core concrete, which increases the strength and ductility of the core concrete and thereby improves the ultimate axial loads, stiffness, ductility, shear-resistance and fire-resistance of CFDST columns. The concrete within the inner circular steel tube not only prevents the local buckling of the inner steel tube but also increases the overall buckling strength and fire-resistance of the inner hollow steel tube. Therefore, thin-walled rectangular CFDST columns are utilized in high-rise composite steel-concrete buildings, industrial

buildings and bridges to support heavy loads. The CFDST columns are characterized by the outward local-buckling of the external rectangular steel tube. However, the local buckling effects have not been incorporated in the fiber-based analysis models for thin-walled CFDST columns and in international design codes including Eurocode 4 [5], ACI 318-11 [6], AISC 360-16 [7] and AIJ [8]. A fiber element simulation technique considering the local buckling effects and concrete confinement is much needed for accurately predicting the axial load-strain responses of rectangular CFDST columns with thin-walled sections.

Computational and experimental investigations on the responses of circular short CFDST columns subjected to axial loading have been undertaken by researchers, such as Peng et al. [9], Hassanein et al. [10], Wan and Zha [11], Xiong et al. [12], and Ekmekyapar and Al-Eliwi [13]. These studies showed that the core concrete was confined by both the inner and outer circular steel tubes, which increased both the ductility and capacity of circular CFDST columns. Ahmed et al. [14] proposed confinement models for the core concrete in short CFDST circular columns based on available test results while the confinement model presented by Hu et al. [15] was adopted to compute the

* Corresponding author.

E-mail address: Qing.Liang@vu.edu.au (Q.Q. Liang).

<https://doi.org/10.1016/j.engstruct.2018.08.032>

Received 17 April 2018; Received in revised form 27 June 2018; Accepted 11 August 2018

Available online 15 August 2018

0141-0296/ © 2018 Elsevier Ltd. All rights reserved.

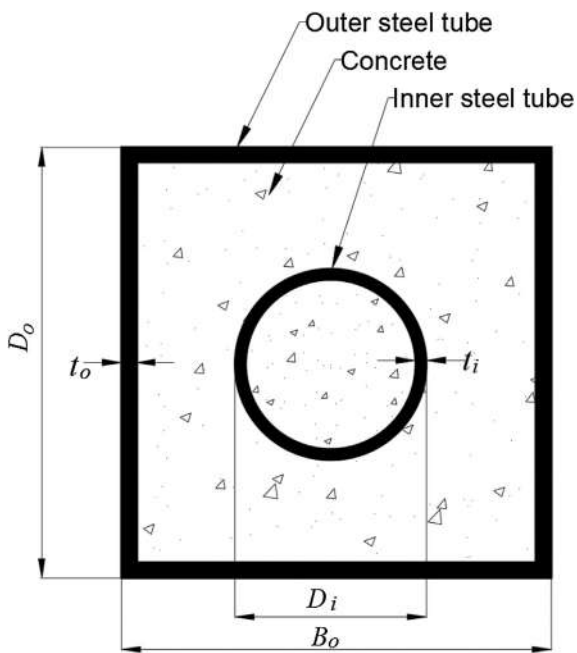


Fig. 1. Cross-section of rectangular CFST column with inner circular steel tube.

maximum compressive strength of the concrete between the two tubes. The fiber technique implementing these confinement models was shown to capture well the behavior of circular CFST short columns.

Relatively limited investigations on the behavior of square CFST columns under static loading were conducted by researchers [16–20]. Lu and Zhao [16] presented a numerical method for computing the load-deflection relationships of eccentrically-loaded square slender CFST columns with various width-to-thickness, loading eccentricity and column slenderness ratios. Pei [18] performed experimental investigations on short and slender square CFST columns subjected to axial and eccentric loading and used the finite element software ANSYS to analyze square CFST short columns. The effects of the inner circular tube with various thicknesses, diameters and steel yield stresses on the performance of CFST columns were examined. The 23 square short CFST columns under axial compressive loads were tested to failure by Qian et al. [19]. The experimental results indicated that the local buckling of the square steel tube occurred outwardly while the sandwiched concrete near the buckled regions crushed. However, these square CFST columns still could withstand about 70% of the ultimate axial loads and had the ultimate axial strains ranging from 0.09 to 0.11. The finite element software ABAQUS was utilized by Qian et al. [19] to analyze short square CFST columns including local buckling effects. Wang et al. [20] undertook tests on 12 square cold-formed thin-walled CFST short columns with stiffeners under axial compression. It was reported that the failure mode of all CFST columns was the outward local buckling of the external square steel tube. The outer steel tube at the stiffeners buckled locally outward because the sandwiched concrete crushed and the stiffeners buckled. No local buckling of the inner circular steel tube was observed so that the core concrete was effectively confined by the internal tube, which improved the column ultimate load and ductility. The finite element software ABAQUS was employed by Wang et al. [20] to study the behavior of short CFST columns.

It should be noted that at the early loading stage, the inner circular steel tube does not provide confinement to the core concrete because the Poisson's ratio of the concrete is less than that of the steel. When the axial compressive stress in concrete is greater than its unconfined compressive strength, the sandwiched concrete crushes and separates from the inner steel tube. Under this high axial compressive stress, the core concrete expands and eventually inserts a lateral pressure on the

inner steel tube so that the inner circular steel tube confines the core concrete. In the numerical analysis, the confinement effect is considered in the stress-strain model for concrete in circular steel tubes when the axial compressive stress in the concrete is greater than its unconfined compressive strength as discussed by Liang [21].

The dynamic and impact responses of CFST columns and double-skin concrete-filled steel tubular (DCFST) columns have been studied in recent years. Han et al. [22] developed a fiber element model for determining the cyclic behavior of square and circular DCFST beam-columns with inner circular tubes. Simple models were proposed that compute the moment-curvature and lateral load-deflection responses of DCFST beam-columns under cyclic lateral loads. The seismic performance of high-strength square CFST columns with various geometric parameters and axial force levels were experimentally investigated by Qian et al. [23]. It was observed that the sandwiched and core concrete crushed and the outer square steel tube buckled locally outward. Wang et al. [24] employed ABAQUS software to quantify the effects of impact height as well as geometric and material properties on the behavior of circular DCFST columns under lateral impact. They reported that the hollow ratio had a significant effect on the dynamic resistance of DCFST columns, which should account for the dynamic increase factor when the confinement factor is greater than 1.03. The blast resistance of square DCFST columns made of high performance steel-fiber reinforced concrete was studied experimentally and numerically by Zhang et al. [25]. The experimental results showed that square DCFST columns could resist a large blast load without failure. Aghdamy et al. [26] utilized the finite element software LS-DYNA to investigate the effects of load-related parameters on the behavior of circular DCFST columns under lateral impact. Large-scale tests and numerical analyses on the flexural behavior of square DCFST members under blast loads were conducted by Ritchie et al. [27]. Their study indicated that increasing the width of the inner steel tube increased the ultimate moment capacity of DCFST columns and the width and thickness of the outer tube had a significant effect on the ductility of DCFST columns.

The local buckling of the external steel tube is one of the main failure modes associated with rectangular CFST short columns with inner circular steel tube. The local buckling of thin steel plates restrained by concrete was studied previously by researchers [28–33]. Liang and Uy [31] derived effective width models for calculating the post-local buckling strength of steel plates in rectangular CFST columns based on finite element analyses. Liang et al. [32] utilized these effective width models in the inelastic analysis of rectangular short CFST columns. Liang et al. [33] also investigated the local and post-local buckling strengths of steel tube walls of rectangular CFST columns under biaxial loads and developed expressions for determining initial local and post-local buckling strengths of clamped steel plates. The expressions were implemented in the fiber based models to include local buckling in the inelastic simulations of CFST columns subjected to biaxial loads by Liang [34,35].

Although the local buckling of the external rectangular steel tube in CFST columns could be considered in the finite element analysis using commercial programs, the nonlinear inelastic finite element analysis of CFST columns is highly time consuming and expensive. This paper presents a computationally efficient fiber-based modeling technique for the simulation of rectangular CFST short columns including the effects of the progressive local and post-local buckling of the outer rectangular steel tube. The fiber-based analysis technique incorporates the confinement to the core concrete offered by the inner circular steel tube. The model validation is performed by comparing the predicted ultimate axial strength and load-strain relationships with the corresponding test results. The developed computer program is then used to evaluate the influences of important variables on the ultimate load and behavior of short CFST columns. A design formula is developed for rectangular short CFST columns considering the concrete confinement and local buckling and verified by independent test results as well as design codes.

Table 1
Comparison of predicted and experimental ultimate axial loads of square CFDST short columns.

Specimen	outer tube			Inner tube			Concrete		Ultimate axial load			Ref.
	$B_o \times D_o \times t_o$ (mm)	$\frac{D_o}{t_o}$	f_{syo} (MPa)	$D_i \times t_i$ (mm)	$\frac{D_i}{t_i}$	f_{syt} (MPa)	f'_{co} (MPa)	f'_{ci} (MPa)	$P_{u,exp}$ (kN)	$P_{u,num}$ (kN)	$\frac{P_{u,num}}{P_{u,exp}}$	
I-CSCFT1	180 × 180 × 3.62	49.7	348	89 × 2.6	34.2	314	89.85	74.38	3643	3436	0.94	[19]
I-CSCFT2	180 × 180 × 3.62	49.7	348	89 × 3.32	26.8	324	89.85	74.38	3583	3487	0.97	
I-CSCFT4	180 × 180 × 3.62	49.7	348	114 × 4.56	25.0	322	89.85	74.38	3820	3707	0.97	
I-CSCFT5	180 × 180 × 3.62	49.7	348	140 × 2.84	49.3	345	89.85	74.38	3940	3541	0.90	
I-CSCFT7	180 × 180 × 5.4	33.3	338	89 × 2.6	34.2	314	89.85	74.38	3865	3784	0.98	
I-CSCFT8	180 × 180 × 5.4	33.3	338	89 × 3.32	26.8	324	89.85	74.38	3947	3836	0.97	
I-CSCFT9	180 × 180 × 5.4	33.3	338	114 × 3.35	34.0	328	89.85	74.38	4045	3976	0.98	
I-CSCFT10	180 × 180 × 5.4	33.3	338	114 × 4.56	25.0	322	89.85	74.38	4121	4063	0.99	
I-CSCFT11	180 × 180 × 5.4	33.3	338	140 × 2.84	49.3	345	89.85	74.38	4251	3874	0.91	
I-CSCFT12	180 × 180 × 5.4	33.3	338	140 × 3.97	35.3	308	89.85	74.38	4258	4147	0.97	
II-CSCFT1	180 × 180 × 3.62	49.7	348	89 × 2.6	34.2	314	74.38	89.85	3355	3186	0.95	
II-CSCFT2	180 × 180 × 3.62	49.7	348	114 × 3.35	34.0	328	74.38	89.85	3686	3493	0.95	
II-CSCFT4	180 × 180 × 5.4	33.3	338	89 × 2.6	34.2	314	74.38	89.85	3814	3553	0.93	
II-CSCFT5	180 × 180 × 5.4	33.3	338	114 × 3.35	34.0	328	74.38	89.85	4043	3867	0.96	
II-CSCFT6	180 × 180 × 5.4	33.3	338	140 × 3.97	35.3	308	74.38	89.85	4428	4172	0.94	
II-CSCFT7	180 × 180 × 5.4	33.3	338	89 × 3.32	26.8	324	74.38	89.85	3855	3601	0.93	
III-CSCFT1	180 × 180 × 3.62	49.7	348	89 × 2.6	34.2	314	74.38	74.38	3198	3096	0.97	
III-CSCFT2	180 × 180 × 3.62	49.7	348	114 × 3.35	34.0	328	74.38	74.38	3415	3343	0.98	
III-CSCFT3	180 × 180 × 3.62	49.7	348	140 × 3.97	35.3	308	74.38	74.38	4120	3588	0.87	
III-CSCFT4	180 × 180 × 5.4	33.3	338	89 × 2.6	34.2	314	74.38	74.38	4021	3463	0.86	
III-CSCFT5	180 × 180 × 5.4	33.3	338	114 × 3.35	34.0	328	74.38	74.38	4165	3716	0.89	
III-CSCFT6	180 × 180 × 5.4	33.3	338	140 × 3.97	35.3	308	74.38	74.38	4436	3965	0.89	
III-CSCFT7	180 × 180 × 5.4	33.3	338	89 × 3.32	26.8	324	74.38	74.38	3900	3515	0.90	
SDS1-40a	200 × 200 × 2.01	99.5	230	136.5 × 1.94	70.4	492.1	43.44	43.44	2450	2379	0.97	[20]
SDS1-40b	200 × 200 × 2.01	99.5	230	136.5 × 1.94	70.4	492.1	43.44	43.44	2383	2379	1.00	
SDS1-70a	200 × 200 × 2.01	99.5	230	136.5 × 1.94	70.4	492.1	43.44	67.83	2997	2728	0.91	
SDS1-70b	200 × 200 × 2.01	99.5	230	136.5 × 1.94	70.4	492.1	43.44	67.83	2806	2728	0.97	
SDS2-40a	200 × 200 × 2.01	99.5	230	114.6 × 3.93	29.2	377.1	43.44	43.44	2366	2429	1.03	
SDS2-40b	200 × 200 × 2.01	99.5	230	114.6 × 3.93	29.2	377.1	43.44	43.44	2463	2429	0.99	
SDS2-70a	200 × 200 × 2.01	99.5	230	114.6 × 3.93	29.2	377.1	43.44	67.83	2765	2659	0.96	
SDS2-70b	200 × 200 × 2.01	99.5	230	114.6 × 3.93	29.2	377.1	43.44	67.83	2884	2659	0.92	
SDS3-40a	200 × 200 × 2.01	99.5	230	140.1 × 3.78	37.1	322.4	43.44	43.44	2505	2502	1.00	
SDS3-40b	200 × 200 × 2.01	99.5	230	140.1 × 3.78	37.1	322.4	43.44	43.44	2479	2502	1.01	
SDS3-70a	200 × 200 × 2.01	99.5	230	140.1 × 3.78	37.1	322.4	43.44	67.83	3144	2881	0.92	
SDS3-70b	200 × 200 × 2.01	99.5	230	140.1 × 3.78	37.1	322.4	43.44	67.83	3100	2881	0.93	
G1-2	120 × 120 × 2.6	46.2	407.5	58.5 × 1.4	41.8	352.5	29.92	29.92	980	946	0.97	[18]
G1-3	120 × 120 × 2.6	46.2	407.5	74 × 0.9	82.2	680	29.92	29.92	1040	1013	0.97	
G1-4	120 × 120 × 2.6	46.2	407.5	83 × 0.9	92.2	597	29.92	29.92	1080	1019	0.94	
Mean											0.95	
Standard Deviation (SD)											0.04	
Coefficients of Variance (COV)											0.04	

2. Fiber element modeling

2.1. Efficiency of the fiber element technique

Although the commercial finite element software such as ABAQUS and ANSYS can be used to develop 3D models for the nonlinear analysis of CFDST columns, the 3D finite element models are tedious to be built and expensive. As pointed out by Liang [36], many 3D elements must be used to divide the column along its length in the finite element modeling so that the model contains many degrees of freedom. The interactions between the concrete and steel tubes are simulated using contact elements. In addition to the development time of the 3D model for each CFDST column, its computational cost is very high compared to the fiber element model that does not require the discretization of the column along its length. The finite element model of Specimen I-CSCFT4 given in Table 1 was developed using ABAQUS and is shown in Fig. 2. The time for creating the 3D finite element model was 13 min while its computational time was 31 min. The mesh of the fiber element model is presented in Fig. 3. The user does not need to create the fiber element model for each CFDST column but needs to input the data of the column. The data input time for Specimen I-CSCFT4 was 15 s while the computational time of the fiber element model was 10 s. The total time for creating and analyzing the finite element model was 2640 s while the total time for creating and analyzing the fiber element model

was only 25 s. This demonstrates that the fiber element technique significantly saves the development and computational time of the composite column model compared to the finite element method. The verification of the fiber element model is given in Section 3.

2.2. Section discretization and stress calculation

The numerical model is formulated based on the fiber element method in this paper. In the fiber analysis, the cross-section of a CFDST column is discretized into small fibers which represent either the steel or concrete [34,37]. The stress of each fiber is computed using the material uniaxial stress-strain constitutive laws for steel or concrete and integrated over the area of the entire cross-section to compute the stress resultants such as the axial load and moment. Fig. 3 shows the typical fiber mesh of the column cross-section. In the computer program, the outer steel tube thickness is divided into layers as specified by the user and the steel tube wall is automatically discretized along the width on the basis of the layer size [34]. The fiber discretization of the sandwiched concrete is undertaken using a mesh generation algorithm proposed by Persson and Strang [38]. The algorithm was derived based on simple mechanical analogy where the nodal locations are solved for equilibrium in 2-D truss structures using the linear force-displacement relationship and reset the topology by the Delaunay algorithm [38]. A non-uniform desire edge length function results in finer resolution for

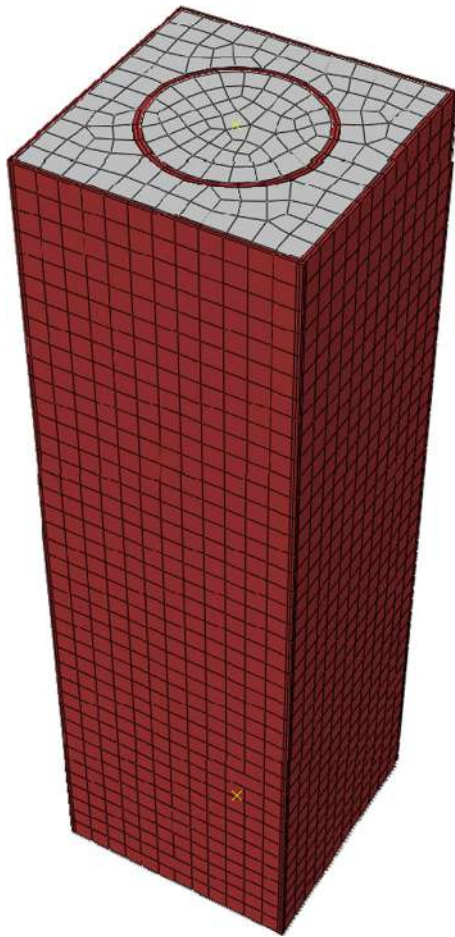


Fig. 2. Finite element model of CFST column.

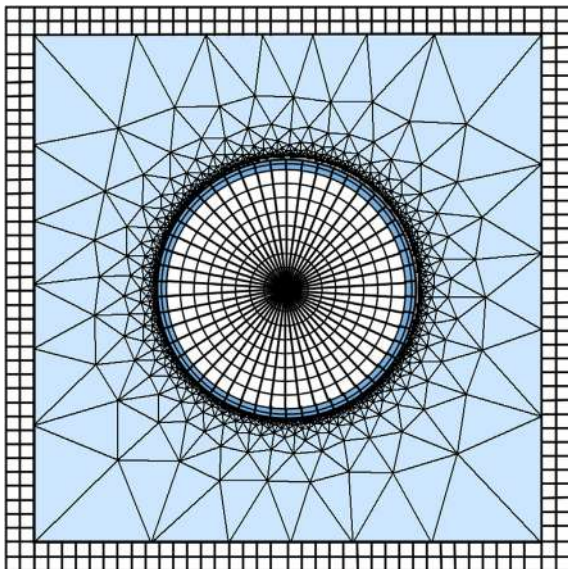


Fig. 3. Typical fiber mesh in CFST column section with inner circular steel tube.

the fibers close to the circle as shown in Fig. 3. The discretization of the inner circular tube and concrete core is similar to the conventional CFST column [39].

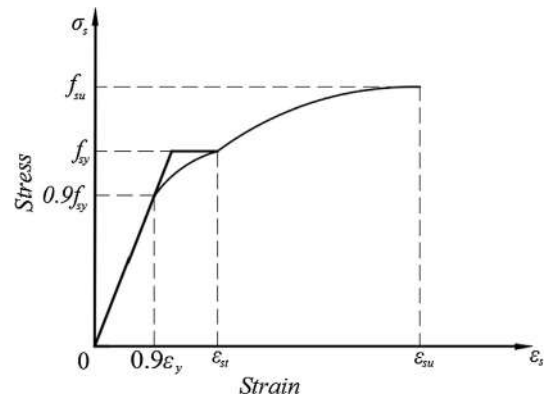


Fig. 4. Stress-strain curve for structural steel.

2.3. Constitutive laws of steels

The stress-strain constitutive laws for structural steels employed in the fiber model are shown in Fig. 4. The idealized stress-strain model for structural steels suggested by Liang [34] is adopted for strain up to the onset of strain-hardening. Beyond this point, the expression given by Mander [40] is used to model the strain hardening behavior. A reduction in the yield stress due to the biaxial stresses on the steel tubes of CFST columns under compression is considered in the stress-strain model. The stress within the strain range of $0.9\epsilon_{sy} < \epsilon_s \leq \epsilon_{st}$ is determined by the following equation derived by Liang [34]:

$$\sigma_s = f_{sy} \left(\frac{\epsilon_s - 0.9\epsilon_{sy}}{\epsilon_{st} - 0.9\epsilon_{sy}} \right)^{\frac{1}{45}} \quad (1)$$

in which σ_s represents the longitudinal steel stress and ϵ_s is the corresponding strain; f_{sy} and ϵ_{sy} denote the yield strength and strain respectively; and ϵ_{st} stands for the strain at the onset of strain hardening which is specified as 0.005 in the nonlinear analysis.

The stress within the strain range of $\epsilon_{st} < \epsilon_s \leq \epsilon_{su}$ is calculated using the expressions developed by Mander [40] as follows:

$$\sigma_s = f_{su} - \left(\frac{\epsilon_{su} - \epsilon_s}{\epsilon_{su} - \epsilon_{st}} \right)^n (f_{su} - f_{sy}) \quad (2)$$

$$n = E_{st} \left(\frac{\epsilon_{su} - \epsilon_{st}}{f_{su} - f_{sy}} \right) \quad (3)$$

where ϵ_{su} is the ultimate strain taken as 0.2, E_{st} is the modulus at the onset of strain hardening taken as $0.02E_s$, and f_{su} denotes the tensile strength of steel.

2.4. Initial local buckling of the external steel tube

The rectangular CFST column made of an outer non-compact or slender steel section is susceptible to local buckling. When the applied axial load attains the initial local buckling stress of the steel plate, the plate undergoes local buckling. Liang et al. [33] derived expressions for computing the initial local-buckling strength of clamped steel plates as part of the CFST column based on the finite element analysis results. Local geometric imperfection and residual stresses of steel plates resulted from the induction of heating and welding during the production were considered in the formulation of these equations. The equation given by Liang et al. [33] is used to estimate the initial local buckling stress of the outer steel tube wall subjected to uniform edge compressive stresses, and is written as

$$\frac{\sigma_{cr}}{f_{syo}} = 0.5507 + 0.005132 \left(\frac{b}{t_o} \right) - 9.869 \times 10^{-5} \left(\frac{b}{t_o} \right)^2 + 1.198 \times 10^{-7} \left(\frac{b}{t_o} \right)^3 \quad (4)$$

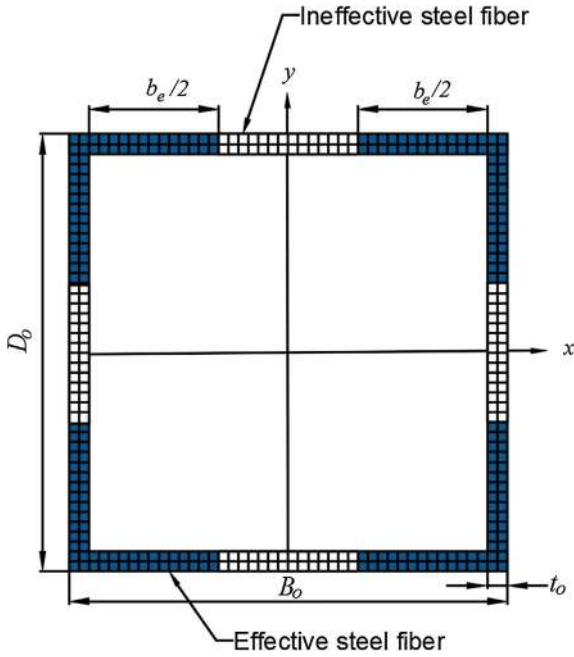


Fig. 5. Effective width of the outer rectangular steel tube.

where σ_{cr} and f_{syo} are the initial local buckling stress and yield strength of the outer steel tube wall with imperfections respectively, and t_o is the thickness of the outer steel tube.

2.5. Post-local buckling of the outer steel tube

After the onset of initial local buckling, the progressive post-local buckling behavior of steel plate under increasing applied load can be described by the method of stress redistribution. The stresses are redistributed to the unloaded edge strips from the central area of the steel plate which heavily buckles and carries lower stresses compared to the edge strips. The post-local buckling strength of the steel plate can be calculated using the effective width illustrated in Fig. 5. The following effective width formula derived by Liang et al. [33] for the steel tube walls of CFST columns subjected to uniform compression is adopted in the present study:

$$\frac{b_e}{b} = 0.5554 + 0.02038 \left(\frac{b}{t_o}\right) - 3.944 \times 10^{-4} \left(\frac{b}{t_o}\right)^2 + 1.921 \times 10^{-6} \left(\frac{b}{t_o}\right)^3 \quad (5)$$

where b and b_e are the clear width and the effective width of the steel tube wall, respectively. At the ultimate strength state, the maximum ineffective width $b_{ne,max}$ of the steel tube wall is computed by

$$b_{ne,max} = b - b_e \quad (6)$$

The ineffective width b_{ne} can be calculated by linear interpolation depending on the stress level of the steel fiber using the following expression [32]:

$$b_{ne} = \left(\frac{\sigma_s - \sigma_{cr}}{f_{syo} - \sigma_{cr}} \right) b_{ne,max} \quad (7)$$

In the computation, the steel fiber stresses are firstly calculated by the stress-strain laws and are checked against the criterial local buckling stress for possible local buckling. For steel tube walls having a b/t_o ratio greater than 30, if $\sigma_s > \sigma_{cr}$, the ineffective width of the steel plate is computed and the fiber stresses within this area are assigned to zero until the maximum $b_{ne,max}$ is attained.

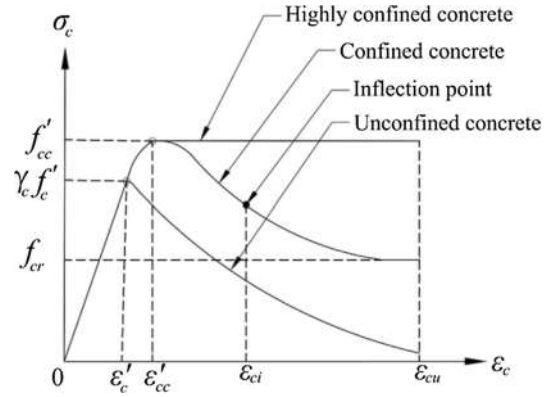


Fig. 6. Stress-strain curves for confined concrete in rectangular CFDST column.

2.6. Constitutive laws of concrete

Confinement models have been proposed for determining the compressive strength of concrete in CFST columns [4,15,39,41–43]. For rectangular CFDST columns with inner circular tube, it is assumed that the outer rectangular steel tube does not induce confinement to the core concrete as well as the sandwiched concrete and the internal circular steel tube offers confinement to the core concrete. Therefore, the stress-strain model given by Liang [34] for concrete in rectangular CFST columns can be applied to the sandwiched concrete while the stress-strain model provided by Liang and Fragomeni [39] for concrete in circular CFST columns can be used for the core concrete in the inner steel tube in CFDST columns. The idealized stress-strain laws of concrete in a rectangular CFDST column presented in Fig. 6 are adopted in the present model. The stress-strain model consists of two Parts: (1) the ascending part and (2) the descending parabolic part. The stress-strain relationships suggested by Liang [34] are used to simulate the ascending branch while the descending branch is described by the equations proposed by Lim and Ozbakkaloglu [44]. The compressive strength of confined concrete (f'_{cc}) and its corresponding strain (ϵ'_{cc}) are calculated by the equations provided by Lim and Ozbakkaloglu [44]. However, the lateral confining pressure model proposed by Liang and Fragomeni [39] is adopted to determine the lateral pressures on the core concrete as it has been well established and verified by experimental data. Moreover, the post-peak behavior of the concrete is modeled by the residual strength and the concrete degradation factor β_c proposed in the present study based on experimental results on CFDST columns.

The ascending branch of the stress-strain curve is defined by the following formula presented by Mander et al. [45]:

$$\sigma_c = \frac{f'_{cc} (\epsilon_c / \epsilon'_{cc})^\lambda}{(\epsilon_c / \epsilon'_{cc})^\lambda + \lambda - 1} \quad (0 \leq \epsilon_c \leq \epsilon'_{cc}) \quad (8)$$

in which σ_c stands for the longitudinal concrete stress, ϵ_c is the corresponding strain and λ is calculated as

$$\lambda = \frac{E_c \epsilon'_{cc}}{E_c \epsilon'_{cc} - f'_{cc}} \quad (9)$$

where E_c represents the Young's modulus of concrete. The original equation for E_c proposed by Lim and Ozbakkaloglu [44] is modified to consider the effect of column size using the factor γ_c as

$$E_c = 4400 \sqrt{\gamma_c f'_c} \text{ (MPa)} \quad (10)$$

where f'_c is the compressive strength of the concrete cylinder, and the reduction factor γ_c is computed as $1.85 D_c^{-0.135}$ suggested by Liang [34] and is limited to $0.85 \leq \gamma_c \leq 1.0$. The parameter D_c is the diameter of the circular concrete core and for rectangular sections, it is taken as the larger of $(B_o - 2t_o)$ and $(D_o - 2t_o)$.

The descending parabolic branch of the stress-strain curve is determined by the following expression given by Lim and Ozbakkaloglu [44]

$$\sigma_c = f'_{cc} - \frac{f'_{cc} - f_{cr}}{\left[1 + \left(\frac{\varepsilon_c - \varepsilon'_{cc}}{\varepsilon_{ci} - \varepsilon'_{cc}}\right)^{-2}\right]} \quad (\varepsilon'_{cc} < \varepsilon_c) \quad (11)$$

where f'_{cc} and ε'_{cc} represent the compressive strength and corresponding strain of the confined concrete, respectively. Lim and Ozbakkaloglu [44] proposed expressions to calculate f'_{cc} and ε'_{cc} based on extensive test results. Their expressions are modified here to consider the effect of column size using the factor γ_c as follows:

$$f'_{cc} = \gamma_c f'_c + 5.2(\gamma_c f'_c)^{0.91} \left(\frac{f_{rp}}{\gamma_c f'_c}\right)^a \quad \text{where } a = (\gamma_c f'_c)^{-0.06} \quad (12)$$

$$\varepsilon'_{cc} = \varepsilon'_c + 0.045 \left(\frac{f_{rp}}{\gamma_c f'_c}\right)^{1.15} \quad (13)$$

$$\varepsilon'_c = \frac{(\gamma_c f'_c)^{0.225}}{1000} \quad (14)$$

in which f_{rp} denotes the lateral pressure applied by the steel tube on the concrete.

The lateral pressure f_{rp} on the sandwiched concrete between the two steel tubes is zero so that its compressive strength is determined as $f'_{cc} = \gamma_c f'_c$. For the core concrete in a CFDST column, the lateral confining pressure is calculated using the confinement model developed by Liang and Fragomeni [39] for concrete in circular CFST columns, which is expressed by

$$f_{rpi} = \begin{cases} 0.7(v_e - v_s) \frac{2t_i}{D_i - 2t_i} f_{syi} & \text{for } \frac{D_i}{t_i} \leq 47 \\ \left(0.006241 - 0.0000357 \frac{D_i}{t_i}\right) f_{syi} & \text{for } 47 < \frac{D_i}{t_i} \leq 150 \end{cases} \quad (15)$$

where D_i and t_i represent the diameter and thickness of the inner circular tube, respectively; v_e and v_s are the Poisson's ratios of the steel tube with and without concrete infill, respectively. In the fiber model, the Poisson's ratio $v_s = 0.5$ is used and v_e is provided by Tang et al. [46] as

$$v_e = 0.2312 + 0.3582v'_e - 0.1524 \left(\frac{\gamma_c f'_c}{f_{syi}}\right) + 4.843v'_e \left(\frac{\gamma_c f'_c}{f_{syi}}\right) - 9.169 \left(\frac{\gamma_c f'_c}{f_{syi}}\right)^2 \quad (16)$$

$$v'_e = 0.881 \times 10^{-6} \left(\frac{D_i}{t_i}\right)^3 - 2.58 \times 10^{-4} \left(\frac{D_i}{t_i}\right)^2 + 1.953 \times 10^{-2} \left(\frac{D_i}{t_i}\right) + 0.4011 \quad (17)$$

In the stress-strain curve shown in Fig. 6, f_{cr} is the residual concrete strength. The expression proposed by Lim and Ozbakkaloglu [44] is utilized to calculate the residual strength of the core concrete within the inner circular steel tube, which is written as

$$f_{cr} = \begin{cases} f'_{cc} & \text{for } \frac{D_i}{t_i} \leq 40 \\ 1.6f'_{cc} \left(\frac{f_{rp}^{0.24}}{\gamma_c f'_c{}^{0.32}}\right) \text{ and } f_{cr} \leq f'_{cc} & \\ -0.15(\gamma_c f'_c) & \text{for } 40 < \frac{D_i}{t_i} \leq 150 \end{cases} \quad (18)$$

The residual concrete strength of the sandwiched concrete can be calculated as $f_{cr} = \beta_c f'_c$, where β_c is the concrete strength degradation factor, which is related to the width-to-thickness ratio (B_s/t_o) of CFDST columns, where B_s is taken as the larger of B_o and D_o of the outer steel tube. Previous research on rectangular CFST columns with $B_s/t_o \leq 24$ is found to be less susceptible to local buckling and recommended β_c value as 1.0 [34]. Based on the previous study on rectangular CFST columns

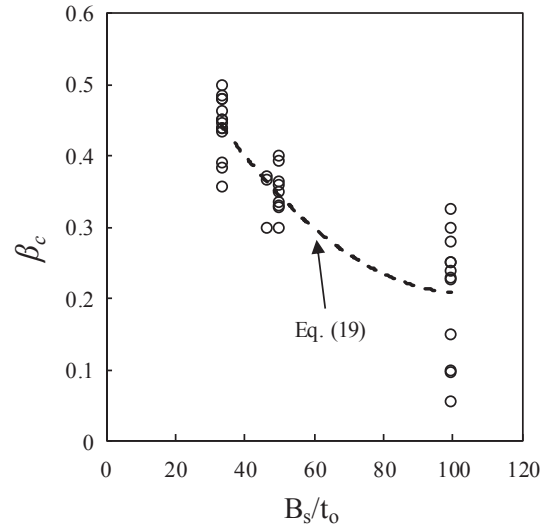


Fig. 7. Verification of the proposed expression for β_c .

[34] and by interpreting the test results of CFDST short columns as shown in Fig. 7, the factor β_c for CFDST columns with $B_s/t_o > 24$ is proposed as

$$\beta_c = \begin{cases} 1 - \frac{(B_s/t_o - 24)}{15} & \text{for } 24 < \frac{B_s}{t_o} \leq 33 \\ 0.000062 \left(\frac{B_s}{t_o}\right)^2 - 0.011225 \left(\frac{B_s}{t_o}\right) + 0.705288 & \text{for } 33 < \frac{B_s}{t_o} \leq 100 \end{cases} \quad (19)$$

In Eq. (11), ε_{ci} is the strain corresponding to the inflection point that determines the shape of the descending curve. For the sandwiched concrete, ε_{ci} is taken as 0.007. For the core concrete, the expression developed by Lim and Ozbakkaloglu [44] and modified using the factor γ_c is used to calculate ε_{ci} as follows:

$$\varepsilon_{ci} = 2.8\varepsilon'_{cc} \left(\frac{f_{cr}}{f'_{cc}}\right) (\gamma_c f'_c)^{-0.12} + 10\varepsilon'_{cc} \left(1 - \frac{f_{cr}}{f'_{cc}}\right) (\gamma_c f'_c)^{-0.47} \quad (20)$$

2.7. Ductility index

The ductility index measures the ductility of a CFDST column and is defined as

$$PI_{sd} = \frac{\varepsilon_u}{\varepsilon_y} \quad (21)$$

where ε_u denotes the axial strain when the axial load drops to 90% of its ultimate load in the post-peak regime or the ultimate strain in the case where column shows ascending stress-strain curve followed by reaching the yielding point. The yield strain (ε_y) is taken as $\varepsilon_{0.75}/0.75$, where $\varepsilon_{0.75}$ stands for the corresponding strain when axial load obtains 75% of its ultimate load.

3. Comparisons of computations with experimental results

The numerical model is validated by comparisons of the predicted ultimate loads and load-strain responses of axially loaded rectangular CFDST short columns with corresponding test data provided by Qian et al. [19], Wang et al. [20] and Pei [18]. The test data of the specimens is given in Table 1. In the numerical analysis, the compressive strength of concrete cylinder f'_c was taken as 85% of the concrete cube strength as suggested by Oehlers and Bradford [47]. In the analysis of the Specimens tested by Wang et al. [20], the local buckling of the outer tube was considered by ignoring the effect of the stiffeners, but the areas of the stiffeners were included. Table 1 shows the computed ultimate axial

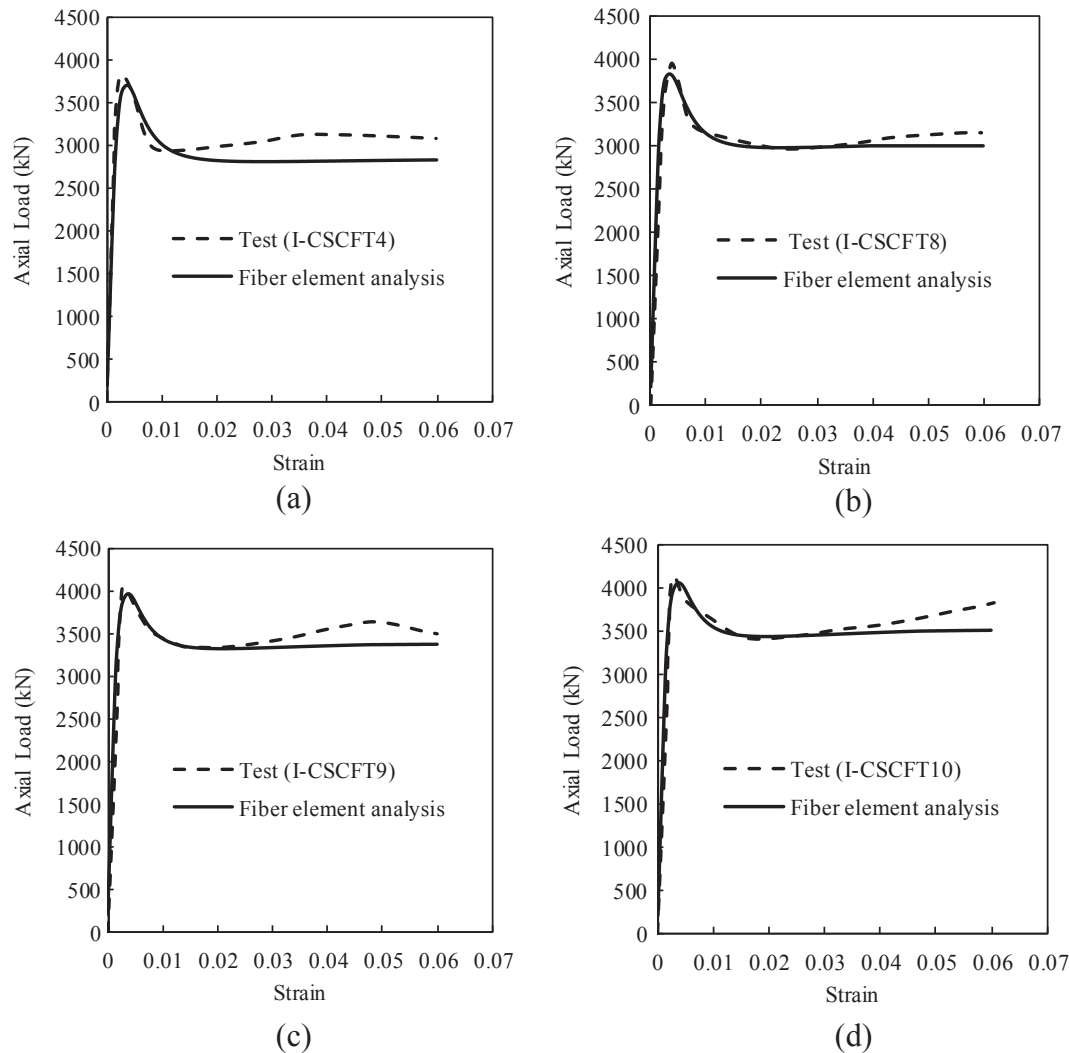


Fig. 8. Comparison of predicted and experimental axial load-strain curves of CFST short columns tested by Qian et al. [19].

strengths ($P_{u,num}$) and experimentally measured strengths ($P_{u,exp}$) of CFST columns. It appears that the fiber-based technique captures well the ultimate loads of axially loaded rectangular CFST short columns. The mean of $P_{u,num}/P_{u,exp}$ is 0.95 with the corresponding standard deviation of 0.04. However, the predicted ultimate axial loads of Specimens III-CSCFT3 to III-CSCFT7 are below or equal to 90% of the experimental results. This is likely caused by the uncertainty of the actual strength of concrete in these specimens. The model is further validated by comparing the measured axial load-strain responses of square CFST short columns with computer solutions in Figs. 8–10. Good agreement between the experimental and predicted responses is obtained. The computed initial stiffness of the columns is in excellent agreement with the measured one. Furthermore, the comparison shows that the proposed fiber-based model predicts the column residual strengths with reasonable accuracy.

4. Parametric study

The performance of rectangular CFST columns with inner circular tube is influenced by both material and geometric properties of the columns. The numerical model proposed was used to examine the influences of key design available on the performance of CFST columns. The material and geometric properties of CFST columns considered are listed in Table 2. The corresponding tensile strengths of steel tubes with the yield stresses of 250, 350, 450 and 520 MPa were taken as 320,

430, 520 and 620 MPa, respectively. The Young's modulus of 200 GPa was used for all steel tubes.

4.1. Effects of inner circular tube

The influences of inner circular tube on the ultimate axial capacity and post-peak behavior of CFST columns were investigated by the fiber-based model. The fiber element analyses of CFST Column C2 and the reference CFST Column C1 given in Table 2 were performed. The two columns had the same cross-section and the same cross-sectional steel area. Fig. 11 illustrates that the ultimate load-carrying capacity of the Column C2 is increased by 10.43% due to the internal circular steel tube compared with that of Column C1. In addition, the circular internal steel tube increases the residual strength of the Column C2 by 32% in comparison with that of Column C1 without an inner steel tube. Moreover, the ductility index increases from 1.75 to 2.23 by strengthening the CFST column (C1) with an inner circular tube. As depicted in Fig. 11, the addition of an inner circular steel tube to the CFST column does not have a notable influence on the column initial stiffness.

The effects of diameter and thickness of the inner circular steel tube on the behavior of CFST short columns were investigated by the fiber modeling technique. Fiber analyses on Columns C2–C5 in Table 2 with diameters ranging from 150 to 300 mm were conducted. The computed axial load-strain responses of the columns are presented in Fig. 12. It is seen that increasing the diameter of the inner steel tube considerably

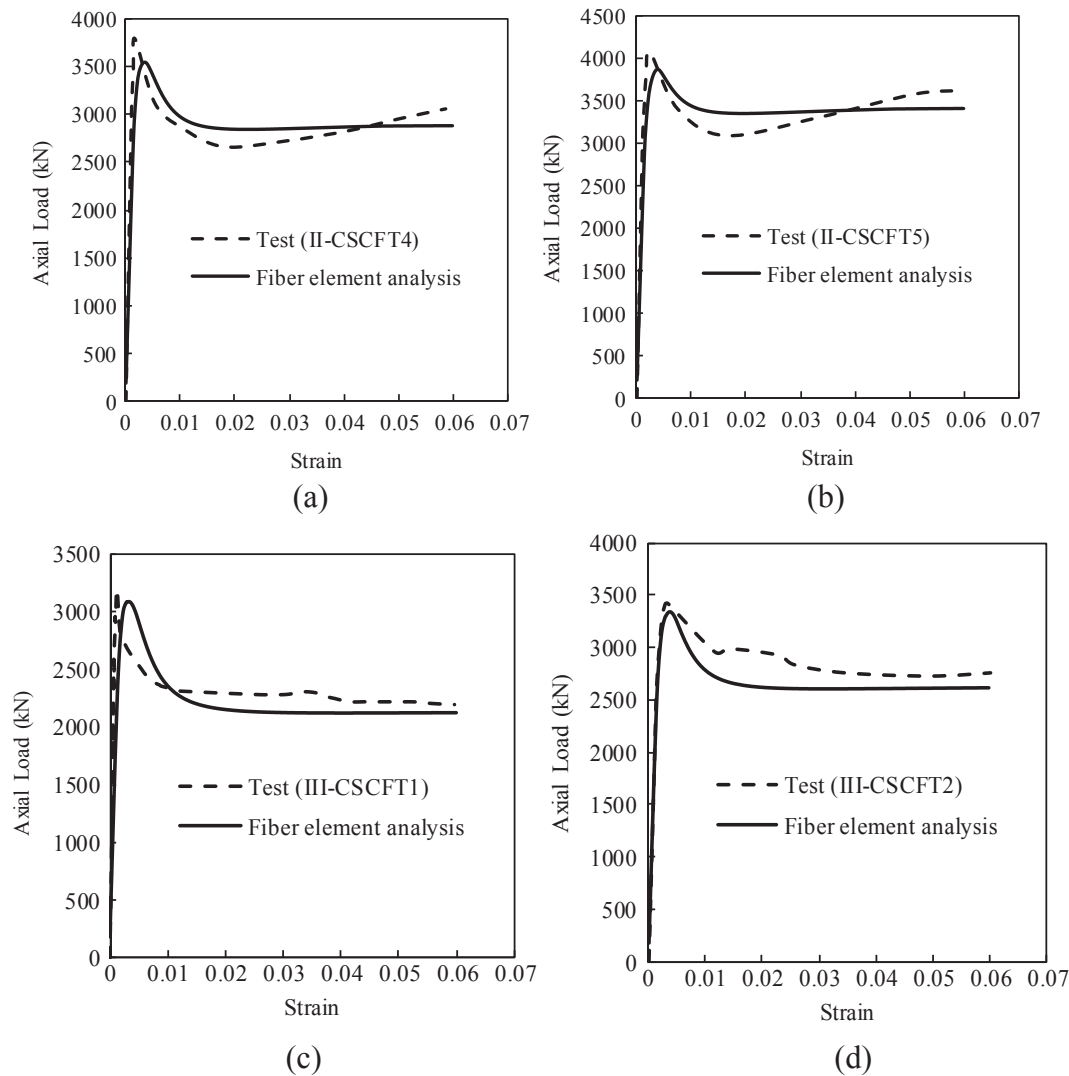


Fig. 9. Comparison of predicted and experimental axial load-strain curves of CFDST columns tested by Qian et al. [19].

increases the ultimate axial loads of CFDST short columns. The column ultimate load is found to increase by 15.2% by increasing the diameter of the inner steel tube from 150 mm to 300 mm. It is noted that the larger of the diameter of the inner steel tube, the larger of the cross-sectional steel area, concrete area confined by the circular steel tube and thus the higher of the column ultimate axial strength. Columns C2 and C6-C8 presented in Table 2 had thickness of the inner steel tube varied from 6.0 to 15.0 mm. Fig. 13 demonstrates the effects of the thickness of the inner steel tube on the behavior of CFDST columns. It appears that the column ultimate axial strength is markedly increased by increasing the thickness of the inner steel tube. When the thickness of the inner steel tube increases from 6.0 to 7.5, 10 and 15 mm, the increase in the column ultimate axial load is 6.0%, 9.8% and 16.5%, respectively. This is attributed to the increase in the steel area and the confinement to the core concrete.

4.2. Effects of local buckling

Column C9 in Table 2 was analyzed to determine the influences of local buckling on the axial load-strain performance of short CFDST columns. The D_o/t_o ratio of the column was 99.5, which was so large that the local buckling of the external square steel tube under compression occurred. Fiber analyses on the column were undertaken by taking into consideration the local buckling of the external steel tube

and ignoring its effect, respectively. Fig. 14 demonstrates that local buckling reduces the column ultimate axial load. When local buckling is not considered, the ultimate load of the CFDST short column is over-estimated by 7.9%. Fig. 14 shows that the residual strength of the CFDST short column is also overestimated by ignoring local buckling effects.

4.3. Effects of concrete strength

To investigate the influences of concrete strengths on the performance of CFDST short column, the Columns C10-C21 filled with concrete with various compressive strengths in Table 2 were analyzed by using the fiber modeling technique. The only variable considered was the concrete compressive strength. Three cases were considered: (1) the strength of the sandwiched and core concrete was the same; (2) the core concrete strength was varied; and (3) the strength of the sandwiched concrete was varied. For the first case, the concrete strength was increased from 35 MPa to 50, 70 and 90 MPa. The axial load capacity of the square CFDST columns increases with increasing the concrete strength as illustrated in Fig. 15. However, the ductility of the columns decreases with increasing the concrete strength. Changing the concrete strength from 35 MPa to 90 MPa results in a decrease in the ductility index from 4.5 to 2.85 as shown in Fig. 16. For the second case, the concrete strength of the sandwiched concrete was 50 MPa while the

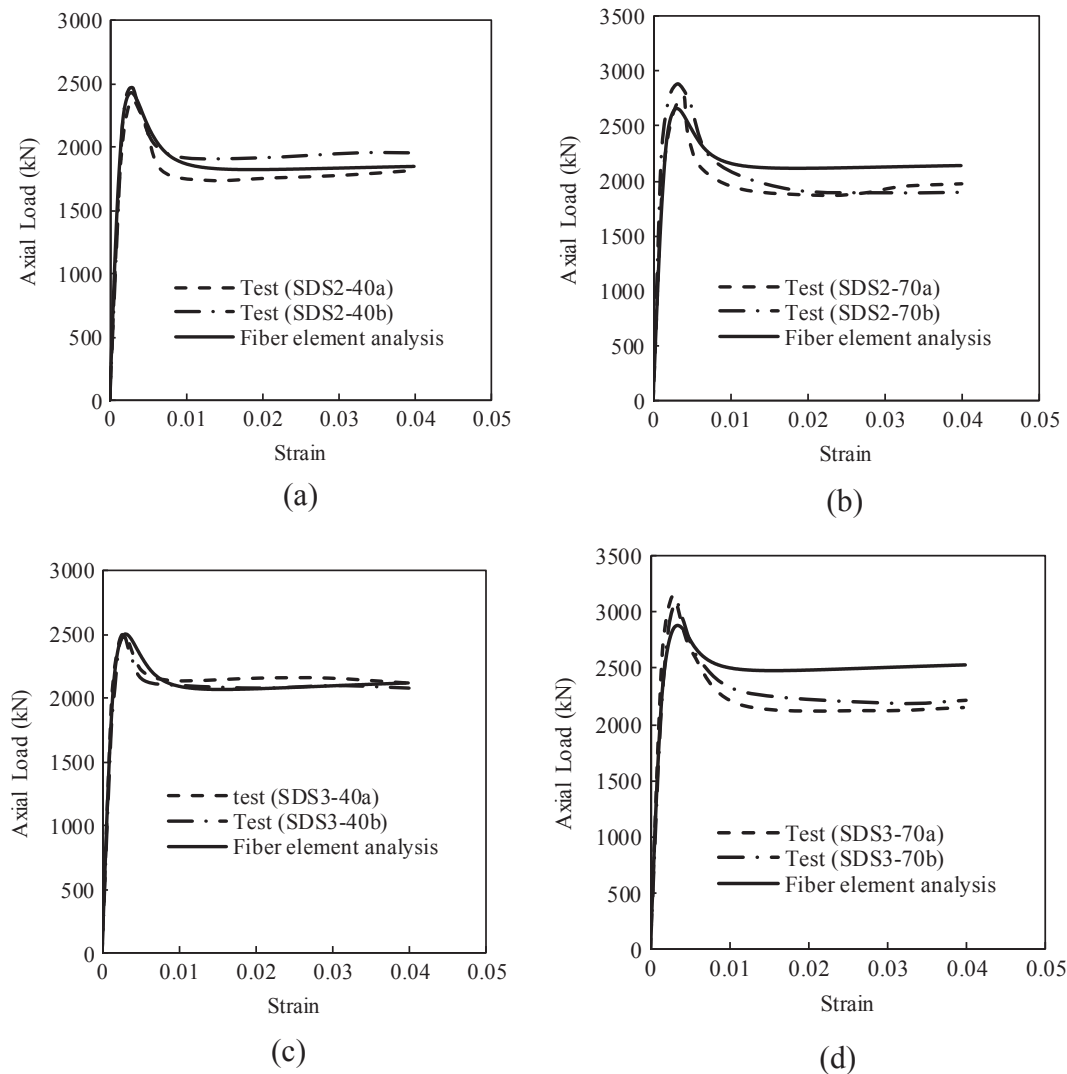


Fig. 10. Comparison of predicted and experimental axial load-strain curves of CFDST columns tested by Wang et al. [20].

strength of the core concrete was increased from 35 MPa to 50, 70 and 90 MPa. The computed axial load-strain relationships of short columns as a function of concrete strength are presented in Fig. 17. The column ultimate axial load is not significantly affected by the core concrete strength. For the third case, the strength of the core concrete was 50 MPa while the strength of the sandwiched concrete was increased from 35 MPa to 50, 70 and 90 MPa. As shown in Fig. 18, the column ultimate strength is increased significantly by increasing the strength of the sandwiched concrete. The column made of concrete with 90 MPa has a ductility index of 2.81 while it is 4.75 for the column with 35 MPa sandwiched concrete.

4.4. Effects of steel yield strength

The computational model was used to study the influences of the yield strength of the steel tubes on the performance of CFDST columns. Two groups of short columns were investigated for this purpose. In the first case, the yield strength (f_{syo}) of the outer steel tubes of Columns C22-C25 in Table 2 was varied while the yield stress of the internal tube f_{syt} was fixed to 350 MPa. In the second case, the yield strength of the internal steel tubes of Columns C26-C29 in Table 2 was changed while the yield stress of the outer tubes was 350 MPa. The predicted load-strain curves of these columns are presented in Figs. 19 and 20. It is observed that the column ultimate axial strength is increased

considerably by increasing the yield stresses of either the outer or the inner steel tube. When the steel yield stress of the inner steel tube is changed from 250 MPa to 350, 450 and 520 MPa, the column ultimate axial load increases by 5.7%, 10.2% and 13.1%, respectively. On the contrary, by increasing f_{syo} from 250 MPa to 350, 450 and 520 MPa, the ultimate load of CFDST columns increases by 6.05%, 11.4% and 14.8%, respectively.

4.5. Effects of B_o/D_o ratio

The width-to-depth ratio (B_o/D_o) influences the performance of CFDST columns. Columns C30-C33 in Table 2 had different B_o/D_o ratios but had an identical inner tube. When the B_o/D_o ratio is increased from 0.5 to 0.75, 1.25 and 1.5, the column ultimate strength increases by 25.5%, 49.8% and 56.8%, respectively. This is due to the fact that the area of the sandwiched concrete is increased by increasing the B_o/D_o ratio and the sandwiched concrete carries most of the load. The load-strain curves of Columns C30-C33 are presented in Fig. 21. It is demonstrated that the larger the B_o/D_o ratio, the poorer the ductility. The residual strength of Column C32 with B_o/D_o ratio of 1.25 is only about 48.3% of the column ultimate strength.

Table 2
Geometric and material properties of CFDST short columns used in the parameter study.

Column	Outer tube			Inner tube			Concrete	
	$B_o \times D_o \times t_o$ (mm)	D_o/t_o	f_{sy0} (MPa)	$D_i \times t_i$ (mm)	D_i/t_i	f_{syi} (MPa)	f'_{co} (MPa)	f'_{ci} (MPa)
C1	450 × 450 × 12.8	35.2	350	–	–	–	–	70
C2	450 × 450 × 7.5	60	350	300 × 10	30	350	70	70
C3	450 × 450 × 7.5	60	350	150 × 10	15	350	70	70
C4	450 × 450 × 7.5	60	350	200 × 10	20	350	70	70
C5	450 × 450 × 7.5	60	350	250 × 10	25	350	70	70
C6	450 × 450 × 7.5	60	350	300 × 6.0	50	350	70	70
C7	450 × 450 × 7.5	60	350	300 × 7.5	40	350	70	70
C8	450 × 450 × 7.5	60	350	300 × 15	20	350	70	70
C9	200 × 200 × 2.01	99.5	492	136.5 × 1.94	70.4	492	35	35
C10	650 × 650 × 10	65	350	350 × 10	35	350	35	35
C11	650 × 650 × 10	65	350	350 × 10	35	350	50	50
C12	650 × 650 × 10	65	350	350 × 10	35	350	70	70
C13	650 × 650 × 10	65	350	350 × 10	35	350	90	90
C14	650 × 650 × 10	65	350	350 × 10	35	350	50	35
C15	650 × 650 × 10	65	350	350 × 10	35	350	50	50
C16	650 × 650 × 10	65	350	350 × 10	35	350	50	70
C17	650 × 650 × 10	65	350	350 × 10	35	350	50	90
C18	650 × 650 × 10	65	350	350 × 10	35	350	35	50
C19	650 × 650 × 10	65	350	350 × 10	35	350	50	50
C20	650 × 650 × 10	65	350	350 × 10	35	350	70	50
C21	650 × 650 × 10	65	350	350 × 10	35	350	90	50
C22	450 × 450 × 7.5	60	250	300 × 10	30	350	70	70
C23	450 × 450 × 7.5	60	350	300 × 10	30	350	70	70
C24	450 × 450 × 7.5	60	450	300 × 10	30	350	70	70
C25	450 × 450 × 7.5	60	520	300 × 10	30	350	70	70
C26	450 × 450 × 7.5	60	350	300 × 10	30	250	70	70
C27	450 × 450 × 7.5	60	350	300 × 10	30	350	70	70
C28	450 × 450 × 7.5	60	350	300 × 10	30	450	70	70
C29	450 × 450 × 7.5	60	350	300 × 10	30	520	70	70
C30	400 × 800 × 12	66.67	450	350 × 10	35	450	90	90
C31	600 × 800 × 12	66.67	450	350 × 10	35	450	90	90
C32	1000 × 800 × 12	66.67	450	350 × 10	35	450	90	90
C33	1200 × 800 × 12	66.67	450	350 × 10	35	450	90	90

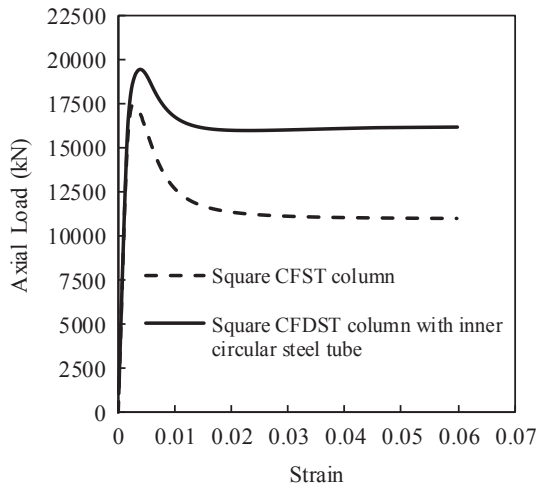


Fig. 11. Effects of the inner steel tube on the axial load-strain responses of CFDST short column.

5. Proposed design model

In this study, a simple design formula was developed for computing the ultimate axial strength of rectangular CFDST short columns as follows:

$$P_{u,des} = f_{sy0}A_{soe} + \gamma_{si}f_{syi}A_{si} + \gamma_{sc}f'_{co}A_{sc} + \gamma_{cc}f'_{cc}A_{cc} \quad (22)$$

where A_{soe} denotes the effective area of the external steel tube considering local buckling effects; A_{si} , A_{sc} and A_{cc} represent the areas of internal steel tube, sandwiched concrete and core concrete,

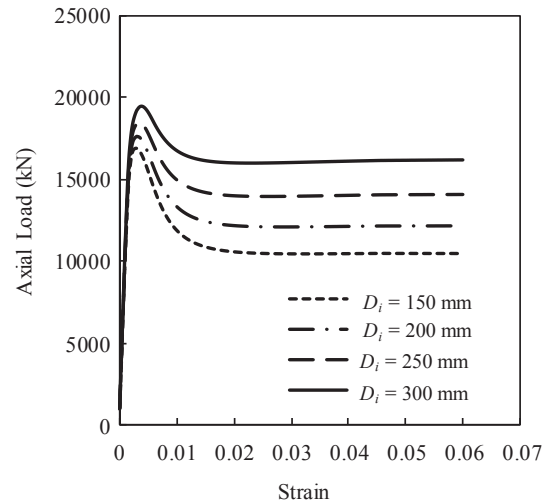


Fig. 12. Effects of the diameter of the inner steel tube on the axial load-strain responses of CFDST short columns.

respectively; f'_{co} is the compressive cylinder strength of the sandwiched concrete; γ_{sc} and γ_{cc} represent the γ_c for the sandwiched concrete and core concrete, respectively; γ_{si} is the strength factor considering the effects of geometric imperfection, strain-hardening and hoop-tension on the inner tube and proposed by Liang and Fragomeni [39] as

$$\gamma_{si} = 1.458 \left(\frac{D_i}{t_i} \right)^{-0.1} \quad (0.9 \leq \gamma_{si} \leq 1.1) \quad (23)$$

To validate the design model proposed, the ultimate strengths of the

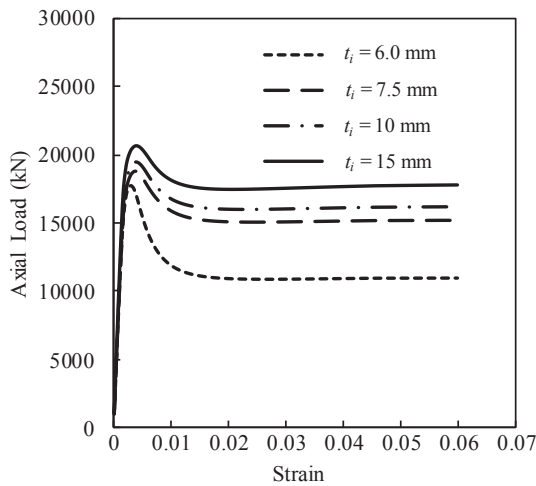


Fig. 13. Effects of the thickness of the inner steel tube on the axial load-strain responses of CFDST short columns.

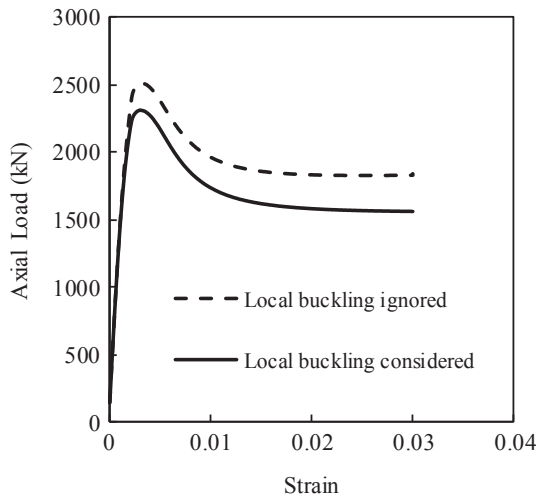


Fig. 14. Effects of local buckling of the outer steel tube on the axial load-strain responses of CFDST short columns.

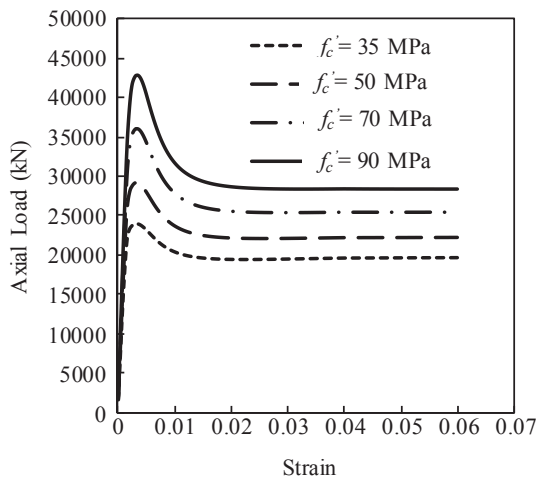


Fig. 15. Effects of concrete compressive strength on the axial load-strain responses of CFDST short columns.

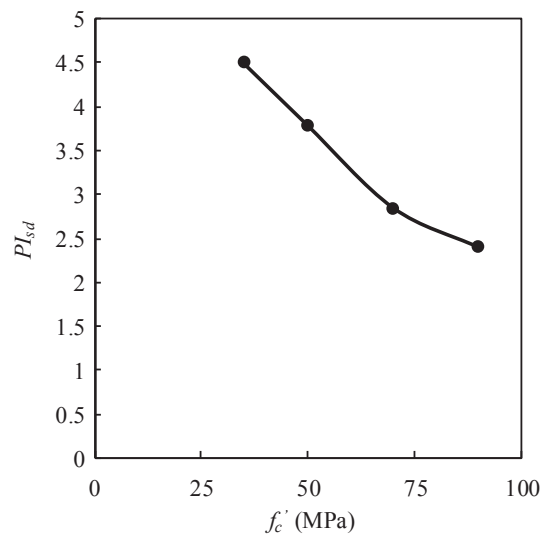


Fig. 16. Strain ductility indices of CFDST short columns with various concrete strengths.

tested columns presented in Table 1 were calculated using Eq. (22) and are compared with the experimental ultimate strengths in Table 3 and Fig. 22. The design model can predict average 97% of the experimental ultimate loads of the short columns. The standard deviation and coefficient of variation of the $P_{u,des}/P_{u,exp}$ ratios are analyzed as 0.05.

The design model was used to investigate the effects of the diameter and thickness of the inner steel tube on the ultimate axial strengths of CFDST short columns. For this purpose, the ultimate axial loads of Columns C2-C8 where the inner steel tubes had various diameters and thicknesses as given in Table 2 were calculated using Eq. (22) and are compared with those predicted by the fiber element modeling technique in Table 4. It can be observed from Table 4 that increasing either the diameter or the thickness of the inner steel tube markedly increases the ultimate axial strengths of CFDST short columns. Excellent agreement between the design calculations and numerical predictions is obtained. The mean $P_{u,des}/P_{u,num}$ of these columns is calculated as 0.98 with a coefficient variance of 0.02. The comparative studies demonstrate that the proposed simple design equation is capable of accurately computing the ultimate axial load of CFDST short columns under axial compression and can be used in the design of such composite columns in practice.

6. Comparisons with design codes

The experimental ultimate strengths of rectangular CFDST columns presented in Table 1 are further compared with the ultimate loads computed by the design methods provided in Eurocode 4 [5], ACI 318-11 [6], AISC 360-16 [7] and Japanese building code AIJ [8] given in Table 5. However, the current design codes do not cover the design of CFDST columns. Table 3 summarizes the code predictions and experimental ultimate load-carrying capacities. It is shown that the ACI 318-11 [6] and AISC 360-16 [7] design codes underestimate the column ultimate strengths remarkably due to neglecting the confinement to the core concrete provided by the inner circular tube. Eurocode 4 [5] and Japanese building code AIJ [8], which account for the confinement effects on the core concrete, generally overestimate the ultimate load-carrying capacities of CFDST short columns because these codes do not consider the local buckling effects of the outer square steel tube. The mean predicted-to-experimental ultimate strength by Eurocode 4 [5] and AIJ [8] was 1.06 and 1.01, respectively. The proposed design formula represented by Eq. (22) considers the local buckling of the outer steel tube and the confinement in the core concrete. It is seen that the design equation developed in the present study yields the best

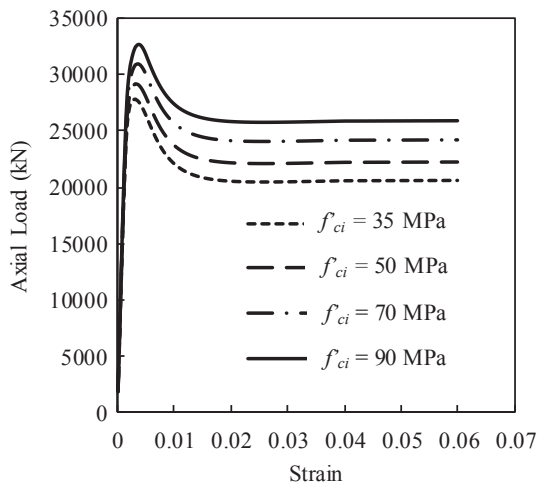


Fig. 17. Effects of core concrete compressive strength on the axial load-strain response of CFDST columns.

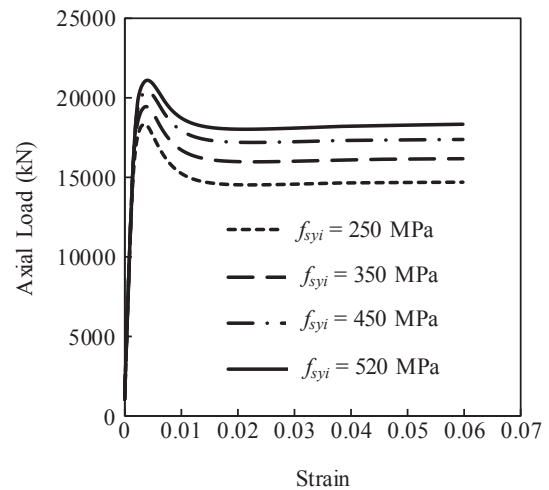


Fig. 20. Effects of the yield strength of the inner steel tube on the axial load-strain responses of CFDST short columns.

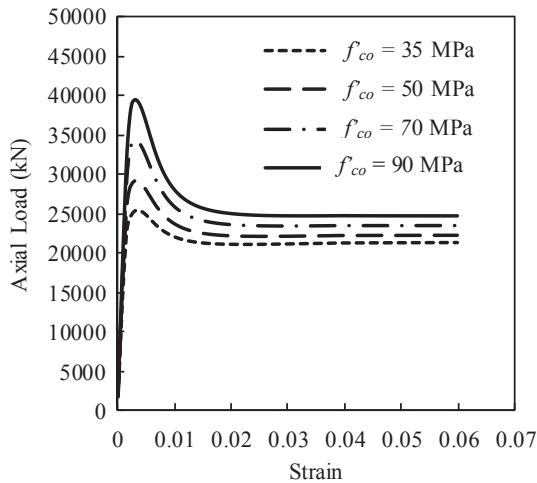


Fig. 18. Effects of sandwiched concrete compressive strength on the axial load-strain responses of CFDST columns.

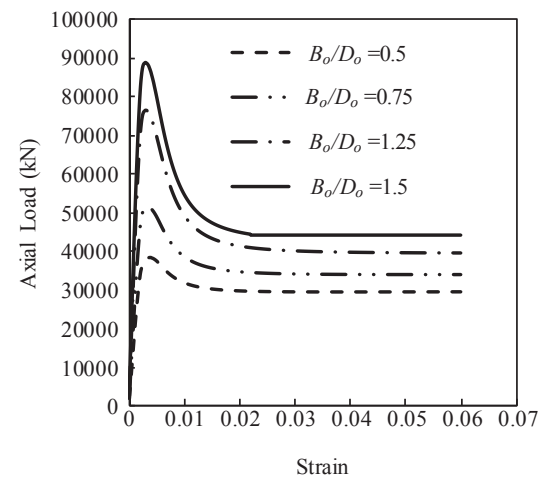


Fig. 21. Effects of the width-to-depth ratios on the axial load-strain responses of CFDST short columns.

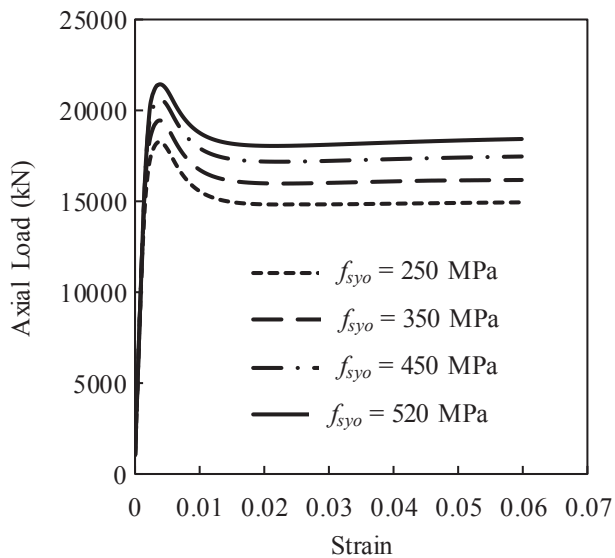


Fig. 19. Effects of the yield strength of the outer steel tube on the axial load-strain responses of CFDST short columns.

estimations of the ultimate loads of CFDST short columns.

7. Conclusions

This paper has presented a computationally efficient fiber-based computational model proposed for the inelastic modeling of rectangular thin-walled CFDST short columns with inner circular steel tube subjected to axial loading. The effects of the progressive local and post-local buckling of the external rectangular steel tube as well as the confinement on the core concrete within the internal circular steel tube have been taken into consideration in the theoretical model. A strength degradation factor for determining the concrete post-peak behavior has been proposed and incorporated in the material constitutive laws of concrete in CFDST columns. The comparisons of computer predictions with experimental data have demonstrated that the fiber-based simulation technology can accurately determine the responses of rectangular CFDST short columns. A design equation has been formulated for computing the ultimate axial strengths of rectangular CFDST short columns.

The conclusions drawn from the studies are:

- (1) The inner circular steel tube remarkably increases the load-carrying capacity, ductility and the residual strength of rectangular short CFDST columns but does not affect the column initial stiffness

Table 3
Comparison of ultimate strengths of rectangular CFDST short columns with the code predictions.

Specimen	$P_{u,exp}$ (kN)	$P_{u,EC4}$ (kN)	$P_{u,ACI}$ (kN)	$P_{u,AISC}$ (kN)	$P_{u,AIJ}$ (kN)	$P_{u,des}$ (kN)	$\frac{P_{u,EC4}}{P_{u,exp}}$	$\frac{P_{u,ACI}}{P_{u,exp}}$	$\frac{P_{u,AISC}}{P_{u,exp}}$	$\frac{P_{u,AIJ}}{P_{u,exp}}$	$\frac{P_{u,des}}{P_{u,exp}}$
I-CSCFT1	3643	3765	3263	3280	3703	3525	1.03	0.90	0.90	1.02	0.97
I-CSCFT2	3583	3852	3319	3334	3775	3599	1.08	0.93	0.93	1.05	1.00
I-CSCFT4	3820	4072	3440	3479	3937	3855	1.07	0.90	0.91	1.03	1.01
I-CSCFT5	3940	3911	3310	3392	3777	3541	0.99	0.84	0.86	0.96	0.90
I-CSCFT7	3865	4049	3556	3574	3980	3844	1.05	0.92	0.92	1.03	0.99
I-CSCFT8	3947	4138	3612	3628	4052	3917	1.05	0.92	0.92	1.03	0.99
I-CSCFT9	4045	4209	3635	3678	4087	4059	1.04	0.90	0.91	1.01	1.00
I-CSCFT10	4121	4364	3733	3772	4213	4173	1.06	0.91	0.92	1.02	1.01
I-CSCFT11	4251	4200	3603	3685	4054	3858	0.99	0.85	0.87	0.95	0.91
I-CSCFT12	4258	4321	3674	3752	4146	4199	1.01	0.86	0.88	0.97	0.99
II-CSCFT1	3355	3489	3025	3053	3423	3263	1.04	0.90	0.91	1.02	0.97
II-CSCFT2	3686	3760	3203	3261	3647	3588	1.02	0.87	0.88	0.99	0.97
II-CSCFT4	3814	3791	3334	3362	3718	3598	0.99	0.87	0.88	0.97	0.94
II-CSCFT5	4043	4067	3512	3570	3942	3923	1.01	0.87	0.88	0.98	0.97
II-CSCFT6	4428	4330	3680	3779	4153	4184	0.98	0.83	0.85	0.94	0.94
II-CSCFT7	3855	3879	3388	3414	3788	3662	1.01	0.88	0.89	0.98	0.95
III-CSCFT1	3198	3405	2953	2973	3338	3188	1.06	0.92	0.93	1.04	1.00
III-CSCFT2	3415	3625	3084	3130	3507	3461	1.06	0.90	0.92	1.03	1.01
III-CSCFT3	4120	3817	3191	3271	3646	3676	0.93	0.77	0.79	0.88	0.89
III-CSCFT4	4021	3709	3262	3283	3633	3524	0.92	0.81	0.82	0.90	0.88
III-CSCFT5	4165	3933	3393	3439	3802	3795	0.94	0.81	0.83	0.91	0.91
III-CSCFT6	4436	4126	3500	3580	3941	4010	0.93	0.79	0.81	0.89	0.90
III-CSCFT7	3900	3798	3318	3337	3705	3597	0.97	0.85	0.86	0.95	0.92
SDS1-40a	2450	2738	2235	2281	2589	2379	1.12	0.91	0.93	1.06	0.94
SDS1-40b	2383	2738	2235	2281	2589	2379	1.15	0.94	0.96	1.09	0.97
SDS1-70a	2997	3064	2522	2597	2926	2728	1.02	0.84	0.87	0.98	0.88
SDS1-70b	2806	3064	2522	2597	2926	2728	1.09	0.90	0.93	1.04	0.95
SDS2-40a	2366	2875	2327	2351	2707	2429	1.22	0.98	0.99	1.14	1.08
SDS2-40b	2463	2875	2327	2351	2707	2429	1.17	0.94	0.95	1.10	1.04
SDS2-70a	2765	3084	2512	2555	2925	2659	1.12	0.91	0.92	1.06	1.03
SDS2-70b	2884	3084	2512	2555	2925	2659	1.07	0.87	0.89	1.01	0.99
SDS3-40a	2505	2889	2324	2370	2705	2502	1.15	0.93	0.95	1.08	1.04
SDS3-40b	2479	2889	2324	2370	2705	2502	1.17	0.94	0.96	1.09	1.05
SDS3-70a	3144	3212	2610	2685	3041	2881	1.02	0.83	0.85	0.97	0.96
SDS3-70b	3100	3212	2610	2685	3041	2881	1.04	0.84	0.87	0.98	0.97
G1-2	980	1031	915	917	997	944	1.05	0.93	0.94	1.02	0.96
G1-3	1040	1124	969	976	1065	998	1.08	0.93	0.94	1.02	0.96
G1-4	1080	1122	968	978	1063	997	1.04	0.90	0.91	0.98	0.92
Mean							1.06	0.88	0.90	1.01	0.97
Standard Deviation (SD)							0.09	0.06	0.06	0.07	0.05
Coefficients of Variance (COV)							0.09	0.07	0.06	0.07	0.05

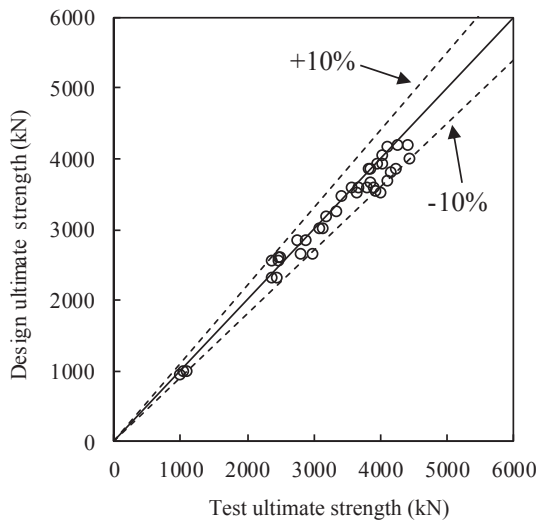


Fig. 22. Verification of the design model.

- notably. Increasing either the diameter or the thickness of the inner circular steel tube considerably increases the ultimate axial strengths of CFDST columns.
- (2) The local buckling of the external steel tube may reduce the axial

Table 4
Comparison of design ultimate strengths of CFDST columns with numerical predictions.

Column	$P_{u,des}$ (kN)	$P_{u,num}$ (kN)	$\frac{P_{u,des}}{P_{u,num}}$
C2	19,376	19,461	1.00
C3	16,393	16,894	0.97
C4	17,368	17,621	0.99
C5	18,367	18,462	0.99
C6	16,835	17,726	0.95
C7	18,462	18,787	0.98
C8	20,897	20,650	1.01
Mean			0.98
Standard Deviation (SD)			0.02
Coefficients of Variance (COV)			0.02

- load capacity of CFDST short columns by about 7.9% and decrease the column residual strengths.
- (3) The ultimate axial loads of CFDST columns are increased significantly by using higher strength sandwiched concrete, but the core concrete strength does not affect the column ultimate loads significantly.
- (4) The ductility of CFDST short columns are decreased by using higher strength concrete.
- (5) The axial load capacity of CFDST short columns is shown to increase with an increase in the yield stress of either the external or

Table 5
Strength prediction formulas for rectangular CFDST short columns by design codes.

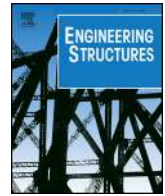
Design codes	Design equations
Eurocode 4 [5]	<p>Circular CFST columns:</p> $P_u = \eta_a A_s f_{sy} + A_c f_c \left(1 + \eta_c \frac{t f_{sy}}{D} \right)$ $\eta_a = 0.25(3 + 2\bar{\lambda})(\eta_a \leq 1.0)$ $\eta_c = 4.9 - 18.5\bar{\lambda} + 17\bar{\lambda}^2 (\eta_c > 0)$ <p>where the relative slenderness ratio is $\bar{\lambda} = \sqrt{\frac{N_{pl,Rk}}{N_{cr}}}$</p> <p>Rectangular CFST columns:</p> $P_u = A_s f_{sy} + A_c f_c'$ <p>Rectangular CFDST columns with inner circular tube:</p> $P_{u,EC4} = A_{so} f_{sy0} + A_{sc} f_c' + \eta_a A_s f_{syi} + A_{cc} f_{cc} \left(1 + \eta_c \frac{t_i f_{syi}}{d_i} \right)$
ACI 318-11 [6]	$P_{u,ACI} = A_{so} f_{sy0} + 0.85 A_{sc} f_{sc} + A_s f_{syi} + 0.85 A_{cc} f_{cc}$
AISC 360-16 [7]	$P_{u,AISC} = \begin{cases} P_o [0.658^{(P_o/P_e)}] & \text{for } P_e \geq 0.44 P_o \\ 0.877 P_e & \text{for } P_e < 0.44 P_o \end{cases}$ $P_o = A_{so} f_{sy0} + C_2 A_{sc} f_{sc} + A_s f_{syi} + C_2 A_{cc} f_{cc}$ $P_e = \frac{\pi^2}{(KL)^2} (EI)_{eff}$ $(EI)_{eff} = E_{so} I_{so} + E_{si} I_{si} + C_4 E_{sc} I_{sc} + C_4 E_{cc} I_{cc}$ $C_4 = 0.6 + 2 \left(\frac{A_s}{A_s + A_c} \right) \leq 0.9$ $C_2 = \begin{cases} 0.95 & \text{for circular cross-section} \\ 0.85 & \text{for rectangular cross-section} \end{cases}$
AIJ [8]	$P_{u,AIJ} = A_{sc} f_c + (1 + \eta) A_{so} f_{sy0} + A_{cc} f_{cc} + (1 + \eta) A_s f_{syi}$ $\eta = \begin{cases} 0.27 & \text{for circular cross-section} \\ 0 & \text{for rectangular cross-section} \end{cases}$

the internal steel tube.

- (6) The B_o/D_o ratio of CFDST columns has a significant influence on the load-carrying capacity of CFDST columns.
- (7) The methods given in Eurocode 4 [5] and AIJ [8] generally overestimate the ultimate axial loads of CFDST short column whereas the design approaches provided in ACI 318-11 [6] and AISC 360-16 [7] codes underestimate the ultimate strengths of CFDST short columns.
- (8) The proposed design formula provides more accurate results of CFDST short columns than the design codes.

References

- [1] Knowles RB, Park R. Strength of concrete filled steel columns. J Struct Division, ASCE 1969;95(12):2565–87.
- [2] Tomii M, Yoshimura K, Morishita Y. Experimental studies on concrete-filled steel tubular stub columns under concentric loading. Procee Int Colloquium Stability Struct Under Static Dyn Loads 1977;718–41.
- [3] Schneider SP. Axially loaded concrete-filled steel tubes. J Struct Eng, ASCE 1998;124(10):1125–38.
- [4] Sakino K, Nakahara H, Morino S, Nishiyama I. Behavior of centrally loaded concrete-filled steel-tube short columns. J Struct Eng, ASCE 2004;130(2):180–8.
- [5] Eurocode 4. Design of composite steel and concrete structures-Part 1-1: general rules and rules for buildings. London, UK: British Standards Institution. EN 1994-1-1; 2004.
- [6] ACI 318–11. Building code requirements for reinforced concrete. Detroit (MI) 2011.
- [7] AISC 360-16. Specification for structural steel buildings. American Institute of Steel Construction, Chicago (IL); 2016.
- [8] AIJ. Recommendations for design and construction of concrete filled steel tubular structures. Japan: Architectural Institute of Japan; 1997.
- [9] Peng YY, Tan KF, Yao Y. Mechanical properties of duplex steel tube high-strength concrete short columns under axial compression. J Wuhan University Technol 2011;33(2):105–9. (in Chinese).
- [10] Hassanein MF, Kharoob OF, Liang QQ. Behaviour of circular concrete-filled lean duplex stainless steel-carbon steel tubular short columns. Eng Struct 2013;56:83–94.
- [11] Wan CY, Zha XX. Nonlinear analysis and design of concrete-filled dual steel tubular columns under axial loading. Steel Compos Struct 2016;20(3):571–97.
- [12] Xiong MX, Xiong DX, Liew JR. Axial performance of short concrete filled steel tubes with high-and ultra-high-strength materials. Eng Struct 2017;136:494–510.
- [13] Ekmekyapar T, Al-Eliwi BJ. Concrete filled double circular steel tube (CFDCST) stub columns. Eng Struct 2017;135:68–80.
- [14] Ahmed M, Liang QQ, Patel VI, Hadi MNS. Numerical modeling of axially loaded circular concrete-filled double steel tubular short columns, Part I: Formulation. Proceeding of the 13th international conference on steel, space and composite structures. Perth, Australia; 2018.
- [15] Hu HT, Huang CS, Wu MH, Wu YM. Nonlinear analysis of axially loaded concrete-filled tube columns with confinement effect. J Struct Eng, ASCE 2003;129(10):1322–9.
- [16] Lu TQ, Zhao GF. Numerical method for analysis of ultimate strength of concrete-filled square steel tubular columns under eccentric compression reinforced by inner circular steel tube. J Dalian University Technol 2001;41(5):612–5. (in Chinese).
- [17] Wang ZH, Cheng R. Axial bearing capacity of composite-sectioned square concrete-filled steel tube. J Tsinghua University, Sci Technol 2005;45(12):1596–9. (in Chinese).
- [18] Pei WJ. Research on mechanical performance of multibarrel tube-confined concrete columns. ME Thesis, Chang'an University, Xi'an, China; 2005 (in Chinese).
- [19] Qian JR, Zhang Y, Ji XD, Cao WL. Test and analysis of axial compressive behavior of short composite-sectioned high strength concrete filled steel tubular columns. J Build Struct 2011;32(12):162–9. (in Chinese).
- [20] Wang Z-B, Tao Z, Yu Q. Axial compressive behaviour of concrete-filled double-tube stub columns with stiffeners. Thin-Walled Struct 2017;120:91–104.
- [21] Liang QQ. Numerical simulation of high strength circular double-skin concrete-filled steel tubular slender columns. Eng Struct 2018;168:205–17.
- [22] Han LH, Huang H, Zhao XL. Analytical behavior of concrete-filled double skin steel tubular (CFDST) beam-columns under cyclic loading. Thin-Walled Struct 2009;47:668–80.
- [23] Qian J, Li N, Ji X, Zhao Z. Experimental study on the seismic behavior of high strength concrete filled double-tube columns. Earthquake Eng Eng Vib 2014;13(1):47–57.
- [24] Wang R, Han LH, Zhao XL, Rasmussen KJR. Analytical behavior of concrete filled double steel tubular (CFDST) members under lateral impact. Thin-Walled Struct 2016;101:129–40.
- [25] Zhang FR, Wu CQ, Zhao XL, Heidarpour A, Li ZX. Experimental and numerical study of blast resistance of square CFDST columns with steel-fibre reinforced concrete. Eng Struct 2017;149:50–63.
- [26] Aghdamy A, Thambiratnam DP, Dhanasekar M, Saiedi S. Effects of load-related parameters on the response of concrete-filled double-skin steel tube columns subjected to lateral impact. J Constr Steel Res 2017;138:642–62.
- [27] Ritchie C, Packer JA, Seica MV, Zhao XL. Flexural behavior of concrete-filled double-skin steel tubes subjected to blast loading. J Struct Eng, ASCE 2018;144(7):04018076.
- [28] Usami T. Effective width of locally buckled plates in compression and bending. J Struct Eng, ASCE 1993;119(5):1358–73.
- [29] Uy B, Bradford MA. Local buckling of thin steel plates in composite construction: experimental and theoretical study. Procee Institution Civil Eng, Struct Build 1995;110(4):426–40.
- [30] Uy B. Strength of concrete filled steel box columns incorporating local buckling. J Struct Eng, ASCE 2000;126(3):341–52.
- [31] Liang QQ, Uy B. Theoretical study on the post-local buckling of steel plates in concrete-filled box columns. Comput Struct 2000;75(5):479–90.
- [32] Liang QQ, Uy B, Liew JYR. Nonlinear analysis of concrete-filled thin-walled steel box columns with local buckling effects. J Constr Steel Res 2006;62(6):581–91.
- [33] Liang QQ, Uy B, Liew JYR. Local buckling of steel plates in concrete-filled thin-walled steel tubular beam-columns. J Constr Steel Res 2007;63(3):396–405.
- [34] Liang QQ. Performance-based analysis of concrete-filled steel tubular beam-columns, Part I: theory and algorithms. J Constr Steel Res 2009;65(2):363–72.
- [35] Liang QQ. Performance-based analysis of concrete-filled steel tubular beam-columns, Part II: verification and applications. J Constr Steel Res 2009;65(2):351–62.
- [36] Liang QQ. Nonlinear analysis of circular double-skin concrete-filled steel tubular columns under axial compression. Eng Struct 2017;131:639–50.
- [37] Patel VI, Liang QQ, Hadi MNS. Nonlinear analysis of concrete-filled steel tubular columns. Germany: Scholar's Press; 2015.
- [38] Persson P-O, Strang G. A simple mesh generator in MATLAB. SIAM Rev 2004;46(2):329–45.
- [39] Liang QQ, Fragomeni S. Nonlinear analysis of circular concrete-filled steel tubular short columns under axial loading. J Constr Steel Res 2009;65(12):2186–96.
- [40] Mander JB. Seismic design of bridge piers. Christchurch, New Zealand: Department of Civil Engineering, University of Canterbury; 1983. Ph.D. Thesis.
- [41] Susantha K, Ge H, Usami T. Uniaxial stress-strain relationship of concrete confined by various shaped steel tubes. Eng Struct 2001;23(10):1331–47.
- [42] Lai Z, Varma AH. Effective stress-strain relationships for analysis of noncompact and slender filled composite (CFT) members. Eng Struct 2016;124:457–72.
- [43] Katwal U, Tao Z, Hassan MK, Wang W-D. Simplified numerical modeling of axially loaded circular concrete-filled steel stub columns. J Struct Eng, ASCE 2017;143(12):04017169.
- [44] Lim JC, Ozbakkaloglu T. Stress-strain model for normal-and light-weight concretes under uniaxial and triaxial compression. Constr Build Mater 2014;71:492–509.
- [45] Mander JB, Priestley MJ, Park R. Theoretical stress-strain model for confined concrete. J Struct Eng, ASCE 1988;114(8):1804–26.
- [46] Tang J, Hino S, Kuroda I, Ohta T. Modeling of stress-strain relationships for steel and concrete in concrete filled circular steel tubular columns. Steel Construct Eng, JSSC 1996;3(11):35–46.
- [47] Oehlers DJ, Bradford MA. Elementary behavior of composite steel and concrete structural members. Oxford U.K.: Butterworth-Heinemann; 1999.



Experimental and numerical studies of square concrete-filled double steel tubular short columns under eccentric loading

Mizan Ahmed^a, Qing Quan Liang^{a,*}, Vipulkumar Ishvarbhai Patel^b, Muhammad N.S. Hadi^c

^a College of Engineering and Science, Victoria University, PO Box 14428, Melbourne, VIC 8001, Australia

^b School of Engineering and Mathematical Sciences, La Trobe University, Bendigo, VIC 3552, Australia

^c School of Civil, Mining and Environmental Engineering, University of Wollongong, Wollongong, NSW 2522, Australia

ARTICLE INFO

Keywords:

Concrete-filled double steel tubes
Local and post-local buckling
Nonlinear analysis

ABSTRACT

Square concrete-filled double steel tubular (CFDST) beam-columns consisting of an internal circular steel tube have increasingly been utilized in composite building structures because of their high structural performance. This paper describes experimental and numerical studies on the structural responses of square thin-walled CFDST columns loaded eccentrically. Tests on twenty short square CFDST columns were undertaken that included sixteen columns under eccentric loading and four columns under concentric loading. The parameters examined in the experiments included the cross-sectional dimensions, the width-to-thickness ratios of outer and internal tubes and loading eccentricity. The measured ultimate strengths, load-shortening responses, load-lateral displacement curves, stress-strain curves and observed failure modes are presented. A numerical model incorporating the fiber analysis is developed that predicts the moment-curvature responses and axial load-moment strength envelopes of CFDST columns. The model explicitly accounts for the influences of the confinement exerted by the internal circular steel tube on the core concrete and the progressive post-local buckling of the external steel tube. Efficient computer algorithms implementing the inverse quadratic method is developed to produce converged solutions to the nonlinear dynamic equilibrium equations generated in the analysis. Measurements from the tests are employed to validate the proposed numerical model. It is shown that there is a good agreement between theory and experiment. The computer model is utilized to demonstrate the significance of various parameters on the behavior of thin-walled short CFDST beam-columns.

1. Introduction

Square concrete-filled double steel tubular (CFDST) columns as depicted in Fig. 1 are used in composite building structures due to their aesthetic appearance and ease of connecting with steel beams in addition to their high structural and fire performance. The external steel tube of a CFDST square column is fabricated by thin-walled section to decrease the usage of steel material for economical designs. However, this may cause the outward local buckling of the steel tube under compression, which has a marked influence on the performance of CFDST columns and should be considered in the nonlinear analysis and design. The internal circular steel tube effectively confines the core-concrete in a loaded CFDST column, which remarkably improves the concrete compressive strength as well as ductility. The CFDST columns in a building structure are likely subjected to eccentric loading or the combination of bending and axial load, and are designed as beam-columns. Little research has been reported on the structural behavior of

thin-walled CFDST square columns that are subjected to eccentric loads. This paper presents experimental and numerical investigations on the behavior of CFDST columns loaded eccentrically to failure.

Most of the investigations on CFDST columns reported previously has focused on circular cross-section [1–12] and tests on short square CFDST columns consisting of an inner circular steel tube have been very limited [13–16]. Pei [13] performed tests to determine the structural performance of stub CFDST square columns under axial and eccentric loads. It was reported that the local buckling of the external steel tube in addition to concrete crushing caused the failure of short CFDST square columns. Experiments on the structural behavior of square CFDST short columns loaded either concentrically or eccentrically to failure were undertaken by Qian et al. [14,15]. The failure of the columns was due to the bending as well as the outward local buckling of the outer steel tube. Since the internal circular tube confined the core concrete, the residual ductility and strength of CFDST columns were dramatically improved. Recently, Wang et al. [16] presented

* Corresponding author.

E-mail address: Qing.Liang@vu.edu.au (Q.Q. Liang).

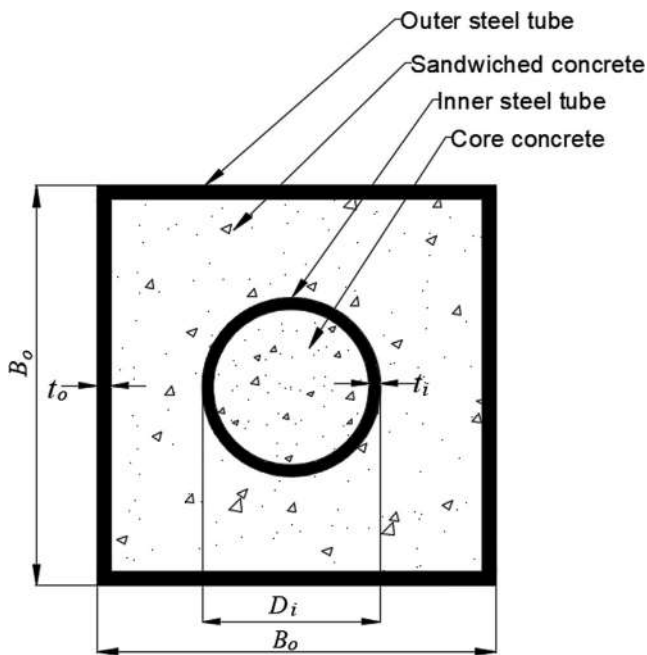


Fig. 1. Cross-section of square CFDST column with inner circular steel tube.

experimental investigations on the characteristics of axially-loaded short square CFDST columns incorporating stiffeners. It was reported that all CFDST columns failed by the outward local-buckling of the outer steel tube walls at the stiffeners coupled with stiffener buckling as well as sandwiched concrete crushing.

Commercial finite element (FE) programs have been employed to model the structural behavior of square CFDST stub columns loaded concentrically to failure by investigators. Pei [13] presented FE models created by using the FE program ANSYS for ascertaining the load-axial strain behavior of short CFDST square columns. The core-concrete was modeled by the stress-strain relations presented by Zhong [17] for concrete confined by circular steel tubes while the sandwiched-concrete was simulated by the material constitutive laws given by Han [18] for concrete in square CFST columns. However, the FE models by Pei [13] did not include the local buckling of the outer steel tube as well as the composite action between the concrete and steel components so that they overestimated the experimentally measured behavior of CFDST columns. Qian et al. [14] utilized the FE software ABAQUS to model the responses of a short square CFDST column loaded concentrically to failure. The nonlinear analysis employed the constitutive model given by Han [18] for sandwiched concrete and the relationship of stress and strain given by Sun and Kenji [19] for core concrete. The FE model presented by Qian et al. [14], which considered the local buckling of the outer steel tube, was shown to predict well the behavior of the concentrically loaded CFDST column. Wang et al. [16] utilized ABAQUS to investigate the interaction behavior of concrete and steel tube in axially loaded stub CFDST columns with outer square sections. The concrete model developed by Tao et al. [20] was adopted for both sandwiched and core concrete. However, the local buckling of the external tube was not included in the modeling.

The effects of local buckling on the structural performance of concrete-filled steel tubular composite columns have been investigated by a number of researchers [21–28]. A fiber-based modeling technique has been proposed by Ky et al. [29] for the response predictions of axially loaded concrete-encased composite (CEC) short and slender columns. The modeling technique, which took into account the local buckling of structural steel, buckling of reinforcement bars, initial geometric imperfection and concrete confinement, was shown to capture well the behavior of CEC columns. Liu et al. [30] developed a numerical model for the inelastic analysis of nonlinear steel–concrete composite beams

curved in-plan. However, very limited experimental and numerical research works have been conducted on the performance of short CFDST square beam-columns. Moreover, no fiber-based computational technique has been proposed for the simulation of the moment-curvature curves and interaction strengths of such beam-columns. To fill this knowledge gap, this paper presents experimental and numerical studies on the structural performance of CFDST square stub columns loaded eccentrically. A total of twenty short columns with different loading eccentricities were tested to failure to examine their structural responses. The experimental program and results obtained are described. A mathematical modeling method for the prediction of the moment-curvature curves and strength envelopes of CFDST beam-columns is developed and validated against test data. The computational model is then utilized to assess the impacts of important design parameters on the structural behavior of short CFDST square beam-columns.

2. Experimental program

2.1. Specimen preparation

Twenty short square CFDST columns fabricated by square outer steel tubes and circular inner steel tubes were tested to failure under either eccentric or concentric loading. The specimens were divided into four groups (G1, G2, G3 and G4). There were five specimens in each group. For Groups G1 and G3, the specimens had an external square cross-section of 125×125 mm and an inner circular tube with a diameter of 76.1 mm. Specimens in Groups G2 and G4 had an outer square cross-section of 150×150 mm and an inner circular tube with a diameter of 88.9 mm. The thickness of the inner steel tubes was varied to investigate their effects on the structural performance. The column specimens were originally designed to be tested using the compression testing machine with a capacity of 2000 kN at Victoria University, Australia. The maximum size of the column specimens that could be tested using this machine was 150×150 mm. For CFDST columns, the cross-section smaller than 125×125 mm was too small to place the inner tube and concrete. The specimens were fabricated by cold-formed steel tubes, which were placed concentrically and welded with two steel bars. Two stiffeners were welded on each face of the ends of the steel square tube to prevent the premature failure of the column ends during the test. A schematic view of the cross-sectional dimensions of short CFDST columns is presented in Fig. 2. Premix concrete was used to construct the columns. Two different batches of concrete mixes were used. The hollow steel tubes were filled with concrete in layers and the compaction of concrete was conducted by a vibrator. The test parameters included loading application (concentric or eccentric loading), load eccentricity ratio (e/B_o) with B_o being the width of the outer steel tube, diameter-to-thickness ratios of the internal tube (D_i/t_i) and steel yield strength. The length of the CFDST columns was three times the width of the external tubes to prevent the overall column buckling. The geometric and material properties of all specimens are provided in Table 1.

2.2. Material properties

The material properties of steel tubes were obtained by conducting tensile coupon tests in accordance with AS 1391 [31]. The average steel yield strengths of steel specimens presented in Table 2 were calculated from the test results of two coupon specimens for each tube. The yield strengths of the external steel tubes of $125 \times 125 \times 4.0$ mm and $150 \times 150 \times 5.0$ mm were measured as 360 MPa and 378 MPa, respectively. The yield strengths of the inner steel tubes varied from 345 MPa to 412 MPa. The stress-strain curves for steel material obtained from tensile coupon tests are presented in Fig. 3.

The material properties of concrete were determined by undertaking compression tests on 100×200 mm concrete cylinders. The concrete compressive strength was averaged from the test results of 42

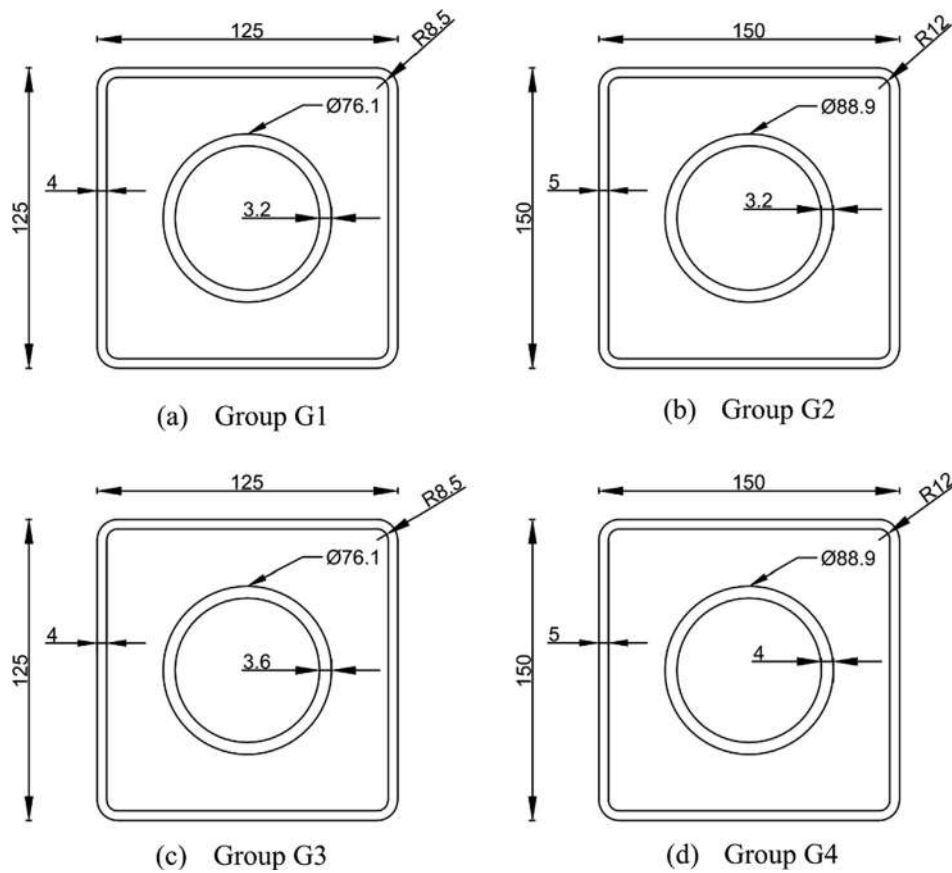


Fig. 2. Dimensions of test specimens (units in mm).

concrete cylinders tested from the start to the end of the experimental program. The average compressive strength of the specimens in Group G1 and G2 was measured as 19.1 MPa while for the specimens in Group G3 and G4 it was measured as 20.6 MPa. The reason for the use of the low concrete compressive strength was because all column specimens were originally designed to be tested using the compression testing

machine with a capacity of 2000 kN at Victoria University, Australia. However, due to the failure of the machine, all column specimens were tested at the University of Wollongong, Australia.

Table 1
Geometry and material properties of square CFDST short columns.

Group	Column	Length L (mm)	Outer Tube		Inner Tube		f'_c (MPa)	e (mm)	e/B_o	$P_{u,exp}$ (kN)
			$B_o \times B_o \times t_o$ (mm)	B_o/t_o	$D_i \times t_i$ (mm)	D_i/t_i				
G1	SC1	375	125 × 125 × 4.0	31.25	76.1 × 3.2	23.8	19.1	0	0	1269
	SC2	375	125 × 125 × 4.0	31.25	76.1 × 3.2	23.8	19.1	10	0.08	1127
	SC3	375	125 × 125 × 4.0	31.25	76.1 × 3.2	23.8	19.1	20	0.16	886
	SC4	375	125 × 125 × 4.0	31.25	76.1 × 3.2	23.8	19.1	30	0.24	721
	SC5	375	125 × 125 × 4.0	31.25	76.1 × 3.2	23.8	19.1	40	0.32	640
G2	SC6	450	150 × 150 × 5.0	30.00	88.9 × 3.2	27.8	19.1	0	0	1852
	SC7	450	150 × 150 × 5.0	30.00	88.9 × 3.2	27.8	19.1	10	0.07	1669
	SC8	450	150 × 150 × 5.0	30.00	88.9 × 3.2	27.8	19.1	20	0.13	1426
	SC9	450	150 × 150 × 5.0	30.00	88.9 × 3.2	27.8	19.1	30	0.20	1191
	SC10	450	150 × 150 × 5.0	30.00	88.9 × 3.2	27.8	19.1	35	0.23	1153
G3	SC11	375	125 × 125 × 4.0	31.25	76.1 × 3.6	21.1	20.6	0	0	1331
	SC12	375	125 × 125 × 4.0	31.25	76.1 × 3.6	21.1	20.6	10	0.08	1087
	SC13	375	125 × 125 × 4.0	31.25	76.1 × 3.6	21.1	20.6	20	0.16	918
	SC14	375	125 × 125 × 4.0	31.25	76.1 × 3.6	21.1	20.6	30	0.24	807
	SC15	375	125 × 125 × 4.0	31.25	76.1 × 3.6	21.1	20.6	40	0.32	597
G4	SC16	450	150 × 150 × 5.0	30.00	88.9 × 4.0	22.2	20.6	0	0	1865
	SC17	450	150 × 150 × 5.0	30.00	88.9 × 4.0	22.2	20.6	10	0.07	1624
	SC18	450	150 × 150 × 5.0	30.00	88.9 × 4.0	22.2	20.6	20	0.13	1377
	SC19	450	150 × 150 × 5.0	30.00	88.9 × 4.0	22.2	20.6	35	0.23	1171
	SC20	450	150 × 150 × 5.0	30.00	88.9 × 4.0	22.2	20.6	45	0.30	1033

Table 2
Material properties of steel tube obtained from tensile coupon tests.

Tube type	No.	Geometry of the tube (mm)	Yield strength, f_{sy} (MPa)	Ultimate strength, f_{su} (MPa)	Yield strain, ϵ_{sy}	Ultimate strain, ϵ_{su}	Elastic modulus, E_s (GPa)
Outer tube $B_o \times B_o \times t_o$	1	125 × 125 × 4.0	360	461	0.0053	0.25	203
	2	150 × 150 × 5.0	378	464	0.0033	0.23	201
Inner tube $D_i \times t_i$	1	76.1 × 3.2	400	458	0.0015	0.188	211
	2	88.9 × 3.2	412	471	0.0013	0.202	200
	3	76.1 × 3.6	353	398	0.0026	0.170	205
	4	88.9 × 4.0	345	372	0.0042	0.193	200

2.3. Test setup and instrumentation

The typical test setup of CFDST short columns is shown in Fig. 4. For CFDST stub columns under concentric loading, the axial load was applied to the concrete and steel simultaneously as illustrated in Fig. 4(a). The column ends were grinded using a concrete grinder prior to placing the column on the compression testing machine to ensure flat and smooth surface ends in order to obtain uniform load distribution. For short CFDST columns under eccentric loading, they were tested under pin-ended conditions by applying the compressive load on the loading heads attached to the column ends as illustrated in Fig. 4(b). The loading heads were designed by Hadi and Widiarsa [32] that consisted of a 50 mm thick square steel cap called the adaptor plate and a 25 mm thick bottom steel plate with a ball joint. The load generated by the compression testing machine was transferred through the bottom plate and ball joint to the adaptor plate with designed eccentricities.

Two strain gauges were attached to the column mid-height (one in each of the adjacent sides of the square column) to capture the axial and transverse strains under concentric loading as illustrated in Fig. 4(a). For columns under eccentric loading, two strain gauges were attached to the columns mid-height (one at each of the compression and tension sides) to capture the axial strain only. The axial shortening of square CFDST columns was averaged from the readings of the two linear variable differential transducers (LVDTs) attached to the two opposite corners of the machine. For columns under eccentric loading, one additional laser triangulation was utilized to capture the column mid-height deflection as shown in Fig. 4(b).

All CFDST columns were tested to failure using the Denison 5000 kN compression testing machine at the structure laboratory in the School of Civil, Mining and Environmental Engineering at the University of Wollongong, Australia. The specimen was initially preloaded to 100 kN using the force-controlled mode to prevent any movement between the specimen and loading head of the testing machine, and then unloaded

to 20 kN before starting recording the data. The column was loaded gradually with a displacement rate of 0.8 mm/min until the failure occurred. The test process was stopped when the external steel tube underwent significant local buckling or the maximum axial shortening reached to 30 mm. The readings of the LVDTs, strain gauges, laser triangulation and applied load were recorded using a data logger.

3. Test results and discussions

3.1. Failure modes and behavior of columns under axial compression

The short CFDST square columns failed by the significant unilateral local buckling of the flanges and webs of the external square steel tubes. The failure patterns of the CFDST short columns with square sections loaded concentrically are shown in Fig. 5. The stiffeners effectively prevented the steel tube ends from the premature failure due to local buckling during the test. Consequently, the outer steel tube generally buckled at the position about one third measured from the column top or bottom end. The outer steel tube of Column SC1 split at the corners where the adjacent tube walls buckled locally outward as shown in Fig. 5. Fig. 6 presents the section view of Column SC1. It can be observed that the crushing of the sandwiched concrete took place at the regions where the local buckling of the external steel tube occurred. As demonstrated in Fig. 6, the core-concrete did not crush because of the confinement offered by the internal circular steel tube.

The measured ultimate loads of CFDST columns loaded concentrically to failure are given in Table 1 while their axial load-shortening curves are depicted in Fig. 7. It would appear from Fig. 7 that short CFDST columns exhibit strain-hardening behavior and very good ductility because of the utilization of internal circular steel tubes. The columns can sustain large axial deformation without a significant strength degradation. The residual strengths of Columns SC1, SC6, SC11 and SC16 were measured as 93%, 96%, 99% and 97% of their

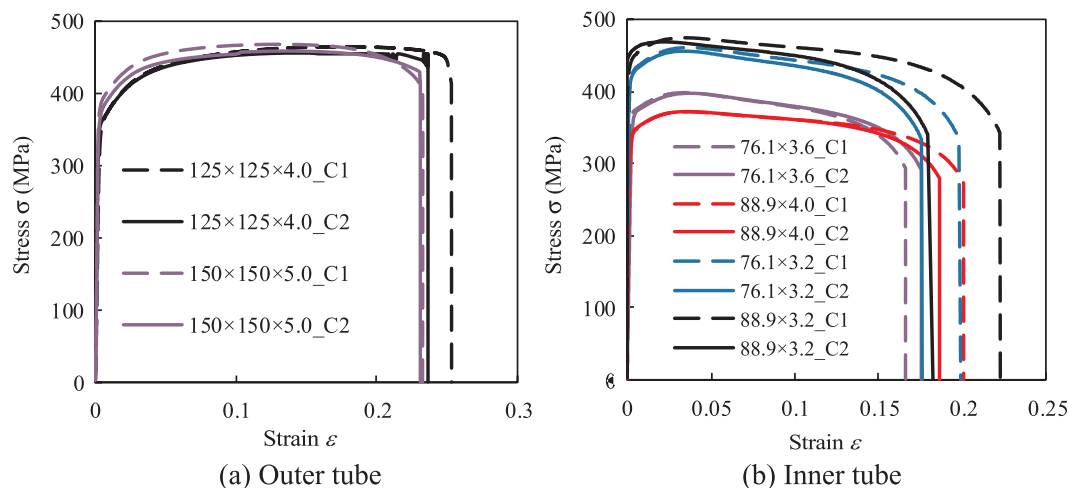


Fig. 3. Measured stress-strain curves for steel tubes.



(a) Under concentric loading



(b) Under eccentric loading

Fig. 4. Test setup of square CFDST short columns.

corresponding ultimate axial strengths, respectively. For the identical external steel tube, increasing the thickness (t_i) of the internal steel tube improves the column ultimate load slightly. Columns SC1 and SC11, SC6 and SC16 had the same outer tube, however, the ultimate loads of Column SC11 and SC16 are higher than those of Columns SC1 and SC6 due to the increased steel areas. The strain distributions in specimens loaded concentrically were measured during the tests and are given in Fig. 8. Fig. 8(a) shows the relationships of the axial load and axial strains as well as lateral strains. In Fig. 8(b), the relationships of the lateral strain (hoop strain) and axial strain are provided. It is seen that both the axial and lateral strains increased at a small rate at the initial state of the loading. This is attributed to the effect of the Poisson's ratio

of concrete, which was smaller than that of steel at the initial stage. However, after a certain load, the lateral strain increased significantly as the load increased due to the rapid expansion of the concrete.

3.2. Failure modes and behavior of columns under eccentric loading

The failure of CFDST square beam-columns loaded eccentrically were caused by the unilateral local buckling of the compression flange and the two adjacent webs in the external steel tube, the crushing of sandwiched concrete at places where local buckling occurred and the significant bending of the beam-columns as illustrated in Fig. 9. It is observed from Fig. 10 that the sandwiched concrete was separated from the internal steel tube. Columns SC5 and SC15 were subjected to eccentric loads with a large eccentricity ratio of 0.32. These two columns failed shortly due to the significant damage of the column bottom end where the load was applied as depicted in Fig. 11. The section view of Column SC14 is given in Fig. 12. It can be seen that the sandwiched concrete crushed at the compression zone where the steel tube wall underwent local buckling.

The load-axial shortening curves of CFDST square columns loaded eccentrically are presented in Fig. 13. It would appear that increasing the loading eccentricity greatly decreases the axial stiffness and ultimate strengths of short columns. The measured column ultimate strengths are tabulated in Table 1. For columns in Group 1, increasing the loading eccentricity from 0 mm to 10 mm, 20 mm, 30 mm and 40 mm reduces its ultimate axial strength by 11.2%, 30.2%, 43.2% and 49.6%, respectively. However, for the identical external steel tube, the reduction in the ultimate strength due to the eccentric loading was generally higher for the columns with thicker inner tube. The columns in Group G3 had a similar external tube as Group G1, however, the reduction in the ultimate axial strength was estimated as 18.3%, 31%, 39.4% and 55.1% for increasing the loading eccentricity from 0 mm to 10 mm, 20 mm, 30 mm and 40 mm, respectively. The experimentally measured load-lateral deflection curves of CFDST columns are provided in Fig. 14. It is evident the initial bending stiffness of CFDST columns decreases as the loading eccentricity increases. Fig. 15 demonstrates the experimental load-axial strain curves of CFDST columns subjected to various end eccentricities. It is observed from Fig. 15 that at the initial loading stage, the CFDST column was subjected to compression. However, as the load increased, the axial strain in one of the steel tube walls became negative, which implies that part of the column was under tension.

4. Numerical model based on fiber element formulation

4.1. The method of fiber analysis

The key aspect of designing square CFDST beam-columns is the



Fig. 5. Failure modes of square CFDST short columns under axial compression.



Fig. 6. Section view of Specimen SC1.

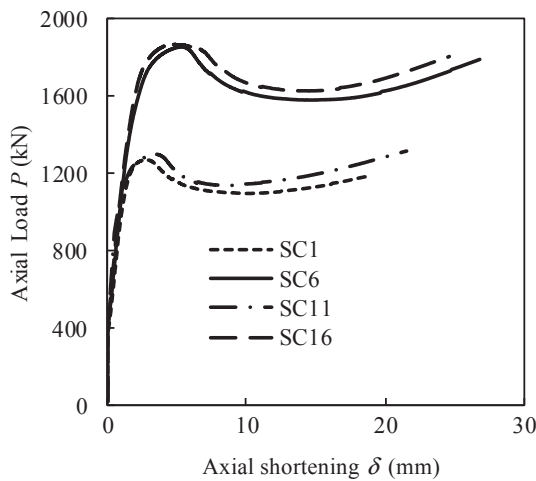


Fig. 7. Measured axial load-shortening curves of square CFDST short columns under axial compression.

calculation of the cross-section strength under eccentric loading. The axial load-moment interaction diagrams (strength envelopes) of composite columns are often used to evaluate the strengths of short and slender composite columns subjected to combined actions. A

mathematical model underlying the theory of fiber analysis has been proposed for calculating the axial load-moment-curvature relationships and strength envelopes of rectangular CFST beam-columns by Liang [33,34]. Fiber elements are used to mesh the column cross-section as shown in Fig. 16. A mesh generator developed by Persson and Strang [35] is employed to discretize the sandwiched concrete in the present study. The formulation assumes that after deformation the plane section remains plane, which implies that a linear strain distribution through the depth of the cross-section is achieved as illustrated in Fig. 16. This assumption ensures the strain compatibility of steel and concrete fibers in the cross-section in the loading history. The stress of each fiber is calculated from its corresponding strain by applying the uniaxial stress-strain laws of concrete and steel materials. The internal bending moment (M) as well as the axial force (P) are determined by integrating the stresses over the cross-section.

4.2. Modeling of local and post-local buckling

The unilateral local buckling of the flanges and webs of a thin-walled CFST square column loaded eccentrically may take place, which leads to a marked reduction in the column ultimate resistance [22,24]. The longitudinal stresses on the steel flanges and webs of the CFST column loaded uniaxially are either non-uniform or uniform as discussed by Liang et al. [24]. Liang et al. [24] developed formulas for ascertaining the initial local buckling strengths of steel flanges and

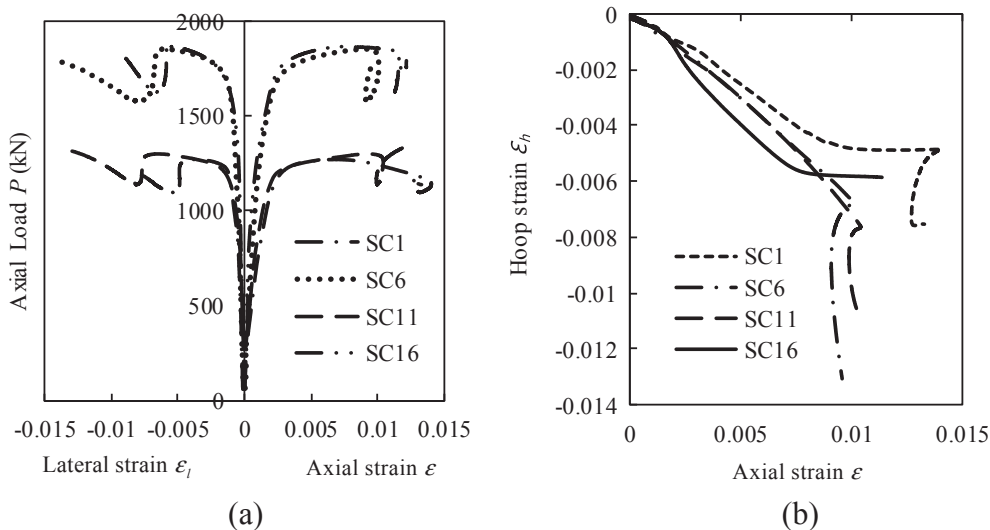


Fig. 8. Strain distributions in square CFDST short columns under axial compression.

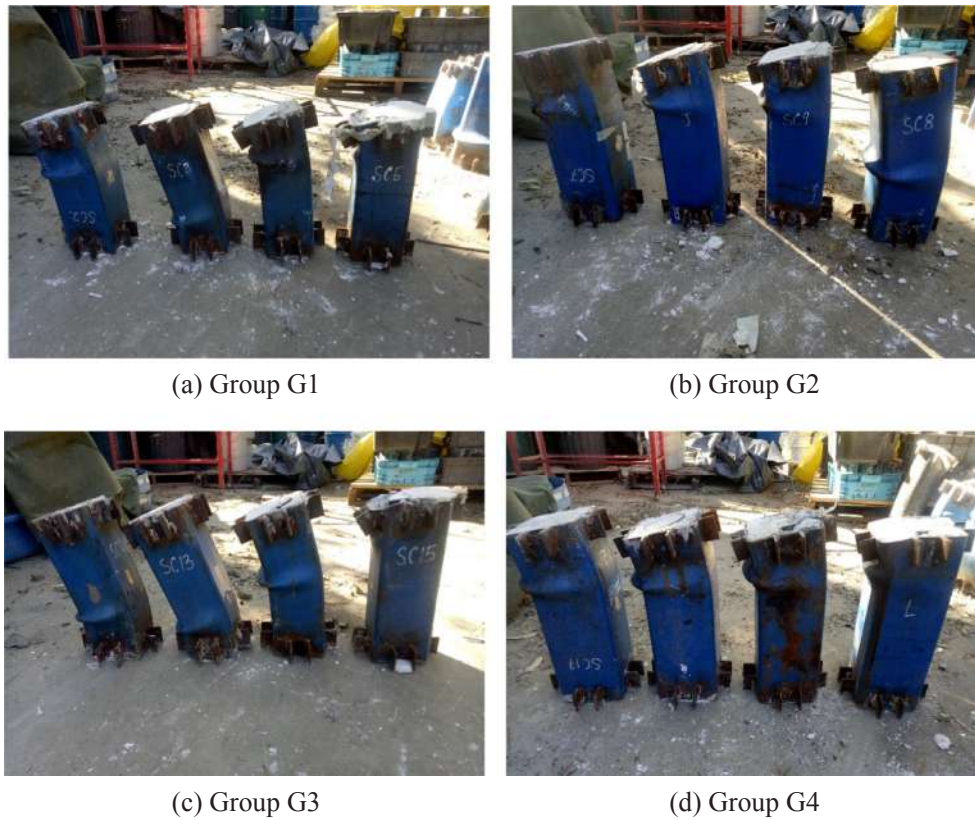


Fig. 9. Failure modes of square CFDST short columns under eccentric loading.



Fig. 10. Separation of sandwiched concrete and inner steel tube in Specimens SC8 and SC14.

webs subjected to non-uniform compressive stresses in CFST rectangular columns. Their expressions are employed in the present mathematical model.

The gradual post-local buckling characteristics of the flanges and webs of a CFDST column loaded eccentrically are modeled by the principle of stress redistributions as shown in Fig. 17. The effective widths of the thin-walled steel tube walls subjected to stress gradients are calculated using the formulas developed by Liang et al. [24]. Their effective width expressions can be used for steel plates with clear width-to-thickness ratios (b/t) ranging from 30 and 100. After the initial local buckling took place, the plate ineffective width increased as the compressive load increased until the plate reached its strength of post-local buckling. The computational scheme for modeling the gradual post-local buckling of a square CFST column loaded eccentrically proposed by Liang [33] is utilized in the present mathematical model.

4.3. Modeling of axial load-moment strength interaction diagrams

An incremental-iterative computational procedure has been developed for quantifying the strength envelopes of short square CFDST beam-columns subjected to axial compression in addition to uniaxial bending. The ultimate axial load (P_u) of the column without bending moment is initially calculated by using the load-axial strain response analysis technique that accounts for post-local buckling influences [33]. For a given axial load (P_u), the curvature (ϕ) of the cross-section is incrementally increased and the corresponding moment is calculated that satisfies the force equilibrium. The section ultimate bending resistance is taken as the maximum moment on the predicted moment-curvature curve. By increasing the axial load from zero to the maximum value (P_u) and calculating the corresponding ultimate bending resistance, a set of ultimate moments and axial loads can be determined, which are used to



Fig. 11. Failure modes of Specimens SC5 and SC15.



Fig. 12. Section view of Specimen SC14.

plot the strength envelop of the CFDST column. The computer flow chart for calculating the strength envelop of a short CFDST column is shown in Fig. 18.

In the analysis, the neutral axis depth (d_n) of the cross-section is adjusted iteratively until the force equilibrium condition is achieved. The inverse quadratic method [36] has been implemented in the computer algorithms to determine the neutral axis depth. In the computational method, three values are initialized to the neutral axis depth. The new neutral axis depth approaching the true value is calculated by means of executing the following equations:

$$d_{n,j+3} = d_{n,j+1} - r_{p,j+1} \left(\frac{A}{C} \right) \quad (1)$$

$$A = (r_{p,j})^2 (d_{n,j+2} - d_{n,j+1}) + r_{p,j} r_{p,j+1} (d_{n,j+1} - d_{n,j+2}) + (r_{p,j+1} - r_{p,j+2}) r_{p,j+2} (d_{n,j} - d_{n,j+1}) \quad (2)$$

$$C = (r_{p,j+1} - r_{p,j})(r_{p,j+2} - r_{p,j})(r_{p,j+2} - r_{p,j+1}) \quad (3)$$

where $r_p = P_u - P$ and j is the iteration number. The initial three values of neutral axis depths are taken as $d_{n,1} = D_0$, $d_{n,2} = D_0/2$ and $d_{n,3} = (d_{n,1} + d_{n,2})/2$. The iterative computational process is stopped when the convergence criterion of $|r_p| < \epsilon_k$ is achieved, where ϵ_k is taken as 10^{-4} .

4.4. Material constitutive laws for steels

The external tube of a square CFDST column is subjected to biaxial stresses under compression. This results in the reduction of steel yield strength which is taken into account in the material laws for structural

steel as illustrated in Fig. 19, where f_{sy} denotes the steel yield strength, ϵ_{sy} the yield strain, ϵ_{st} the strain at the onset of strain-hardening, f_{su} the tensile strength and ϵ_{su} the ultimate strain of steel. The rounded part of the stress-strain curve between $0.9\epsilon_{sy}$ and ϵ_{st} is represented by the expression proposed by Liang [33] while formulas suggested by Mander [37] are used to determine the stresses after the strain hardening occurs. The strain ϵ_{st} and the ultimate strain ϵ_{su} are taken as 0.005 and 0.2, respectively.

4.5. Material constitutive laws for concrete

The internal and external tubes provide little confinement to the sandwiched concrete in a square CFDST column so that the sandwiched-concrete is treated as unconfined concrete. However, the core concrete is confined by the internal circular steel tube in a square CFDST column and this confinement is recognized in the material stress-strain relations for core-concrete in the present study. The material constitutive models for sandwiched-concrete and core-concrete in rectangular CFDST columns have been validated against experimental data by Ahmed et al. [27]. The general stress-strain curves for both confined concrete and unconfined concrete are schematically illustrated in Fig. 20.

The ascending branch of the stress-strain curves are described by the following expressions suggested by Mander et al. [38]

$$\sigma_c = \frac{f'_{cc} (\epsilon_c / \epsilon'_{cc})^\lambda}{(\epsilon_c / \epsilon'_{cc})^\lambda + \lambda - 1} \quad \text{for } 0 \leq \epsilon_c \leq \epsilon'_{cc} \quad (4)$$

$$\lambda = \frac{E_c \epsilon'_{cc}}{E_c \epsilon'_{cc} - f'_{cc}} \quad (5)$$

where σ_c and ϵ_c represent the longitudinal concrete compressive stress and corresponding strain, respectively; f'_{cc} and ϵ'_{cc} the compressive strength and corresponding strain of confined concrete, respectively; E_c the concrete elastic modulus [12], which is taken as

$$E_c = 4400 \sqrt{\gamma_c f'_c} \quad (\text{MPa}) \quad (6)$$

where $\gamma_c = 1.85 D_c^{-0.135}$ stands for the reduction factor given by Liang [33], which considers the column size effect on the concrete compressive strength, and D_c is taken as $(B_o - 2t_o)$.

The maximum compressive strength as well as its corresponding strain of the core-concrete are calculated by

$$f'_{cc} = \gamma_c f'_c + 5.2 (\gamma_c f'_c)^{0.91} \left(\frac{f_{rp}}{\gamma_c f'_c} \right)^a \quad \text{where } a = (\gamma_c f'_c)^{-0.06} \quad (7)$$

$$\epsilon'_{cc} = \epsilon'_c + 0.045 \left(\frac{f_{rp}}{\gamma_c f'_c} \right)^{1.15} \quad (8)$$

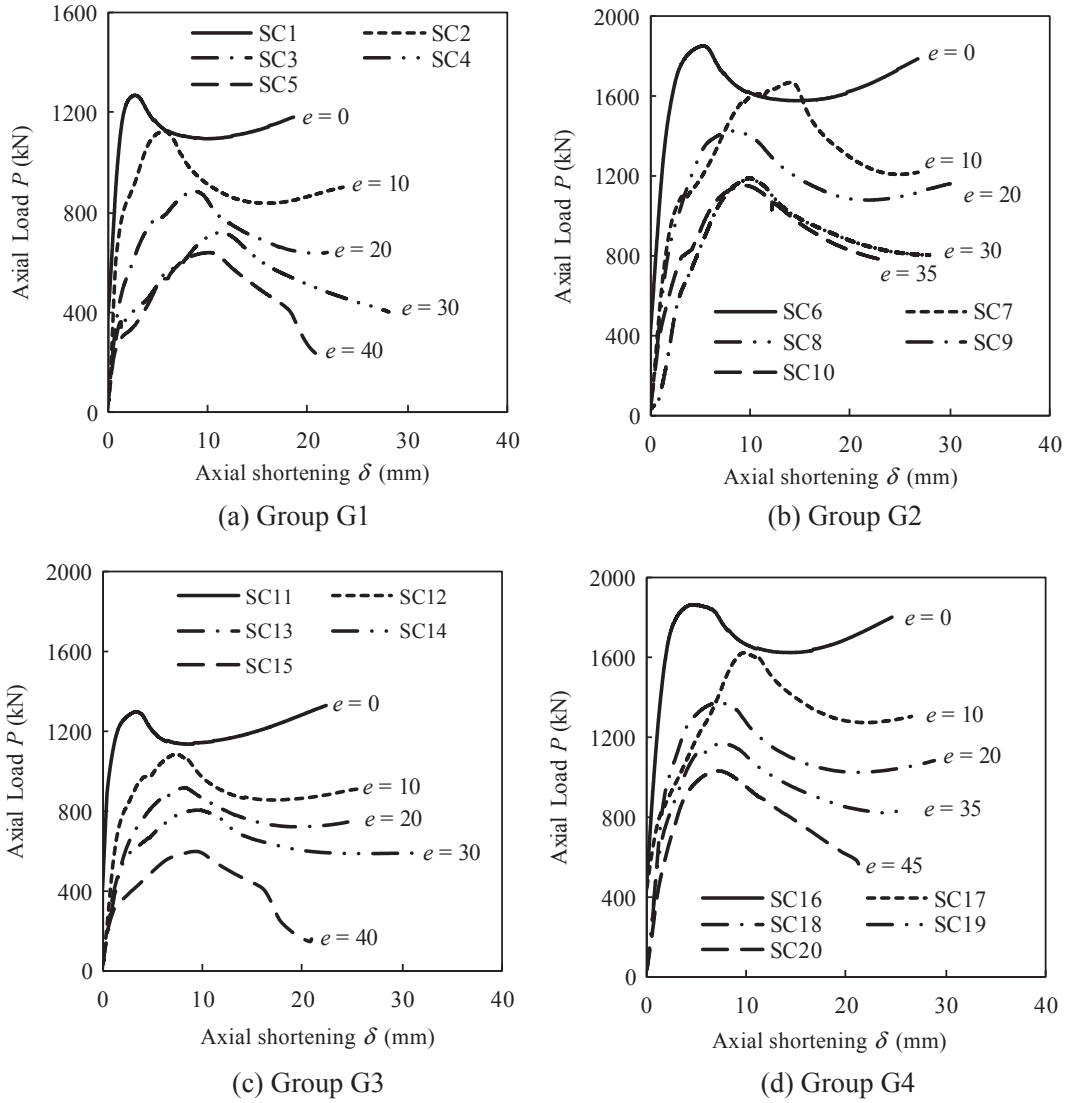


Fig. 13. Effects of loading eccentricity on the axial load-shortening curves of square CFDST columns.

$$\epsilon'_c = \frac{(\gamma_c f'_c)^{0.225}}{1000} \tag{9}$$

where f_{fp} stands for the lateral pressure on the core-concrete, which is computed by the following equation suggested by Liang and Fragomeni [39]:

$$f_{fp} = \begin{cases} 0.7(v_e - v_s) \frac{2t_i}{D_i - 2t_i} f_{syi} & \text{for } \frac{D_i}{t_i} \leq 47 \\ \left(0.006241 - 0.0000357 \frac{D_i}{t_i}\right) f_{syi} & \text{for } 47 < \frac{D_i}{t_i} \leq 150 \end{cases} \tag{10}$$

in which v_e and v_s stand for the Poisson's ratios of the steel tube with and without concrete infill. In the numerical analysis, $v_s = 0.5$ and the v_e suggested by Tang et al. [40] are adopted.

The equation formulated by Lim and Ozbakkaloglu [41] is used to describe the descending branch of the stress-strain responses of confined concrete as well as the unconfined one, and is expressed as

$$\sigma_c = f'_{cc} - \frac{f'_{cc} - f_{cr}}{\left[1 + \left(\frac{\epsilon_c - \epsilon_{ci}}{\epsilon_{ci} - \epsilon'_{cc}}\right)^{-2}\right]} \text{ for } \epsilon_c > \epsilon'_{cc} \tag{11}$$

in which f_{cr} denotes the residual strength of concrete and ϵ_{ci} the strain at the inflection point. The expressions suggested by Lim and Ozbakkaloglu [41] are used to determine f_{cr} for the core concrete while f_{cr} is

equal to $\beta_c f'_c$ for the sandwiched-concrete. By analyzing the available test data, Ahmed et al. [27] proposed β_c as

$$\beta_c = \begin{cases} 1 & \text{for } 0 \leq \frac{B_o}{t_o} \leq 24 \\ 1 - \frac{1}{15} \left(\frac{B_o}{t_o} - 24\right) & \text{for } 24 < \frac{B_o}{t_o} \leq 33 \\ 0.000062 \left(\frac{B_o}{t_o}\right)^2 - 0.011225 \left(\frac{B_o}{t_o}\right) + 0.705288 & \text{for } 33 < \frac{B_o}{t_o} \leq 100 \end{cases} \tag{12}$$

The strain (ϵ_{ci}) at the inflection point is specified as 0.007 for the sandwiched-concrete. The equation given by Lim and Ozbakkaloglu [41] is employed to calculate ϵ_{ci} for the core-concrete, taking into account the column size effect [27].

The stress-strain curves for concrete under tension is illustrated in Fig. 20, where the tensile strength is equal to $0.6 \sqrt{\gamma_c f'_c}$ and the ultimate tensile strain is taken as ten times the strain at cracking.

4.6. Curvature ductility index

The curvature ductility of a CFDST column in bending is expressed by the following curvature ductility indicator:

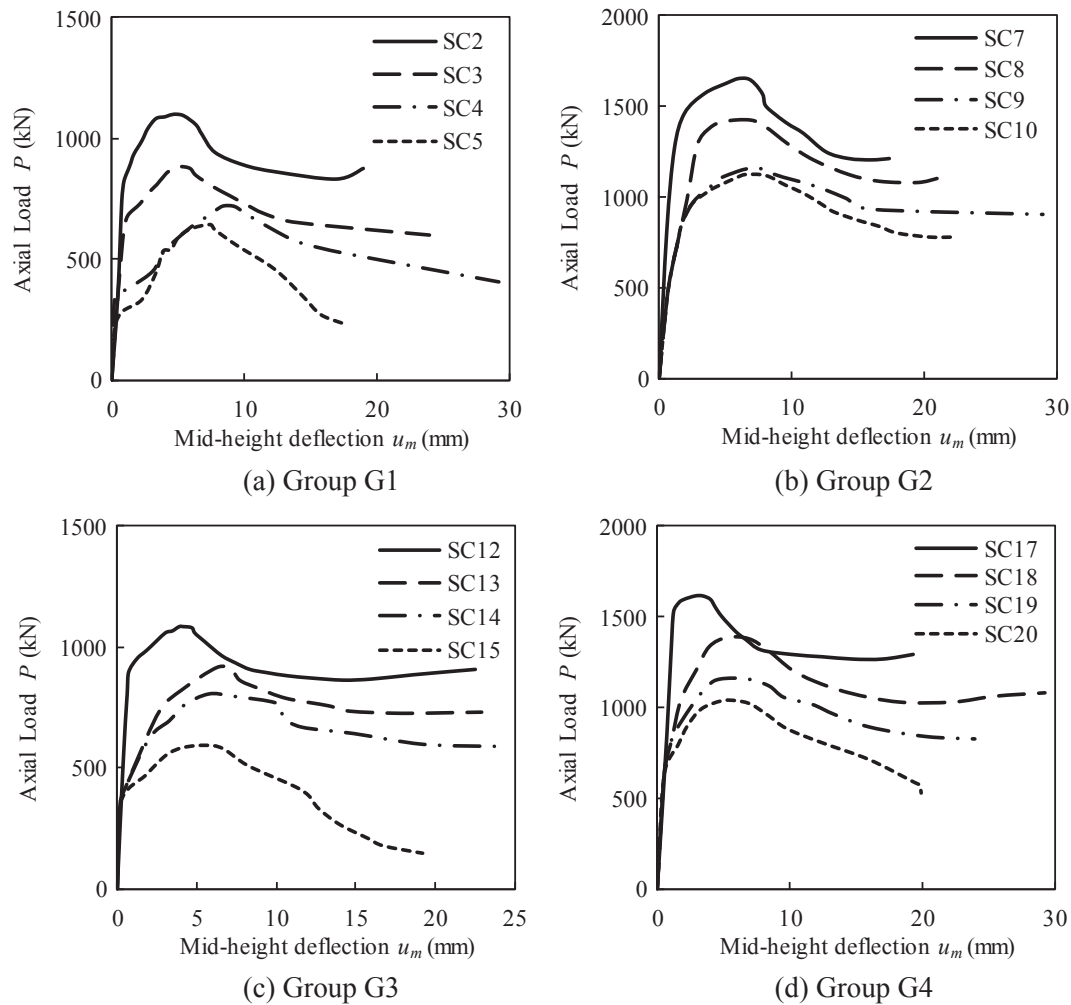


Fig. 14. Measured axial load-lateral deflection curves of square CFDST short columns under eccentric loading.

$$PI_{cd} = \frac{\phi_u}{\phi_y} \tag{13}$$

where ϕ_u represents the curvature of the CFDST column when the moment reduces to 90% of its ultimate moment capacity in the post-peak range or the ultimate curvature where column shows ascending moment-curvature relationships. The yield curvature (ϕ_y) is taken as $\phi_{0.75}/0.75$, where $\phi_{0.75}$ stands for the curvature when moment attains 75% of the column ultimate moment capacity.

5. Experimental verification

The mathematical modeling technique developed is validated by comparing the simulated strength envelopes with experimentally measured data in Fig. 21. The experimental ultimate moments were calculated as $M_{u,exp} = P_{u,exp} \times e$, where $P_{u,exp}$ denotes the ultimate axial load obtained from experiments provided in Table 1 and e stands for the loading eccentricity. In the moment-curvature analysis of each CFDST column, the ultimate concrete strain was taken as the concrete strain corresponding to the column ultimate axial load. It can be observed from Fig. 21 that the agreement between experimental results and numerical predictions is generally good. The ultimate moments of Specimens SC2 and SC7 obtained from the experiments are slightly higher than the computed results. The cause for this is likely due to the fact that the actual concrete strengths in the tested specimens were unknown and the average concrete strength was specified in the non-linear analyses. As shown in Fig. 21, the experimental ultimate bending

resistances of Specimens SC4, SC5 and SC15 are considerably lower than the predicted values. This is because Specimens SC4, SC5 and SC15 with large loading eccentricities failed prematurely by the damage of the column ends under the applied load as shown in Figs. 9 and 11. For columns subjected to a large loading eccentricity, it is suggested for future tests that a cantilever should be rigidly connected to the column ends to prevent the premature failure of the column ends. The limitation of the proposed numerical model is that it does not predict the premature failure of the loading heads.

6. Parametric study

The computer simulation program developed was used to determine the axial load-moment-curvature relationships and strength envelopes of square short CFDST columns with various width-to-thickness (B_o/t_o) ratios of the external tube, the diameter-to-thickness (D_i/t_i) ratio of the internal tube, concrete strength (f'_c), steel yield strength (f_{sy}), axial load ratio (P_u/P_o) and local buckling effects. The details of the reference CFDST column are as follows: $B_o = 500$ mm, $t_o = 10$ mm, $D_i = 250$ mm, $t_i = 5$ mm, $f_{syo} = f_{syi} = 350$ MPa, $E_s = 200$ GPa, $f'_{co} = f'_{ci} = 40$ MPa.

6.1. Effects of B_o/t_o ratio

The influences of the B_o/t_o ratio of the external square tube on the structural behavior of CFDST columns were examined by using the computational technique. The thickness of the reference column was varied to give the B_o/t_o ratios of 30, 50, 75 and 100 while the other

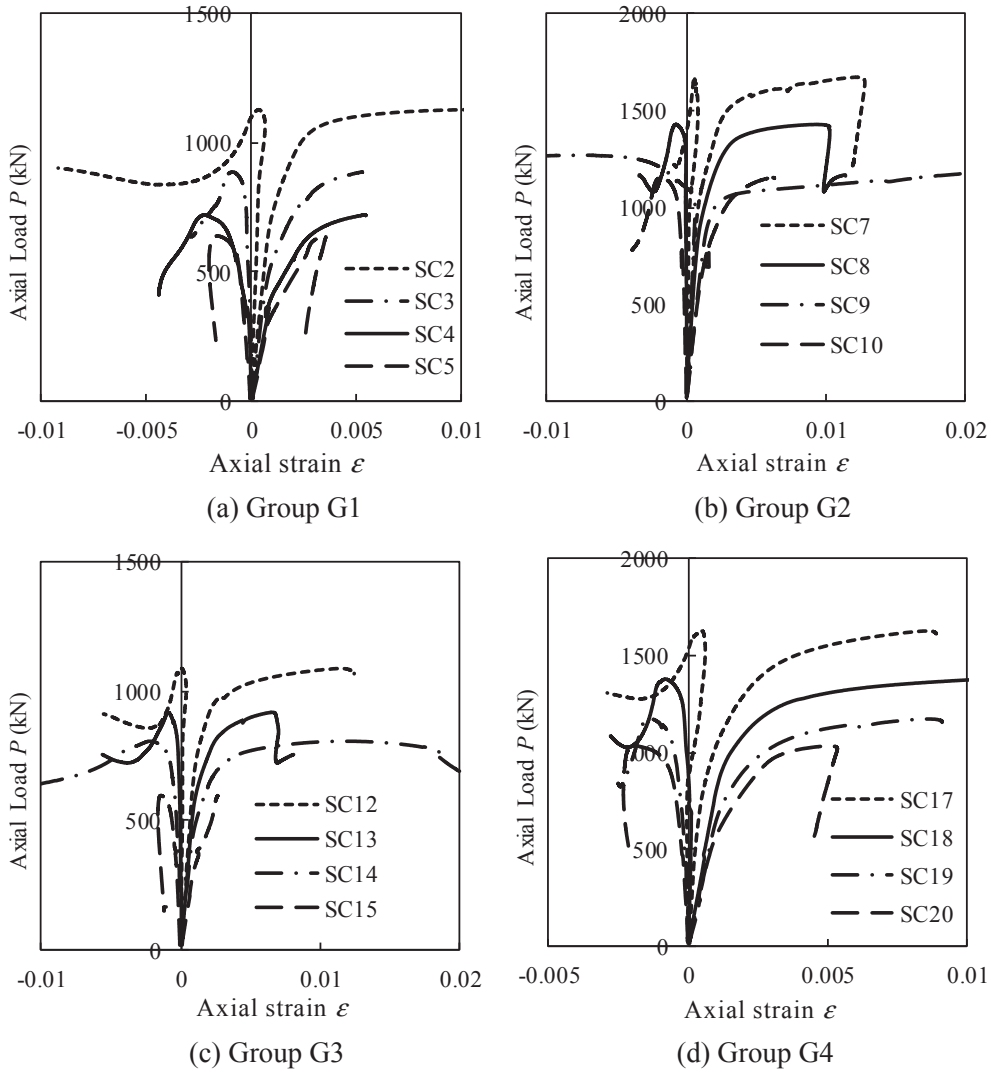


Fig. 15. Measured axial load-strain curves of square CFDST short columns under eccentric loading.

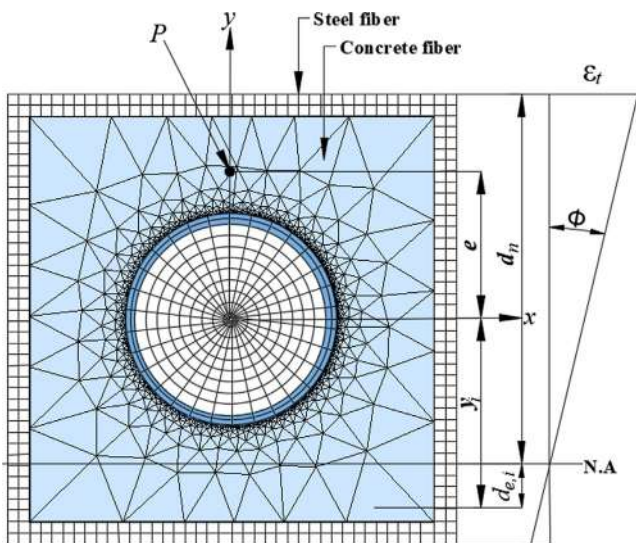


Fig. 16. Typical fiber discretization and strain distribution in the cross-section of square CFDST column.

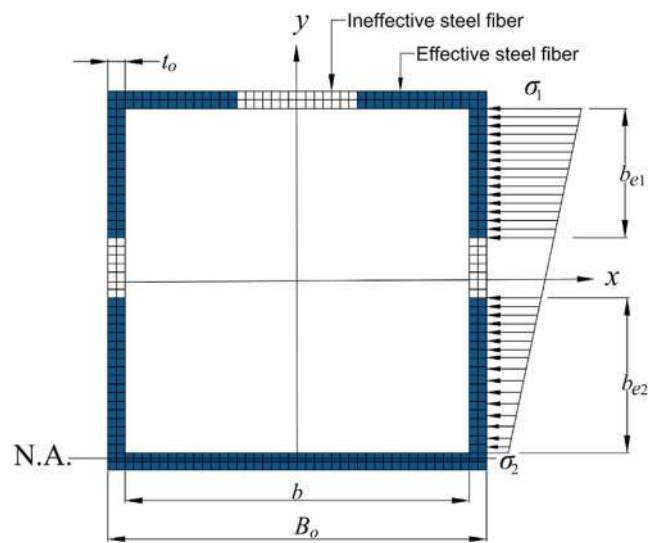


Fig. 17. Effective widths of the external steel tube of square CFDST column under eccentric loading.

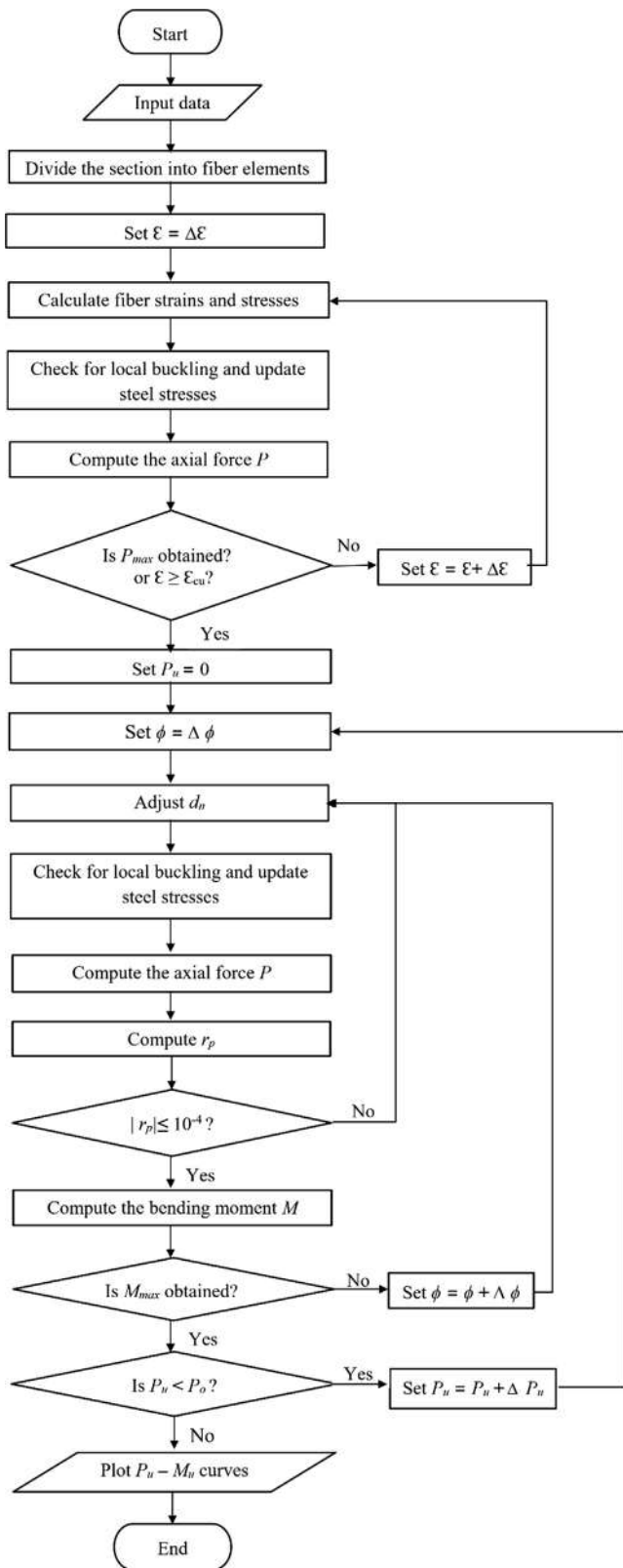


Fig. 18. Computer flowchart for calculating axial load-moment interaction curves.

parameters were unchanged. Fig. 22 presents the moment-curvature responses of the CFDST columns having various B_o/t_o ratios under a constant axial load (P_u), which was taken as 60% of the pure ultimate axial load of the column with the B_o/t_o ratio of 100. It is clearly shown

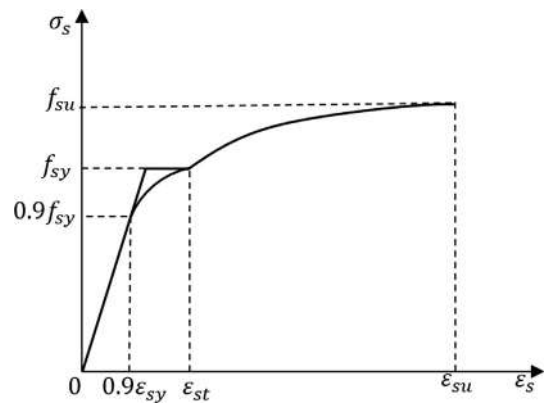


Fig. 19. Stress-strain curve for structural steels.

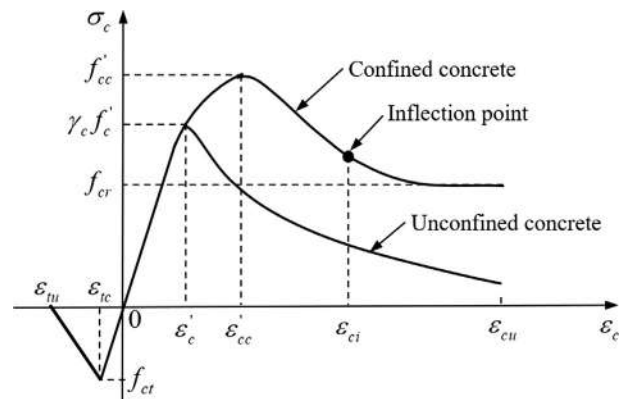


Fig. 20. Stress-strain curves for confined and unconfined concrete.

that increasing the B_o/t_o ratio remarkably reduces the column initial bending stiffness and ultimate moment capacity. This is due to the reduction in the thickness and area of the steel tube and because of local buckling. The reduction in the ultimate moment capacity was calculated as 66.9% by changing the B_o/t_o ratio from 30 to 100. The curvature ductility of CFDST columns also decreases as the B_o/t_o ratio increases. When increasing the B_o/t_o ratio from 30 to 50, 75 and 100, the curvature ductility index decreases from 4.62 to 3.75, 3.03 and 2.78, respectively. Furthermore, increasing the B_o/t_o ratio greatly reduces the pure ultimate axial load (P_o) and pure ultimate moment (M_o) of the CFDST columns as can be seen from the strength envelopes presented in Fig. 23. However, the B_o/t_o ratio has the most prominent influence on the pure ultimate bending resistance than on the pure ultimate axial load (P_o). Changing the B_o/t_o ratio from 30 to 100 reduces the pure ultimate axial load by 39.0% and the pure ultimate moment by 62.1%, respectively.

6.2. Effects of D_i/t_i ratio

The computer simulation program was employed to ascertain the significance of the D_i/t_i ratio on the responses of the CFDST columns. The D_i/t_i ratios of 20, 30, 40 and 50 were obtained by altering the thickness t_i of the internal tube only. Fig. 24 presents the influences of the D_i/t_i ratio on the axial load-moment-curvature behavior of CFDST columns under the axial load of $P_u = 9388$ kN. It would appear that the D_i/t_i ratio has a minor influence on the initial bending stiffness of CFDST columns. However, increasing the D_i/t_i ratio considerably reduces the column ultimate bending resistance. The column ultimate moment is reduced by 8.9%, 14.3% and 19.3%, respectively, by changing the D_i/t_i ratio from 20 to 30, 40 and 50. Varying the D_i/t_i ratio from 20 to 50 decreases the curvature ductility index from 5.46 to 3.35. The strength envelopes of CFDST columns as a function of D_i/t_i ratios are

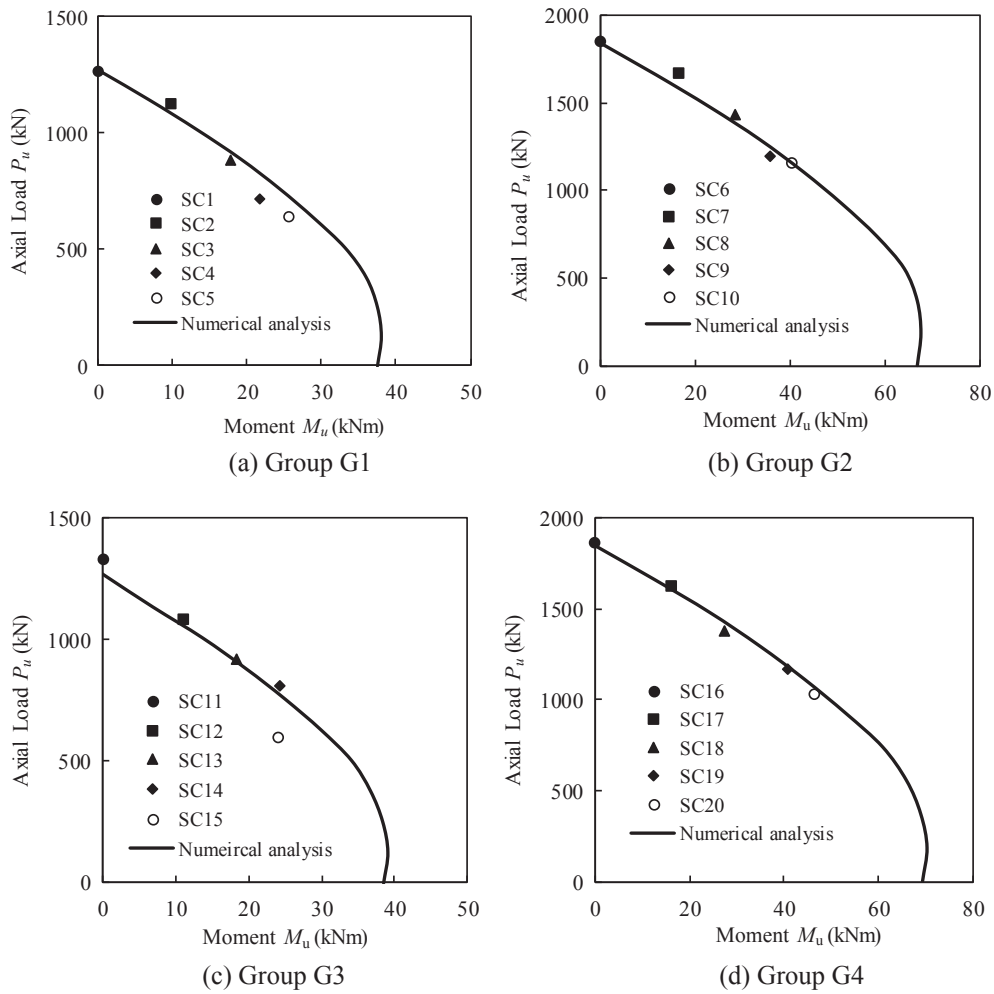


Fig. 21. Comparison of predicted strength envelopes of square CFDST columns with test results.

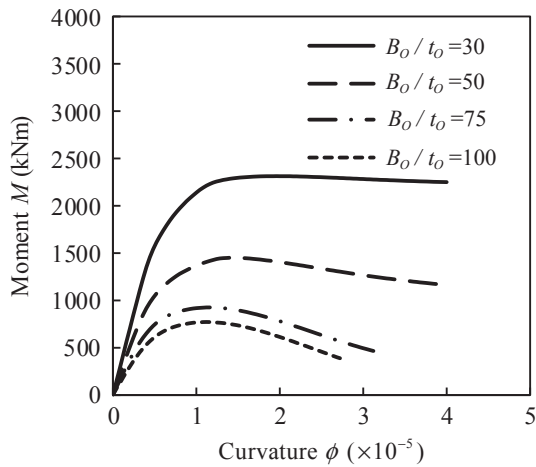


Fig. 22. Effects of B_o/t_o ratio on the moment-curvature curves of square CFDST columns.

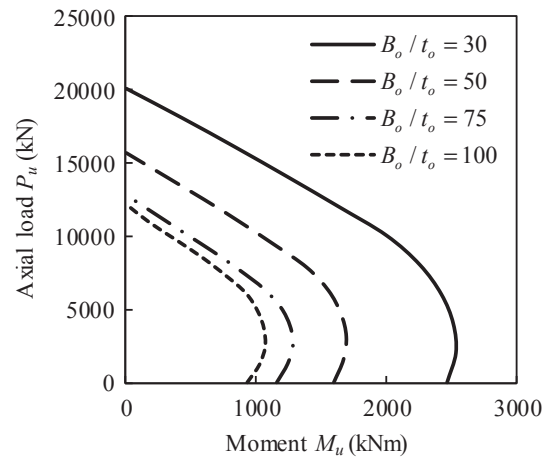


Fig. 23. Effects of B_o/t_o ratio on the strength envelopes of square CFDST columns.

given in Fig. 25. It is seen that the D_i/t_i ratio has a moderate influence on the column ultimate axial and bending resistances. When the D_i/t_i ratio is increased from 20 to 50, the column pure ultimate axial and bending strengths are found to reduce by 11% and 8.5%, respectively. This is because increasing the D_i/t_i ratio reduces the confinement exerted on the core-concrete, which reduces the column ultimate resistances.

6.3. Effects of steel yield strength

The sensitivities of the moment-curvature and interaction behavior of CFDST columns to the steel yield strength f_{sy} were investigated by varying f_{sy} from 250 MPa to 690 MPa. The predicted moment-curvature relationships of CFDST columns subjected to the same axial load of $P_u = 9388$ kN have been plotted in Fig. 26. It is discovered that the

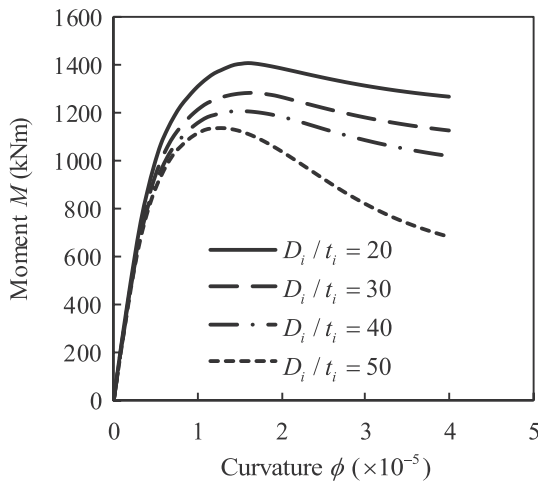


Fig. 24. Effects of D_i/t_i ratio on the moment-curvature curves of square CFDST columns.

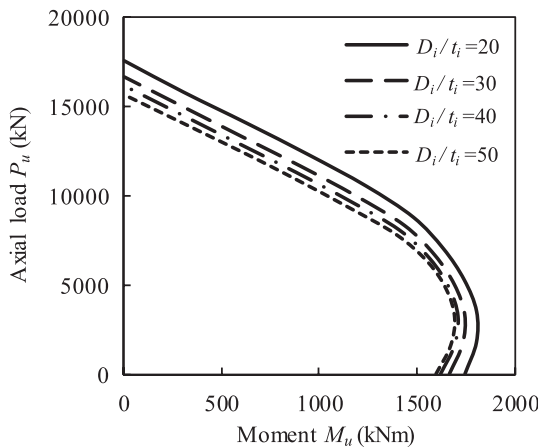


Fig. 25. Effects of D_i/t_i ratio on the strength envelopes of square CFDST columns.

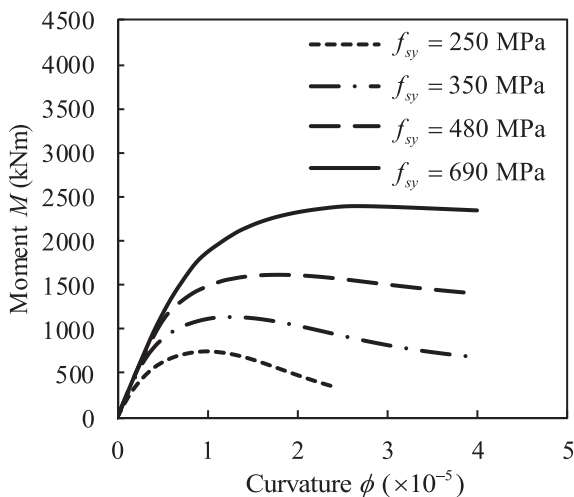


Fig. 26. Effects of steel yield strength on the moment-curvature curves of square CFDST columns.

initial bending stiffness and ultimate bending resistance of CFDST columns are markedly improved by using steel tube with higher yield strength. When altering the yield strength from 250 MPa to 350 MPa, 480 MPa and 690 MPa, the column bending resistance increases by 52.1%, 116.0%, and 220.1%, respectively. As shown in Fig. 26, the

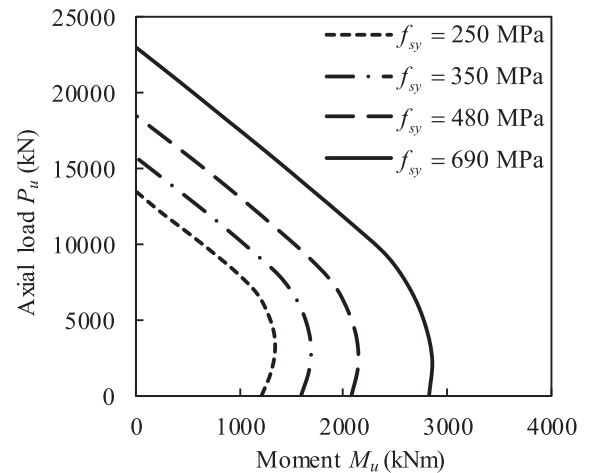


Fig. 27. Effects of steel yield strength on the strength envelopes of square CFDST columns.

column curvature ductility also improves as the yield strength increases. The calculated column curvature ductility indices with yield strengths of 250 MPa, 350 MPa and 480 MPa are 2.69, 3.35 and 4.34, respectively. Fig. 27 gives the strength envelopes of CFDST columns, which have been plotted by demonstrating the effect of steel yield strength. It is illustrated that the use of higher strength steel tube remarkably improves the ultimate bending and axial resistances of CFDST columns. The numerical results show that changing the yield strength from 250 MPa to 690 MPa leads to 70.5% improvement in the pure ultimate axial load and 133.2% increase in the pure ultimate bending resistance of the column.

6.4. Effects of concrete strength

Fiber analyses on CFDST short columns constructed by concrete with different compressive strengths were performed to ascertain the effects of concrete strength on their moment-curvature and interaction strength characteristics. The CFDST columns were made of concrete with strengths ranging from 40 MPa to 100 MPa. The simulated moment-curvature curves for the CFDST columns under a constant load of $P_u = 9388$ kN are provided in Fig. 28. The initial bending stiffness and ultimate bending resistance of CFDST columns are shown to considerably improve by using higher strength concrete. As a result of changing the concrete strength from 40 MPa to 100 MPa, the column

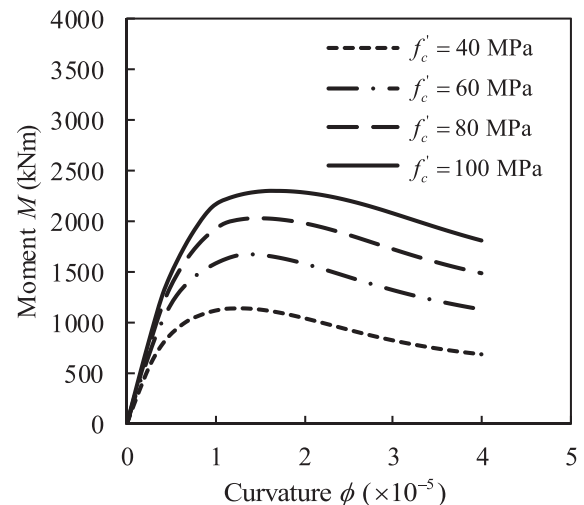


Fig. 28. Effects of concrete strength on the moment-curvature curves of square CFDST columns.

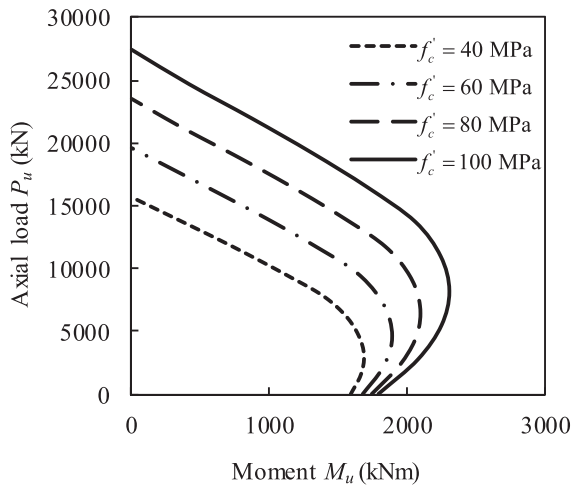


Fig. 29. Effects of concrete strength on the strength envelopes of square CFDST columns.

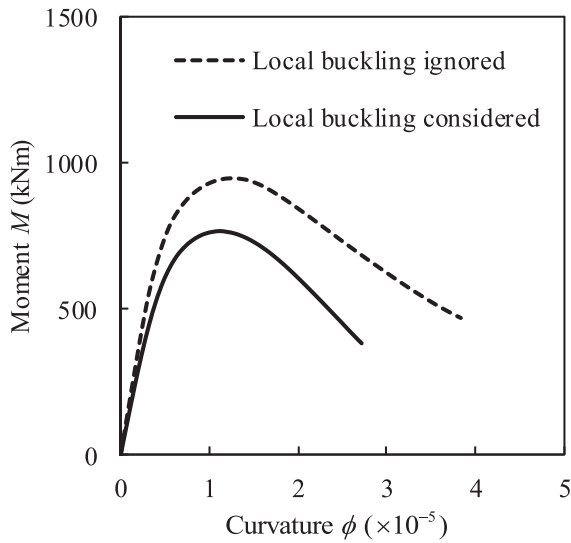


Fig. 30. Effects of the local buckling of the outer steel tube on the moment-curvature curves of square CFDST columns.

ultimate bending resistance increases by 102.3%. However, using higher strength concrete in CFDST columns decreases their curvature ductility. The column with 100 MPa concrete has a curvature ductility index of 2.9 while the column with 40 MPa concrete has a value of 3.35. Fig. 29 shows the complete axial load-bending resistance curves for CFDST columns with different concrete strengths. It is confirmed that using higher strength concrete improves both the ultimate bending and axial strengths of CFDST columns. However, the effect of concrete strength on the column pure ultimate axial load is more prominent than on its pure bending resistance. When the concrete strength is changed from 40 MPa to 100 MPa, the increase in the pure ultimate axial load and pure ultimate bending resistance is 75.8% and 12.9%, respectively.

6.5. Effects of local buckling

The local buckling effects on the axial load-moment-curvature and interaction responses of axial load and moment in the CFDST columns were ascertained by means of using the computational model proposed. The nonlinear analyses on the reference column with a B_o/t_o ratio of 100 were undertaken by ignoring and including local buckling, respectively. The local buckling effect on the moment-curvature behavior of the CFDST column under the axial load of $P_u = 7351$ kN is

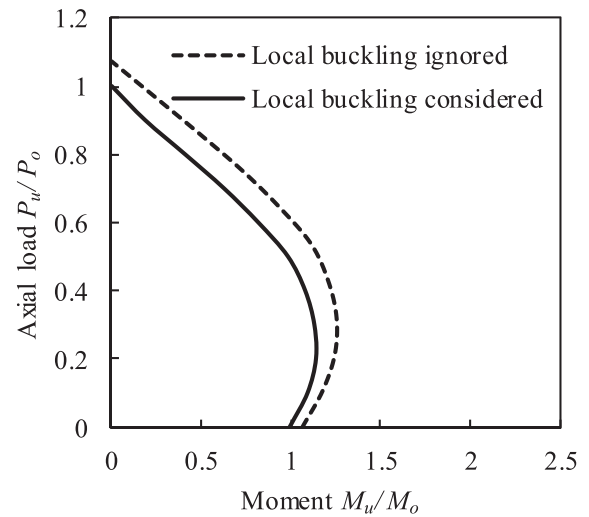


Fig. 31. Effects of the local buckling of the outer steel tube on the normalized strength envelopes of square CFDST columns.

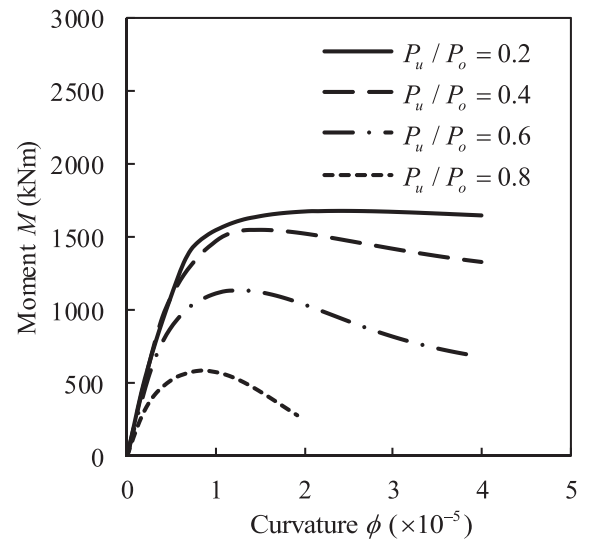


Fig. 32. Effects of axial load ratio on the moment-curvature curves of square CFDST columns.

demonstrated in Fig. 30. It is evident that the local buckling of the outer steel tube markedly reduces the column initial bending stiffness, ultimate bending resistance and curvature ductility. If the tube local buckling was not included in the analysis, the column ultimate bending resistance is overestimated by 23.6%. Fig. 31 illustrates the local buckling influence on the complete strength envelopes. It is confirmed that the interaction strengths of the CFDST column are markedly reduced by the outward local buckling. The column ultimate axial capacity and pure bending resistance are overestimated by 7.4% and 9.5%, respectively by ignoring the effect of local buckling.

6.6. Effects of axial load ratio

The significance of the axial load ratio (P_u/P_o) on the moment-curvature responses of CFDST beam-columns loaded eccentrically was examined by incorporating the axial load ratios from 0.2 to 0.8. The predicted moment-curvature responses have been plotted in Fig. 32. It is demonstrated that the influence of the axial load on the moment-curvature responses is remarkable. Increasing the axial load ratio significantly decreases the column initial bending stiffness, ultimate bending resistance and curvature ductility. The column ultimate

bending resistance is found to reduce by 7.7%, 32.4% and 65.1% by increasing the P_u/P_o ratio from 0.2 to 0.4, 0.6 and 0.8, respectively. For the axial load ratios of 0.2, 0.4, 0.6 and 0.8, the curvature ductility indices were estimated as 4.61, 4.35, 3.35 and 2.72, respectively. This means that the column curvature ductility reduces by 6%, 27% and 41%, respectively, as the P_u/P_o ratio increases from 0.2 to 0.4, 0.6 and 0.8.

7. Conclusions

Experimental and numerical investigations on the structural performance of square CFDST stub columns loaded eccentrically have been presented in this paper. The experimental failure modes and behavior of twenty square CFDST columns tested have been reported. A numerical model has been proposed for computing the axial load-moment-curvature relationships and interaction strengths of square CFDST stub columns incorporating local and post-local buckling. Efficient computational algorithms implementing the inverse quadratic method have been developed to obtain converged solutions. Good agreement between predictions and experimental data has been obtained. The computer model developed has been employed to perform a parametric study on the responses of CFDST columns considering important geometric and material parameters.

The following concluding remarks are given:

1. Square CFDST short columns loaded concentrically failed by the outward local buckling of the four walls of the external steel tube and the crushing of the sandwiched concrete. The CFDST columns tested under eccentric loading failed by the outward local buckling of the compression walls of the external steel tube, the crushing of the sandwiched-concrete and significant column bending. The core concrete in CFDST columns did not crush because the internal circular tube effectively confined the core-concrete.
2. Test results indicate that increasing the loading eccentricity markedly reduces the column ultimate loads as well as initial bending stiffness.
3. Numerical results demonstrate that the initial bending stiffness and ultimate axial and bending resistances of CFDST columns are remarkably decreased by increasing the B_o/t_o ratio and the axial load ratio but are only slightly decreased by increasing the D_i/t_i ratio.
4. Using higher yield strength tubes and high strength concrete appreciably improves the column initial bending stiffness, ultimate axial load and ultimate bending resistance, but the concrete strength has a more pronounced effect on the pure ultimate load than on the pure bending strength.
5. The unilateral local buckling of the outer steel tube considerably reduces the ultimate axial and bending resistances of CFDST columns.

Square CFDST columns composed of an inner circular steel tube offer great benefits, such as high strength, high stiffness, high ductility and ease of connecting with steel beams, and can be used in high-rise composite buildings. To maximize their strengths and stiffness while maintaining good ductility, CFDST beam-columns should be designed with small B_o/t_o ratios, high strength steel tubes, suitable D_i/t_i ratios so that the inner tube effectively confines the concrete-core and high strength concrete within the inner tube.

Acknowledgements

The financial support provided by Victoria University, Australia and La Trobe University, Australia to conduct the experiments described in this paper is gratefully acknowledged. The authors would like to thank the technicians at both Victoria University and the University of Wollongong, Australia, particularly Mr. Ritchie McLean and Mr. Duncan Best at the University of Wollongong, Australia, for their

assistance and help during the experiments.

References

- [1] Peng YY, Tan KF, Yao Y. Mechanical properties of duplex steel tube high-strength concrete short columns under axial compression. *J Wuhan Univ Technol* 2011;33(2):105–9. (In Chinese).
- [2] Liew JYR, Xiong DX. Ultra-high strength concrete filled composite columns for multi-storey building construction. *Adv Struct Eng* 2012;15(9):1487–503.
- [3] Hassanein MF, Kharoob OF, Liang QQ. Behaviour of circular concrete-filled lean duplex stainless steel-carbon steel tubular short columns. *Eng Struct* 2013;56:83–94.
- [4] Romero ML, Espinós A, Portolés J, Hospitaler A, Ibañez C. Slender double-tube ultra-high strength concrete-filled tubular columns under ambient temperature and fire. *Eng Struct* 2015;99:536–45.
- [5] Wan CY, Zha XX. Nonlinear analysis and design of concrete-filled dual steel tubular columns under axial loading. *Steel Compo Struct* 2016;20(3):571–97.
- [6] Ekmekyapar T, Al-Eliwi BJ. Concrete filled double circular steel tube (CFDCST) stub columns. *Eng Struct* 2017;135:68–80.
- [7] Ibañez C, Romero ML, Espinós A, Portolés JM, Albero V. Ultra-high strength concrete on eccentrically loaded slender circular concrete-filled dual steel columns. *Structures* 2017;12:64–74.
- [8] Romero ML, Ibañez C, Espinós A, Portolés J, Hospitaler A. Influence of ultra-high strength concrete on circular concrete-filled dual steel columns. *Structures* 2017;9:13–20.
- [9] Xiong MX, Xiong DX, Liew JYR. Axial performance of short concrete filled steel tubes with high-and ultra-high-strength materials. *Eng Struct* 2017;136:494–510.
- [10] Xiong MX, Xiong DX, Liew JYR. Behaviour of steel tubular members infilled with ultra high strength concrete. *J Constr Steel Res* 2017;138:168–83.
- [11] Zheng Y, He C, Zheng L. Experimental and numerical investigation of circular double-tube concrete-filled stainless steel tubular columns under cyclic loading. *Thin-Walled Struct* 2018;132:151–66.
- [12] Ahmed M, Liang QQ, Patel VI, Hadi MN. Numerical analysis of axially loaded circular high strength concrete-filled double steel tubular short columns. *Thin-Walled Struct* 2019;138:105–16.
- [13] Pei WJ. Research on Mechanical Performance of Multibarrel Tube-Confined Concrete Columns. ME Thesis, Chang'an University, Xian, China, 2005 (in Chinese).
- [14] Qian J, Zhang Y, Ji X, Cao W. Test and analysis of axial compressive behavior of short composite-sectioned high strength concrete filled steel tubular columns. *J Build Struct* 2011;32(12):162–9. (in Chinese).
- [15] Qian J, Zhang Y, Zhang W. Eccentric compressive behavior of high strength concrete filled double-tube short columns. *J Tsinghua Univ, Sci Technol* 2015;55(1):1–7. (in Chinese).
- [16] Wang ZB, Tao Z, Yu Q. Axial compressive behaviour of concrete-filled double-tube stub columns with stiffeners. *Thin-Walled Struct* 2017;120:91–104.
- [17] Zhong ST. Concrete Filled Steel Tubular Structures. Beijing: Tsinghua University Press; 2003. (in Chinese).
- [18] Han LH. Concrete Filled Steel Tubular Structures: Theory and Practice. Science Press, Beijing, 1st Edition, 2000; Second Edition, 2007 (in Chinese).
- [19] Sun YP, Kenji S. A comprehensive stress-strain model for high-strength concrete confined by circular transverse reinforcement. *Proc of the Sixth Inter Conf on Steel-Concrete Compo Struct*, Los Angeles, USA, 2000; 1067–1074.
- [20] Tao Z, Wang ZB, Yu Z. Finite element modelling of concrete-filled steel stub columns under axial compression. *J Constr Steel Res* 2013;89(10):121–31.
- [21] Uy B. Local and post-local buckling of concrete filled steel welded box columns. *J Constr Steel Res* 1998;47(1–2):47–72.
- [22] Liang QQ, Uy B. Theoretical study on the post-local buckling of steel plates in concrete-filled box columns. *Comput Struct* 2000;75(5):479–90.
- [23] Liang QQ, Uy B, Liew JR. Nonlinear analysis of concrete-filled thin-walled steel box columns with local buckling effects. *J Constr Steel Res* 2006;62(6):581–91.
- [24] Liang QQ, Uy B, Liew JYR. Local buckling of steel plates in concrete-filled thin-walled steel tubular beam-columns. *J Constr Steel Res* 2007;63(3):396–405.
- [25] Huang Z, Li D, Uy B, Thai H-T, Hou C. Local and post-local buckling of fabricated high-strength steel and composite columns. *J Constr Steel Res* 2019;154:235–49.
- [26] Song Y, Li J, Chen YY. Local and post-local buckling of normal/high strength steel sections with concrete infill. *Thin-Walled Struct* 2019;138:155–69.
- [27] Ahmed M, Liang QQ, Patel VI, Hadi MNS. Nonlinear analysis of rectangular concrete-filled double steel tubular short columns incorporating local buckling. *Eng Struct* 2018;175:13–26.
- [28] Ahmed M, Liang QQ, Patel VI, Hadi MNS. Local-global interaction buckling of square high strength concrete-filled double steel tubular slender beam-columns. *Thin-Walled Struct* 2019;143:106244.
- [29] Ky VS, Tangaramvong S, Thepchatri T. Inelastic analysis for the post-collapse behavior of concrete encased steel composite columns under axial compression. *Steel Compo Struct* 2015;19:1237–58.
- [30] Liu X, Bradford MA, Erkmen RE. Non-linear inelastic analysis of steel-concrete composite beams curved in-plan. *Eng Struct* 2013;57:484–92.
- [31] AS 1391. *Metallic Materials-Tensile Testing at Ambient Temperature*. Standards Australia, Sydney, NSW, Australia, 2007.
- [32] Hadi MNS, Widiarsa IBR. Axial and flexural performance of square RC columns wrapped with CFRP under eccentric loading. *J Compos Constr ASCE* 2012;16(6):640–9.
- [33] Liang QQ. Performance-based analysis of concrete-filled steel tubular beam-columns, part I: theory and algorithms. *J Constr Steel Res* 2009;65(2):363–72.
- [34] Liang QQ. Performance-based analysis of concrete-filled steel tubular

- beam-columns, part II: verification and applications. *J Constr Steel Res* 2009;65(2):351–62.
- [35] Persson P-O, Strang G. A simple mesh generator in MATLAB. *SIAM Rev* 2004;46(2):329–45.
- [36] Epperson JF. *An Introduction to Numerical Methods and Analysis*. Wiley-Interscience; 2007.
- [37] Mander JB. *Seismic design of bridge piers*. Ph.D. Thesis, Department of Civil Engineering, Christchurch, New Zealand: University of Canterbury; 1983.
- [38] Mander JB, Priestley MJ, Park R. Theoretical stress-strain model for confined concrete. *J Struct Eng ASCE* 1988;114(8):1804–26.
- [39] Liang QQ, Fragomeni S. Nonlinear analysis of circular concrete-filled steel tubular short columns under axial loading. *J Constr Steel Res* 2009;65(12):2186–96.
- [40] Tang J, Hino S, Kuroda I, Ohta T. Modeling of stress-strain relationships for steel and concrete in concrete filled circular steel tubular columns. *Steel Constr Eng, JSSC* 1996;3(11):35–46.
- [41] Lim JC, Ozbakkaloglu T. Stress-strain model for normal-and light-weight concretes under uniaxial and triaxial compression. *Constr Build Mater* 2014;71:492–509.

Experimental and numerical investigations of eccentrically loaded rectangular concrete-filled double steel tubular columns by M. Ahmed, Q.Q. Liang, V.I. Patel, and M.N.S. Hadi was published in the peer review journal, *Journal of Constructional Steel Research*, 167, 2020.

The full-text of this article is subject to copyright restrictions, and cannot be included in the online version of the thesis.

The published version is available from: <https://doi.org/10.1016/j.jcsr.2020.105949>

3.2 CONCLUDING REMARKS

Numerical and experimental studies on the behavior of square and rectangular CFDST stub columns with either an inner circular tube or a rectangular/square inner tube have been reported in this chapter. New constitutive relationship for modeling the concrete post-peak behavior has been derived. The computer modeling method incorporating this new relationship and local buckling has been found to predict well the experimental behavior of CFDST rectangular columns having an internal circular tube. The design formulas proposed have yielded accurate calculations of the capacities of CFDST stub columns. The experimental results presented have provided new insight into the failure modes, load-deformation characteristics and the capacities of rectangular and square CFDST short columns. The numerical models incorporating local buckling and confinement have been formulated to predict the moment-curvature relationships in addition to the strength envelopes of short CFDST columns loaded eccentrically. New computer solution algorithms, which have implemented the inverse quadratic method, have been developed to solve the nonlinear dynamic equilibrium equations of eccentrically loaded CFDST columns. It has been shown the computer modeling methods developed can predict well the responses of CFDST composite columns and have been used to conduct parametric studies.

Chapter 4

CIRCULAR CFDST SHORT COLUMNS

4.1 INTRODUCTION

This chapter presents numerical and experimental research studies on the behavior of circular CFDST columns composed of a circular internal tube. A new confinement model of the core-concrete of circular CFDST stub columns and a new strength degradation coefficient for the post-peak concrete strength are proposed by interpreting the existing test data and incorporated in the computational model developed for quantifying the axial strain responses of CFDST circular columns to concentric loads. An extensive parameter study is performed to examine the behavior of such composite columns under axial load. A design formula is proposed for the calculation of the capacity of CFDST columns under axial compression. Experimental programs on the behavior of short CFDST circular columns loaded either concentrically or eccentrically are presented. The tests examine the influences of loading application (axial and eccentric), diameter-to-thickness ratios of steel sections as well as loading eccentricity on the structural performance of CFDST circular columns. A mathematical model is also developed for simulating the moment and curvature relationships as well as the strength envelopes of eccentrically loaded CFDST circular short columns, incorporating the proposed confinement model and strength degradation factor. The computer simulation model is employed to ascertain the effects

of design variables on the moment-curvature responses, strength interaction envelopes and moment distributions in concrete and steel components of CFDST short columns.

This chapter includes the following papers:

1. **Ahmed, M.**, Liang, Q. Q., Patel, V. I. and Hadi, M. N. (2019). Numerical analysis of axially loaded circular high strength concrete-filled double steel tubular short columns. *Thin-Walled Structures*, 138, 105-116.
2. **Ahmed, M.**, Liang, Q. Q., Patel, V. I. and Hadi, M. N. S. (2019). Behavior of eccentrically loaded double circular steel tubular short columns filled with concrete. *Engineering Structures*, 201, 109790.

OFFICE FOR RESEARCH TRAINING, QUALITY AND INTEGRITY

DECLARATION OF CO-AUTHORSHIP AND CO-CONTRIBUTION: PAPERS INCORPORATED IN THESIS

This declaration is to be completed for each conjointly authored publication and placed at the beginning of the thesis chapter in which the publication appears.

Title of
Paper/Journal/Book:

Ahmed, M., Liang, Q. Q., Patel, V. I. and Hadi, M. N. S. (2019). Numerical analysis of axially loaded circular high strength concrete-filled double steel tubular short columns. *Thin-Walled Structures*, 138: 105-116.

Surname:

First
name:

Institute:

Candidate's Contribution (%):

Status:

Accepted and in press:

Date:

Published:

Date:

2. CANDIDATE DECLARATION

I declare that the publication above meets the requirements to be included in the thesis as outlined in the HDR Policy and related Procedures – policy.vu.edu.au.

Mizan Ahmed Digitally signed by Mizan Ahmed
Date: 2019.12.18 12:52:06 +11'00'

18-12-2019

Signature

Date

3. CO-AUTHOR(S) DECLARATION

In the case of the above publication, the following authors contributed to the work as follows:

The undersigned certify that:

1. They meet criteria for authorship in that they have participated in the conception, execution or interpretation of at least that part of the publication in their field of expertise;
2. They take public responsibility for their part of the publication, except for the responsible author who accepts overall responsibility for the publication;

3. There are no other authors of the publication according to these criteria;
4. Potential conflicts of interest have been disclosed to a) granting bodies, b) the editor or publisher of journals or other publications, and c) the head of the responsible academic unit; and
5. The original data will be held for at least five years from the date indicated below and is stored at the following **location(s)**:

R:\CFDST Columns

Name(s) of Co-Author(s)	Contribution (%)	Nature of Contribution	Signature	Date
Mizan Ahmed	60	Methodology, Software, Validation, Formal analysis, Investigation, Data curation, Writing–Original draft, Visualization.	Mizan Ahmed Digitally signed by Mizan Ahmed Date: 2019.12.18 12:52:18 +11'00'	18-12-2019
Qing Quan Liang	20	Conceptualization, Methodology, Software, Validation, Writing–Review and Editing, Supervision, Project administration.	Qing Quan Liang Digitally signed by Qing Quan Liang Date: 2019.12.18 13:13:26 +11'00'	18-12-2019
Vipulkumar I. Patel	10	Validation, Writing–Review and Editing, Supervision.	Vipul Patel Digitally signed by Vipul Patel Date: 2019.12.18 13:32:19 +11'00'	18-12-2019
Muhammad N.S. Hadi	10	Validation, Writing–Review and Editing, Supervision.	Muhammad Hadi Digitally signed by Muhammad Hadi DN: cn=Muhammad Hadi, o=University of Wollongong, ou=School of CME, email=mhadi@uow.edu.au, c=AU Date: 2019.12.18 14:49:06 +11'00'	18-12-2019

OFFICE FOR RESEARCH TRAINING, QUALITY AND INTEGRITY

DECLARATION OF CO-AUTHORSHIP AND CO-CONTRIBUTION: PAPERS INCORPORATED IN THESIS

This declaration is to be completed for each conjointly authored publication and placed at the beginning of the thesis chapter in which the publication appears.

Title of
Paper/Journal/Book:

Ahmed, M., Liang, Q. Q., Patel, V. I. and Hadi, M. N. S. (2019). Behavior of eccentrically loaded double circular steel tubular short columns filled with concrete. Engineering Structures, 201, 109790.

Surname:

First
name:

Institute:

Candidate's Contribution (%):

Status:

Accepted and in press:

Date:

Published:

Date:

2. CANDIDATE DECLARATION

I declare that the publication above meets the requirements to be included in the thesis as outlined in the HDR Policy and related Procedures – policy.vu.edu.au.

Mizan Ahmed Digitally signed by Mizan Ahmed
Date: 2019.12.18 12:56:10 +11'00'

Signature

18-12-2019

Date

3. CO-AUTHOR(S) DECLARATION

In the case of the above publication, the following authors contributed to the work as follows:

The undersigned certify that:

1. They meet criteria for authorship in that they have participated in the conception, execution or interpretation of at least that part of the publication in their field of expertise;
2. They take public responsibility for their part of the publication, except for the responsible author who accepts overall responsibility for the publication;

3. There are no other authors of the publication according to these criteria;
4. Potential conflicts of interest have been disclosed to a) granting bodies, b) the editor or publisher of journals or other publications, and c) the head of the responsible academic unit; and
5. The original data will be held for at least five years from the date indicated below and is stored at the following **location(s)**:

R:\CFDST Columns

Name(s) of Co-Author(s)	Contribution (%)	Nature of Contribution	Signature	Date
Mizan Ahmed	60	Methodology, Software, Validation, Formal analysis, Investigation, Data curation, Writing–Original draft, Visualization.	Mizan Ahmed Digitally signed by Mizan Ahmed Date: 2019.12.18 12:56:21 +11'00'	18-12-2019
Qing Quan Liang	20	Conceptualization, Methodology, Software, Validation, Writing–Review and Editing, Supervision, Project administration, Funding acquisition.	Qing Quan Liang Digitally signed by Qing Quan Liang Date: 2019.12.18 13:21:11 +11'00'	18-12-2019
Vipulkumar I. Patel	10	Validation, Writing–Review and Editing, Supervision, Funding acquisition.	Vipul Patel Digitally signed by Vipul Patel Date: 2019.12.18 13:40:38 +11'00'	18-12-2019
Muhammad N.S. Hadi	10	Validation, Investigation, Writing–Review and Editing, Supervision.	Muhammad Hadi Digitally signed by Muhammad Hadi DN: cn=Mohammad Hadi, o=University of Wollongong, ou=School of CME, email=mhadi@uow.edu.au, c=AU Date: 2019.12.18 14:53:06 +11'00'	18-12-2019



Full length article

Numerical analysis of axially loaded circular high strength concrete-filled double steel tubular short columns



Mizan Ahmed^a, Qing Quan Liang^{a,*}, Vipulkumar Ishvarbhai Patel^b, Muhammad N.S. Hadi^c

^a College of Engineering and Science, Victoria University, PO Box 14428, Melbourne, VIC 8001, Australia

^b School of Engineering and Mathematical Sciences, La Trobe University, Bendigo, VIC 3552, Australia

^c School of Civil, Mining and Environmental Engineering, University of Wollongong, Wollongong, NSW 2522, Australia

ARTICLE INFO

Keywords:

Concrete-filled double steel tubes
Composite columns
High-strength concrete
Numerical modeling

ABSTRACT

Circular high-strength concrete-filled double steel tubular (CFDST) columns are high performance members where the internal and external steel tubes offer significant confinement to the concrete infill. The confinement remarkably improves the concrete compressive strength and ductility. However, no fiber element models have been formulated for computing the responses of CFDST columns with circular steel tubes filled with high-strength concrete incorporating accurate confinement to the core and sandwiched concrete. In this paper, a new fiber-based numerical model is developed that computes the axial load-strain responses of circular high-strength CFDST short columns under axial loading. Based on existing experimental results, a new confining pressure model is developed for the determination of the confining pressures on the core-concrete in CFDST columns with circular sections. A new strength degradation parameter is also proposed that allows the concrete post-peak characteristics to be quantified. The fiber-based numerical model validated by experimental data is used to assess the responses of high-strength CFDST columns considering important parameters, which include the inner steel tube, external tube diameter-to-thickness ratio and concrete and steel strengths. A simple expression is derived for the estimation of the axial load-carrying capacities of circular short CFDST columns and comparisons with several design codes are made. The proposed fiber-based analysis technique and design equation can accurately determine the responses of short circular high-strength CFDST columns.

1. Introduction

A circular concrete-filled double steel tubular (CFDST) column is fabricated by means of filling concrete into two concentrically-placed circular hollow steel tubes as illustrated in Fig. 1. The CFDST columns have higher ductility and strength performance than conventional circular concrete-filled steel tubular (CFST) columns because the internal steel tube offers additional confinement to the core-concrete. In addition, CFDST columns could be constructed by high-strength concrete that allows further improvement in the column ultimate strengths, but its brittleness affects the ductility of the columns. Analytical and experimental investigations on circular high-strength CFDST columns constructed by carbon steel tubes have been very limited. The confinement induced by the inner and external steel tubes to the core-concrete in CFDST columns with circular sections has not been fully understood and quantified. Furthermore, limited studies on CFDST columns have not resulted in the development of appropriate design specifications in international standards for circular CFDST columns.

Therefore, it is important to propose an accurate numerical model that can accurately quantify the confinement effects in circular CFDST columns to determine the behavior of CFDST columns and propose design recommendation based on numerical solutions.

The performance of CFST columns made of circular and rectangular sections has been studied by means of conducting experiments [1–6]. Portolés et al. [3] performed tests on slender circular CFST columns exposed to eccentric loadings. It was observed from the tests that the high-strength concrete increased the strength of shorter columns under small load eccentricities. However, increasing the end eccentricity improved the column ductility. Their comparative studies showed that the strengths of eccentrically-loaded slender CFST columns calculated by the design approach given in Eurocode 4 [7] were conservative compared to test data. Similar conclusions were given by O'Shea and Bridge [4] for circular CFST short columns under combined actions. Xiong et al. [6] studied the experimental behavior of short CFST circular columns constructed by means of using ultra-high-strength concrete (UHSC). They reported that UHSC CFST short columns attained their

* Corresponding author.

E-mail address: Qing.Liang@vu.edu.au (Q.Q. Liang).

<https://doi.org/10.1016/j.tws.2019.02.001>

Received 21 September 2018; Received in revised form 16 January 2019; Accepted 1 February 2019

0263-8231/© 2019 Elsevier Ltd. All rights reserved.

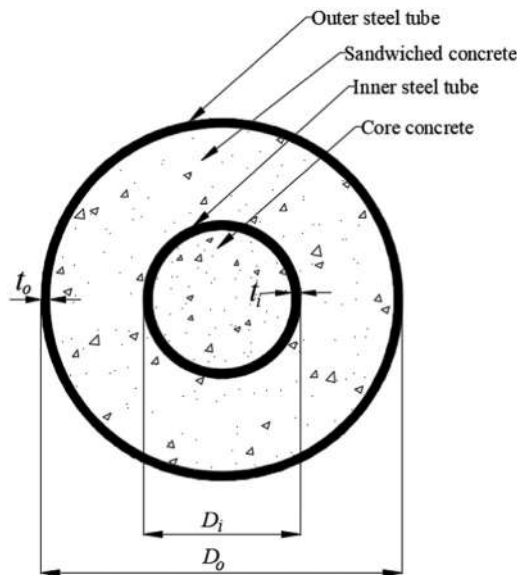


Fig. 1. Cross-section of circular CFST column.

ultimate axial strengths at small strains before the core-concrete was confined by the steel tubes. In addition, the applied loads on the UHSC CFST columns dropped sharply after the maximum load had been attained owing to the brittleness of high-strength concrete.

In comparisons with experimental studies on CFST columns, only limited experimental investigations on CFST columns with circular sections were performed by researchers, such as Xiong et al. [6], Peng et al. [8], Liew and Xiong [9], Romero et al. [10], Wan and Zha [11], Ekmekyapar and Al-Eliwi [12] and Ibañez et al. [13]. Peng et al. [8] tested axially-loaded short CFST circular columns to failure. The cube strengths of the filled concrete in these specimens varied from 66 MPa to 102 MPa. The diameter-to-thickness (D_o/t_o) ratios of the external tube varied from 27 to 65.4 and the internal steel tube D_i/t_i ratios ranged from 14.1 to 22.8. Experimental observations indicated that the column ultimate strengths were reduced by increasing the D_o/t_o ratios of the outer tube. Xiong et al. [6] conducted experiments on circular CFST short columns where ultra-high-strength concrete was employed. The yield stress of inner and outer tubes was up to 428 MPa. The compressive cylindrical strengths of the filled concrete varied from 51 to 184 MPa. It was found that CFST short columns with circular sections had higher axial strengths than circular CFST short columns. Liew and Xiong [9] and Romero et al. [10] reported that the performance of CFST columns was dependent on the sectional configurations of steel tubes. Filling the inner tube with ultra-high-strength concrete and the external tube with normal-strength concrete resulted in considerable improvement in the column ultimate axial strengths with superior ductility than any other combinations of concrete strength. Chang et al. [14] and Zheng et al. [15] undertook experiments on short concrete-filled stainless steel-carbon steel tubular (CFSCST) circular columns where the outer circular tube was constructed by stainless steel and the internal circular tube was made of carbon steel. Although CFSCST columns can be regarded as another form of CFST columns, their behavior sustainably differs from that of CFST columns.

Computational models were proposed that calculated the responses of CFST columns and double-skin CFST columns with circular sections by researchers [16–24]. Hu et al. [16], Liang and Fragomeni [18], and Lai and Varma [21] proposed confinement models for the determination of the lateral confining pressures and the post-peak strength degradation of core concrete and implemented them in the nonlinear analysis procedures for CFST columns with circular sections. Numerical studies on CFSCST columns made of circular sections were undertaken by Chang et al. [14] and Hassanein et al. [23,24]. In these

investigations, the finite element program ABAQUS was employed to create 3D models for the nonlinear analysis of CFSCST columns. The confinement models proposed for the concrete core in circular CFST columns were employed to determine the confinement induced by the internal and external tubes to the core-concrete in CFSCST columns. The stress-strain model for stainless steel obtained by the tensile coupon tests was applied to the external stainless-steel tube [25]. However, Quach et al. [26] reported that the compressive stress-strain responses of stainless steels is greatly different from the tension behavior. The adoption of the constitutive model for stainless steel based on the tensile coupon tests may lead to the underestimation of the ultimate loads of CFSCST circular columns [19].

Numerical studies on circular CFST short column constructed by carbon steel tubes have been extremely scarce [11,27]. Wan and Zha [11] proposed a confining pressure model and a softening reduction factor as a function of confining factors for determining the post-peak responses of concrete in CFST columns. However, it was found that the computed axial load-strain curves deviated considerably from experimental data. This highlights that further studies on the confinement mechanism are necessary and important in order to determine the actual responses of CFST columns constructed by circular sections. Ahmed et al. [28] formulated a fiber-based mathematical model for short CFST columns where the external tube was rectangular and the internal tube was circular. The local buckling of rectangular steel tube and concrete confinement were considered. The fiber analysis technique was demonstrated to simulate well the responses of rectangular short CFST columns.

The above literature review shows that no fiber-based mathematical models have been proposed for the simulation of concentrically-loaded circular CFST short columns constructed by carbon steel tubes. To accurately determine the responses of short CFST columns made of circular sections, an accurate confinement model recognizing the effects of material properties and geometry of CFST circular sections needs to be developed. In this paper, a fiber-based numerical method is formulated for the simulation of the axial behavior of CFST columns with circular sections filled with high-strength concrete incorporating concrete confinement. A new formula is proposed based on experimental results for evaluating the confining pressures on the core-concrete. An expression for the estimation of the residual concrete strength in the post-yield regime is also given. Verified by experimental results, the numerical technique is utilized to undertake a parametric study on the behavior of CFST columns. An expression is given for calculating the column ultimate axial strengths and compared with experimental data and several design codes.

2. The fiber-based numerical model

A numerical modeling technique has been proposed based on fiber element formulations for the determination of the performance of short CFST columns made of circular sections subjected to concentric axial loading. A column having a slenderness ratio (L/r) less than 22 is defined as a short column whose strengths are governed by its section capacities [29]. The method of fiber analysis is computationally efficient and accurate numerical technique for composite columns [28–32]. The method discretizes the cross-section of the CFST column into many small fiber elements as illustrated in Fig. 2. Steel fibers are assigned to steel material properties while concrete fibers are assigned to concrete material properties. The assumptions of the mathematical formulation are: (a) the bond at the interface of the steel tubes and concrete is perfect; (b) the strain is linearly distributed through the cross-sectional depth; and (c) the concrete shrinkage and creep are ignored. The computational procedure starts with initializing a small strain and then calculating the fiber stresses by means of employing the uniaxial stress-strain models for concrete and steel materials. The axial force P is computed by integrating stresses over the column cross-section. The analysis is repeated by incrementally increasing the axial

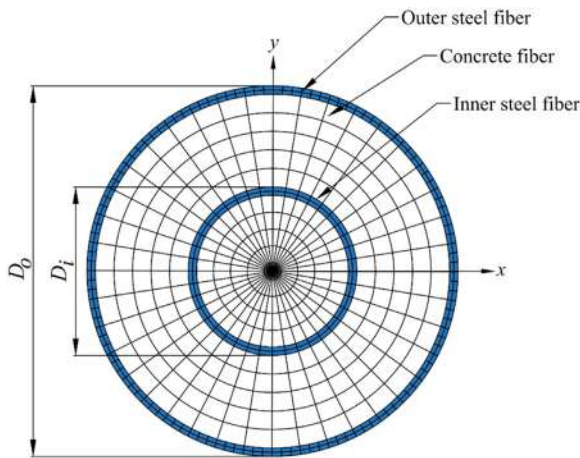


Fig. 2. Typical discretization of circular CFDST column section in the fiber element analysis.

strain until the axial load drops to 50% of the column ultimate axial load or the specified ultimate concrete strain ϵ_{cu} is exceeded.

The ductility of a CFDST column in axial compression is expressed by the following indicator:

$$PI_{sd} = \frac{\epsilon_u}{\epsilon_y} \tag{1}$$

in which ϵ_u is the strain at the axial load that falls to 90% of the column ultimate strength in the post-peak range or the ultimate strain in the post-yield ascending stress-strain branch. The yield strain ϵ_y is calculated as $\epsilon_{0.75}/0.75$, where $\epsilon_{0.75}$ represents the strain under the axial load that achieves 75% of the column ultimate axial load in the ascending branch [22,33,34]

3. Material model for steel tubes

The internal and external steel tubes in a CFDST column with circular section are under biaxial stresses resulting from the longitudinal compression and either hoop compression or tension which lowers the yield stress of the steel tubes. To consider this effect, the yield stress is reduced by a factor of 0.9 in the constitutive model for structural steels as shown in Fig. 3. The parabolic curve in the strain range of $0.9\epsilon_{sy} < \epsilon_s \leq \epsilon_{st}$ applied to cold-formed steels is defined using the expression proposed by Liang [30] as

$$\sigma_s = f_{sy} \left(\frac{\epsilon_s - 0.9\epsilon_{sy}}{\epsilon_{st} - 0.9\epsilon_{sy}} \right)^{\frac{1}{4.5}} \tag{2}$$

where σ_s denotes the axial steel stress; ϵ_s represents the axial steel strain; f_{sy} stands for the steel yield strength; ϵ_{sy} is the yield strain; and ϵ_{st} is the

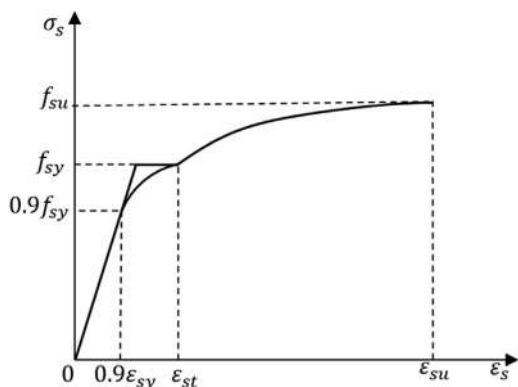


Fig. 3. General material stress-strain curve for structural steels.

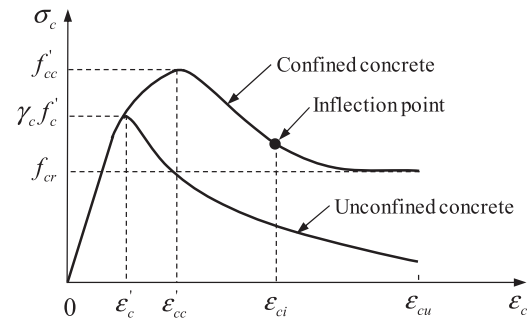


Fig. 4. Stress-strain curves for confined concrete in circular CFDST columns.

strain at the onset of strain-hardening

and is taken as 0.005 in the present study.

The equations given by Mander [35] are utilized to calculate the stress from the axial strain when the strain is in the range of $\epsilon_{st} < \epsilon_s \leq \epsilon_{su}$, written as

$$\sigma_s = f_{su} - \left(\frac{\epsilon_{su} - \epsilon_s}{\epsilon_{su} - \epsilon_{st}} \right)^n (f_{su} - f_{sy}) \tag{3}$$

$$n = E_{st} \left(\frac{\epsilon_{su} - \epsilon_{st}}{f_{su} - f_{sy}} \right) \tag{4}$$

in which f_{su} denotes the steel tensile strength, $\epsilon_{su} = 0.2$ is the ultimate strain and E_{st} represents the steel modulus at the onset of strain-hardening and a value of $0.02E_s$ is used.

4. Material model for confined concrete

4.1. General stress-strain curve

The two-stage stress-strain model presented in Fig. 4 is employed to model the responses of confined concrete in CFDST columns with circular sections under axial compression. In the first stage ($0 \leq \epsilon_c \leq \epsilon'_{cc}$), the following formula by Mander et al. [36] is employed to calculate the stress of the confined concrete from the axial strain:

$$\sigma_c = \frac{f'_{cc} (\epsilon_c / \epsilon'_{cc})^\lambda}{(\epsilon_c / \epsilon'_{cc})^\lambda + \lambda - 1} \tag{5}$$

where σ_c is the axial stress in compression and ϵ_c denotes the corresponding strain; f'_{cc} and ϵ'_{cc} represent the compressive strength and corresponding strain of the confined concrete, respectively; and λ controls the initial slope and the curvature of the ascending branch and given by

$$\lambda = \frac{\epsilon'_{cc} E_c}{\epsilon'_{cc} E_c - f'_{cc}} \tag{6}$$

in which E_c represents the concrete modulus of elasticity. Lim and Ozbakkaloglu [37] derived an expression for estimating E_c by analyzing many experimental results on concrete cylinders. Their expression was modified by Ahmed et al. [28] to consider the effect of column size as follows:

$$E_c = 4400 \sqrt{\gamma_c f'_c} \text{ (MPa)} \tag{7}$$

where γ_c stands for the reduction factor applied to the concrete strength considering the influence of the column size, proposed by Liang [30] for CFST columns as

$$\gamma_c = 1.85 D_c^{-0.135} \quad (0.85 \leq \gamma_c \leq 1.0) \tag{8}$$

in which D_c denotes the concrete-core diameter of circular CFST and CFDST columns, and taken as $(D_o - 2t_o)$ for sandwiched concrete and $(D_i - 2t_i)$ for core-concrete in circular CFDST columns.

In the second stage ($\epsilon_c > \epsilon'_{cc}$), the descending stress-strain branch of

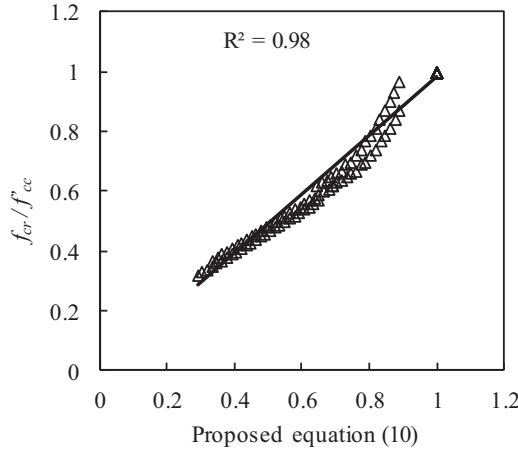


Fig. 5. Verification of the proposed expression for determining the residual concrete strength.

confined-concrete is defined by the equation formulated by Lim and Ozbakkaloglu [37] as

$$\sigma_c = f'_{cc} - \frac{f'_{cc} - f_{cr}}{\left[1 + \left(\frac{\epsilon_c - \epsilon'_{ci}}{\epsilon_{ci} - \epsilon'_{ci}}\right)^{-2}\right]} \quad (9)$$

where f_{cr} represents the concrete residual strength and ϵ_{ci} denotes the concrete strain corresponding to the inflection point, which defines the shape of the stress-strain curve in the post-peak range as illustrated in Fig. 4.

Parameters studies show that the f_{cr}/f'_{cc} ratio is mainly influenced by the D/t ratio and f'_c . Based on the regression analyses, an expression is proposed for f_{cr}/f'_{cc} as follows:

$$\frac{f_{cr}}{f'_{cc}} = 1.2420 - 0.0029 \left(\frac{D}{t}\right) - 0.0044 \gamma_c f'_c \quad \left(0 \leq \frac{f_{cr}}{f'_{cc}} \leq 1.0\right) \quad (10)$$

The accuracy of the proposed Eq. (10) for calculating the normalized residual strength of concrete (f_{cr}/f'_{cc}) is examined in Fig. 5 against the results obtained from the parametric study on 92 test data [1,2,6,8,9,11,12,38,39].

Lim and Ozbakkaloglu [37] provided a formula for determining the strain (ϵ_{ci}) at the inflection point based on extensive test results. Their formula was modified by Ahmed et al. [28] by using γ_c to incorporate the column size effect as follows:

$$\epsilon_{ci} = 2.8\epsilon'_{cc} (\gamma_c f'_c)^{-0.12} \left(\frac{f_{cr}}{f'_{cc}}\right) + 10\epsilon'_{cc} (\gamma_c f'_c)^{-0.47} \left(1 - \frac{f_{cr}}{f'_{cc}}\right) \quad (11)$$

The concrete ultimate strain (ϵ_{cu}) as illustrated in Fig. 4 is specified and used as the stopping criterion in the numerical analysis.

4.2. Compressive strength and strain of confined concrete

As illustrated in Fig. 4, when the axial compressive concrete stress exceeds the effective strength $\gamma_c f'_c$ of concrete in a CFDST column with circular section, the concrete is said to be confined by the steel tubes. This implies that the confined-concrete compressive strength increases from $\gamma_c f'_c$ to the maximum value f'_{cc} with increasing the axial load [22]. The maximum strength (f'_{cc}) and its corresponding strain (ϵ'_{cc}) of the concrete confined are determined by the formulas provided by Mander et al. [36] incorporating the factor γ_c given by Liang and Fragomeni [18] as follows:

$$f'_{cc} = \left(1 + \frac{k_1 f_{rp}}{\gamma_c f'_c}\right) \gamma_c f'_c \quad (12)$$

$$\epsilon'_{cc} = \epsilon'_c + \frac{k_2 f_{rp} \epsilon'_c}{\gamma_c f'_c} \quad (13)$$

in which f_{rp} represents the confining pressure on the concrete offered by the tubes. In the present study, $k_1 = 4.1$ and $k_2 = 20.5$ provided by Richart et al. [40] are used. The axial strain ϵ'_c at f'_c depends on the effective concrete strength in compression. The following equation given by De Nicolo et al. [41] for computing the strain ϵ'_c is adopted in the present study:

$$\epsilon'_c = 0.00076 + \sqrt{(0.626\gamma_c f'_c - 4.33) \times 10^{-7}} \quad (14)$$

4.3. Confining pressure model for sandwiched concrete

Experimental results showed that the outer tube of a circular CFDST column was forced to buckle locally outward and the sandwiched concrete crushed where the steel tube buckled [6,11,12]. The finite element analyses on circular CFST and CFDST columns conducted by Chang et al. [21] indicated that the longitudinal compressive stress in the core-concrete in the circular CFDST column was higher than that in the corresponding concrete in the CFST column. However, the longitudinal compressive stress in the sandwiched concrete in the CFDST column was similar to that in the corresponding concrete in the CFST column. This implies that in a CFDST short column under axial compression, the core-concrete is confined by both the outer and inner steel tubes but the sandwiched-concrete is confined mainly by the outer steel tube and the confinement provided by the inner steel tube on the sandwiched concrete is insignificant and can be ignored. In this study, the lateral pressure on the sandwiched concrete (f_{rpo}) in CFDST columns made of circular sections is estimated by the following expressions provided by Hu et al. [16]:

$$\frac{f_{rpo}}{f_{sy0}} = \begin{cases} 0.043646 - 0.000832\left(\frac{D_o}{t_o}\right) & \text{for } 21.7 \leq \frac{D_o}{t_o} \leq 47 \\ 0.006241 - 0.0000357\left(\frac{D_o}{t_o}\right) & \text{for } 47 < \frac{D_o}{t_o} \leq 150 \end{cases} \quad (15)$$

4.4. Proposed confining pressure model for core concrete

The confining pressure model for the core concrete was developed by means of interpreting the experimental data of 34 circular short CFDST columns given in Table 1 [6,8,9,11,12]. The maximum axial load on the axial load-strain curve with softening was used as the ultimate axial strength of the CFDST column. For specimens without softening behavior, the axial load at the ultimate strain was assumed to reach its ultimate state. The compressive strength for the confined core-concrete was calculated by subtracting the capacities of the sandwiched concrete and internal and external steel tubes. The lateral pressure ($f_{rpi,exp}$) on the core concrete obtained from experiments was then determined using Eq. (16). By undertaking the regression analyses on the experimental data given in Table 1, a new expression for quantifying the confining pressure exerted on the core-concrete in CFDST columns with circular sections is proposed as

$$f_{rpi} = 2.2897 + 0.0066\left(\frac{D_o}{t_o}\right) - 0.1918\left(\frac{D_i}{t_i}\right) - \left[0.0585\left(\frac{D_o}{t_o}\right) - 0.3801\left(\frac{D_i}{t_i}\right)\right] \zeta^{-1} \quad (f_{rpi} \geq 0) \quad (16)$$

in which D_i and D_o are the diameters of the internal and external steel tubes, respectively; t_i and t_o are the thickness of the inner and outer tubes, respectively; and ζ is the confinement factor which is expressed by

$$\zeta = \frac{A_{s0} f_{sy,0} + A_{si} f_{sy,i}}{A_{sc} \gamma_c f'_{sc} + A_{cc} \gamma_c f'_{cc}} \quad (17)$$

Table 1
Geometric and material properties of tested circular CFDST short columns.

Specimen	Outer tube					Inner tube					Concrete		Ref.
	$D_o \times t_o$ (mm)	$\frac{D_o}{t_o}$	$f_{sy,o}$ (MPa)	$f_{su,o}$ (MPa)	$E_{s,o}$ (GPa)	$D_i \times t_i$ (mm)	$\frac{D_i}{t_i}$	$f_{sy,i}$ (MPa)	$f_{su,i}$ (MPa)	$E_{s,i}$ (GPa)	$f'_{c,o}$ (MPa)	$f'_{c,i}$ (MPa)	
C1-1	133×4.5	29.6	361	410	200	55.9×3.4	16.4	361	410	200	56.1	56.1	[8]
C1-2	133×4.5	29.6	361	410	200	56×3.4	16.6	361	410	200	56.1	56.1	
C2-1	132.5×3.0	44.2	361	410	200	56×3.0	18.7	361	410	200	56.1	56.1	
C2-2	132.5×3.0	44.2	361	410	200	56×3.0	18.7	361	410	200	56.1	56.1	
C2-3	132.3×3.2	41.3	361	410	200	56.1×3.2	17.5	361	410	200	79.9	79.9	
C2-4	132×3.0	44.0	361	410	200	56.1×3.2	17.5	361	410	200	79.9	79.9	
C2-5	132.1×3.1	42.6	361	410	200	56×3.4	16.5	361	410	200	86.7	86.7	
C2-6	132×3.2	41.3	361	410	200	56.1×3.0	18.7	361	410	200	86.7	86.7	
C3-1	131.8×2.1	62.8	361	410	200	54.8×2.4	22.8	361	410	200	56.1	56.1	
C3-2	130.8×2.0	65.4	361	410	200	54.2×2.6	20.8	361	410	200	56.1	56.1	
C4-1	108×4.0	27.0	361	410	200	48×3.0	16.0	361	410	200	56.1	56.1	
C4-2	106.5×2.3	46.3	361	410	200	48×3.4	14.1	361	410	200	56.1	56.1	
C5-1	107.5×3.1	34.7	361	410	200	47.6×3.0	15.9	361	410	200	56.1	56.1	
C5-2	107.6×3.1	34.7	361	410	200	47.6×3.1	15.4	361	410	200	56.1	56.1	
S3-1-1	219×5.0	43.8	377	511	205	114×3.6	31.7	406	505	213	51	51	[9]
S3-1-2	219×5.0	43.8	377	511	205	114×3.6	31.7	406	505	213	167	167	
S3-1-3	219×5.0	43.8	377	511	205	114×3.6	31.7	406	505	213	51	167	
S3-1-4	219×5.0	43.8	377	511	205	114×3.6	31.7	406	505	213	51	184	
S3-2-1	219×10	21.9	381	509	212	114×6.3	18.1	428	521	209	51	51	
S3-2-2	219×10	21.9	381	509	212	114×6.3	18.1	428	521	209	167	167	
S3-2-3	219×10	21.9	381	509	212	114×6.3	18.1	428	521	209	51	167	
S3-2-4	219×10	21.9	381	509	212	114×6.3	18.1	428	521	209	51	184	
A1-1	426×7.73	55.1	298	408	206	133×6.6	20.2	331.4	478	200	25.9	25.9	[11]
A2-1	426×7.52	56.6	302	407	206	133×6.6	20.2	460	683	200	25.9	25.9	
A1-2	426×7.52	56.6	302	407	206	219×6.7	32.7	316.8	460	200	25.9	25.9	
A2-2	426×7.52	56.6	302	407	206	219×6.7	32.7	478	660	200	25.9	25.9	
A1-3	426×7.52	56.6	302	407	206	273×6.5	42.0	322	415	200	25.9	25.9	
A2-3	426×7.52	56.6	302	407	206	273×6.5	42.0	447	626	200	25.9	25.9	
CC1-SC1-OT1	139.7×3.3	42.3	290	350	200	88.9×4.25	20.9	375	450	200	29.1	29.1	[12]
CC1-SC1-OT2	139.7×5.9	23.7	355	410	200	88.9×4.25	20.9	375	450	200	29.1	29.1	
CC1-SC2-OT1	139.7×3.3	42.3	290	350	200	88.9×4.25	20.9	375	450	200	64.9	29.1	
CC1-SC2-OT2	139.7×5.9	23.7	355	410	200	88.9×4.25	20.9	375	450	200	64.9	29.1	
CC2-SC1-OT1	139.7×3.3	42.3	290	350	200	88.9×4.25	20.9	375	450	200	29.1	64.9	
CC2-SC1-OT2	139.7×5.9	23.7	355	410	200	88.9×4.25	20.9	375	450	200	29.1	64.9	
CC2-SC2-OT1	139.7×3.3	42.3	290	350	200	88.9×4.25	20.9	375	450	200	64.9	64.9	
CC2-SC2-OT2	139.7×5.9	23.7	355	410	200	88.9×4.25	20.9	375	450	200	64.9	64.9	
DC-09	219.1×6.3	34.8	300	467	202	114×6.3	18.1	428	519	209	155	155	[6]
DC-10	219.1×6.3	34.8	300	467	202	114×6.3	18.1	428	519	209	167	167	
DC-11	219.1×6.3	34.8	300	467	202	114×6.3	18.1	428	519	209	142	142	
DC-12	219.1×6.3	34.8	300	467	202	114×6.3	18.1	428	519	209	166	166	

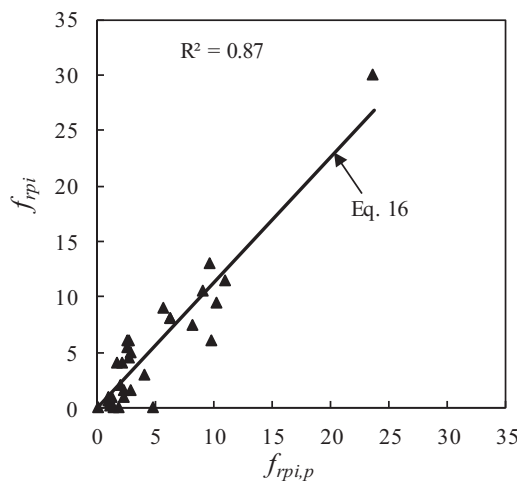


Fig. 6. Verification of the proposed expression for determining the lateral pressure on core concrete with the test results.

in which A_{so} , A_{si} , A_{sc} and A_{cc} are the cross-sectional areas of the outer tube, inner tube, sandwiched-concrete and core-concrete, respectively; f'_{cc} and f'_{sc} are the strengths of the core concrete and sandwiched concrete in compression, respectively; f_{syi} and f_{syo} are the yield stresses of

the internal and external tubes, respectively. Fig. 6 shows that the lateral pressures calculated by the proposed Eq. (16) are in good correlation with test data.

5. Comparisons of computer solutions with test results

The accuracy of the fiber-based numerical model incorporating the proposed confining pressure model and material constitutive laws is established by means of comparing computations with corresponding measurements provided by Xiong et al. [6], Peng et al. [8], Liew and Xiong [9], Wan and Zha [11] and Ekmekyapar and Al-Eliwi [12]. Table 1 gives the material and geometric properties of 40 tested CFDST short columns. The unconfined concrete strengths were determined by the compression tests on concrete cubes (f'_{cu}), concrete cylinders of 100×200 mm ($f'_{c,100}$) or concrete cylinders of 150×300 mm (f'_c). For consistency, the unconfined concrete strengths were converted to f'_c using the conversion of $f'_{ck,100}/1.05$ and $0.85f'_{cu}$, respectively.

The predicted ultimate axial loads ($P_{u,num}$) by the numerical model and the experimental values ($P_{u,exp}$) are given in Table 2. It is observed that the fiber modeling technique accurately determines the capacities of short CFDST circular columns. The statistical study indicates that the mean $P_{u,num}/P_{u,exp}$ ratio is 0.97 while both the coefficient of variation and standard deviation are 0.08. The simulated axial load-strain behavior of high-strength CFDST columns are provided in Fig. 7. The measured axial load-strain performance of the tested columns was

Table 2
Ultimate axial strengths of circular CFDST short columns.

Specimen	$P_{u,exp}$ (kN)	$P_{u,num}$ (kN)	$P_{u,EC4}$ (kN)	$P_{u,ACI}$ (kN)	$P_{u,AISC}$ (kN)	$P_{u,des}$ (kN)	$\frac{P_{u,num}}{P_{u,exp}}$	$\frac{P_{u,EC4}}{P_{u,exp}}$	$\frac{P_{u,ACI}}{P_{u,exp}}$	$\frac{P_{u,AISC}}{P_{u,exp}}$	$\frac{P_{u,des}}{P_{u,exp}}$
C1-1	1942	1818	1847	1407	1455	1823	0.94	0.95	0.72	0.75	0.94
C1-2	1911	1818	1846	1407	1455	1823	0.95	0.97	0.74	0.76	0.95
C2-1	1683	1409	1546	1196	1249	1425	0.84	0.92	0.71	0.74	0.85
C2-2	1592	1409	1546	1196	1249	1425	0.89	0.97	0.75	0.78	0.90
C2-3	1831	1730	1852	1470	1544	1781	0.94	1.01	0.80	0.84	0.97
C2-4	1875	1694	1811	1442	1516	1718	0.90	0.97	0.77	0.81	0.92
C2-5	1870	1813	1916	1532	1612	1837	0.97	1.02	0.82	0.86	0.98
C2-6	1925	1831	1908	1524	1605	1853	0.95	0.99	0.79	0.83	0.96
C3-1	1434	1214	1327	1042	1097	1231	0.85	0.93	0.73	0.77	0.86
C3-2	1425	1190	1303	1026	1080	1204	0.84	0.91	0.72	0.76	0.84
C4-1	1432	1276	1042	979	1009	1281	0.89	0.73	0.68	0.70	0.89
C4-2	1106	931	875	810	842	948	0.84	0.79	0.73	0.76	0.86
C5-1	1256	1110	947	883	915	1121	0.88	0.75	0.70	0.73	0.89
C5-2	1182	1110	953	888	920	1126	0.94	0.81	0.75	0.78	0.95
S3-1-1	3626	4051	3460	3207	3351	3790	1.12	0.95	0.88	0.92	1.05
S3-1-2	8529	7834	7295	6467	6938	8022	0.92	0.86	0.76	0.81	0.94
S3-1-3	4968	4950	4499	4091	4323	5014	1.00	0.91	0.82	0.87	1.01
S3-1-4	5239	5175	4652	4220	4465	5193	0.99	0.89	0.81	0.85	0.99
S3-2-1	6300	6558	4891	4670	4783	5918	1.04	0.78	0.74	0.76	0.94
S3-2-2	9817	8943	8252	7526	7930	9211	0.91	0.84	0.77	0.81	0.94
S3-2-3	7022	6798	5828	5466	5660	6897	0.97	0.83	0.78	0.81	0.98
S3-2-4	7160	6794	5966	5583	5788	7041	0.95	0.83	0.78	0.81	0.98
A1-1	8142	8804	7260	6756	7043	7410	1.08	0.89	0.83	0.87	0.91
A2-1	9830	9079	7563	7057	7341	7720	0.91	0.76	0.71	0.74	0.78
A1-2	9830	9383	7725	7227	7506	7956	0.95	0.79	0.74	0.76	0.81
A2-2	10,025	10,189	8446	7947	8216	8586	1.02	0.84	0.79	0.82	0.86
A1-3	9740	9767	8037	7542	7818	8275	1.00	0.83	0.77	0.80	0.85
A2-3	10,739	10,801	8717	8222	8488	8755	1.01	0.81	0.77	0.79	0.82
CC1-SC1-OT1	1435.05	1460	1306	1247	1282	1429	1.02	0.91	0.87	0.89	1.00
CC1-SC1-OT2	1977.94	2090	1658	1605	1635	1972	1.06	0.84	0.81	0.83	1.00
CC1-SC2-OT1	1606.89	1673	1514	1412	1475	1661	1.04	0.94	0.88	0.92	1.03
CC1-SC2-OT2	2044.44	2278	1908	1817	1871	2237	1.11	0.93	0.89	0.92	1.09
CC2-SC1-OT1	1570.15	1627	1415	1328	1381	1563	1.04	0.90	0.85	0.88	1.00
CC2-SC1-OT2	2153.11	2255	1849	1767	1815	2182	1.05	0.86	0.82	0.84	1.01
CC2-SC2-OT1	1784.39	1839	1704	1574	1655	1877	1.03	0.96	0.88	0.93	1.05
CC2-SC2-OT2	2274.77	2374	2099	1979	2051	2448	1.04	0.92	0.87	0.90	1.08
DC-09	7640	7346	7038	6309	6727	7504	0.96	0.92	0.83	0.88	0.98
DC-10	7209	7699	7414	6629	7078	7878	1.07	1.03	0.92	0.98	1.09
DC-11	6882	6961	6631	5963	6346	7100	1.01	0.96	0.87	0.92	1.03
DC-12	8375	7699	7383	6602	7049	7847	0.92	0.88	0.79	0.84	0.94
Mean							0.97	0.89	0.79	0.83	0.95
Standard Deviation (SD)							0.08	0.08	0.06	0.07	0.08
Coefficients of Variance (COV)							0.08	0.09	0.08	0.08	0.08

determined by the mathematical model with reasonable accuracy. The experimentally measured column initial axial stiffness slightly differs from the predicted one. The fiber-based modeling method also gives a good simulation of the post-yield responses of the CFDST columns. The discrepancy between the predictions and measurements is caused by the uncertainty of the actual concrete strength and stiffness in the tested specimens and the average concrete strength was used in the numerical analyses.

6. Parametric study

The mathematical model proposed was utilized to examine the structural behavior of short circular high-strength CFDST columns. The details on the CFDST columns under investigations are provided in Table 3. Steel tubes having the yield stresses of 250 MPa, 300 MPa, 350 MPa, 400 MPa and 450 MPa were used in the numerical analyses and their corresponding tensile strengths were 320 MPa, 400 MPa, 420 MPa, 500 MPa and 520 MPa, respectively. In the parametric study, the ultimate concrete strain ε_{cu} was taken as 0.04 which gives conservative results of columns with ascending stress-strain behavior in the post-yield range.

6.1. Influences of the internal steel tube

The effects of the internal tube on the strength as well as ductility of the CFDST column were examined by comparing its axial load-strain response with that of the conventional CFST column. For this purpose, analyses on Columns C1 and C2 presented in Group G1 in Table 3 were undertaken by the mathematical model. Both columns had the same outer tube diameter as well as the steel area and were made of high-strength concrete of 60 MPa. Fig. 8 shows that the CFDST column has 4.85% higher strength than the CFST column due to the inclusion of the internal circular tube. The reason for the strength increase is that the inner steel tube provides additional confinement to the core-concrete, which increases the strength of the core-concrete thereby the column ultimate strength. The CFDST column also has a better ductility than the CFST column. However, the column initial stiffness is not affected by the internal tube.

The influences of the internal tube diameter on the column behavior were evaluated by analyzing Columns C3–C6 in Group G1 in Table 3. Only the inner tube diameter (D_i) was varied in this investigation. Fig. 9 presents the calculated axial loads as a function of axial strains for these CFDST columns. The ultimate axial loads of short circular CFDST columns are found to increase significantly as D_i increases. By increasing the diameter D_i from 157.5 mm to 202.5 mm, 247.5 mm and 292.5 mm, the percentage increases in the column ultimate strengths are 3.4%,

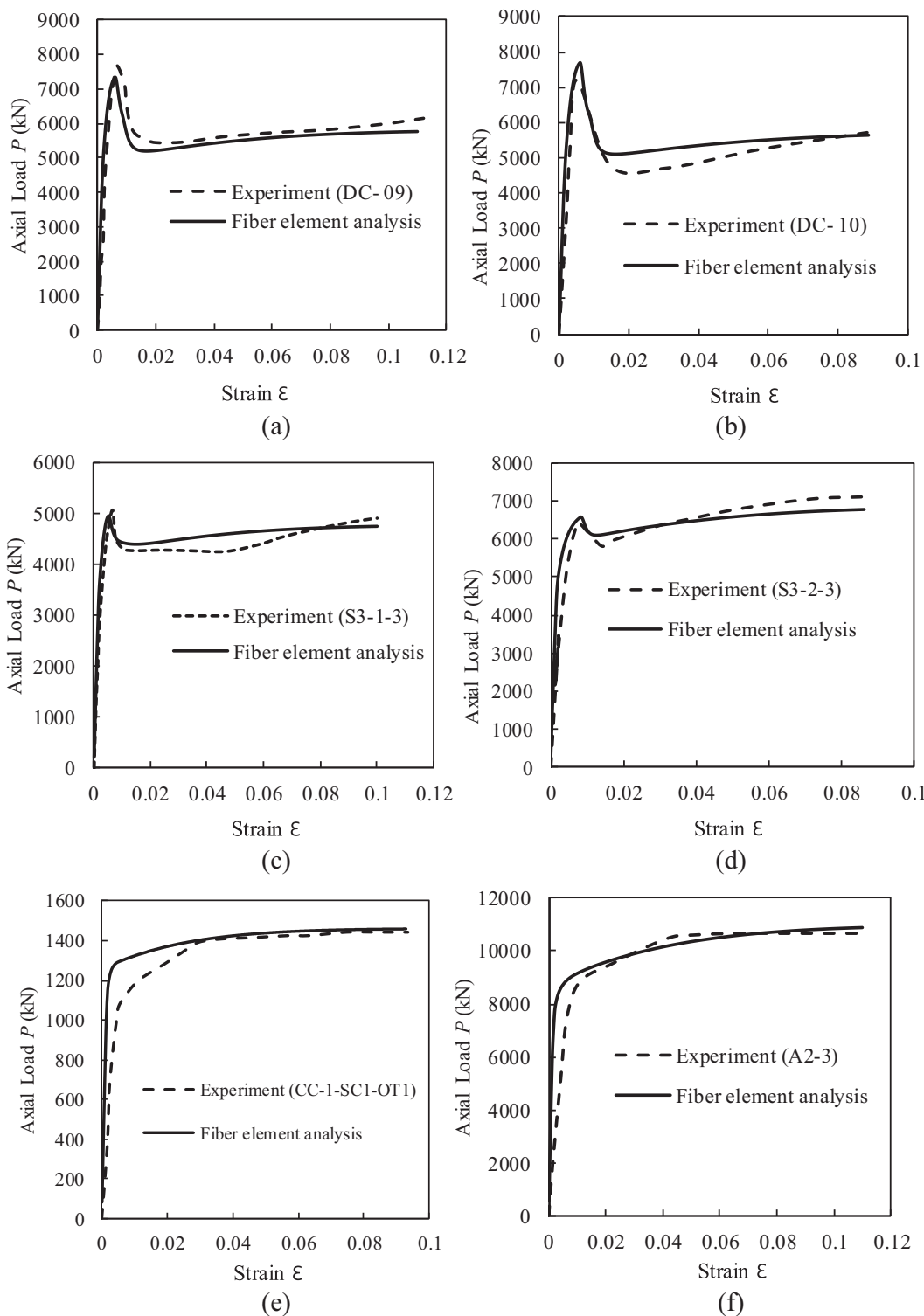


Fig. 7. Comparison of computational and experimental axial load-strain curves for circular CFDST short columns.

7.1% and 11.4%, respectively. It would appear that increasing the diameter D_i reduces the sandwiched-concrete area but increases the core-concrete area. This implies that more concrete would be confined by the internal tube. Consequently, the strength of the CFDST column increases. Fig. 9 indicates that the column initial axial stiffness is slightly affected by the inner tube diameter. The computed ductility indices of CFDST columns having different diameters are provided in Fig. 10. It would appear that circular CFDST short columns have very good ductility with a strain ductility index greater than 16.0. It is

discovered that the ductility index of CFDST columns has a slight decrease as the inner steel tube diameter reduces.

Investigations were undertaken on the influences of the internal tube thickness on the behavior of CFDST columns. Columns C7–C10 in Group G1 in Table 3 with thickness ranged from 6.67 mm to 20 mm were analyzed. The results computed by the numerical technique are shown in Fig. 11. It appears that the ultimate axial strength of CFDST column increases considerably with increasing the thickness of the internal tube. The increase in the column ultimate strength is 14.1%

Table 3
Geometric and material properties of circular CFDST short columns utilized in the parametric study.

Group	Column	Outer tube				Inner tube				Concrete f'_c (MPa)	Ultimate strength			
		D_o (mm)	t_o (mm)	$\frac{D_o}{t_o}$	f_{syo} (MPa)	D_i (mm)	t_i (mm)	$\frac{D_i}{t_i}$	f_{syt} (MPa)		$P_{u,num}$ (kN)	$P_{u,des}$ (kN)	$\frac{P_{u,des}}{P_{u,num}}$	
G1	C1	500	12.88	38.8	350	–	–	–	–	60	18,973	18,387	0.97	
	C2	500	10	50	350	280	5	56	350	60	19,751	19,849	1.00	
	C3	450	10	45	350	157.5	8	19.68	350	60	14,831	14,696	0.99	
	C4	450	10	45	350	202.5	8	25.31	350	60	15,330	15,249	0.99	
	C5	450	10	45	350	247.5	8	30.93	350	60	15,889	15,868	1.00	
	C6	450	10	45	350	292.5	8	36.56	350	60	16,520	16,534	1.00	
	C7	600	10	60	450	200	6.67	30	450	40	21,648	20,403	0.94	
	C8	600	10	60	450	200	10	20	450	40	22,343	21,168	0.95	
	C9	600	10	60	450	200	15	13.33	450	40	23,520	22,396	0.95	
	C10	600	10	60	450	200	20	10	450	40	24,694	23,559	0.95	
G2	C11	280	8	35	350	140	5	28	350	60	7180	7127	0.99	
	C12	320	8	40	350	140	5	28	350	60	8428	8417	1.00	
	C13	360	8	45	350	140	5	28	350	60	9601	9607	1.00	
	C14	400	8	50	350	140	5	28	350	60	10,968	11,000	1.00	
	C15	450	9	50	350	200	8	25	350	70	15,806	15,844	1.00	
	C16	450	10	45	350	200	8	25	350	70	16,568	16,523	1.00	
	C17	450	11.25	40	350	200	8	25	350	70	17,840	17,683	0.99	
	C18	450	12.86	35	350	200	8	25	350	70	19,123	18,966	0.99	
G3	C19	480	12	40	350	200	8	25	350	55	18,311	17,655	0.96	
	C20	480	12	40	350	200	8	25	350	75	20,817	20,537	0.99	
	C21	480	12	40	350	200	8	25	350	95	23,653	23,420	0.99	
	C22	480	12	40	350	200	8	25	350	115	26,449	26,302	0.99	
G4	C23	720	12	60	250	280	8	35	250	60	31,692	30,722	0.97	
	C24	720	12	60	300	280	8	35	300	60	33,175	31,866	0.96	
	C25	720	12	60	350	280	8	35	350	60	34,072	33,229	0.98	
	C26	720	12	60	400	280	8	35	400	60	35,949	34,729	0.97	
	C27	720	12	60	450	280	8	35	450	60	37,836	36,319	0.96	
Mean														0.98
Standard Deviation (SD)														0.02
Coefficients of Variance (COV)														0.02

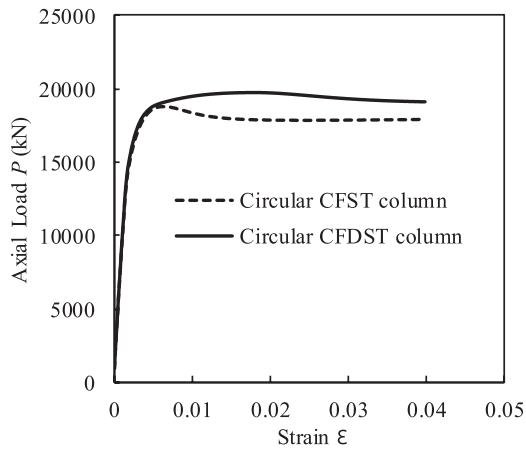


Fig. 8. Effects of the inner steel tube on the axial load-strain curves.

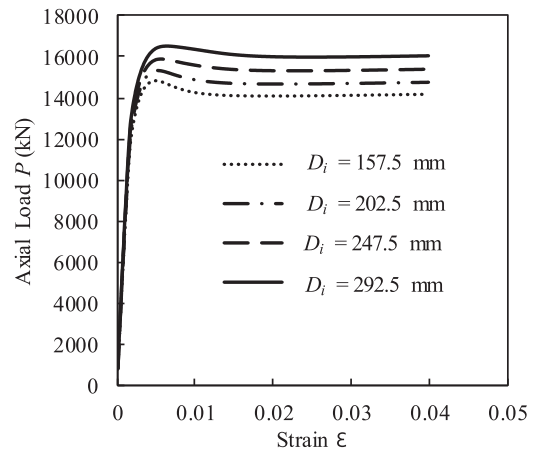


Fig. 9. Effects of the diameter of the inner steel tube on the axial load-strain curves of circular CFDST short columns.

when the thickness t_i is increased from 6.67 mm to 20 mm. This can be explained by the fact that increasing the inner tube thickness leads to an increase in the steel area with yield stress of 450 MPa but the same reduction in the core-concrete area with compressive strength of 40 MPa, which results in a considerable increase in the ultimate axial strength of the column. As demonstrated in Fig. 12, reducing the thickness t_i causes a slight decrease in the ductility because of the reduction in the internal tube area. The numerical results presented in Fig. 12 indicate that when the thickness t_i is reduced from 20 mm to 15 mm, 10 mm and 6.67 mm, the axial ductility index decreases from 17.40 to 17.35, 17.31 to 17.20, respectively.

It has been demonstrated that circular CFDST columns possess higher strength and ductility than circular CFST columns. High strength

inner steel tubes may be used to further increase the column capacity. The use of the inner steel tube instead of reinforcing bars certainly speeds up the construction process. Moreover, the existing conventional CFST column can be strengthened by using an additional external steel tube filled with concrete and it becomes a CFDST column. However, to achieve economical and efficient designs, the cross-sections of CFDST columns must be properly designed. The proposed computational model can be used to analyze the cross-sectional capacities of CFDST columns to determine the optimal designs of CFDST columns.

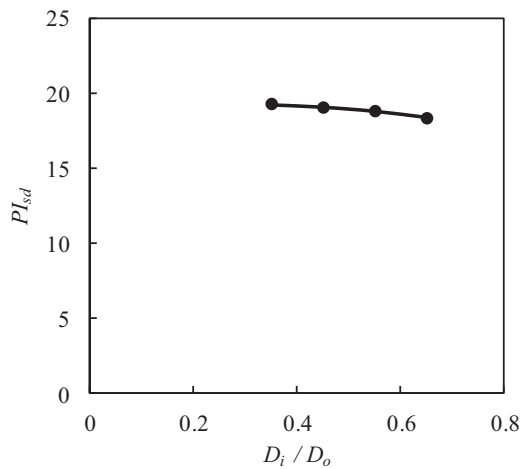


Fig. 10. Effects of D_i / D_o ratio on the strain ductility index of circular CFDST short columns.

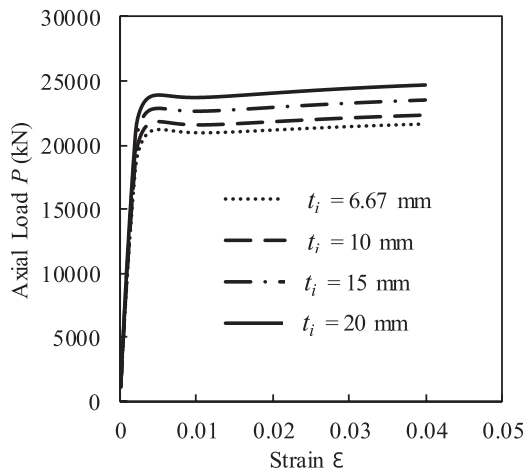


Fig. 11. Effects of the thickness of the inner steel tube on the axial load-strain curves of circular CFDST short columns.

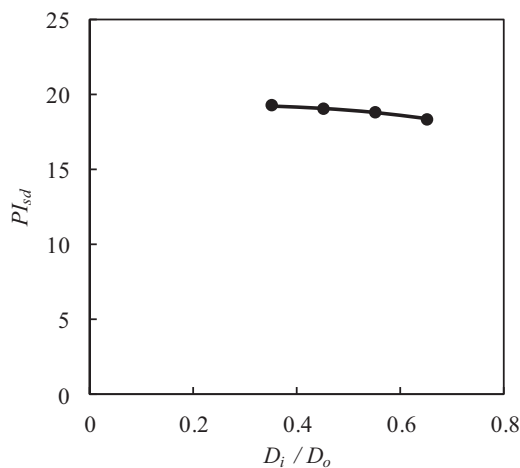


Fig. 12. Effects of D_i / t_i ratio on the strain ductility index of circular CFDST short columns.

6.2. Influences of D_o / t_o ratio

The behavior of CFDST columns is significantly dependent on the D_o / t_o ratios. Two scenarios were considered to examine the effects of D_o / t_o ratios. The CFDST columns with D_o / t_o ratios of 35, 40, 45 and 50

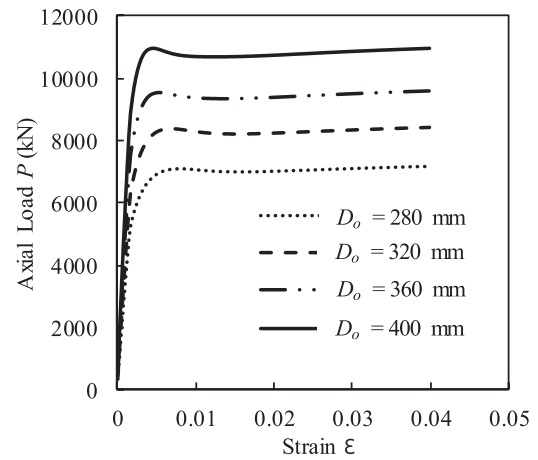


Fig. 13. Effects of the diameter of the outer steel tube on the axial load-strain curves of circular CFDST short columns.

given in Group G2 in Table 3 were examined in the first scenario by changing the outer tube diameter D_o only. Fig. 13 gives the computed load-strain relationships of these columns. It would appear that increasing the external steel tube diameter D_o significantly increases the column axial strength. By increasing D_o from 280 mm to 320 mm, 360 mm and 400 mm, the increases in the column axial strengths are 17.4%, 33.7% and 52.8%, respectively. This is because increasing the diameter of the outer tube increases the areas of both steel tube and concrete so that the column ultimate axial load increases. As depicted in Fig. 13, the column initial stiffness increases considerably with an increase in the D_o / t_o ratio, however, it has an insignificant impact on the post-peak responses of CFDST columns. The axial strain ductility indices are given in Fig. 14. The ductility indices are found to vary with D_o / t_o ratios. The computed axial ductility indexes are 16.3, 17.32, 18.73 and 19.63 for columns with D_o / t_o ratios of 35, 40, 45 and 50, respectively.

In the second scenario, only the external tube thickness t_o was changed to determine the D_o / t_o ratios as 35, 40, 45 and 50 as shown in Group G2 in Table 3. The axial load-strain curves predicted are given in Fig. 15. It would appear that decreasing the thickness t_o significantly decreases the column ultimate strength. The strength reductions are computed as 6.7%, 13.4% and 17.3%, respectively when the thickness t_o is reduced from 12.86 mm to 11.25 mm, 10 mm and 9 mm, respectively. The reason for this is that decreasing the outer tube thickness reduces the steel tube area and the confinement on the sandwiched and core concrete so that the column axial loads decrease significantly. It can be seen from Fig. 15 that the D_o / t_o ratio influences the post-yield curves.

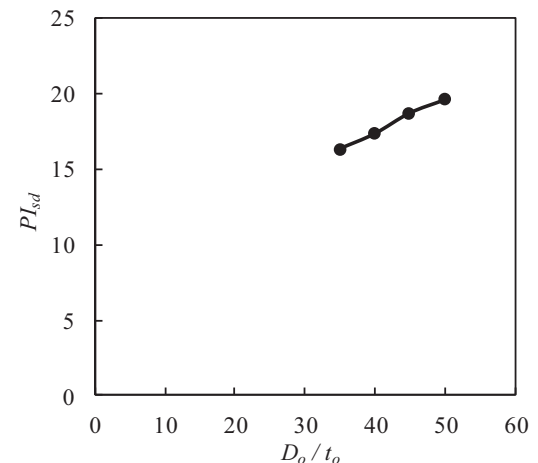


Fig. 14. Effects of D_o / t_o ratio by varying diameter of the outer steel tube on the strain ductility index of circular CFDST short columns.

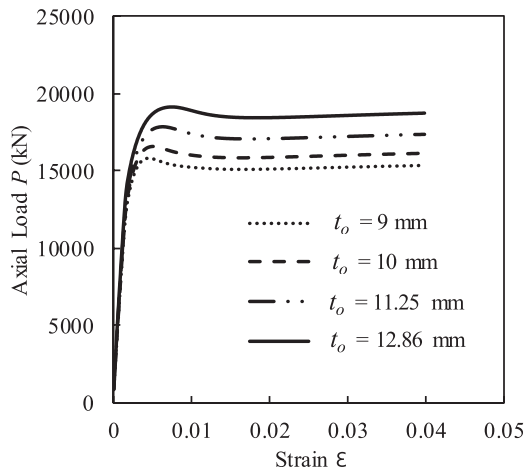


Fig. 15. Effects of the thickness of the outer steel tube on the axial load-strain curves of circular CFDST short columns.

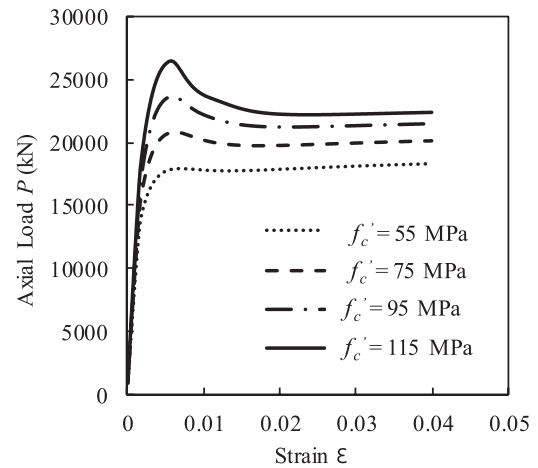


Fig. 17. Effects of concrete compressive strength on the axial load-strain curves of circular CFDST short columns.

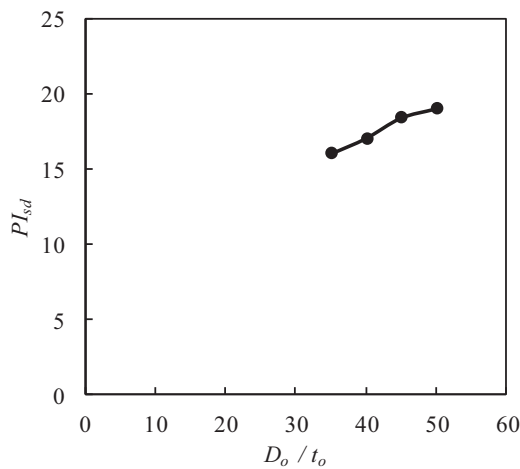


Fig. 16. Effects of D_o/t_o ratio by varying thickness of the outer steel tube on the strain ductility index of circular CFDST short columns.

Fig. 16 illustrates that increasing the D_o/t_o ratio improves the axial ductility. For CFDST short columns with D_o/t_o ratio of 35, 40, 45 and 50, the calculated strain ductility indexes are 16.05, 17.08, 18.44 and 19.06, respectively.

6.3. Influences of concrete compressive strength

In Group G3 in Table 3, the concrete of different strengths was used to construct CFDST columns. The compressive concrete strengths of 55 MPa, 75 MPa, 95 MPa and 115 MPa were considered in the fiber analysis. The predicted load-strain responses presented in Fig. 17 indicate that using higher strength concrete significantly improves the ultimate strength of CFDST columns. When f'_c increases from 55 MPa to 75 MPa, 95 MPa and 115 MPa, the increases in the column ultimate strengths are 13.7%, 29.2% and 44.4%, respectively. This can be explained by the fact that the ultimate axial load of short CFDST columns is governed by its section and material properties such as the concrete compressive strength. However, it is noticed that CFDST columns constructed using high-strength concrete are less ductile due to its brittle behavior.

6.4. Influences of steel yield strength

The yield stress of steel tubes has influences on the behavior of CFDST columns and its effect was studied by using the fiber-based

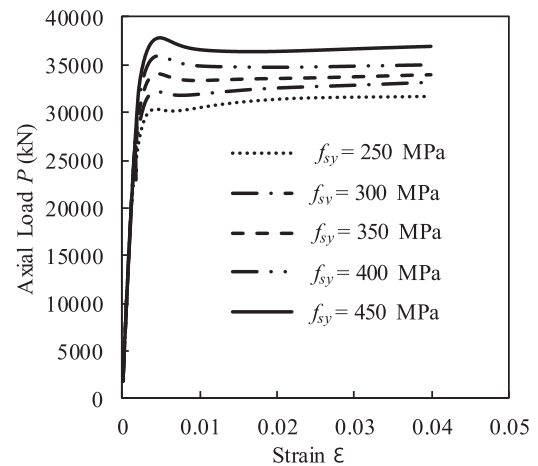


Fig. 18. Effects of steel yield strength on the axial load-strain curves of circular CFDST short columns.

model. The Columns in Group G4 in Table 3 were considered for this study. The calculated responses of these CFDST columns constructed by steel tubes having various yield stresses are given Fig. 18. It is observed that the ultimate strength of the CFDST column significantly increases when the steel yield stress is increased. When the yield stress is increased from 250 MPa to 300 MPa, 350 MPa, 400 MPa and 450 MPa, the column ultimate strength is found to increase by 4.7%, 7.5%, 13.4% and 19.4%, respectively. The reason for the column strength increase is that the ultimate axial strength of a short CFDST column is governed by its section and material properties such as the steel yield strength. The strain ductility indices of CFDST columns are depicted in Fig. 19. It is shown that the ductility index of the column increases with an increase in its steel yield strength up to 350 MPa and after that it decreases as its steel yield strength increases.

7. Proposed design model

Currently, there are no design specifications available for the design of stub CFDST columns constructed by circular carbon steel tubes. Previously, Liang and Fragomeni [18] proposed a formula for the computation of the ultimate axial capacities of CFST columns with circular cross-sections under axial loading considering confinement effects. Liang [22] also derived design formulas for double-skin CFST short columns in axial compression. Hassanein et al. [23] recommended a formula for the design of CFSCST columns where the outer tube was made of duplex stainless steel. Based on the proposed model for lateral

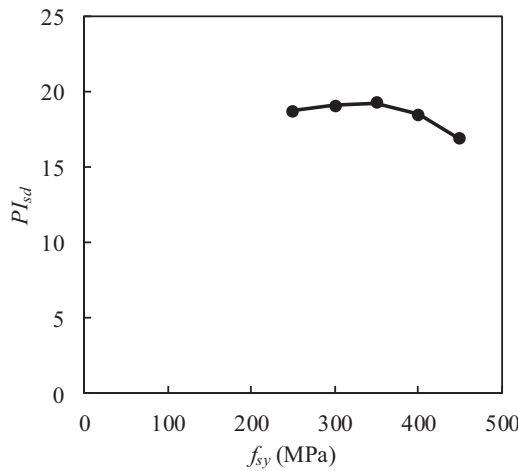


Fig. 19. Effects of steel yield strength on the strain ductility index of circular CFDST short columns.

pressures on core-concrete and the previously cited work [18,22], a new simple expression for the estimation of the ultimate strength of short circular CFDST columns is proposed as

$$P_{u,design} = \gamma_{so} f_{sy0} A_{so} + \gamma_{si} f_{syt} A_{st} + (\gamma_{sc} f'_c + 4.1 f_{rpo}) A_{sc} + (\gamma_{cc} f'_c + 4.1 f_{rpt}) A_{cc} \tag{18}$$

where γ_{so} and γ_{si} are strength factors, accounting for the influences of hoop-tension, strain hardening as well as imperfections on the outer tube and inner tube, respectively and were developed by Liang and Fragomeni [18] as

$$\gamma_{so} = 1.458 \left(\frac{D_o}{t_o} \right)^{-0.1} \quad (0.9 \leq \gamma_{so} \leq 1.1) \tag{19}$$

$$\gamma_{si} = 1.458 \left(\frac{D_i}{t_i} \right)^{-0.1} \quad (0.9 \leq \gamma_{si} \leq 1.1) \tag{20}$$

The proposed design equation is verified by comparing calculations with test data of 40 CFDST columns in Table 2, where $P_{u,des}$, $P_{u,exp}$ and $P_{u,num}$ are the ultimate axial loads calculated using Eq. (18), obtained from experiments and determined by the fiber analysis, respectively. It is observed that the mean $P_{u,des}/P_{u,exp}$ ratio is 0.97 and the calculated coefficient of variance and standard deviation are 0.08. The strength computations of circular CFDST columns by the design model are further validated by numerical predictions in Table 3. It is shown that the strengths computed by the design model agree extremely well with corresponding numerical predictions. The proposed design formula can predict 98% of the numerical strengths with a coefficient of variance of 0.02.

8. Comparisons with design codes

The applicability of the existing design specifications for short circular CFST columns given in Eurocode 4 [7], ACI 318-11 [42] and AISC 360-16 [43] to circular CFDST columns is examined herein. Table 4 presents the specifications of the design codes to calculate the ultimate axial strengths. Eurocode 4 accounts for the influence of concrete confinement on the strength calculations of CFST circular columns whereas ACI 318-11 and AISC 360-16 neglect this effect. Table 2 summaries the comparisons between design calculations and measured results on 40 tested CFDST short columns. The calculated ultimate strengths using ACI 318-11 and AISC 360-16 codes are very conservative compared to test results. Although the design method specified in Eurocode 4 yields better estimations of the load-carrying capacities of CFDST columns than ACI 318-11 and AISC 360-16, but it could not capture the actual improvement in the core concrete strength. The

Table 4 Design formulas for circular CFDST short columns given in design codes.

Design codes	Design equations
Eurocode 4 [7]	<p>Circular CFST columns:</p> $P_{u,outer} = \eta_a A_{so} f_{sy0} + A_{sc} f_{sc} \left(1 + \eta_c \frac{t_o}{D_o} \frac{f_{sy0}}{f_{sc}} \right)$ $P_{u,inner} = \eta_a A_{si} f_{syt} + A_{cc} f_{cc} \left(1 + \eta_c \frac{t_i}{D_i} \frac{f_{syt}}{f_{cc}} \right)$ $P_{EC4} = P_{u,outer} + P_{u,inner}$ $\eta_a = 0.25 \left(3 + 2\bar{\lambda} \right) \quad \left(\eta_a \leq 1.0 \right)$ $\eta_c = 4.9 - 18.5\bar{\lambda} + 17\bar{\lambda}^2 \quad \left(\eta_c > 0 \right)$ <p>where the relative slenderness ratio is $\bar{\lambda} = \sqrt{\frac{N_{pl,Rk}}{N_{cr}}}$</p>
ACI 318-11 [42]	$P_{u,ACI} = A_{so} f_{sy0} + 0.85 A_{sc} f_{sc} + A_{si} f_{syt} + 0.85 A_{cc} f_{cc}$
AISC 360-16 [43]	$P_{u,AISC} = \begin{cases} P_c [0.658^{(P_c/R_c)}] & \text{for } P_c \geq 0.44P_c \\ 0.877P_c & \text{for } P_c < 0.44P_c \end{cases}$ $P_c = A_{so} f_{sy0} + C_2 A_{sc} f_{sc} + A_{si} f_{syt} + C_2 A_{cc} f_{cc}$ $P_c = \frac{\pi^2}{(KL)^2} (EI)_{eff}$ $(EI)_{eff} = E_{so} I_{so} + E_{si} I_{si} + C_4 E_{sc} I_{sc} + C_4 E_{cc} I_{cc}$ $C_4 = 0.6 + 2 \left(\frac{A_s}{A_s + A_c} \right) \leq 0.9$ $C_2 = 0.95 \text{ for circular section}$

mean calculated-to-measured ultimate axial strengths calculated by using Eurocode 4, ACI 318-11 and AISC 360-16 are 0.89, 0.79 and 0.83, respectively. On the contrary, the proposed design model generally yields better strength predictions of short CFDST columns than design codes. The current design equation given in Eurocode 4 [7] for CFST columns is simpler than the proposed Eq. (18), but Eq. (18) yields more accurate results than the current design provision. Further studies should focus on developing a more simple revision to the current design provision in Eurocode 4 for the design of CFDST columns.

9. Conclusions

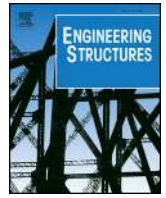
This paper has described a fiber-based mathematical model formulated for the numerical simulations of short circular CFDST columns subjected to axial loading. A new model for computing the confining pressures on the core-concrete has been proposed based on existing test data together with a new strength-degradation parameter for quantifying the post-peak responses of confined concrete. The accuracy of the developed numerical analysis technique incorporating the new proposals of material constitutive laws has been examined by comparisons with experimental results of CFDST columns. Details parametric studies have been conducted considering various columns geometry and material properties. A new design formula has been derived and verified by test results. Furthermore, the applicability of the existing design rules recommended by Eurocode 4 [7], ACI 318-11 [42] and AISC 360-16 [43] for circular CFST columns to circular CFDST columns has been investigated.

The conclusions are given as follows:

- (1) The fiber-based mathematical model developed produces predictions which are in good correlations with experimental data of circular CFDST columns under axial compression.
- (2) If both circular CFDST and CFST columns have the same external tube diameter and the same steel area, the CFDST column has higher strength and ductility than the CFST column.
- (3) Increasing the inner steel-tube diameter remarkably improves the ultimate strength of the CFDST column.
- (4) Increasing the thickness of the inner tube considerably increases the ultimate axial loads of CFDST columns made of normal strength concrete but its effect diminishes when high-strength concrete is used.
- (5) The use of higher strength steel tubes and concrete results in higher axial capacities, but it considerably affects the column axial ductility.
- (6) The design rules specified in Eurocode 4 [7], ACI 318-11 [42] and AISC 360-16 [43] for circular CFST columns give conservative calculations of the ultimate axial strengths of short CFDST columns made of circular steel sections.
- (7) The design formula proposed yields more accurate ultimate strength predictions of CFDST columns than the design approaches provided in existing design codes.

References

- [1] K. Sakino, H. Nakahara, S. Morino, I. Nishiyama, Behavior of centrally loaded concrete-filled steel-tube short columns, *J. Struct. Eng. ASCE* 130 (2) (2004) 180–188.
- [2] G. Giakoumelis, D. Lam, Axial capacity of circular concrete-filled tube columns, *J. Constr. Steel Res.* 60 (7) (2004) 1049–1068.
- [3] J.M. Portolés, M.L. Romero, J.L. Bonet, F.C. Filippou, Experimental study of high strength concrete-filled circular tubular columns under eccentric loading, *J. Constr. Steel Res.* 67 (4) (2011) 623–633.
- [4] M.D. O'Shea, R.Q. Bridge, Design of circular thin-walled concrete filled steel tubes, *J. Struct. Eng. ASCE* 126 (11) (2000) 1295–1303.
- [5] J.Y.R. Liew, M.X. Xiong, D.X. Xiong, Design of concrete filled tubular beam-columns with high strength steel and concrete, *Structures* 8 (2016) 213–226.
- [6] M.X. Xiong, D.X. Xiong, J.Y.R. Liew, Axial performance of short concrete filled steel tubes with high-and ultra-high-strength materials, *Eng. Struct.* 136 (2017) 494–510.
- [7] Eurocode 4, Design of Composite Steel and Concrete Structures-Part 1-1: General Rules and Rules for Buildings, European Committee for Standardization, CEN, Brussels, Belgium, 2004.
- [8] Y.Y. Peng, K.F. Tan, Y. Yao, Mechanical properties of duplex steel tube high-strength concrete short columns under axial compression, *J. Wuhan. Univ. Technol.* 33 (2) (2011) 105–109 (In Chinese).
- [9] J.Y.R. Liew, D.X. Xiong, Ultra-high strength concrete filled composite columns for multi-storey building construction, *Adv. Struct. Eng.* 15 (9) (2012) 1487–1503.
- [10] M.L. Romero, A. Espinós, J. Portolés, A. Hospitaler, C. Ibañez, Slender double-tube ultra-high strength concrete-filled tubular columns under ambient temperature and fire, *Eng. Struct.* 99 (2015) 536–545.
- [11] C.Y. Wan, X.X. Zha, Nonlinear analysis and design of concrete-filled dual steel tubular columns under axial loading, *Steel Compos. Struct.* 20 (3) (2016) 571–597.
- [12] T. Ekmekyapar, B.J. Al-Eliwi, Concrete filled double circular steel tube (CFDCST) stub columns, *Eng. Struct.* 135 (2017) 68–80.
- [13] C. Ibañez, M.L. Romero, A. Espinós, J. Portolés, V. Albero, Ultra-high strength concrete on eccentrically loaded slender circular concrete-filled dual steel columns, *Structures* 12 (2017) 64–74.
- [14] X. Chang, Z.L. Ru, W. Zhou, Y.B. Zhang, Study on concrete-filled stainless steel-carbon steel tubular (CFSCST) stub columns under compression, *Thin-Walled Struct.* 63 (2013) 125–133.
- [15] Y. Zheng, C. He, L. Zheng, Experimental and numerical investigation of circular double-tube concrete-filled stainless steel tubular columns under cyclic loading, *Thin-Walled Struct.* 132 (2018) 151–166.
- [16] H.T. Hu, C.S. Huang, M.H. Wu, Y.M. Wu, Nonlinear analysis of axially loaded concrete-filled tube columns with confinement effect, *J. Struct. Eng. ASCE* 129 (10) (2003) 1322–1329.
- [17] E. Ellobody, B. Young, D. Lam, Behaviour of normal and high strength concrete-filled compact steel tube circular stub columns, *J. Constr. Steel Res.* 62 (7) (2006) 706–715.
- [18] Q.Q. Liang, S. Fragomeni, Nonlinear analysis of circular concrete-filled steel tubular short columns under axial loading, *J. Constr. Steel Res.* 65 (12) (2009) 2186–2196.
- [19] V.I. Patel, Q.Q. Liang, M.N.S. Hadi, Nonlinear analysis of axially loaded circular concrete-filled stainless steel tubular short columns, *J. Constr. Steel Res.* 101 (2014) 9–18.
- [20] F.C. Wang, L.H. Han, W. Li, Analytical behavior of CFDST stub columns with external stainless steel tubes under axial compression, *Thin-Walled Struct.* 127 (2018) 756–768.
- [21] Z. Lai, A.H. Varma, Effective stress-strain relationships for analysis of noncompact and slender filled composite (CFT) members, *Eng. Struct.* 124 (2016) 457–472.
- [22] Q.Q. Liang, Nonlinear analysis of circular double-skin concrete-filled steel tubular columns under axial compression, *Eng. Struct.* 131 (2017) 639–650.
- [23] M.F. Hassanein, O.F. Kharoob, Q.Q. Liang, Behaviour of circular concrete-filled lean duplex stainless steel-carbon steel tubular short columns, *Eng. Struct.* 56 (2013) 83–94.
- [24] M.F. Hassanein, M. Elchalakani, V.I. Patel, Overall buckling behaviour of circular concrete-filled dual steel tubular columns with stainless steel external tubes, *Thin-Walled Struct.* 115 (2017) 336–348.
- [25] K.J. Rasmussen, Full-range stress-strain curves for stainless steel alloys, *J. Constr. Steel Res.* 59 (1) (2003) 47–61.
- [26] W. Quach, J.G. Teng, K. Chung, Three-stage full-range stress-strain model for stainless steels, *J. Struct. Eng. ASCE* 134 (9) (2008) 1518–1527.
- [27] D. Pons, A. Espinos, V. Albero, M.L. Romero, Numerical study on axially loaded ultra-high strength concrete-filled dual steel columns, *Steel Compos. Struct.* 26 (6) (2018) 705–717.
- [28] M. Ahmed, Q.Q. Liang, V.I. Patel, M.N.S. Hadi, Nonlinear analysis of rectangular concrete-filled double steel tubular short columns incorporating local buckling, *Eng. Struct.* 175 (2018) 13–26.
- [29] Q.Q. Liang, Analysis and Design of Steel and Composite Structures, CRC Press, Taylor and Francis Group, Boca Raton and London, 2014.
- [30] Q.Q. Liang, Performance-based analysis of concrete-filled steel tubular beam-columns, Part I: theory and algorithms, *J. Constr. Steel Res.* 65 (2) (2009) 363–372.
- [31] Q.Q. Liang, Performance-based analysis of concrete-filled steel tubular beam-columns, Part II: verification and applications, *J. Constr. Steel Res.* 65 (2) (2009) 351–362.
- [32] V.I. Patel, Q.Q. Liang, M.N.S. Hadi, Concrete-Filled Stainless Steel Tubular Columns, CRC Press, Taylor and Francis Group, Boca Raton and London, 2018.
- [33] R. Park, Evaluation of ductility of structures and structural subassemblages from laboratory testing, *Bull. N.Z. Soc. Earthq. Eng.* 22 (3) (1989) 155–166.
- [34] Z. Tao, L.H. Han, Z.L. Zhao, Behavior of concrete-filled double skin (CHS inner and CHS outer) steel tubular stub columns and beam-columns, *J. Constr. Steel Res.* 60 (2004) 1129–1158.
- [35] J.B. Mander, Seismic Design of Bridge Piers (Ph.D. Thesis), Depart. of Civil Eng. Uni. of Canterbury, Christchurch, New Zealand, 1983.
- [36] J.B. Mander, M.J. Priestley, R. Park, Theoretical stress-strain model for confined concrete, *J. Struct. Eng. ASCE* 114 (1988), pp. 1804–1826.
- [37] J.C. Lim, T. Ozbakkaloglu, Stress-strain model for normal- and light-weight concretes under uniaxial and triaxial compression, *Constr. Build. Mater.* 2014 (71) (2014) 492–509.
- [38] S.P. Schneider, Axially loaded concrete-filled steel tubes, *J. Struct. Eng.* 124 (10) (1998) 1125–1138.
- [39] L.H. Han, G.H. Yao, X.L. Zhao, Tests and calculations for hollow structural steel (HSS) stub columns filled with self-consolidating concrete (SCC), *J. Constr. Steel Res.* 61 (9) (2005) 1241–1269.
- [40] F.E. Richart, A. Brandtzaeg, R.L. Brown, A Study of the Failure of Concrete Under Combined Compressive Stresses, University of Illinois at Urbana Champaign, College of Eng. Exp. Station, 1928.
- [41] B. De Nicolò, L. Pani, E. Pozzo, Strain of concrete at peak compressive stress for a wide range of compressive strengths, *Mater. Struct.* 27 (4) (1994) 206–210.
- [42] ACI 318-11, Building Code Requirements for Reinforced Concrete, American Concrete Institute, Detroit, MI, 2011.
- [43] AISC 360-16, Specification for Structural Steel Buildings, American Institute of Steel Construction, Chicago, IL, 2016.



Behavior of eccentrically loaded double circular steel tubular short columns filled with concrete

Mizan Ahmed^a, Qing Quan Liang^{a,*}, Vipulkumar Ishvarbhai Patel^b, Muhammad N.S. Hadi^c

^a College of Engineering and Science, Victoria University, PO Box 14428, Melbourne, VIC 8001, Australia

^b School of Engineering and Mathematical Sciences, La Trobe University, Bendigo, VIC 3552, Australia

^c School of Civil, Mining and Environmental Engineering, University of Wollongong, Wollongong, NSW 2522, Australia

ARTICLE INFO

Keywords:

Concrete-filled double steel tubes
Beam-columns
Composite columns
Fiber element modeling
Nonlinear analysis
Short columns

ABSTRACT

Circular concrete-filled double steel tubular (CFDST) columns in high-rise building structures possess high ductility and strength performance owing to the concrete confinement exerted by the external and internal circular steel tubes. However, the behavior of circular CFDST short columns that are loaded eccentrically has not been investigated either experimentally or numerically. Particularly, numerical studies on the moment-curvature responses, strength envelopes, confinement effects and moment distributions in circular CFDST beam-columns have not been reported. In this paper, experimental and computational investigations into the structural responses of circular CFDST short columns loaded eccentrically are presented. Nineteen short circular CFDST columns with various parameters under axial and eccentric loads were tested to failure to measure their structural responses. Test results are presented and discussed. A mathematical simulation model underlying the method of fiber analysis is proposed that simulates the axial load-moment-curvature relationships as well as the strength interaction curves of CFDST beam-columns composed of circular sections. The mathematical modeling technique explicitly takes into account the confinement of concrete on the responses of CFDST columns. The computational procedure and solution method are given. The accuracy of the computer simulation model is evaluated by comparing computations against experimental data. The significance of material and geometric properties, concrete confinement and axial load ratio on the responses of moment-curvature and strength envelopes of CFDST columns and the moment distributions in concrete and steel components are investigated. The mathematical model proposed not only simulates well the experimentally observed responses of CFDST columns but also can monitor the moment distributions in the steel and concrete components of such composite columns.

1. Introduction

Circular concrete-filled double steel tubular (CFDST) columns as schematically depicted in Fig. 1 have increasingly been used in high-rise as well as super high-rise buildings to support heavy loads because of their high ductility and strength performance. The circular CFDST column may be formed by strengthening an existing concrete-filled steel tubular (CFST) circular column with an outer circular steel tube that is filled by either normal or high strength concrete. In a circular CFDST column loaded in compression, the inner steel tube effectively confines the core-concrete while the external tube exerts confinement to both the sandwiched-concrete and the core concrete [1–3]. The effective design of a CFDST column may be achieved by using the outer and inner tubes with different strengths and filling the tubes with concrete of different strengths. In composite buildings, CFDST columns

are often subjected to eccentric loads. Therefore, understanding their performance under eccentric loading is vital for effective design purpose. The current design codes, which include Eurocode 4 [4] and ANSI/AISC 360–16 [5], have not provided design rules for designing circular CFDST beam-columns because experimental and computational studies on their behavior have been extremely rare. This paper addresses this issue.

The experimental behavior of CFDST short columns composed of circular steel sections that were loaded axially has been reported by a number of investigators [6–9]. Test results presented by Xiong et al. [6] showed that utilizing an internal circular tube increased the ultimate axial loads of short circular CFDST columns significantly. However, the effect of the internal tube was more pronounced on the CFDST columns constructed by normal strength concrete than those made of ultra-high-strength concrete. They also studied the effects of using concrete with

* Corresponding author.

E-mail address: Qing.Liang@vu.edu.au (Q.Q. Liang).

<https://doi.org/10.1016/j.engstruct.2019.109790>

Received 9 July 2019; Received in revised form 10 October 2019; Accepted 10 October 2019

0141-0296/ © 2019 Elsevier Ltd. All rights reserved.

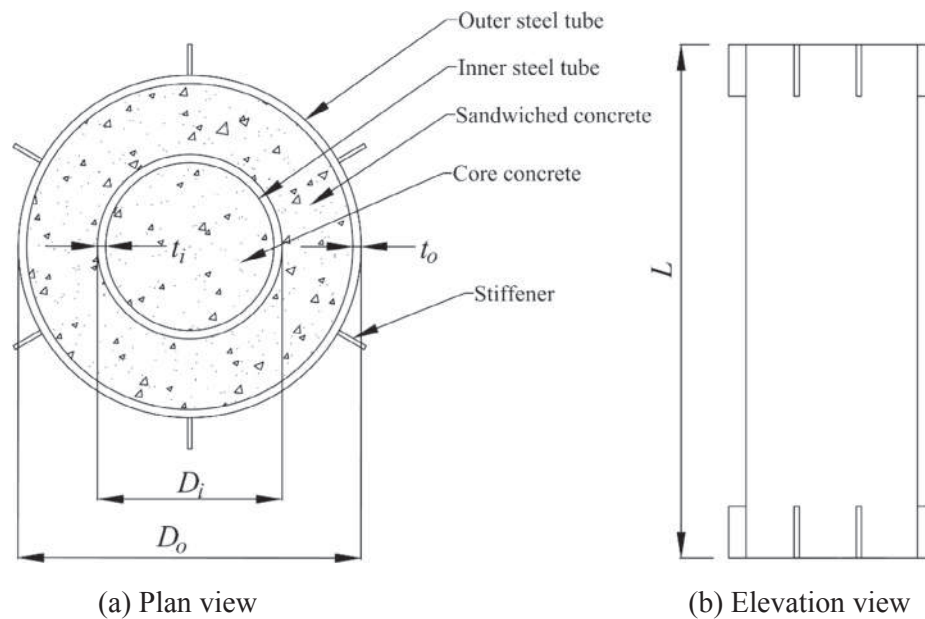


Fig. 1. Schematic view of circular CFDST column.

different strengths to fill the sandwiched space and the internal tube on the structural behavior of CFDST columns. Peng et al. [7] reported that the ultimate loads of the tested circular CFDST columns decreased with increasing the diameter-to-thickness ratio of the steel tubes. The CFDST slender and short columns loaded in axial compression by Wan and Zha [8] failed in a ductile manner. It was reported that increasing the steel ratio of the internal tube improved the ultimate strengths of CFDST short and slender columns markedly. Ekmekyapar and Al-Eliwi [9] investigated the possibility of repairing highly deformed CFST column by placing an outer tube and filling the hollow section with concrete to form a CFDST column. It was observed that the repaired CFST columns exhibited similar performance to that of the freshly fabricated CFDST columns. However, the tested CFDST columns failed prematurely due to the lack of sufficient end restraints. Moreover, Romero et al. [10] performed tests on circular CFDST slender columns at ambient and elevated temperatures. The parameters chosen for the study included the thickness of steel tubes as well as concrete strength. Ibañez et al. [11] investigated the influences of ultra-high-strength concrete on the structural behavior of CFDST slender circular columns that were under eccentric compression. Chang et al. [2] and Zheng et al. [12] studied the strengths of concrete-filled stainless steel-carbon steel tubular (CFSCST) columns with an external stainless steel tube. However, as discussed by Patel et al. [13,14] owing to the difference of the material behaviors between carbon steel and stainless steel, the performance of CFSCST columns is different from that of CFDST columns.

Computer modeling techniques have been employed to compute the performance of nonlinear inelastic circular CFDST columns that were loaded concentrically [1,3,8,15,16]. Chang et al. [2] and Hassanein et al. [3] developed finite element (FE) models for analyzing nonlinear short CFSST columns using the general-purpose FE program ABAQUS. The lateral pressure on the core-concrete was computed by simply adding the lateral pressures induced by the outer stainless-steel tube and by the inner carbon-steel tube. Zheng and Tao [15] developed FE models for circular and square CFDST columns and suggested design equations to estimate the ultimate strength, compressive stiffness and ultimate strain of CFDST columns. The material laws of steel proposed by Katwal et al. [17] and the stress-strain curve for concrete given by Tao et al. [18] were utilized to model the behavior of CFDST columns. The confinement exerted by the external tube on the strength enhancement of the core-concrete was not considered, but confinement factors for the sandwiched-concrete and core-concrete were used. It was

shown that the FE models predicted well the structural behavior. Ahmed et al. [1] developed a new confinement model based on the available experimental data for the core-concrete in circular CFDST columns while the lateral pressures provided by the external steel tube to the sandwiched-concrete were quantified using the model of Hu et al. [19]. The computational technique implementing the new confinement model predicted well the behavior of CFDST short circular columns that were axially loaded.

It would appear that no experimental and computational studies on the responses of short CFDST columns composed of circular sections under eccentric loading have been reported. In this paper, experimental and computational investigations into the structural performance of short CFDST circular columns loaded eccentrically are presented for the first time. The paper is organized as follows. The test program is presented first and the test results obtained are then described. The non-linear numerical analysis procedure for modeling the moment-curvature behavior and strength envelopes of CFDST columns is presented. This is followed by the experimental verification of the numerical procedure. Parametric studies on the structural performance of CFDST short columns that are eccentrically loaded are conducted by means of utilizing the computer model developed and the results obtained are discussed.

2. Test program

2.1. General

A total of nineteen short CFDST columns composed of circular tubes were tested to failure to investigate their structural performance. The short columns were loaded either axially or eccentrically during the tests. This is for the very first time, tests on eccentrically loaded circular short CFDST columns had been carried out. The test parameters mainly focused on the application of loading (axial and eccentric), the diameter-to-thickness ratios of the inner and outer steel tubes and loading eccentricity.

2.2. CFDST column specimens

The hollow circular tubes of CFDST column specimens were constructed by cold-formed thin-walled steel tubes, which were cut into the design length from the long steel tubes supplied by the steel supplier.

Table 1
Geometric and material properties of circular CFDST short columns.

Group	Column	Length L (mm)	Outer tube		Inner tube		f'_c (MPa)	e (mm)	e/D_o	$P_{u,exp}$ (kN)
			$D_o \times t_o$ (mm)	$\frac{D_o}{t_o}$	$D_i \times t_i$ (mm)	$\frac{D_i}{t_i}$				
G1	CC1	420	139.7 × 5.0	27.9	76.1 × 3.6	21.1	19.1	0	0	1605
	CC2	420	139.7 × 5.0	27.9	76.1 × 3.6	21.1	19.1	10	0.07	1268
	CC3	420	139.7 × 5.0	27.9	76.1 × 3.6	21.1	19.1	25	0.18	951
	CC4	420	139.7 × 5.0	27.9	76.1 × 3.6	21.1	19.1	30	0.21	871
G2	CC5	495	165.1 × 5.0	33.0	88.9 × 4.0	22.2	19.1	0	0	1721
	CC6	495	165.1 × 5.0	33.0	88.9 × 4.0	22.2	19.1	0	0	1717
	CC7	495	165.1 × 5.0	33.0	88.9 × 4.0	22.2	19.1	10	0.06	1327
	CC8	495	165.1 × 5.0	33.0	88.9 × 4.0	22.2	19.1	20	0.12	1184
	CC9	495	165.1 × 5.0	33.0	88.9 × 4.0	22.2	19.1	35	0.21	893
G3	CC10	420	139.7 × 3.5	39.9	76.1 × 3.2	23.8	20.6	0	0	1491
	CC11	420	139.7 × 3.5	39.9	76.1 × 3.2	23.8	20.6	0	0	1489
	CC12	420	139.7 × 3.5	39.9	76.1 × 3.2	23.8	20.6	10	0.07	1023
	CC13	420	139.7 × 3.5	39.9	76.1 × 3.2	23.8	20.6	20	0.14	918
	CC14	420	139.7 × 3.5	39.9	76.1 × 3.2	23.8	20.6	30	0.21	765
G4	CC15	495	165.1 × 3.5	47.2	88.9 × 3.2	27.8	20.6	0	0	1911
	CC16	495	165.1 × 3.5	47.2	88.9 × 3.2	27.8	20.6	0	0	1915
	CC17	495	165.1 × 3.5	47.2	88.9 × 3.2	27.8	20.6	10	0.06	1440
	CC18	495	165.1 × 3.5	47.2	88.9 × 3.2	27.8	20.6	20	0.12	1231
	CC19	495	165.1 × 3.5	47.2	88.9 × 3.2	27.8	20.6	35	0.21	961

The specimen length was three times the diameter of the external tube to prevent the column from overall buckling. A typical circular CFDST short column specimen is depicted in Fig. 1, where D_o and t_o are the outer diameter and thickness of the external tube; D_i and t_i the outer diameter and thickness of the internal tube. The column specimens were divided into four groups namely Groups G1, G2, G3 and G4. The material properties as well as geometry of column specimens are given in Table 1, where f'_c is the compressive strength of concrete cylinder, e the loading eccentricity, and $P_{u,exp}$ the experimental ultimate load. Each group consisted of 5 column specimens in which two identical specimens were loaded concentrically to failure except Group G1. The nominal cross-sectional dimensions of the outer steel tubes in Groups G1 and G3 were 139.7×5.0 mm while those in Group G2 and G4 were 165.1×5.0 mm. The nominal sizes of the inner tubes in Group G1, G2, G3 and G4 were 76.1×3.6 mm, 88.9×4.0 mm, 76.1×3.2 mm and 88.9×3.2 mm, respectively. The fabrication of CFDST column specimens was performed by placing the outer and inner hollow steel tubes concentrically and the two tubes were welded with two steel bars to secure their concentric position. Six stiffeners of 32×50 mm with the same thickness as the tube were welded to the ends of the circular outer steel tube around the circumference at 60° apart to avoid premature local buckling at the column end during the test. Ready-mix concrete was utilized to fill the hollow steel tubes. Two different concrete mixes were employed where the aggregate size was 12 mm. The concrete was poured into the tubes in layers and compacted by using a vibrator.

2.3. Material properties

Tensile coupon samples were cut from the steel tubes that were employed to fabricate the circular CFDST columns. Two coupon samples were prepared from each tube and tested according to the requirements of AS 1391 [20]. The curves of stress and strain for the tensile coupon samples are presented in Fig. 2, where the cross-sectional dimensions of the tube were used to identify the individual curve associated with a code designated by C1 or C2. The steel yield strengths of coupon samples varied from 332 to 412 MPa while their tensile strengths ranged from 372 to 510 MPa. The strains of the test coupon samples corresponding to the tensile strength ranged from 0.17 to 0.27 with an average value of 0.21. The measured yield strengths, tensile strengths and their corresponding strains with the calculated modulus of elasticity are listed in Table 2.

Concrete cylinders (100 mm × 200 mm) were also casted and cured in the same environment as the circular CFDST column specimens. Compression tests on concrete cylinders were undertaken to determine their compressive concrete strengths at least after 28 days of the casting. The concrete compressive strengths were averaged from 42-cylinder test results collected from the start and end of the experimental work. The average concrete compressive strength for CFDST column specimens in Groups G1 and G2 was 19.1 MPa while for Groups G3 and G4 it was 20.6 MPa. The reason for using the low strength concrete was because all column specimens were originally designed to be tested using the 2000 kN compression testing machine at Victoria University, Australia. However, due to the failure of the machine, all column specimens were then tested at the University of Wollongong, Australia.

2.4. Test set up

All circular CFDST column specimens were loaded to failure using the Denison compression testing machine having 5000 kN capacity at the structure laboratory in the School of Civil, Mining and Environmental Engineering at the University of Wollongong, Australia. The actual test configurations of column specimens under axial loading and eccentric loading are illustrated in Fig. 3. As shown in Fig. 3(a), for column specimens subjected to concentric loading, the compression load was directly applied on the column specimens. The ends of axially loaded CFDST column specimens were grinded using a concrete grinder to ensure maximum uniform contact between the specimens and the loading heads of the machine. On the other hand, the specially designed loading heads were utilized to simulate the pinned-end conditions of the column specimen that was eccentrically loaded as illustrated in Fig. 3(b). The loading heads, which were designed by Hadi and Wi-diarsa [21], had a round adaptor plate and a 25 mm thick bottom steel plate with a ball joint. The loading heads were grooved with different offsets to obtain different loading eccentricities. Both ends of the column specimen were plastered to the loading heads. The strain distributions of circular CFDST columns were measured by strain gauges. Two strain gauges were mounted at the mid-height of the column specimen under axial compression where one strain gauge was used to capture the axial strain and another strain gauge was used to record the transverse strain of the columns. However, for the column specimen subjected to eccentric loading, both strain gauges were mounted at the compression and tension sides of the column mid-height to record the

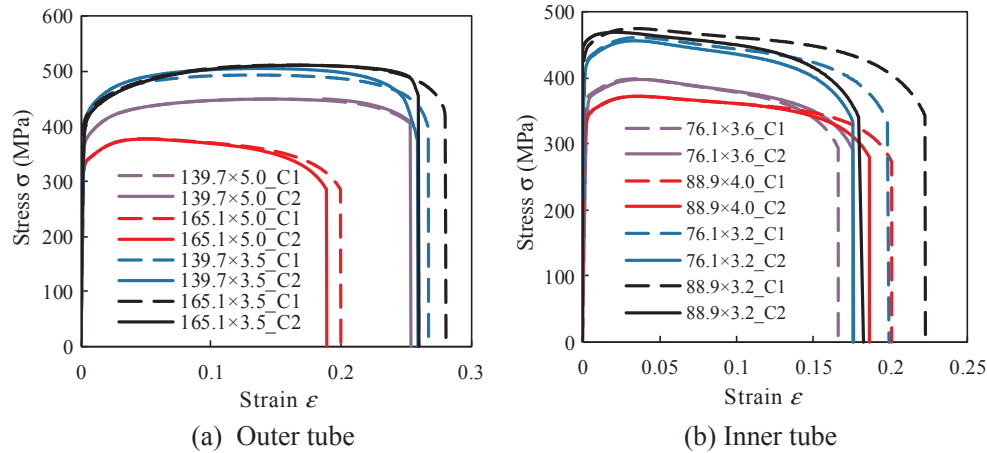


Fig. 2. Measured stress-strain curves of steel tube materials.

axial strain only. Two linear variable differential transducers (LVDTs) were installed at the opposite corners of the testing machine to measure the axial shortening of the column specimen as illustrated in Fig. 3. An additional laser triangulation was employed to measure the deflection at the mid-height of the column specimen tested under eccentric loading as shown in Fig. 3(b).

The column specimen was initially preloaded to 100 kN at a rate of 1.67 kN/s to prevent any slip that could occur during the tests and then unloaded to 20 kN before finally started recording the data. The column specimens were loaded by using the displacement control method with a rate of 0.8 mm/min until failure. A digital data acquisition system was employed to record the readings of LVDTs, strain gauges, laser triangulation and applied load.

3. Test results and discussions

3.1. CFDST column specimens under axial loading

Circular CFDST short column specimens were tested up to large axial deformations. The stopping criterion for testing was either the column specimen buckled significantly or the axial load increment became small enough around the axial shortening of 30 mm. The failure of the column specimens loaded concentrically was caused by the outward local buckling of the outer steel tube as shown in Fig. 4 and the concrete crushing at the locations of the tube local buckling. Fig. 4 demonstrates that the stiffeners successfully prevented the local failure of the column ends from occurring. It can be observed from the sectional view of Specimen CC10 presented in Fig. 5 that there was a composite interaction between the external tube and the sandwiched-concrete and that between the internal tube and core-concrete. The crushing of the sandwiched concrete took place at the regions where the steel tube buckled locally. However, the local buckling of the internal steel tube was effectively prevented by the rigid concrete.

Table 2
Material properties of steel tubes obtained from tensile coupon tests.

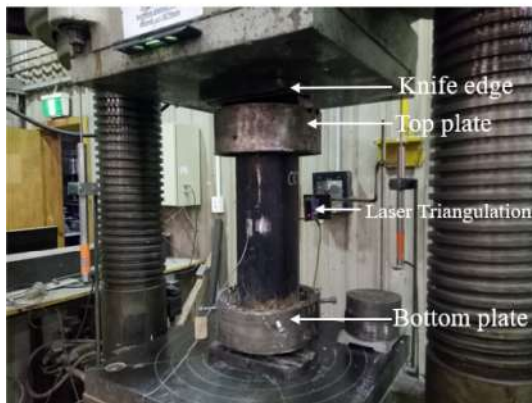
Tube type	No.	Geometry of the tube $D \times t$ (mm)	Yield strength, f_{sy} (MPa)	Ultimate strength, f_{su} (MPa)	Yield strain, ϵ_{sy} ($\mu\epsilon$)	Elongation Δ (%)	Elastic modulus, E_s (GPa)
Outer tube	1	139.7 × 5.0	365	449	2827	20.02	210
	2	165.1 × 5.0	332	377	3346	19.47	208
	3	139.7 × 3.5	412	498	4368	26.53	205
	4	165.1 × 3.5	398	510	2689	26.95	196
Inner tube	1	76.1 × 3.6	353	398	2652	17.06	205
	2	88.9 × 4.0	345	372	4156	19.28	200
	3	76.1 × 3.2	400	458	1493	18.76	211
	4	88.9 × 3.2	412	471	1359	20.18	200

The measured axial load-axial shortening curves of CFDST columns have been plotted in Fig. 6 and ultimate axial loads ($P_{u,exp}$) are tabulated in Table 1. It would appear from Fig. 6 that CFDST circular columns have a good ductility as well as large deformation capability. The axial load-shortening curves of the two columns loaded axially in each group are almost the same. Due to the concrete confinement, the ultimate loads of axially loaded columns in Groups G1, G2, G3 and G4 are 23.6%, 11.6%, 26.4% and 31.9% higher than their theoretical ultimate loads without considering concrete confinement. The inconsistency of the increase in the percentage of the ultimate loads of column specimens in Group G2 compared to other Groups was caused by the uncertainty of the actual strengths of concrete in these column specimens as the average concrete compressive strength was employed to calculate the theoretical ultimate loads. It is observed from Table 1 that the column ultimate load increases with an increase in the steel ratio. The D_o/t_o ratios of the column Specimens CC1 and CC10 with the same D_o were 27.9 and 39.9, respectively. The ultimate axial load of Specimen CC1 is 7.6% higher than that of Specimen CC10. Moreover, increasing the D_o/t_o ratio by using a larger diameter of the outer tube increased the cross-sectional areas of the confined concrete and steel. Therefore, the strength of the columns was improved. However, the column ultimate strength was also influenced by the thickness of the external steel tube. The ultimate load of the Specimen CC5 is 7.2% higher than that of Specimen CC1. However, the ultimate axial load of Specimen CC15 is 28.2% higher than that of Specimen CC10. The test results show that the larger the concrete cross-sectional area, the higher the column ultimate load. The reason for this is that the concrete carries most of the load in a CFDST column.

The axial load-axial strain curves in addition to the axial load-hoop strain responses provide important information about the delamination of CFDST columns and contact stresses between the confined concrete and steel tubes. Fig. 7 presents the measured axial loads vs axial and hoop strain curves of column specimens that were concentrically



(a) Under axial compression



(b) Under eccentric compression

Fig. 3. Test setup of circular CFDST columns.

loaded. The axial and hoop strains of circular CFDST short columns increased linearly at the elastic stage without confinement because the steel material had a larger Poisson's ratio than the concrete. However, as the load increased, the sandwiched concrete expanded more than that of the outer tube. Therefore, the hoop strains of the column specimens increased rapidly as shown in Fig. 7. The presence of the hoop strain-induced lateral pressures on the concrete, which increased the compressive strength of the concrete.

3.2. CFDST columns under eccentric loading

The failure of eccentrically loaded CFDST column specimens was



Fig. 4. Failure modes of axially loaded circular CFDST short columns.



Fig. 5. Section view of Specimen CC10.

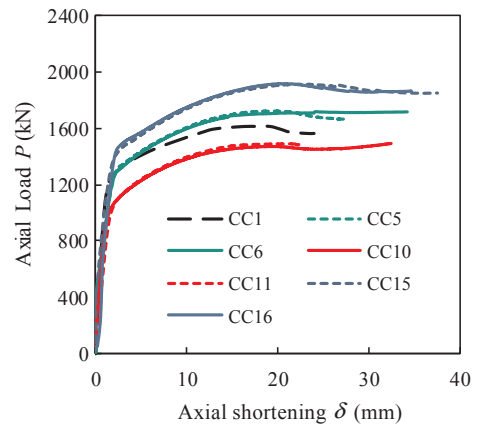


Fig. 6. Load-axial shortening curves of circular CFDST short columns under axial compression.

caused by the outward local buckling of the outer steel tubes in the compression regions near the mid-height of the column specimens, the concrete crushing at the locations of tube buckling, and the column bending as shown in Fig. 8. For columns under a large loading eccentricity, the external steel tube near the column ends underwent significant buckling. The sandwiched concrete in some column specimens was separated from the inner tubes as depicted in Fig. 9. The section view of Specimen CC13 is illustrated in Fig. 10. It is confirmed that the core-concrete in the CFDST columns loaded eccentrically was confined effectively by the steel tubes and did not crush. The main difference between the fundamental behaviors of circular CFST columns and CFDST columns is that the CFDST column has higher strength and ductility than the CFST column for the same outer tube diameter, steel

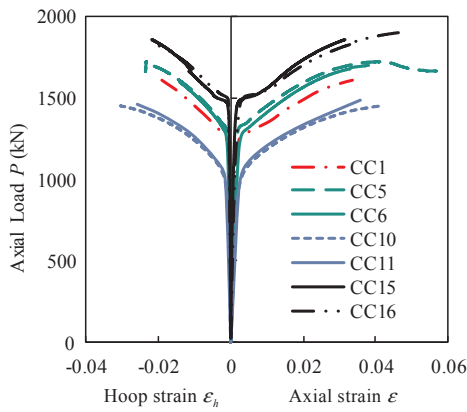


Fig. 7. Measured axial load-strain curves of axially loaded circular CFDST short columns.

cross-sectional area and material strengths as reported by Ahmed et al. [1]. Circular CFST short columns under eccentric loading may fail by the outward local buckling and crushing of the concrete in the compression zone. Circular CFDST columns under eccentric loading may fail by the outward local buckling and crushing of the sandwiched concrete in the compression zone, but the core concrete does not crush due to the confinement provided by both steel tubes.

The experimentally measured axial load-shortening curves for the tested specimens have been plotted in Fig. 11. It is clearly illustrated that increasing the loading eccentricity ratio (e/D_o) significantly reduces the ultimate axial loads of the column specimens. The ultimate axial loads of column specimens in Group G4 were reduced by 30%, 43% and 59% by changing the e/D_o ratio from 0 to 0.06, 0.12 and 0.21, respectively. The measured responses of load-axial shortening and axial



Fig. 9. Separation of sandwiched concrete and inner steel tube of Specimen CC19.

load-lateral deflection of column specimens under eccentric compression are given in Figs. 11 and 12, respectively, where u_m is the lateral deflection at the column mid-height. It is observed that increasing the e/D_o ratio considerably reduces the axial stiffness of the beam-columns. However, all tested column specimens exhibited good ductility and deformation capability. The measured load vs longitudinal strain distributions for specimens loaded eccentrically are illustrated in Fig. 13. The negative strain represents tensile strain while the positive strain means compressive strain. The measured compressive strains were larger than the tensile strains as can be seen from Fig. 13.



Fig. 8. Failure modes of eccentrically loaded circular CFDST short columns.



Fig. 10. Section view of Specimen CC13.

4. Nonlinear analysis

4.1. Basic concepts

A mathematical model underlying the theory of fiber analysis is developed to simulate the nonlinear inelastic moment-curvature relationships and strength envelopes of eccentrically loaded circular CFDST columns. The fiber element method is an accurate and computationally efficient numerical modeling method for the simulation of nonlinear composite columns over the traditional finite element method as pointed out by Liang [22] and Ahmed et al. [23]. The typical fiber discretization of the concrete and steel components in the cross-

section of a circular CFDST is illustrated in Fig. 14, where d_n is the depth of the plastic neutral axis in the cross-section, y_i the distance from the section centroid to the centroid of the i th fiber element, $d_{e,i}$ the distance from the neutral axis to the element centroid, ϕ the curvature, ε_i the compressive strain at the extreme fiber, and $\varepsilon_{e,i}$ the strain of the i th fiber element. The plane section is assumed to remain plane after deformation in the fiber analysis technique. This implies a linear distribution of strains through the depth of the column cross-section as illustrated in Fig. 14. Under the axial loading combined with uniaxial bending, the fiber strain is computed from the curvature and the neutral axis depth of the cross-section [14,24,25]. The stresses in steel and concrete fibers are determined from the material uniaxial stress-strain relationships of steel and concrete given in Section 5. The internal force (P) as well as moment (M) are calculated as stress resultants over the entire cross-section.

4.2. Computer simulation procedure

The moment vs curvature curves of circular CFDST columns loaded eccentrically are simulated by increasing the curvature incrementally and computing the corresponding moment. The force equilibrium condition must be maintained for each increment of the curvature by adjusting the neutral axis depth (d_n) of the cross-section. The internal moment (M) is determined by the integration of fiber stresses over the entire cross-section. The complete moment-curvature curve for a given axial load can be obtained by repeating the process of analysis.

The strength envelope, which represents the axial load (P_u) and ultimate moment (M_u) interaction diagram, of a short circular CFDST column is used in designing columns subjected to eccentric loading. In

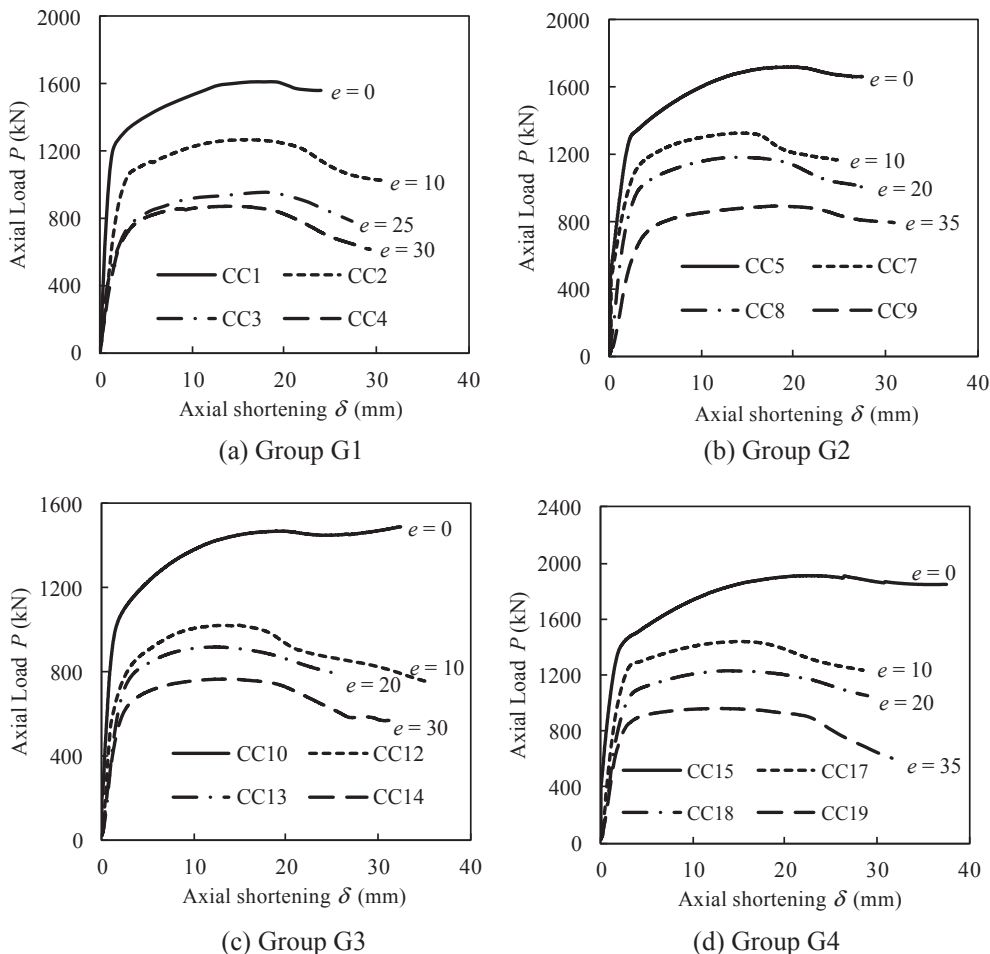


Fig. 11. Effects of load eccentricity on the axial load-shortening curves of circular CFDST columns.

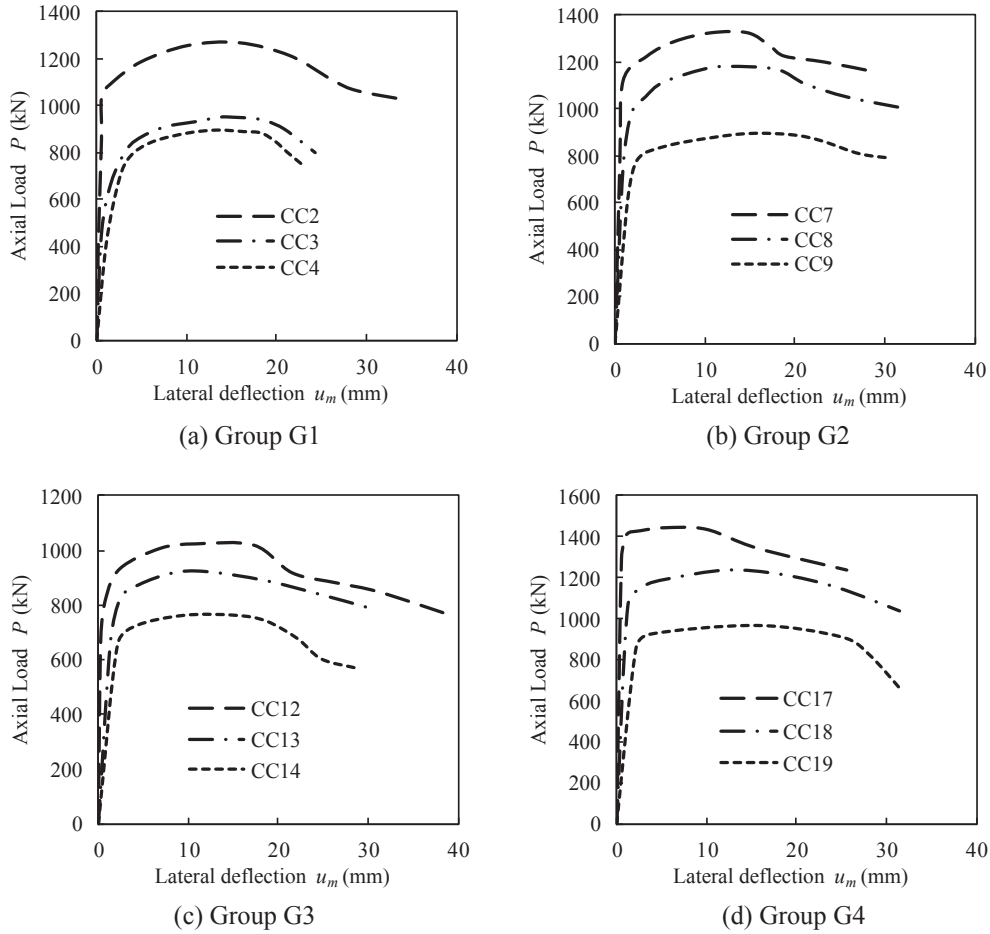


Fig. 12. Measured axial load-lateral deflection curves of eccentrically loaded circular CFDST columns.

the simulation of the interaction curve, the ultimate axial load (P_o) of the CFDST column loaded concentrically is firstly calculated by the axial load-strain analysis procedure considering the concrete confinement. The axial load (P_u) is increased gradually from zero to the maximum ultimate load (P_o), and the corresponding ultimate moment (M_u) of the composite section is ascertained from the moment-curvature relationships. The equilibrium condition for each curvature increment must be maintained by ensuring the internal axial load (P) calculated is the same as the applied axial load (P_u). To achieve this condition, the neutral axis depth (d_n) of the column section is adjusted iteratively by efficient numerical algorithms. The inverse quadratic method has been implemented in the mathematical programming scheme to solve the highly dynamic equilibrium functions [26]. The computer flowchart for calculating the strength envelope of a short CFDST column is given in Fig. 15, where $\Delta\varepsilon$ is the axial strain increment, P_{max} the maximum axial load that can be applied to the column, ε_{cu} the ultimate strain of concrete in compression, $\Delta\phi$ the curvature increment, r_p the residual force expressed as $r_p = P_u - P$, and ΔP_u the axial load increment.

4.3. Computational solution algorithms

Computational solution algorithms implementing the inverse quadratic method have been developed by Ahmed et al. [26,27] for quantifying the neutral axis depth (d_n) during the loading history of CFDST columns. The inverse quadratic method requires three initial values of d_n taken as $d_{n,1} = D_0$, $d_{n,2} = D_0/2$ and $d_{n,3} = (d_{n,1} + d_{n,2})/2$ to be initialized to start the computation process. The new true d_n is then calculated by the following equations:

$$d_{n,j+3} = d_{n,j+1} - r_{p,j+1} \left(\frac{A}{C} \right) \quad (1)$$

$$A = (r_{p,j})^2(d_{n,j+2} - d_{n,j+1}) + r_{p,j}r_{p,j+1}(d_{n,j+1} - d_{n,j+2}) + (r_{p,j+1} - r_{p,j+2})r_{p,j+2}(d_{n,j} - d_{n,j+1}) \quad (2)$$

$$C = (r_{p,j+1} - r_{p,j})(r_{p,j+2} - r_{p,j})(r_{p,j+2} - r_{p,j+1}) \quad (3)$$

where the residual force $r_p = P_u - P$ and j is the iteration number. The stopping criterion of the computational process is determined as $|r_p| < \varepsilon_k$, in which ε_k is taken as 10^{-4} .

4.4. Curvature ductility index

The curvature ductility indicator evaluates the ductility of a circular CFDST column eccentrically loaded and is defined as

$$PI_{cd} = \frac{\phi_u}{\phi_y} \quad (4)$$

in which ϕ_u denotes the ultimate curvature of the column when the moment falls to 90% of its ultimate moment capacity in the post-peak range or the ultimate curvature where column shows ascending moment-curvature relationships in the post-yield regime. The yield curvature ϕ_y is taken as the curvature corresponding to 75% of the column ultimate moment capacity [24].

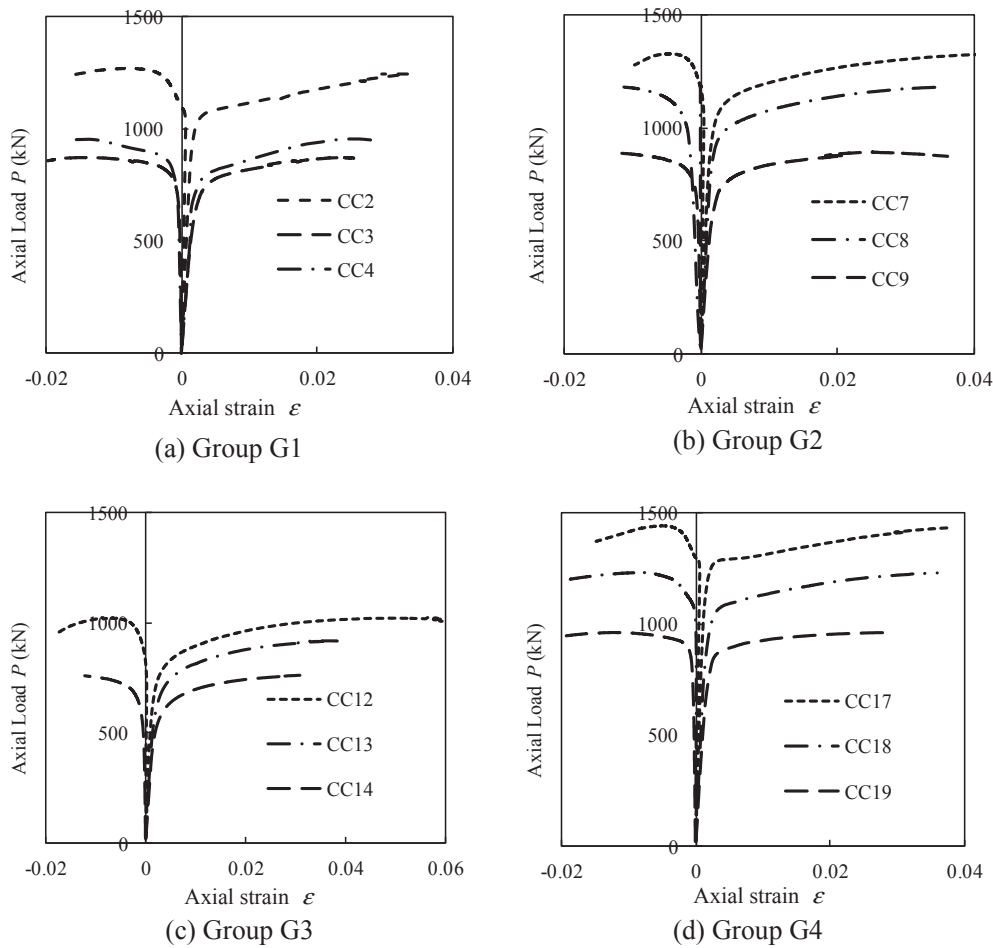


Fig. 13. Measured load-strain curves of eccentrically loaded circular CFDST short columns.

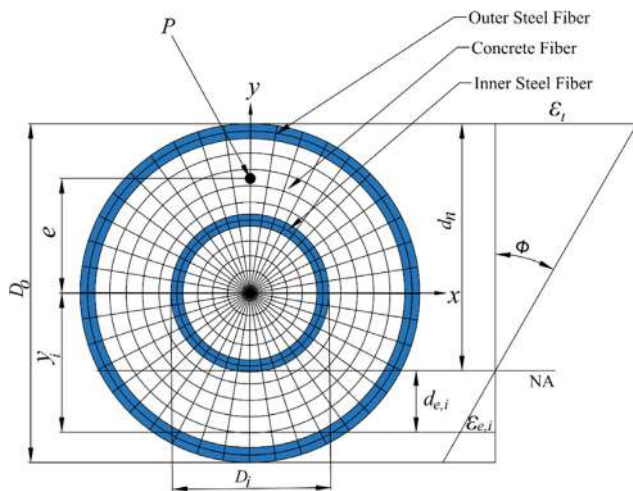


Fig. 14. Typical fiber discretization and strain distribution in the cross-section of circular CFDST column.

5. Material constitutive laws

5.1. Structural steels

The steel tubes in CFDST columns are subjected to biaxial stresses which reduce their yield strength in the longitudinal direction. The stress and strain relationships of structural steel material are given in Fig. 16, where σ_s and ϵ_s are the longitudinal stress and strain in steel,

respectively; ϵ_{st} and ϵ_{stH} are the strains at the onset of strain-hardening and at the ultimate strain, and taken as 0.005 and 0.2, respectively. Liang [24] suggested that a reduction factor of 0.9 should be used to reduce the steel yield strength shown in Fig. 16 to consider the effects of biaxial stresses on the steel tube. The formulas to calculate the rounded-part in the stress-strain curve was also suggested by Liang [24] for cold-formed steel while the expression provided by Mander [28] is employed to determine the stresses in the range of strain hardening.

5.2. Concrete

The current and existing test results [6–9] indicate that the effective confinement provided by the circular steel tube significantly increases the ductility as well as the strength of CFDST columns composed of circular tubes. Moreover, the results obtained from finite element analyses presented by Chang et al. [2] confirmed that longitudinal stress in sandwiched concrete was similar to the concrete in circular CFST columns while the core-concrete in a circular CFDST column loaded was subjected to a higher compressive longitudinal stress than the sandwiched-concrete. When the compressive load increases, the sandwiched-concrete and the core-concrete expand more than the steel tubes, the external steel tube confines the sandwiched-concrete. The sandwiched-concrete under lateral compression exerts lateral pressure on the internal steel tube which therefore confines the core-concrete. Therefore, it can be assumed that the sandwiched-concrete is mainly confined by the external tube while the core-concrete is effectively confined by both the external and internal tubes in a circular CFDST column [1–3]. Ahmed et al. [1] proposed constitutive laws of confined concrete in circular CFDST columns. The two-stage stress and strain

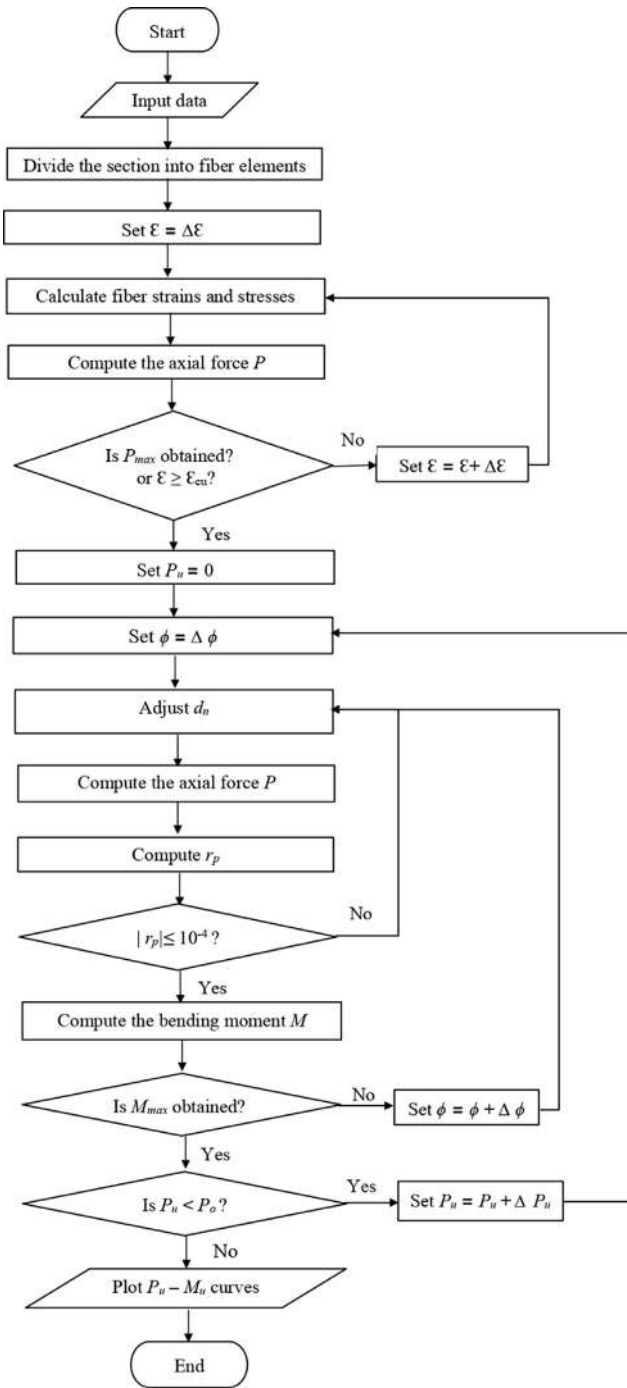


Fig. 15. Computer flowchart for calculating axial load-moment interaction curves.

curves for unconfined and confined concrete illustrated in Fig. 17 was originally derived by Lim and Ozbakkaloglu [29]. A general stress-strain model is adopted for both sandwiched-concrete and core-concrete, but different lateral confining pressure models are used to determine the confinement on the sandwiched-concrete and ore-concrete. The ascending branch of the curves is expressed by the equations presented by Mander et al. [30] as

$$\sigma_c = \frac{f'_{cc} (\epsilon_c / \epsilon'_{cc})^\lambda}{(\epsilon_c / \epsilon'_{cc})^\lambda + \lambda - 1} \quad (5)$$

$$\lambda = \frac{\epsilon'_{cc} E_c}{\epsilon'_{cc} E_c - f'_{cc}} \quad (6)$$

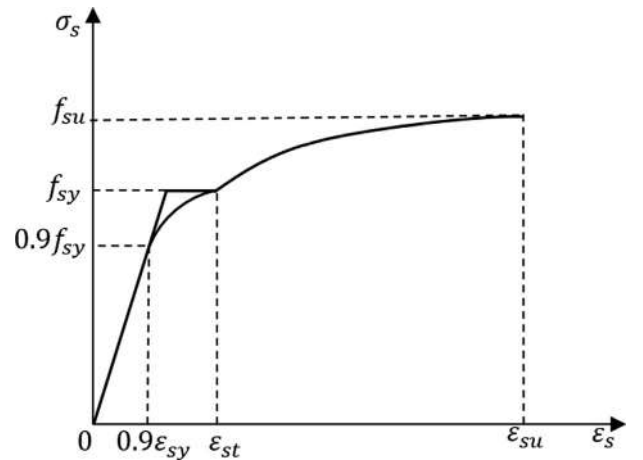


Fig. 16. Typical stress-strain curve for structural steels.

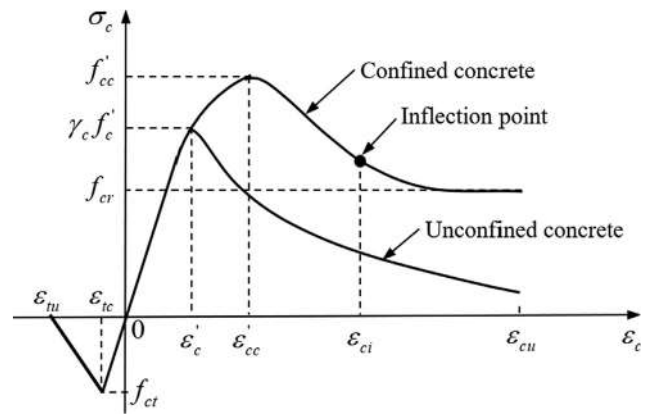


Fig. 17. Typical stress-strain curves for confined and unconfined concrete.

in which σ_c and ϵ_c denote the longitudinal stress and the corresponding strain; f'_{cc} and ϵ'_{cc} represent the maximum strength of compressive concrete and its corresponding strain, respectively; E_c is the modulus of elasticity of concrete, calculated as [23]

$$E_c = 4400 \sqrt{\gamma_c f'_c} \text{ (MPa)} \quad (7)$$

in which $\gamma_c = 1.85 D_c^{-0.135}$ is the reduction factor applied to the concrete compressive strength taking into account the column size effect, in which D_c stands for the concrete-core diameter and is $(D_i - 2t_i)$ for core-concrete and $(D_o - 2t_o)$ for sandwiched concrete.

The confinement is explicitly taken into account in the stress-strain model for confined concrete. As shown in Fig. 4, the confinement effect is included when the compressive stress in the concrete fibers is greater than $\gamma_c f'_c$. The confinement increases the concrete compressive strength from $\gamma_c f'_c$ to the maximum value of f'_{cc} . The maximum compressive strength (f'_{cc}) together with the corresponding strain (ϵ'_{cc}) are calculated as

$$f'_{cc} = \gamma_c f'_c + 4.1 f_{rp} \quad (8)$$

$$\epsilon'_{cc} = \epsilon'_c + \frac{20.5 f_{rp} \epsilon'_c}{\gamma_c f'_c} \quad (9)$$

where f_{rp} generally defines the lateral pressure on the confined concrete. For the sandwiched concrete, the lateral pressure (f_{rpo}) is calculated by the equation proposed by Hu et al. [19] as

$$f_{rpo} = \begin{cases} 0.043646 - 0.000832 \left(\frac{D_o}{t_o}\right) & \text{for } 21.7 \leq \frac{D_o}{t_o} \leq 47 \\ 0.006241 - 0.0000357 \left(\frac{D_o}{t_o}\right) & \text{for } 47 < \frac{D_o}{t_o} \leq 150 \end{cases} \quad (10)$$

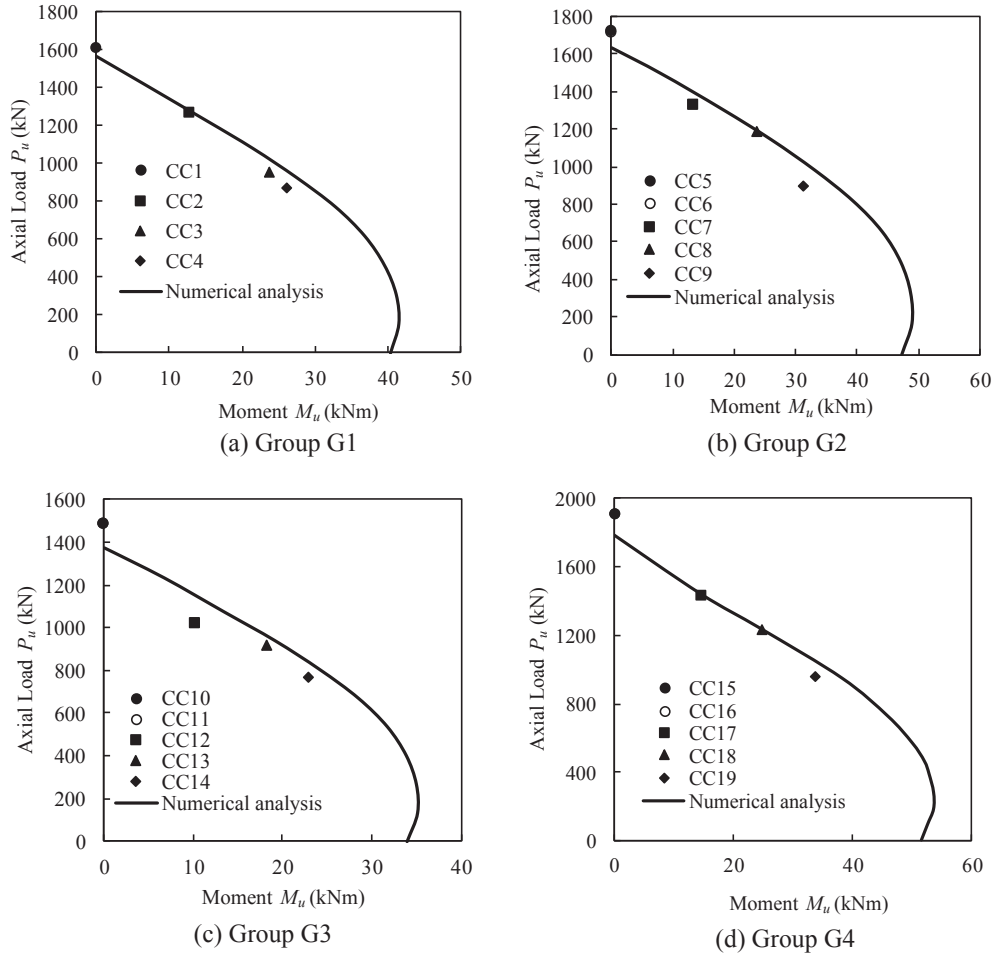


Fig. 18. Comparison of predicted strength envelopes of circular CFDST columns with test results.

in which f_{sy0} is the yield strength of the outer steel tube.

Based on the test results, Ahmed et al. [1] proposed an equation for estimating the lateral pressure on the core-concrete (f_{rpi}) in CFDST columns, expressed as

$$f_{rpi} = 2.2897 + 0.0066 \left(\frac{D_o}{t_o} \right) - 0.1918 \left(\frac{D_i}{t_i} \right) - \left[0.0585 \left(\frac{D_o}{t_o} \right) - 0.3801 \left(\frac{D_i}{t_i} \right) \right] \zeta^{-1} \quad (f_{rpi} \geq 0) \quad (11)$$

in which the confinement factor ζ is defined as

$$\zeta = \frac{A_{so} f_{sy,0} + A_{si} f_{sy,i}}{A_{sc} \gamma_c f'_c + A_{cc} \gamma_c f'_c} \quad (12)$$

The strain (ϵ'_c) corresponding to the maximum strength f'_c of the unconfined compressive concrete shown in Fig. 17 is calculated using the expression given by De Nicolo et al. [31] as

$$\epsilon'_c = 0.00076 + \sqrt{(0.626 \gamma_c f'_c - 4.33) \times 10^{-7}} \quad (13)$$

Lim and Ozbakkaloglu [29] proposed an equation to express the descending branch of stress-strain curves as

$$\sigma_c = f'_{cc} - \frac{f'_{cc} - f_{cr}}{\left[1 + \left(\frac{\epsilon_c - \epsilon'_{cc}}{\epsilon_{ct} - \epsilon'_{cc}} \right)^{-2} \right]} \quad (14)$$

where f_{cr} is the residual strength of concrete, which was proposed by Ahmed et al. [1] as

$$\frac{f_{cr}}{f'_{cc}} = 1.2420 - 0.0029 \left(\frac{D}{t} \right) - 0.0044 \gamma_c f'_c \left(0 \leq \frac{f_{cr}}{f'_{cc}} \leq 1.0 \right) \quad (15)$$

The original equation developed by Lim and Ozbakkaloglu [29] for calculating the strain at the inflection point (ϵ_{ci}) is modified to consider the column size effects as

$$\epsilon_{ci} = 2.8 \epsilon'_{cc} (\gamma_c f'_c)^{-0.12} \left(\frac{f_{cr}}{f'_{cc}} \right) + 10 \epsilon'_{cc} (\gamma_c f'_c)^{-0.47} \left(1 - \frac{f_{cr}}{f'_{cc}} \right) \quad (16)$$

The relationships of stress and strain of concrete in tension are illustrated in Fig. 17, where f_{ct} and ϵ_{st} are the tensile strength and corresponding strain of concrete. The ultimate strength (f'_{ct}) of concrete in tension is specified as $0.6 \sqrt{\gamma_c f'_c}$ and the corresponding strain ϵ_{tu} is determined as ten times the cracking strain.

6. Experimental verification

The accuracy of the mathematical modeling technique proposed is assessed by means of comparing the predicted strength envelopes with experimental results in Fig. 18. The experimental ultimate moment ($M_{u,exp}$) was determined as the product of the ultimate axial load ($P_{u,exp}$) and eccentricity (e). It can be observed from the comparisons that the computational results are generally in good agreement with measurements. However, the ultimate loads of CFDST columns under concentric loads are slightly underestimated by the numerical model and experimental ultimate moments of Columns CC7 and CC12 are slightly lower than the predicted values. The uncertainty in the actual concrete strengths in the tested specimens may cause these discrepancies as the

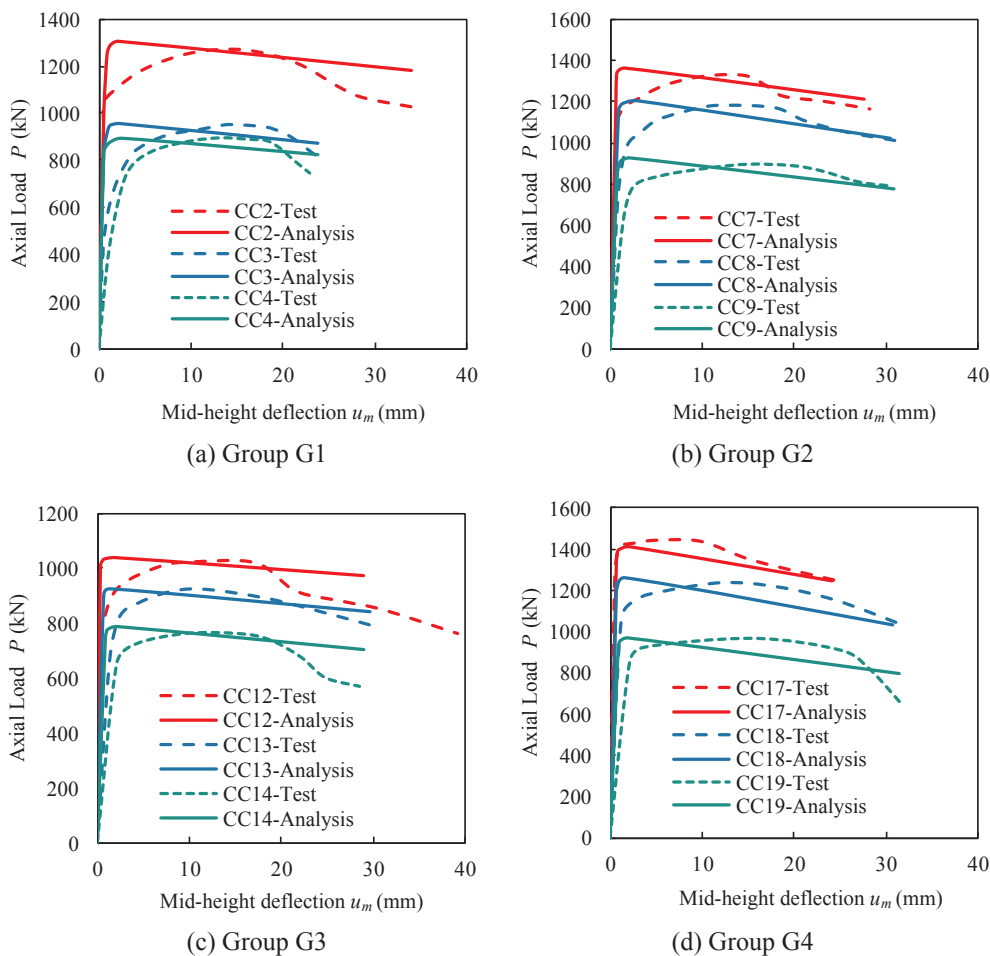


Fig. 19. Comparison of tested and predicted axial load-mid-height deflection curves of circular CFDST columns.

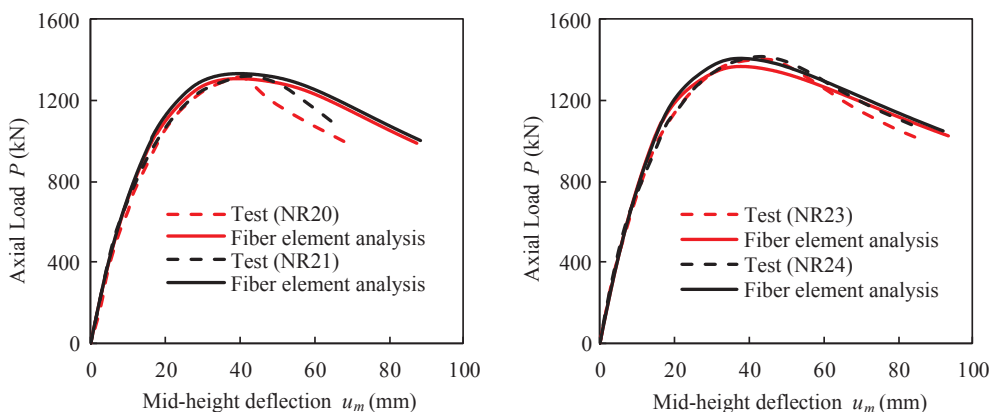


Fig. 20. Comparison of predicted and experimental load-mid-height deflection curves of circular CFDST slender columns tested by Ibañez et al. [11].

average compressive strengths of concrete were specified in the numerical analyses. The difference between the experimental and predicted ultimate moments of Columns CC9, CC14 and CC19 is caused by the failure of the column ends subjected to large loading eccentricities as shown in Fig. 8.

The computational model proposed has been further developed to simulate the load-deflection responses of circular CFDST short and slender columns loaded eccentrically [26]. The accuracy of the computational model is validated by comparing the calculations with the measured load-deflection curves of eccentrically loaded circular CFDST short and slender columns tested by the authors and Ibañez et al. [11].

The initial eccentricity of the tested short columns was taken as $L/650$ in the numerical analyses. It would appear from Fig. 19 that reasonable agreement between test data and numerical results for short CFDST columns is obtained. The difference between experiments and computations is likely attributed to the uncertainty in the actual strengths of concrete in the tested columns. Moreover, as the concrete strength is very low, the concrete model adopted might not accurately capture the behavior of low strength concrete. However, the numerical model predicts well the complete load-deflection curves of slender CFDST columns as depicted in Fig. 20. This approves that the mathematical model proposed can accurately predict the structural behavior of

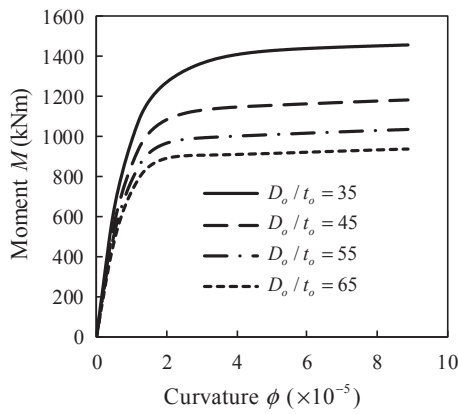


Fig. 21. Moment-curvature curves of circular CFDST columns with various D_o/t_o ratios.

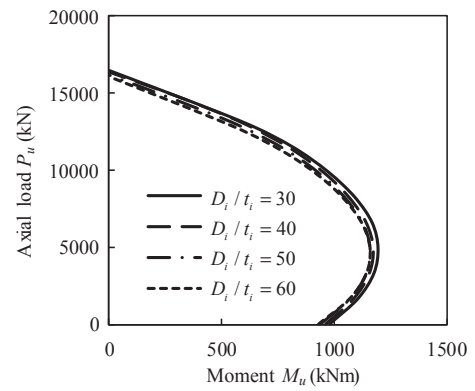


Fig. 24. Strength envelopes of circular CFDST columns with various D_i/t_i ratios.

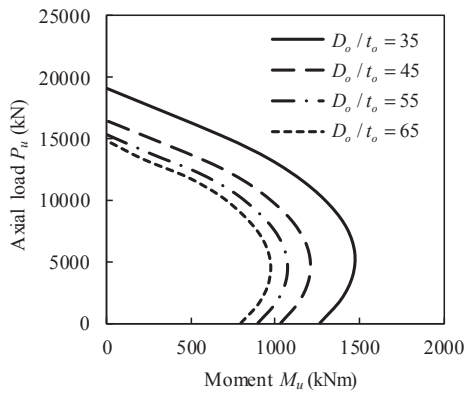


Fig. 22. Strength envelopes of circular CFDST columns with various D_o/t_o ratios.

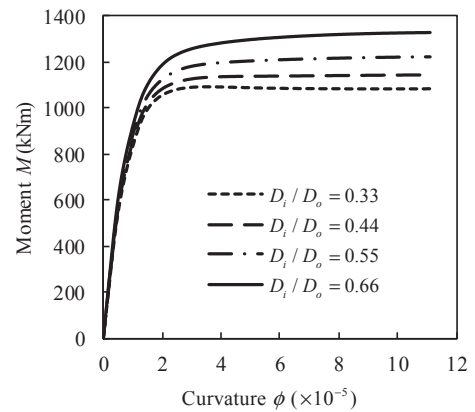


Fig. 25. Moment-curvature curves of circular CFDST columns as a function of D_i/D_o ratio.

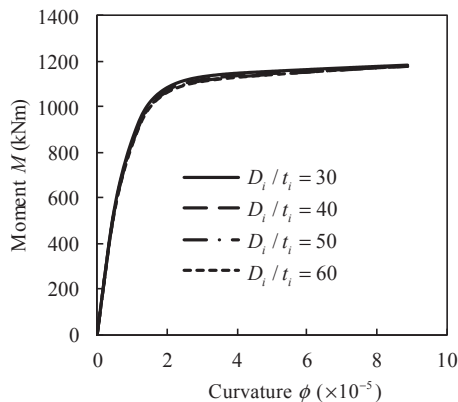


Fig. 23. Moment-curvature curves of circular CFDST columns with various D_i/t_i ratios.

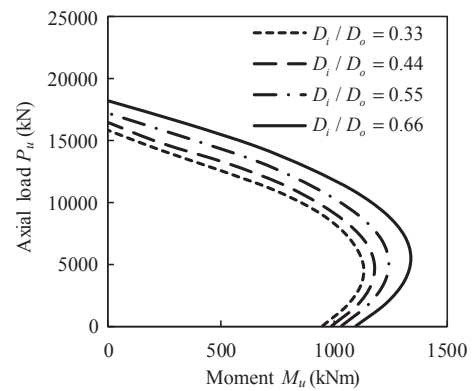


Fig. 26. Strength envelopes of circular CFDST columns as a function of D_i/D_o ratio.

circular CFDST columns loaded eccentrically.

7. Parametric studies

The mathematical model, which was implemented in a computer program, was employed to examine the sensitivities of moment-curvature responses and strength envelopes of CFDST columns composed circular sections to various important design parameters. The stress-strain model for concrete in circular CFDST columns has been verified by experimental results by the authors [1], and can be used to model the material behavior of both normal and high strength concrete in CFDST columns. For practical applications, the concrete strength used

in CFDST columns is usually above 40 MPa. Therefore, the concrete strengths varying from 40 MPa to 100 MPa were used in the parametric studies. The following data were used for the reference column: $D_o = 450$ mm, $t_o = 10$ mm, $D_i = 200$ mm, $t_i = 6.67$ mm, $f_{syo} = f_{syi} = 350$ MPa, $E_s = 200$ GPa, the concrete strength of the sandwiched-concrete and the core-concrete was taken as $f'_{co} = f'_{ci} = 70$ MPa, and the load ratio was specified as $P_u/P_o = 0.4$.

7.1 D_o/t_o ratio

The effects of the ratio of D_o/t_o on the structural behavior of CFDST circular columns were examined by utilizing the computational model developed. The D_o/t_o ratio of CFDST columns was varied from 35 to 45, 55 and 65 by altering the thickness of the external tube only. The

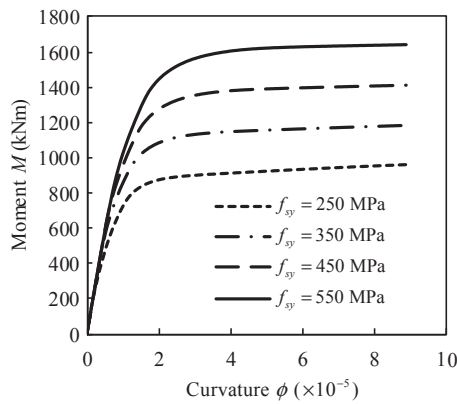


Fig. 27. Effects of steel yield strength on the moment-curvature curves of circular CFDST columns.

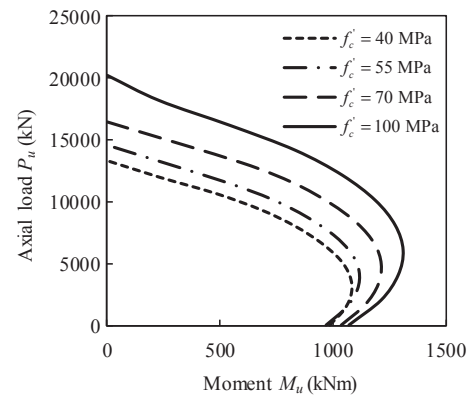


Fig. 30. Effects of concrete strength on the strength envelopes of circular CFDST columns.

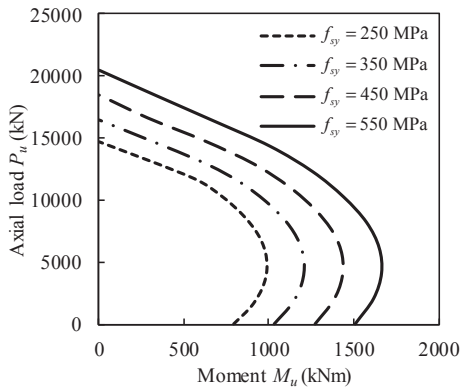


Fig. 28. Effects of steel yield strength on the strength envelopes of circular CFDST columns.

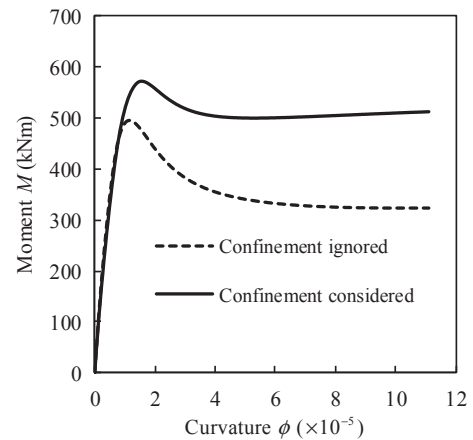


Fig. 31. Influences of concrete confinement on the moment-curvature curves of circular CFDST columns.

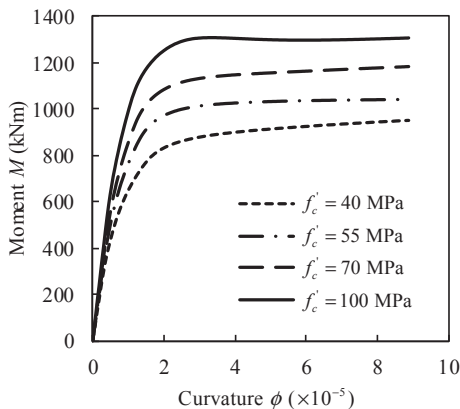


Fig. 29. Effects of concrete strength on the moment-curvature curves of circular CFDST columns.

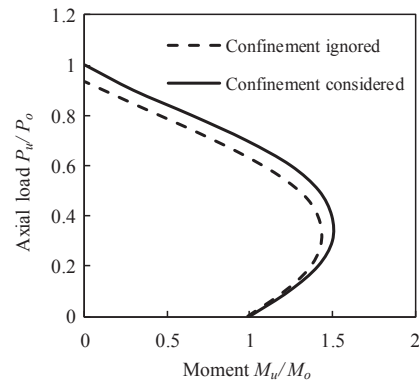


Fig. 32. Influences of concrete confinement on the normalized strength envelopes of circular CFDST columns.

moment-curvature curves and strength envelopes of CFDST columns are presented in Figs. 21 and 22, respectively. Under the constant axial load of 6591 kN, increasing ratio of D_o/t_o remarkably reduces both the initial bending stiffness and resistance of CFDST columns as demonstrated in Fig. 21. This is caused by the decrease in the steel area of the outer tube. The ultimate moment capacity is decreased by 35.7% by increasing the ratio D_o/t_o from 35 to 65. Moreover, Fig. 22 indicates that the ratio D_o/t_o has a considerable influence on the pure ultimate axial and the pure bending moment. Changing the D_o/t_o ratio from 35 to 45, 55 and 65 causes an increase in the pure ultimate axial strength of the columns by 13.7%, 19.6% and 22.5%, respectively, while the increases in the pure bending resistance were calculated as 18.1%, 29.2% and 36.69%,

respectively.

7.2 D_i/t_i ratio

The sensitivities of the structural responses of circular CFDST columns to the ratio D_i/t_i were examined by altering the thickness of the inner tube only. The moment-curvature relations of CFDST columns under a constant axial load of 6591 kN are given in Fig. 23. It is observed that the ratio D_i/t_i has a minor effect on the moment-curvature behavior of the CFDST columns. The bending resistance of the CFDST columns decreases by only 0.3% when the ratio D_i/t_i increases from 30 to 60. The curvature ductility index of CFDST columns having the D_i/t_i

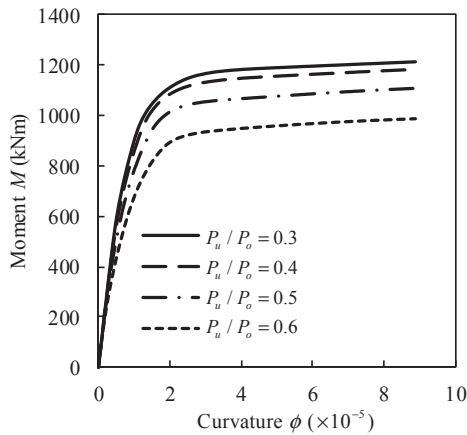


Fig. 33. Influences of axial load ratio on the moment-curvature curves of circular CFDST column.

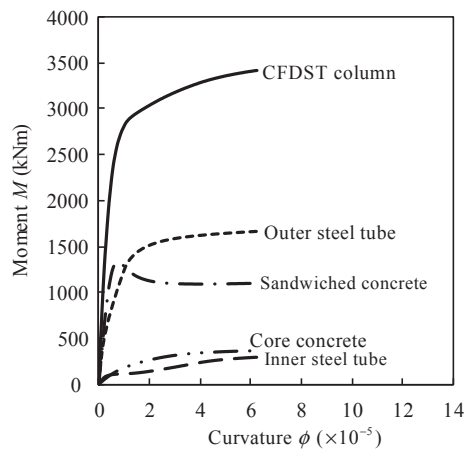


Fig. 34. Moment distributions in a circular CFDST beam-column.

ratio of 30 is 18.13 but it is 15.11 for the CFDST column having the D_i/t_i ratio of 60. The strength curves generated by the computational model are given in Fig. 24. It is apparent that the influence of the D_i/t_i ratio on the strength envelopes is insignificant. The decreases in the pure ultimate axial and the bending strengths are only 2.3% and 5.2%, respectively when the ratio D_i/t_i is changed from 30 to 60.

7.3. D_i/D_o ratio

The diameter of the inner tube was changed to investigate the significance of the ratio D_i/D_o on the responses of CFDST columns. The moment-curvature curves for the columns that were loaded by a constant axial load of 6591 kN are given in Fig. 25. It is evident that increasing the ratio D_i/D_o slightly increases the initial bending stiffness but improves the ultimate bending strength of CFDST columns considerably. When the ratio D_i/D_o is changed from 0.33 to 0.44, 0.55 and 0.66, the column ultimate moment increases by 4.7%, 11.9% and 21.6%, respectively. The curvature ductility index of CFDST columns increases from 20.1 to 23.3 by changing the ratio D_i/D_o from 0.33 to 0.66. The computed strength envelopes of CFDST columns have been drawn in Fig. 26. The change of the D_i/D_o ratio from 0.33 to 0.66 improves the pure ultimate axial load by 15% and the pure ultimate moment of the CFDST column by 15.1%.

7.4. Steel yield strength

The steel yield stress of circular CFDST columns was varied from 250 MPa to 550 MPa to ascertain its influences on their structural performance. The influences of steel yield stress on the moment-

curvature behavior of the CFDST columns subjected to the constant axial load of 6591 kN are shown in Fig. 27. It would appear from Fig. 27 that the initial bending stiffness of the columns is appreciably improved by using the steel tubes with higher yield stress. Changing the steel yield stress from 250 MPa to 650 MPa causes a marked increase in the ultimate moment by 70.8%. However, the column ductility index reduces from 17.89 to 14.11 when the steel tubes with the yield stress of 650 MPa are used instead of those with the yield stress of 250 MPa. The sensitivity of the interaction behavior to the steel yield stress is demonstrated in Fig. 28. The figure indicates that the higher the yield stress of the steel tubes, the higher the pure ultimate axial and bending strengths of the column. However, the steel yield stress has the most pronounced impact on the pure bending moment. The pure ultimate axial and pure bending strengths increase by 38.7% and 90.4%, respectively when changing the steel yield stress from 250 MPa to 650 MPa.

7.5. Concrete compressive strength

The sensitivities of the moment-curvature and strength interaction responses of CFDST columns to the concrete compressive strengths varied from 40 MPa to 100 MPa were examined. The simulated moment-curvature curves for the columns loaded by the constant axial load of 6591 kN are given in Fig. 29. The column's initial bending stiffness has a marked improvement due to the increase in the concrete compressive strength. Changing the concrete strength from 40 MPa to 100 MPa increases the ultimate moment capacity of the column by 37.5%, however, its ductility index decreases from 18.67 to 9.01. Fig. 30 shows that the concrete strength has a greater effect on the pure ultimate axial load of the CFDST column than on its pure bending moment. As a result of increasing the concrete strength from 40 MPa to 100 MPa, the pure ultimate axial load increases by 51.7% while the pure ultimate moment increases only 8.9%.

7.6. Concrete confinement

The concrete confinement is an important feature that has a remarkable effect on the responses of circular CFDST columns loaded eccentrically. The computer program developed was employed to ascertain this effect. The thickness t_o of the reference column was changed to produce a D_o/t_o ratio of 100 while D_i was changed to $D_i = D_o/3$. The other parameters of the reference column remained the same. The moment-curvature and interaction strength curves of the CFDST column with and without considering the confinement effect are provided in Figs. 31 and 32, respectively. It is discovered that ignoring the confinement effect considerably underestimates the performance of the CFDST column. When the confinement is not considered in the numerical modeling, the column ultimate and residual moment capacity is underestimated by 13.4% and 37% as indicated in Fig. 31. Moreover, the confinement has a considerable influence on the interaction curves of CFDST columns as demonstrated in Fig. 32. If the confinement is not considered in the simulation, the pure ultimate axial load of the columns is underestimated by 7.4% while the pure bending moment is underestimated by 1.1%.

7.7. Axial load ratio

The computer model was used to ascertain the influences of the applied axial load ratio (P_u/P_o) on the responses of CFDST columns. The moment-curvature curves of the CFDST column with the P_u/P_o ratios varied from 0.3 to 0.4, 0.5 and 0.6 are presented in Fig. 33. The initial bending stiffness and moment capacity are markedly decreased by increasing the load ratio. However, this effect is more significant for the P_u/P_o ratio larger than 0.5. If the axial load ratio is changed from 0.3 to 0.4 and 0.5, the bending resistance of the CFDST column decreases by only 2.5% and 8.7%, respectively. However, when the P_u/P_o ratio

increases from 0.3 to 0.6, the ultimate moment reduces by 18.7%. The ductility performance of the CFDST column is insignificantly influenced by the P_u/P_o ratio as indicated in Fig. 33.

7.8. Moment distributions in CFDST columns

The moment distributions in circular CFDST columns loaded eccentrically have not been investigated. To provide information on the moment distributions, the circular CFDST beam-column that had the following geometric and material properties was analyzed by the computational model: $D_o = 800$ mm, $t_o = 8$ mm, $D_i = 400$ mm, $t_i = 8$ mm, $f_{sy0} = f_{sy1} = 350$ MPa, $E_s = 200$ GPa and $f'_{co} = f'_{ci} = 50$ MPa. In the moment-curvature analysis, the axial load of 22,289 kN was applied to the beam-column. The predicted moment distributions in the external steel tube, inner steel tube, sandwiched concrete and core-concrete as a function of the curvature are schematically presented in Fig. 34, where the moment-curvature curve for the CFDST column is also shown. At the maximum moment, the moments carried by the external steel tube, the sandwiched concrete, the core-concrete and the internal steel tube were calculated as 48.7%, 32.1%, 10.6% and 8.6%, respectively. The results indicate that the external steel tube and sandwiched-concrete withstand a large portion of the ultimate moment. The reason for this is that the sandwiched-concrete and external steel tube have larger cross-sectional areas and are located farther from the section centroid than the internal steel tube and core concrete.

8. Conclusions

This paper has described experimental and computational investigations into the behavior of CFDST short columns composed of circular tubes that are axially and eccentrically loaded. The experimental results have been employed to verify the computer modeling technique developed for quantifying the moment-curvature and strength interaction behavior of circular CFDST columns incorporating concrete confinement effects. Parametric studies on the structural responses of CFDST columns including various important features have been conducted.

Experiments conducted indicate that the local buckling of the internal steel tube is effectively prevented by the rigid concrete and the core-concrete in circular CFDST columns does not crush due to the confinement provided by the steel tubes. The experimental data on circular CFDST short columns under eccentric loading presented in this paper for the first time can be used to validate other numerical models. The fiber-based computational method proposed is shown to be efficient and accurate, and can be employed to analyze and design of CFDST beam-columns in practice. Numerical results presented on the moment-curvature responses, strength envelopes, concrete confinement effect, and moment distributions in circular CFDST short columns loaded eccentrically provide a better understanding of the fundamental behavior of CFDST columns. It has been demonstrated that the outer steel tube carries the largest portion of the moment followed by the sandwiched concrete while the core-concrete and inner steel tube make less contributions to the moment capacity of the CFDST column.

Declaration of Competing Interest

Authors declare that there is no conflicts of interest.

Acknowledgements

The experimental work discussed in this paper was financially supported by both Victoria University and La Trobe University, Australia. The financial support is gratefully acknowledged. The authors thank the technicians at both Victoria University and the University of Wollongong, Australia for their technical support,

particularly Mr. Ritchie McLean and Mr. Duncan Best in the structure laboratory at the University of Wollongong, Australia for their helpful assistance during the experiments.

References

- [1] Ahmed M, Liang QQ, Patel VI, Hadi MNS. Numerical analysis of axially loaded circular high strength concrete-filled double steel tubular short columns. *Thin-Walled Struct* 2019;138:105–16.
- [2] Chang X, Ru ZL, Zhou W, Zhang YB. Study on concrete-filled stainless steel-carbon steel tubular (CFSCT) stub columns under compression. *Thin-Walled Struct* 2013;63:125–33.
- [3] Hassanein MF, Kharoob OF, Liang QQ. Behaviour of circular concrete-filled lean duplex stainless steel-carbon steel tubular short columns. *Eng Struct* 2013;56:83–94.
- [4] Eurocode 4, Design of composite steel and concrete structures-Part 1-1: General rules and rules for buildings, European Committee for Standardization, CEN, Brussels, Belgium, 2004.
- [5] ANSI/AISC 360-16, Specification for Structural Steel Buildings, American Institute of Steel Construction, Chicago, IL, 2016.
- [6] Xiong MX, Xiong DX, Liew JYR. Axial performance of short concrete filled steel tubes with high-and ultra-high-strength materials. *Eng Struct* 2017;136:494–510.
- [7] Peng YY, Tan KF, Yao Y. Mechanical properties of duplex steel tube high-strength concrete short columns under axial compression. *J Wuhan Univ Tech* 2011;33(2):105–9. (In Chinese).
- [8] Wan CY, Zha XX. Nonlinear analysis and design of concrete-filled dual steel tubular columns under axial loading. *Steel Comp Struct* 2016;20(3):571–97.
- [9] Ekmekyapar T, Al-Eliwi BJ. Concrete filled double circular steel tube (CFDCST) stub columns. *Eng Struct* 2017;135:68–80.
- [10] Romero ML, Espinós A, Portolés J, Hospitaller A, Ibañez C. Slender double-tube ultra-high strength concrete-filled tubular columns under ambient temperature and fire. *Eng Struct* 2015;99:536–45.
- [11] Ibañez C, Romero ML, Espinós A, Portolés JM, Albero V. Ultra-high strength concrete on eccentrically loaded slender circular concrete-filled dual steel columns. *Struct* 2017;12:64–74.
- [12] Zheng Y, He C, Zheng L. Experimental and numerical investigation of circular double-tube concrete-filled stainless steel tubular columns under cyclic loading. *Thin-Walled Struct* 2018;132:151–66.
- [13] Patel VI, Liang QQ, Hadi MNS. Nonlinear analysis of axially loaded circular concrete-filled stainless steel tubular short columns. *J Constr Steel Res* 2014;101:9–18.
- [14] Patel VI, Liang QQ, Hadi MNS. Concrete-filled stainless steel tubular columns. Taylor and Francis, Boca Raton and London: CRC Press; 2018.
- [15] Zheng Y, Tao Z. Compressive strength and stiffness of concrete-filled double-tube columns. *Thin-Walled Struct* 2019;134:174–88.
- [16] Hassanein MF, Elchalakani M, Patel VI. Overall buckling behaviour of circular concrete-filled dual steel tubular columns with stainless steel external tubes. *Thin-Walled Struct* 2017;115:336–48.
- [17] Katwal U, Tao Z, Hassan MK, Wang WD. Simplified numerical modeling of axially loaded circular concrete-filled steel stub columns. *J Struct Eng ASCE* 2017;143(12):04017169.
- [18] Tao Z, Wang Z-B, Yu Q. Finite element modelling of concrete-filled steel stub columns under axial compression. *J Constr Steel Res* 2013;89:121–31.
- [19] Hu HT, Huang CS, Wu MH, Wu YM. Nonlinear analysis of axially loaded concrete-filled tube columns with confinement effect. *J Struct Eng* 2003;129(10):1322–9.
- [20] AS 1391-2007. *Metallic materials - Tensile testing at ambient temperature*, Standards Australia, Sydney, NSW, Australia, 2007.
- [21] Hadi MNS, Widiarsa IBR. Axial and flexural performance of square RC columns wrapped with CFRP under eccentric loading. *J Comp Constr* 2012;16(6):640–9.
- [22] Ahmed M, Liang QQ, Patel VI, Hadi MNS. Nonlinear analysis of rectangular concrete-filled double steel tubular short columns incorporating local buckling. *Eng Struct* 2018;175:13–26.
- [23] Liang QQ. Nonlinear analysis of circular double-skin concrete-filled steel tubular columns under axial compression. *Eng Struct* 2017;131:639–50.
- [24] Liang QQ. Performance-based analysis of concrete-filled steel tubular beam-columns, part I: theory and algorithms. *J Constr Steel Res* 2009;65(2):363–72.
- [25] Patel VI, Liang QQ, Hadi MNS. Nonlinear analysis of concrete-filled steel tubular columns. Germany: Scholar's Press; 2015.
- [26] Ahmed M, Liang QQ, Patel VI, Hadi MNS. Local-global interaction buckling of square high strength concrete-filled double steel tubular slender beam-columns. *Thin-Walled Struct* 2019;143:106244.
- [27] Ahmed M, Liang QQ, Patel VI, Hadi MNS. Experimental and numerical studies of square concrete-filled double steel tubular short columns under eccentric loading. *Eng Struct* 2019;143:109419.
- [28] J. B. Mander, Seismic design of bridge piers, (Ph.D. Thesis), Christchurch, New Zealand, Dep. Civ. Eng., Uni. Cant., 1983.
- [29] Lim JC, Ozbakkaloglu T. Stress-strain model for normal-and light-weight concretes under uniaxial and triaxial compression. *Const Build Mat* 2014;71:492–509.
- [30] Mander JB, Priestley MJ, Park R. Theoretical stress-strain model for confined concrete. *J Struct Eng* 1988;114(8):1804–26.
- [31] De Nicolò B, Pani L, Pozzo E. Strain of concrete at peak compressive stress for a wide range of compressive strengths. *Mat Struct* 1994;27(4):206–10.

4.2 CONCLUDING REMARKS

In this chapter, a new confining pressure model and a strength degradation parameter have been derived for the confined concrete of CFDST circular columns having an inner circular tube. This concrete constitutive model has been incorporated in the computational models, which have been developed for the determination of axial load-strain behavior, strength envelopes and moment-curvature relationships of short CFDST columns of circular section. Experimental results obtained from this research and existing test data have been used to validate the mathematical models. It has been demonstrated that the mathematical models developed can accurately capture the behavior of CFDST columns and the proposed design formula can be used to design CFDST columns. Experimental and numerical results presented provide important information on the structural performance of CFDST short circular columns and can be employed to verify numerical modeling techniques.

Chapter 5

LOCAL-GLOBAL INTERACTION BUCKLING OF SQUARE CFDST SLENDER COLUMNS

5.1 INTRODUCTION

The failure of square CFDST slender columns composed of a circular inner steel tube under applied loads is characterized by the interaction of the local buckling of the outer thin-walled steel tube and global buckling. This interaction buckling problem is so complicated that it has not been included in any existing fiber-based model for the nonlinear modeling of CFDST columns. In this chapter, a mathematical model underlying the theory of fiber elements is described for quantifying the ultimate load and deflection responses of slender square thin-walled CFDST columns having a circular inner tube loaded eccentrically. The important features of square CFDST columns including the concrete confinement, interaction of local-global buckling, initial geometric imperfections, second-order effect and nonlinearities of material and geometry are incorporated in the mathematical model. The formulation of the mathematical model and computational procedures are presented. The computationally efficient solution algorithms are developed to solve the highly dynamic equilibrium functions. The mathematical modeling technique is verified by comparing with the independent test results. The effects of important design parameters on the performance of slender CFDST

columns are examined by means of utilizing the mathematical model developed. Design formulas are proposed for designing slender CFDST columns loaded either concentrically or eccentrically.

This chapter includes the following paper:

1. **Ahmed, M.**, Liang, Q. Q., Patel, V. I. and Hadi, M. N. S. (2019). Local-global interaction buckling of square high strength concrete-filled double steel tubular slender beam-columns. *Thin-Walled Structures*, 143, 106244.

OFFICE FOR RESEARCH TRAINING, QUALITY AND INTEGRITY

DECLARATION OF CO-AUTHORSHIP AND CO-CONTRIBUTION: PAPERS INCORPORATED IN THESIS

This declaration is to be completed for each conjointly authored publication and placed at the beginning of the thesis chapter in which the publication appears.

Title of
Paper/Journal/Book:

Ahmed, M., Liang, Q. Q., Patel, V. I. and Hadi, M. N. S. (2019). Local-global interaction buckling of square high strength concrete-filled double steel tubular slender beam-columns. *Thin-Walled Structures*, 143, 106244.

Surname:

First
name:

Institute:

Candidate's Contribution (%):

Status:

Accepted and in press:

Date:

Published:

Date:

2. CANDIDATE DECLARATION

I declare that the publication above meets the requirements to be included in the thesis as outlined in the HDR Policy and related Procedures – policy.vu.edu.au.

Mizan Ahmed

Digitally signed by Mizan
Ahmed
Date: 2019.12.18 12:52:45
+11'00'

18-12-2019

Signature

Date

3. CO-AUTHOR(S) DECLARATION

In the case of the above publication, the following authors contributed to the work as follows:

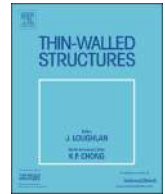
The undersigned certify that:

1. They meet criteria for authorship in that they have participated in the conception, execution or interpretation of at least that part of the publication in their field of expertise;
2. They take public responsibility for their part of the publication, except for the responsible author who accepts overall responsibility for the publication;

3. There are no other authors of the publication according to these criteria;
4. Potential conflicts of interest have been disclosed to a) granting bodies, b) the editor or publisher of journals or other publications, and c) the head of the responsible academic unit; and
5. The original data will be held for at least five years from the date indicated below and is stored at the following **location(s)**:

R:\CFDST Columns

Name(s) of Co-Author(s)	Contribution (%)	Nature of Contribution	Signature	Date
Mizan Ahmed	60	Methodology, Software, Validation, Formal analysis, Investigation, Data curation, Writing–Original draft, Visualization.	Mizan Ahmed Digitally signed by Mizan Ahmed Date: 2019.12.18 12:52:59 +11'00'	18-12-2019
Qing Quan Liang	20	Conceptualization, Methodology, Software, Validation, Writing–Review and Editing, Supervision, Project administration.	Qing Quan Liang Digitally signed by Qing Quan Liang Date: 2019.12.18 13:14:47 +11'00'	18-12-2019
Vipulkumar I. Patel	10	Validation, Writing–Review and Editing, Supervision.	Vipul Patel Digitally signed by Vipul Patel Date: 2019.12.18 13:34:24 +11'00'	18-12-2019
Muhammad N.S. Hadi	10	Validation, Writing–Review and Editing, Supervision.	Muhammad Hadi Digitally signed by Muhammad Hadi DN: cn=Muhammad Hadi, o=University of Wollongong, ou=School of CME, email=mhadi@uow.edu.au, c=AU Date: 2019.12.18 14:49:41 +11'00'	18-12-2019



Full length article

Local-global interaction buckling of square high strength concrete-filled double steel tubular slender beam-columns



Mizan Ahmed^a, Qing Quan Liang^{a,*}, Vipulkumar Ishvarbhai Patel^b, Muhammad N.S. Hadi^c

^a College of Engineering and Science, Victoria University, PO Box 14428, Melbourne, VIC, 8001, Australia

^b School of Engineering and Mathematical Sciences, La Trobe University, Bendigo, VIC, 3552, Australia

^c School of Civil, Mining and Environmental Engineering, University of Wollongong, Wollongong, NSW, 2522, Australia

ARTICLE INFO

Keywords:

Concrete-filled double steel tubes
High-strength
Slender beam-columns
Local-global interaction buckling
Nonlinear analysis

ABSTRACT

High-strength square concrete-filled double steel tubular (CFDST) slender beam-columns with a circular internal steel tube subjected to eccentric loads may undergo interaction local-global buckling. No computational studies on the interaction local-global buckling of slender square CFDST beam-columns have been reported and their behavior has not been fully understood. This paper describes a mathematical model for the simulation of the interaction local-global buckling behavior of square high-strength CFDST slender beam-columns under axial compression in combination with uniaxial bending. The mathematical model is formulated by the fiber approach, accounting for confinement provided by the internal circular steel tube, and geometric and material nonlinearities. An incremental-iterative numerical procedure is designed to quantify the local-global interaction buckling responses of slender CFDST columns. Efficient numerical solution algorithms implementing the inverse quadratic method are developed for solving the nonlinear equilibrium dynamic functions of CFDST columns. The formulation proposed is verified by existing experimental data on CFDST columns as well as double-skin concrete-filled steel tubular (DCFST) slender columns. The developed computational model is employed to study the local-global interaction buckling behavior of CFDST columns made of high-strength materials with various important parameters. Simplified design models are proposed for determining the ultimate axial strengths of slender square CFDST columns under axial compression and the interaction curves of CFDST slender beam-columns loaded eccentrically. It is demonstrated that the computational and design models predict well the interaction local-global buckling behavior and strength of slender square CFDST beam-columns.

1. Introduction

The applications of concrete-filled double steel tubular (CFDST) beam-columns made of high strength materials in tall buildings have been increased in recent years. The CFDST square columns as depicted in Fig. 1(a) combine the advantage properties of concrete and steel materials. In addition, CFDST columns offer improved ductility, stiffness, strength, and fire-resistance in comparison with square concrete-filled steel tubular (CFST) columns. The cross-sectional sizes of CFDST columns can be reduced by means of using high-strength steel and concrete and this greatly increases the space usage in composite buildings. A column having a slenderness ratio (L/r) greater than 22 is defined as a slender column in AS 3600-2009 [1]. Eccentrically loaded slender square CFDST thin-walled beam-columns may encounter the problem of local-global interaction instability. The nonlinear analysis and design of slender square CFDST columns under combined actions

are complicated as the formulation must consider the material nonlinearities, second-order effects as well as the interaction of local-global buckling. However, no attempt has been made to computationally investigate the inelastic responses of slender square high-strength CFDST columns loaded eccentrically, incorporating the interaction local-global buckling. To bridge this knowledge gap, a computationally-efficient mathematical model needs to be developed.

Experimental investigations on the strength and behavior of slender CFST columns with rectangular and square sections made of high-strength materials were carried out by researchers in the past. Varma et al. [2] conducted tests on slender high-strength CFST beam-columns which were subjected to constant axial load in combination with monotonically increasing moment. The steel tubes were made of either high-strength or normal strength steel and had the width-to-thickness ratio (b/t) of either 32 or 48. These columns were fabricated by using high-strength concrete of 110 MPa. It was shown that slender CFST

* Corresponding author.

E-mail address: Qing.Liang@vu.edu.au (Q.Q. Liang).

<https://doi.org/10.1016/j.tws.2019.106244>

Received 11 December 2018; Received in revised form 1 May 2019; Accepted 11 June 2019

0263-8231/ © 2019 Elsevier Ltd. All rights reserved.

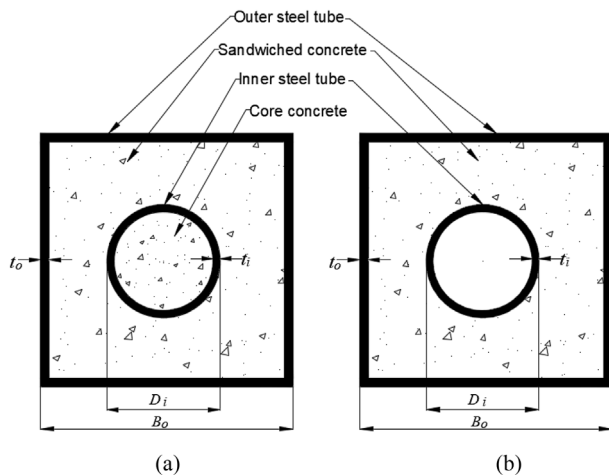


Fig. 1. Cross-section of square concrete-filled steel tubular columns: (a) CFDST column; (b) DCFST column.

square columns failed by the local-global interaction buckling with concrete crushing. The axial load and b/t ratio had remarkable effects on the column curvature ductility. The responses of square slender CFST columns loaded eccentrically to failure were studied experimentally by Mursi and Uy [3]. The steel tubes had the b/t ratios of 36, 46.4 and 56.8 and were filled with 60 MPa concrete. Mursi and Uy [4] undertook further tests on eccentrically-loaded square slender CFST columns constructed by steel tubes having a yield stress of 761 MPa and 20 MPa concrete. It was reported that the failure mode associated with slender CFST square columns was the global column buckling coupled with outward local buckling. The behavior of high-strength CFST rectangular columns that were loaded eccentrically to failure was experimentally studied by Liu [5]. Steel tubes having 550 MPa yield stress and high-strength concrete of either 70.8 MPa or 82.1 MPa were used to construct these columns. Liu [5] reported that the failure of CFST slender columns was caused by the outward local buckling and concrete crushing coupled with overall column buckling. More recently, Du et al. [6,7] carried out an experimental research on eccentrically loaded slender CFST columns with rectangular sections, incorporating b/t ratios of high-strength steel tubes ranging from 21 to 42.6. The observed failure modes of rectangular slender CFST columns with high-strength steel tubes were the column global buckling, local buckling, concrete crushing, and weld cracking.

The performance of double-skin CFST (DCFST) columns with hollow inner tube as depicted in Fig. 1(b) has been studied by Tao et al. [8,9], Zhao et al. [10,11] and Han et al. [12,13]. Square DCFST slender columns under combined actions and DCFST members under cyclic loading were tested to failure by Han et al. [12,13]. The parameters chosen for the study included the member slenderness, loading eccentricity, and the section hollow ratio. Han et al. [12] also developed a theoretical model for quantifying the structural behavior of square DCFST slender columns loaded uniaxially. Moreover, a simplified method for calculating the design strengths of DCFST columns was proposed. Xiong et al. [14] performed tests on square CFST and DCFST slender columns incorporating an inner square steel tube. It was observed that the incorporation of an internal steel tube improved the ultimate strength of CFST columns.

Only limited experiments on the responses of CFDST columns having square outer sections were performed by Pei [15], Qian et al. [16–18], Xiong et al. [14,19], and Wang et al. [20]. Pei [15] reported that short square CFDST columns failed by the outward local buckling of the outer square steel tubes while slender square CFDST columns failed by the local-global interaction buckling. The concrete with cube compressive strength up to 103 MPa was used to construct CFDST short columns by Qian et al. [17,18]. The inner circular steel tube was found

to provide an effective confinement to the concrete core, which resulted in improved ductility of the tested columns as well as their strengths. The residual strengths of the tested columns were found to be about 75% of their ultimate axial strengths. Xiong et al. [14] tested one circular and one rectangular CFDST slender column under eccentric loading. The aforementioned tests showed that for the same design parameters, the ultimate strength of CFDST slender columns was higher than that of conventional CFST and DCFST slender columns.

The inelastic analysis procedures were utilized to simulate the structural responses of slender CFST rectangular and square columns [21–24]. Shanmugam et al. [21] proposed a theoretical formulation for the determination of the axial load-buckling performance of slender CFST columns with either slender or non-compact sections where local buckling occurs. A numerical model was described by Mursi and Uy [3,4] that predicted the strength of slender thin-walled CFST rectangular columns loaded eccentrically about one principal axis and including local buckling. However, the numerical model given by Mursi and Uy [3,4] employed the expressions for the effective widths of steel plates subjected to uniform stresses, which are not applicable to steel webs in CFST columns with rectangular sections under non-uniform stresses induced by uniaxial bending. Moreover, their model did not consider the progressive post-local buckling. Patel et al. [23] and Liang et al. [24] proposed fiber-based mathematical models for the predictions of local-global interaction buckling behavior of CFST rectangular columns which were designed to support axial compression as well as uniaxial or biaxial bending. The mathematical models were shown to be capable of simulating the gradual post-local buckling of steel tube walls under non-uniform stresses. Du et al. [6,7] and Xiong et al. [14] employed the finite-element (FE) program ABAQUS to analyze rectangular CFST slender columns loaded eccentrically without the consideration of local buckling.

Computational research into the behavior of slender and short CFDST columns with rectangular section has been very limited. The FE models were created by Pei [15] and Wang et al. [20] using the commercial FE software ABAQUS for analyzing nonlinear square CFDST short columns. The computer modeling technique using fiber approach proposed by Ahmed et al. [25] for short CFDST rectangular columns made of high-strength materials loaded concentrically incorporated the influences of confinement as well as the local buckling of the outer steel tube. Lü and Zhao [26] presented an analytical method for the simulation of nonlinear slender CFDST columns with square outer sections. The influences of the member slenderness, loading eccentricity as well as the outer tube thickness on the load-deflection behavior were studied. However, the aforementioned numerical models have not considered the influences of the interaction local-global buckling on the performance of CFDST slender columns made of square sections.

This paper extends the mathematical model proposed by Ahmed et al. [25] to the simulation of slender square high-strength CFDST beam-columns loaded eccentrically, including the interaction local-global buckling. The confinement effect induced by steel tubes is considered in the stress-strain relations of concrete. The theory and computational procedures for the calculations of the interaction local-global buckling responses of square CFDST columns under uniaxial bending and axial compression are described. Efficient numerical solution algorithms are developed for obtaining solutions to the nonlinear equilibrium dynamic functions. The validation of the computational modeling method against experimental data and parametric studies are conducted and discussed. Design models are proposed for estimating the ultimate strengths of slender square CFDST columns under axial compression and interaction curves of CFDST slender columns.

2. Formulation of the mathematical model

2.1. Inelastic analysis of cross-sections including local buckling

The mathematical model simulating the inelastic buckling of slender

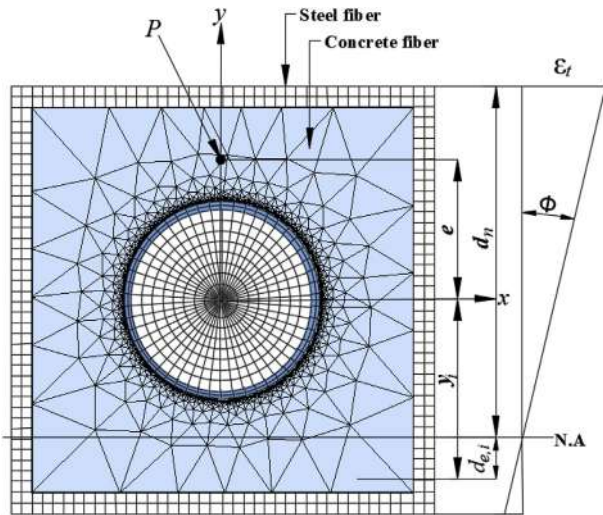


Fig. 2. Discretization and strain distribution of square CFDST column.

square CFDST columns is formulated by the method of fiber elements [27–30]. Fig. 2 illustrates the typical mesh of fibers and the distribution of strain in the cross-section of a square CFDST column. The mesh generator developed by Persson and Strang [31] is used to discretize the sandwiched concrete while the discretization of the core concrete is similar to that of circular CFDST columns [29,32]. It is assumed that the plane section remains plane after deformation. This results in a linear strain distribution through the depth of the cross-section as depicted in Fig. 2. The perfect bond between steel and concrete is assumed. These assumptions ensure that the strain compatibility in the cross-section throughout the loading history is achieved [29,30]. The stresses of fibers are computed from fiber strains by the stress-strain relations of concrete and steel. Under combined actions, the fiber strain is calculated using the function of curvature (ϕ) and neutral axis depth (d_n) as shown in Fig. 2 [27]. The internal axial force (P) and moment (M) are calculated by integrating fiber stresses over the cross-section as stress resultants [27].

The steel tubular walls restrained by concrete in a rectangular CFDST column are susceptible to the outward local buckling. The ultimate strength of CFDST columns is reduced considerably by local buckling [27,28]. The outward local-buckling is included in the present numerical modeling of square CFDST columns to accurately predict their inelastic behavior. The external steel flange and webs of a square CFDST column subjected to axial load in combination with bending about one principal axis are under either non-uniform or uniform stresses. Liang et al. [33] derived expressions that determine the initial local-buckling stresses of steel tube walls of CFST columns under non-uniform stresses. Experiments [15,17,18] indicated that the outer steel tube of a square CFDST column buckled locally outward, which is similar to that of a conventional CFST column. Therefore, the expressions proposed by Liang et al. [33] are implemented directly in the present mathematical modeling procedures for CFDST columns.

The progressive post-local buckling of steel tubes is modeled by gradually redistributing the in-plane stresses in the buckled walls. For this purpose, the effective width expressions of Liang et al. [33] are utilized. The effective widths b_{e1} and b_{e2} of the steel tube walls in a square CFDST column subjected to axial compression in addition to uniaxial bending are illustrated in Fig. 3, and are quantified by the following equations formulated by Liang et al. [33]:

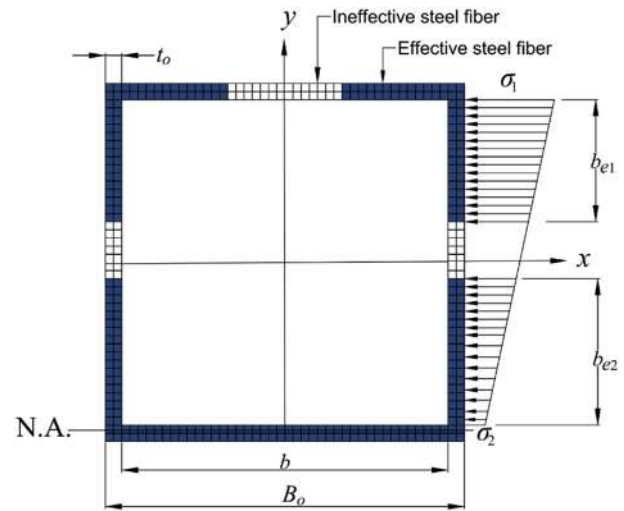


Fig. 3. Effective width of the external steel tube of square CFDST column.

$$\frac{b_{e1}}{b} = \begin{cases} 0.2777 + 0.01019\left(\frac{b}{t_o}\right) - 1.972 \times 10^{-4}\left(\frac{b}{t_o}\right)^2 \\ + 9.605 \times 10^{-7}\left(\frac{b}{t_o}\right)^3 \quad (\alpha_s > 0.0) \\ 0.4186 + 0.002047\left(\frac{b}{t_o}\right) + 5.355 \times 10^{-5}\left(\frac{b}{t_o}\right)^2 - 4.685 \times 10^{-7}\left(\frac{b}{t_o}\right)^3 \quad (\alpha_s \\ = 0.0) \end{cases} \quad (1)$$

$$\frac{b_{e2}}{b} = (2 - \alpha_s) \frac{b_{e1}}{b} \quad (2)$$

where b denotes the clear width of the external steel tube wall as presented in Fig. 3, t_o represents the outer tube thickness, α_s is the stress-gradient coefficient, which is taken $\alpha_s = \sigma_2/\sigma_1$, where σ_2 and σ_1 represent the minimum and maximum edge stressed on the plate, respectively.

The maximum ineffective width ($b_{ne,max}$) of a steel plate corresponding to the ultimate axial load applied is determined as $(b - b_{e1} - b_{e2})$. The ineffective width (b_{ne}) between zero and $b_{ne,max}$ is computed by means of the linear interpolation approach based on the steel fiber stress level, which can be written as

$$b_{ne} = \left(\frac{\sigma_1 - \sigma_{cr}}{f_{syo} - \sigma_{cr}} \right) b_{ne,max} \quad (3)$$

in which σ_{cr} stands for the stress at the onset of the initial local-buckling of the outer steel tube wall, and f_{syo} represents the yield strength of the external steel tube.

The modeling scheme developed by Liang [27] for the progressive post-local buckling characterized by thin steel plates is used in the present computational modeling approach to incorporate post-local buckling into the global buckling simulation of CFST slender square columns.

2.2. Incremental-iterative global buckling analysis

A mathematical model is formulated for simulating the interaction local-global buckling responses of slender CFDST columns of square sections under uniaxial bending as well as axial compression. The formulation extends the numerical models proposed by Liang [34], Patel et al. [23] and Liang et al. [24] for conventional CFST slender columns to the simulation of slender CFDST columns. It should be noted that in the fiber analysis, the strain compatibility is used to control the deformations of the adjacent fiber elements while the displacement shape

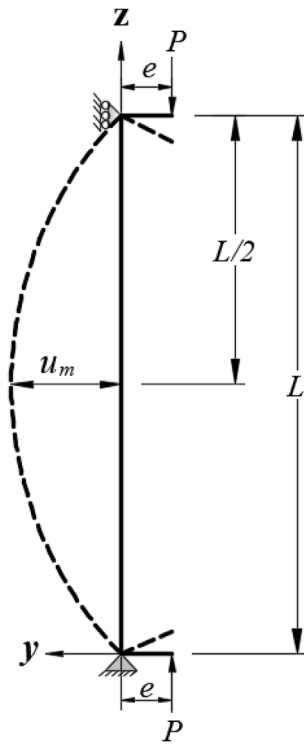


Fig. 4. Pin-ended CFDST slender beam-column.

function is employed to control the overall deflection of the column. Unlike the finite element method, the computational model using the method of fiber elements does not need to use contact elements to model the interface of steel tube and concrete. Fig. 4 illustrates the schematic view of the pin-ended CFDST slender column having equal loading eccentricity (e) and under single curvature bending. The column deflected shape is a part of a sinewave. The curvature at the column mid-length (ϕ_m) is obtained from the buckling shape function [34] as

$$\phi_m = u_m \left(\frac{\pi}{L} \right)^2 \tag{4}$$

where u_m stands for the lateral deflection that occurs at the mid-length of the column, and L is the effective length of the pin-ended column.

The geometric imperfection (u_0) initially presented in the column and the second-order effect induced by the interaction of the axial load and buckling displacement (u_m) are included in the formulation. The external moment at the column mid-length is computed by

$$M_{ext} = P(e + u_m + u_0) \tag{5}$$

The default initial geometric imperfection (u_0) at the column mid-height is taken as $L/1000$ in the mathematical model. The global buckling analysis of square CFDST slender columns is formulated by means of employing the displacement-control method. The computational method incrementally increases the buckling displacement (u_m) at the mid-length of the column and calculates the internal axial force (P) and moment (M) considering local buckling effects [23,24]. The internal axial force satisfying the equilibrium condition of moment at the column mid-height is treated as the axial load applied at the column ends. The complete axial load-buckling displacement curve for the slender CFDST column can be computed by iteratively executing this computational process.

In the calculations by the numerical method, the equilibrium condition at the column mid-height is satisfied if the following residual moment is sufficiently small:

$$r_p = M - P(e + u_m + u_0) \tag{6}$$

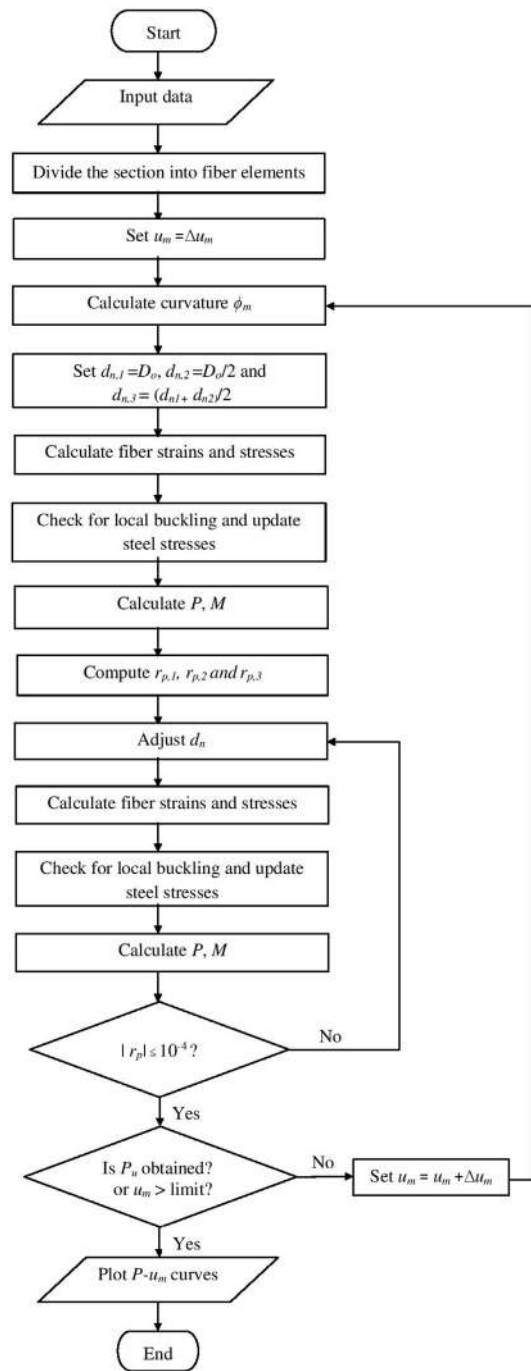


Fig. 5. Computer flowchart for calculating the axial load-deflection curves of square CFDST slender beam-columns.

In mathematical form, the equilibrium condition is achieved if $|r_p| < \epsilon_k = 10^{-4}$. The computer flowchart for the computation of the axial load-buckling displacement curve of slender CFST columns made of square sections is depicted in Fig. 5.

2.3. Solution algorithms implementing the inverse quadratic method

In the global buckling analysis of a slender column, the depth of the neutral axis of the section is iteratively adjusted to achieve the force and moment equilibrium at the mid-length of the column. The residual moment function (r_p) is changing in the computational process and is a highly nonlinear dynamic function, which is not derivative with respect to variables. Numerical solution algorithms implementing the secant

approach and Müller's method have been programed by Liang [34], Patel et al. [23] and Liang et al. [24] for determining the neutral axis depth. Although the secant and Müller's methods are effective numerical techniques for finding the roots of nonlinear functions, they are not used in the present study. Efficient numerical algorithms using the inverse quadratic method are developed to solve the dynamic functions. The solution algorithms developed in the present study are completely different from those presented by Liang [34], Patel et al. [23] and Liang et al. [24]. The inverse quadratic method requires three initial values to be assigned to the neutral axis depths $d_{n,1}$, $d_{n,2}$ and $d_{n,3}$ to facilitate the computation. The following equations are programed to adjust the neutral axis depth d_n :

$$d_{n,j+3} = d_{n,j+1} - r_{p,j+1} \left(\frac{A}{C} \right) \tag{7}$$

$$A = (r_{p,j})^2 (d_{n,j+2} - d_{n,j+1}) + r_{p,j} r_{p,j+1} (d_{n,j+1} - d_{n,j+2}) + (r_{p,j+1} - r_{p,j+2}) r_{p,j+2} (d_{n,j} - d_{n,j+1}) \tag{8}$$

$$C = (r_{p,j+1} - r_{p,j})(r_{p,j+2} - r_{p,j})(r_{p,j+2} - r_{p,j+1}) \tag{9}$$

where j is the iteration number. The iteration of searching for the true neutral axis depth d_n continues until the criterion of convergence $|r_p| < \epsilon_k = 10^{-4}$ is satisfied. The prescribed value for the convergence criterion is sufficiently small that the solutions obtained are adequate for engineering purpose.

In the numerical analysis, the initial depths of the neutral axis are taken as $d_{n,1} = D_0$, $d_{n,2} = D_0/2$ and $d_{n,3} = (d_{n,1} + d_{n,2})/2$. The inverse quadratic method is found to be very fast and efficient to determine the neutral axis depth of CFDST columns considering local buckling.

3. Stress-strain relations of structural steels

The three-stage stress-strain relations of structural steels presented in Fig. 6 consider the reduction of the steel yield strength as a result of biaxial stresses on the steel tube under compression. The rounded-part of the stress-strain curves is defined by the equation proposed by Liang [27]. The model for describing the strain-hardening behavior of structural steels by Mander [35] is adopted in the present numerical model, and is different from that used by Liang [34], Patel et al. [23] and Liang et al. [24]. The model by Mander [35] is expressed as

$$\sigma_s = f_{su} - \left(\frac{\epsilon_{su} - \epsilon_s}{\epsilon_{su} - \epsilon_{st}} \right)^n (f_{su} - f_{sy}) \quad \text{for } \epsilon_{st} < \epsilon_s \leq \epsilon_{su} \tag{10}$$

where σ_s and ϵ_s denote the longitudinal steel stress and corresponding strain, respectively; f_{sy} is the steel yield strength at the yield strain ϵ_{sy} ; ϵ_{st} and ϵ_{su} represent the hardening strain and ultimate strain taken as 0.005 and 0.2, respectively. The strain-hardening exponent n is determined as

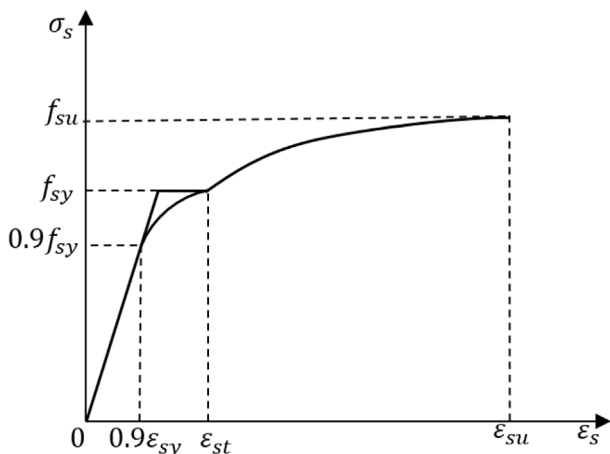


Fig. 6. Stress-strain curve for structural steels.

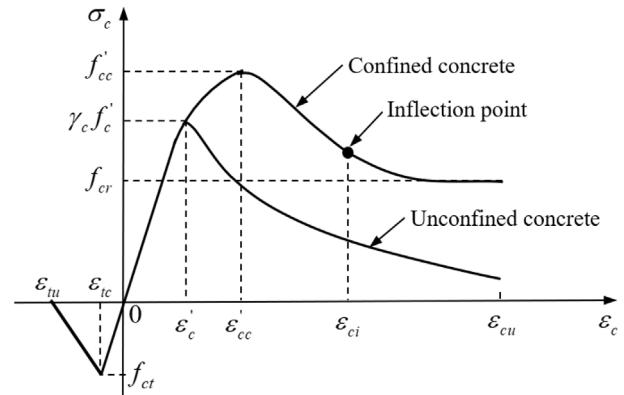


Fig. 7. Stress-strain curves for confined and unconfined concrete.

$$n = E_{st} \left(\frac{\epsilon_{su} - \epsilon_{st}}{f_{su} - f_{sy}} \right) \tag{11}$$

in which E_{st} is taken as $0.02 E_s$, where E_s represents the Young's modulus of steel.

4. Stress-strain relations of confined concrete

4.1. General stress-strain curve

The two-stage constitutive laws of confined and unconfined concrete under compression are given in Fig. 7. The ascending part of the stress-strain curve is expressed by using the following expression of Mander et al. [36]:

$$\sigma_c = \frac{f'_{cc} (\epsilon_c / \epsilon'_{cc})^\lambda}{(\epsilon_c / \epsilon'_{cc})^\lambda + \lambda - 1} \tag{12}$$

in which σ_c and ϵ_c denote the longitudinal concrete stress and corresponding strain, respectively; f'_{cc} and ϵ'_{cc} are the ultimate compressive strength and corresponding strain of confined concrete, respectively; the parameter λ is given as

$$\lambda = \frac{E_c \epsilon'_{cc}}{E_c \epsilon'_{cc} - f'_{cc}} \tag{13}$$

$$E_c = 4400 \sqrt{\gamma_c f'_{cc}} \quad (\text{MPa}) \tag{14}$$

in which γ_c was proposed by Liang [27] as $1.85 D_c^{-0.135}$ to consider the column size effects, and D_c is calculated as $(B_0 - 2t_o)$.

The descending branch of the stress-strain curves given in Fig. 7 defines the post-peak responses of concrete. The equation presented by Lim and Ozbakkaloglu [37] is used to describe the descending branch in the present computational model and is completely different from those employed by Liang [34], Patel et al. [23] and Liang et al. [24]. The equation of Lim and Ozbakkaloglu [37] is written as

$$\sigma_c = f'_{cc} - \frac{f'_{cc} - f_{cr}}{\left[1 + \left(\frac{\epsilon_c - \epsilon'_{cc}}{\epsilon_{ci} - \epsilon'_{cc}} \right)^{-2} \right]} \tag{15}$$

in which f_{cr} represents the concrete residual strength and ϵ_{ci} stands for the strain that defines the inflection point.

4.2. Compressive strength and strain of confined concrete

The lateral pressure exerted by the circular inner steel tube to the core-concrete improves the ductility as well as the compressive strength of concrete [32]. This effect is considered in the constitutive relationships by quantifying the lateral pressure on the concrete using the formula suggested by Lim and Ozbakkaloglu [37]. Ahmed et al. [25]

modified the original expression to consider the column size effects (γ_c) as follows:

$$f'_{cc} = 5.2(\gamma_c f'_c)^{0.91} \left(\frac{f_{rp}}{\gamma_c f'_c} \right)^a + \gamma_c f'_c \quad (16)$$

where $a = (\gamma_c f'_c)^{-0.06}$, and f_{rp} stands for the lateral pressure on the core-concrete.

The compressive concrete strain ϵ'_{cc} is calculated by

$$\epsilon'_{cc} = \epsilon'_c + 0.045 \left(\frac{f_{rp}}{\gamma_c f'_c} \right)^{1.15} \quad (17)$$

$$\epsilon'_c = \frac{(\gamma_c f'_c)^{0.225}}{1000} \quad (18)$$

where ϵ'_c is the strain corresponding to $\gamma_c f'_c$.

As discussed by Wang et al. [20], the confinement induced by the external square steel tube to the sandwiched-concrete is so small that the lateral pressure (f_{rpo}) on the sandwiched concrete is assumed to be zero as suggested by Ahmed et al. [25]. However, the core-concrete is passively confined by the circular inner steel tube. The confining-pressure (f_{rpi}) on the core-concrete is estimated using the expressions of Liang and Fragomeni [38] based on the work of Hu et al. [39] and Tang et al. [40], which are written as

$$f_{rpi} = \begin{cases} 0.7(v_e - v_s) \left(\frac{2t_i}{D_i - 2t_i} \right) f_{syi} & \text{for } \frac{D_i}{t_i} \leq 47 \\ \left(0.006241 - 0.0000357 \frac{D_i}{t_i} \right) f_{syi} & \text{for } 47 < \frac{D_i}{t_i} \leq 150 \end{cases} \quad (19)$$

in which v_e and v_s stand for the Poisson's ratios of the concrete-filled steel tube and of the hollow tube, respectively, and are given by Tang et al. [40].

4.3. Residual concrete strength and inflection point

The accurate determination of the residual concrete strength (f_{cr}) and the concrete strain (ϵ_{ci}) at the inflection point is vital to the accurate prediction of the post-peak behavior of square CFDST columns. The residual strength (f_{cr}) of the core-concrete is estimated by the expressions of Lim and Ozbakkaloglu [37], written as

$$f_{cr} = \begin{cases} f'_{cc} & \text{for } \frac{D_i}{t_i} \leq 40 \\ 1.6f'_{cc} \left[\frac{f_{rpi}^{0.24}}{(\gamma_c f'_c)^{0.32}} \right] \text{ and } f_{cr} \leq f'_{cc} - 0.15(\gamma_c f'_c) & \text{for } 40 < \frac{D_i}{t_i} \leq 150 \end{cases} \quad (20)$$

On the other hand, the residual concrete strength (f_{cr}) of the sandwiched concrete is determined as $f_{cr} = \beta_c f'_c$ where β_c is the strength degradation parameter for the sandwiched concrete. Ahmed et al. [25] proposed β_c based on the test results as

$$\beta_c = \begin{cases} 1 & \text{for } 0 \leq \frac{B_o}{t_o} \leq 24 \\ 1 - \frac{1}{15} \left(\frac{B_o}{t_o} \right) - 24 & \text{for } 24 < \frac{B_o}{t_o} \leq 33 \\ 0.000062 \left(\frac{B_o}{t_o} \right)^2 - 0.011225 \left(\frac{B_o}{t_o} \right) + 0.705288 & \text{for } 33 < \frac{B_o}{t_o} \leq 100 \end{cases} \quad (21)$$

For the sandwiched concrete, a value of 0.07 is used for the strain at the inflection point (ϵ_{ci}) as suggested by Ahmed et al. [25]. The equation proposed by Lim and Ozbakkaloglu [37] is utilized for the core-concrete, incorporating the column size effect by Ahmed et al. [25] as

$$\epsilon_{ci} = 2.8\epsilon'_{cc} (\gamma_c f'_c)^{-0.12} \left(\frac{f_{cr}}{f'_{cc}} \right) + 10\epsilon'_{cc} (\gamma_c f'_c)^{-0.47} \left(1 - \frac{f_{cr}}{f'_{cc}} \right) \quad (22)$$

4.4. Tensile behavior of concrete

When subjected to eccentric loading, part of the concrete in a square CFDST slender column is in tension. The tensile stress-strain relationship of concrete is given in Fig. 7. The stress under tension increases linearly up to the tensile strength at which the concrete cracks and then linearly decreases to zero. The tensile strength of concrete is prescribed as $0.6\sqrt{\gamma_c f'_c}$ in the numerical model and the ultimate tensile strain is equal to ten times the concrete cracking strain.

5. Comparisons of computational results with experimental data

In the absence of experimental data on CFDST slender columns with square sections under eccentric loading, test results on CFDST short columns provided by Qian et al. [18] and on DCFST slender columns given by Han et al. [12] are used to validate the developed numerical model. Qian et al. [18] carried out experiments on eccentrically loaded short CFDST square columns with a length of 600 mm. The dimensions of the outer steel tubes were 180×180 mm with the thickness of either 3.62 mm or 5.40 mm. High strength concrete was used to construct these columns. The specimens were tested with the loading eccentricity varied from 18 to 54 mm. The cylindrical concrete strength f'_c was estimated by applying a reduction factor of 0.85 to the cube concrete strength as suggested by Oehlers and Bradford [41]. Table 1 gives the test data of the specimens tested by Qian et al. [18]. The predicted ultimate axial strengths using the mathematical model are found to be consistent with the test results tabulated in Table 1, in which $P_{u,num}$ and $P_{u,exp}$ are the numerical and experimental ultimate axial loads of the columns, respectively. The mean $P_{u,num}/P_{u,exp}$ ratio is 0.97. The predicted axial load-lateral displacement responses of CFDST columns are compared against experimental ones in Fig. 8 and Fig. 9. In general, the computed axial load-lateral deflection curves are correlated well with corresponding test data. The small discrepancy between experimental and computational solutions is observed. It is likely caused by fact that the actual stiffness and strength of concrete in the tested specimens are unknown.

Table 2 presents the material as well as geometric properties of slender square double-skin concrete-filled steel tubes given by Han et al. [12]. The initial geometric imperfection of the columns was taken as $L/1000$ in the analyses. The measured ultimate loads of DCFST columns as well as predictions are also provided in Table 2. There is a good agreement between computed column strengths and measured values with a mean $P_{u,num}/P_{u,exp}$ ratio of 0.96. The axial load-buckling displacement curves of DCFST columns are given in Fig. 10. The experimentally measured curves are generally captured well by the mathematical modeling procedure developed. However, the measured post-yield curves differ slightly from the computational ones and the ductility of the test columns is slightly overestimated as the actual concrete strength and stiffness in tested columns are uncertain.

6. Local-global interaction buckling behavior

The mathematical model was implemented in a computer program, which was used to examine the influences of various factors on the interaction local-global buckling of CFDST square columns. The parameters investigated include the width-to-thickness ratio (B_o/t_o) of the external tube, the diameter-to-thickness ratio (D_i/t_i) of the internal tube, diameter-to-width ratio (D_i/B_o), column slenderness ratio (L/r), the loading eccentricity ratio (e/B_o), concrete strength (f'_c), and steel yield strength (f_{sy}). The material and geometric properties of the reference column used in the parametric studies were: $B_o = 450$ mm, $t_o = 7.5$ mm, $D_i = 150$ mm, $t_i = 3.75$ mm, $f_{syo} = f_{syi} = 350$ MPa, $E_s = 200$ GPa, $f'_{co} = f'_{ci} = 70$ MPa, $e/B_o = 0.3$, $L/r = 50$ and initial geometric imperfection = $L/1000$.

Table 1
Comparison of predicted and experimental ultimate axial loads of square CFDST beam-columns.

Specimen	Outer Tube			Inner Tube			Concrete		e (mm)	Ultimate load			Ref.
	$B_o \times B_o \times t_o$ (mm)	$\frac{B_o}{t_o}$	f_{sy0} (MPa)	$D_i \times t_i$ (mm)	$\frac{D_i}{t_i}$	f_{syi} (MPa)	f'_{co} (MPa)	f'_{ci} (MPa)		$P_{u,exp}$ (kN)	$P_{u,num}$ (kN)	$\frac{P_{u,num}}{P_{u,exp}}$	
I-CFDT1-1	180 × 180 × 3.62	49.7	348	89 × 2.6	34.2	314	89.85	74.38	18	2690	2585	0.96	[18]
I-CFDT3-1	180 × 180 × 3.62	49.7	348	114 × 3.35	34.0	328	89.85	74.38	18	2712	2746	1.01	
I-CFDT3-2	180 × 180 × 3.62	49.7	348	114 × 3.35	34.0	328	89.85	74.38	36	2177	2200	1.01	
I-CFDT3-3	180 × 180 × 3.62	49.7	348	114 × 3.35	34.0	328	89.85	74.38	54	1927	1801	0.93	
I-CFDT5-1	180 × 180 × 3.62	49.7	348	140 × 2.84	49.3	345	89.85	74.38	45	1933	1982	1.03	
I-CFDT7-1	180 × 180 × 5.40	33.3	338	89 × 2.6	34.2	314	89.85	74.38	18	3127	2879	0.92	
I-CFDT9-1	180 × 180 × 5.40	33.3	338	114 × 3.35	34.0	328	89.85	74.38	18	3186	3237	1.02	
I-CFDT9-2	180 × 180 × 5.40	33.3	338	114 × 3.35	34.0	328	89.85	74.38	36	2474	2388	0.97	
I-CFDT9-3	180 × 180 × 5.40	33.3	338	114 × 3.35	34.0	328	89.85	74.38	27	2897	2640	0.91	
I-CFDT11-1	180 × 180 × 5.40	33.3	338	140 × 2.84	49.3	345	89.85	74.38	27	2752	2605	0.95	
II-CFDT3-1	180 × 180 × 3.62	49.7	348	114 × 3.35	34.0	328	74.38	89.85	18	2624	2591	0.99	
II-CFDT3-2	180 × 180 × 3.62	49.7	348	114 × 3.35	34.0	328	74.38	89.85	36	2087	2112	1.01	
II-CFDT3-3	180 × 180 × 3.62	49.7	348	114 × 3.35	34.0	328	74.38	89.85	54	1797	1715	0.95	
III-CFDT3-1	180 × 180 × 3.62	49.7	348	114 × 3.35	34.0	328	74.38	74.38	18	2623	2495	0.95	
III-CFDT3-2	180 × 180 × 3.62	49.7	348	114 × 3.35	34.0	328	74.38	74.38	36	2123	2042	0.96	
III-CFDT3-3	180 × 180 × 3.62	49.7	348	114 × 3.35	34.0	328	74.38	74.38	54	1740	1670	0.96	
Mean												0.97	
Standard Deviation (SD)												0.04	
Coefficients of Variance (COV)												0.04	

6.1. Influences of L/r ratio

Investigations on the influences of L/r ratio on the interaction local-global buckling responses of eccentrically loaded CFDST square columns were undertaken by means of altering the column length only.

The calculated axial load-buckling displacement curves for the columns are plotted in Fig. 11. It would appear from Fig. 11 that the ultimate strength and initial stiffness of the CFDST columns decrease significantly as a result of increasing the L/r ratio. Fig. 12 presents the column strength curve which is a function of the member slenderness

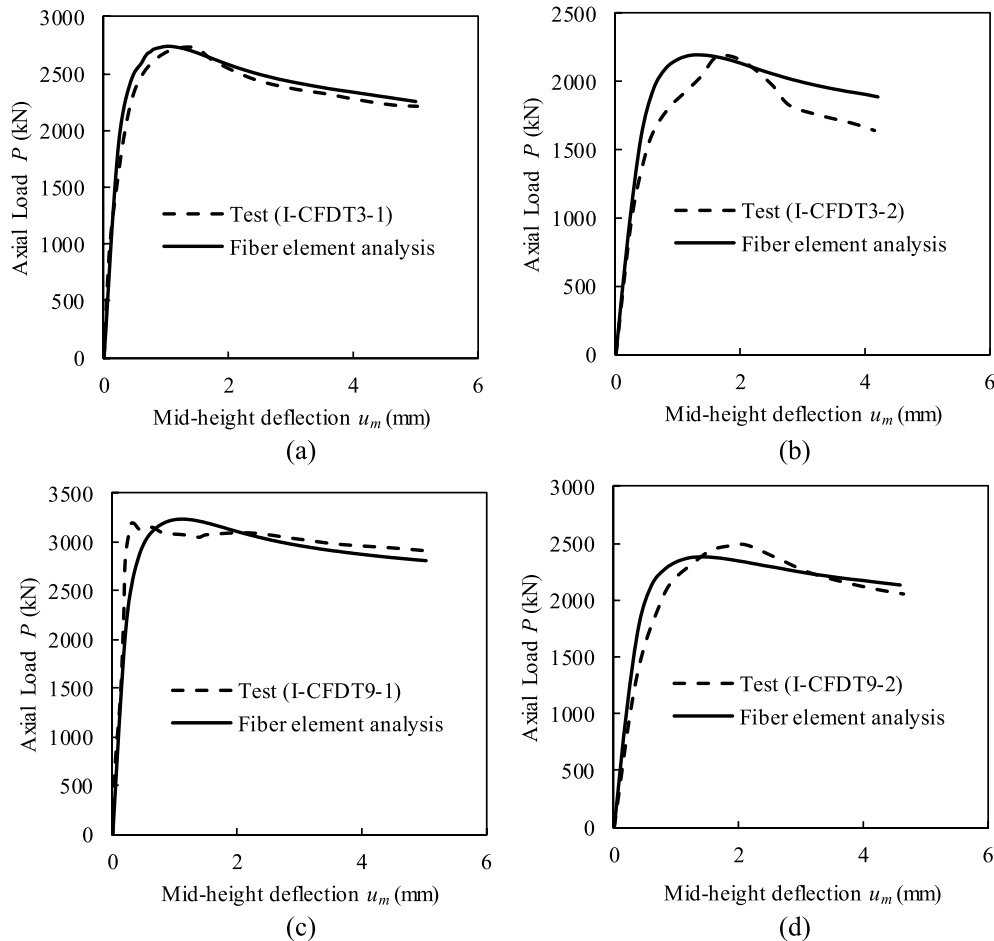


Fig. 8. Comparison of predicted and experimental axial load-deflection curves of square CFDST beam-columns tested by Qian et al. [18].

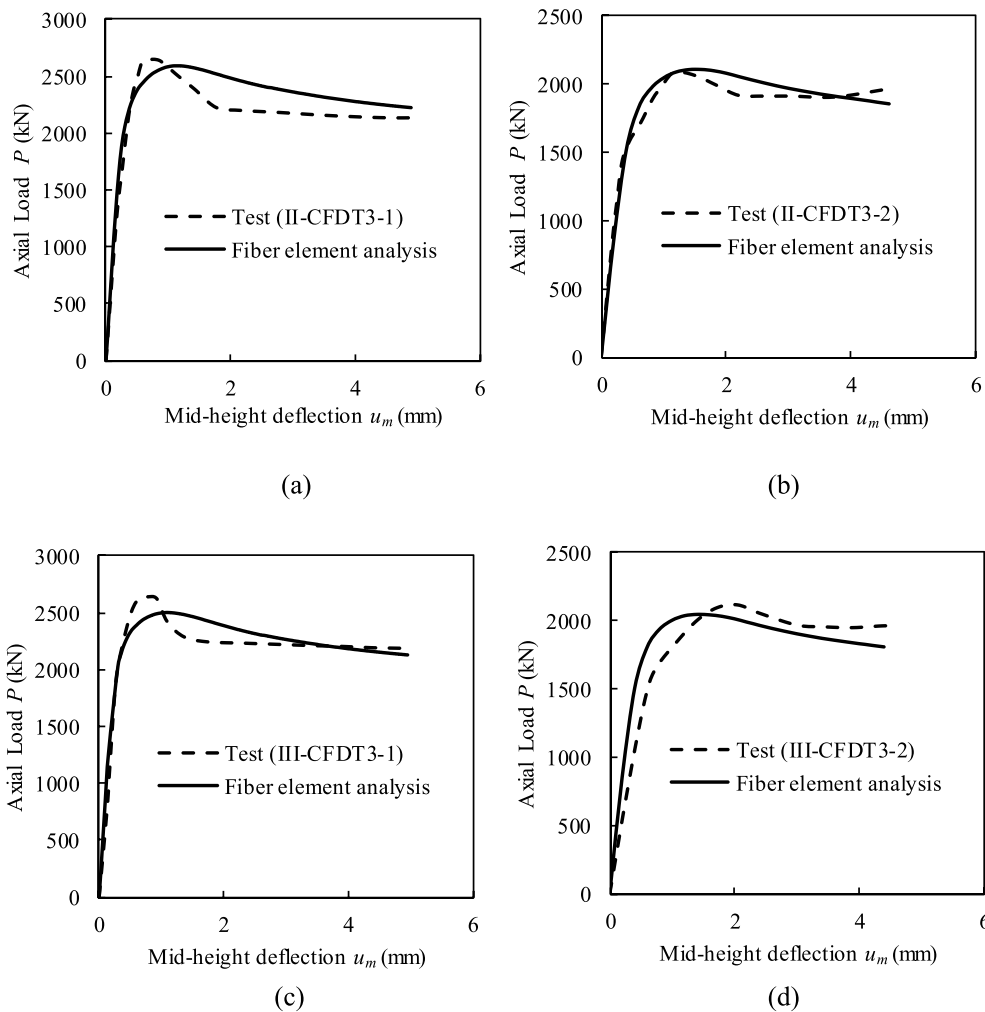


Fig. 9. Comparison of predicted and experimental axial load-deflection curves of square CFDT3 beam-columns tested by Qian et al. [18].

ratio. When the column is short, its ultimate strength is reduced by only 5% by means of changing the L/r ratio from 0.0 to 22. However, the ultimate load of the slender column represented as P_u in Fig. 12 incorporating an L/r ratio of 140 is 30% of the ultimate strength P_{oa} , which is the ultimate load of the eccentrically loaded column with the column slenderness ratio approaching zero.

6.2. Influences of B_o/t_o ratio

The sensitivities of the local-global interaction buckling strengths of CFDT3 columns to the B_o/t_o ratio were investigated by using the computer program. Changes were made only to the thickness of the external steel tube to produce the B_o/t_o ratios of 40, 60, 80 and 100, respectively. The column interaction responses of local-global buckling are provided in Fig. 13. The use of steel tube with a larger B_o/t_o ratio causes a

Table 2 Comparison of predicted and experimental ultimate axial loads of square DCFST slender beam-columns.

Specimen	L (mm)	Outer tube			Inner tube			Concrete	e (mm)	Ultimate load			Ref.
		$B_o \times B_o \times t_o$ (mm)	B_o/t_o	f_{syo} (MPa)	$D_i \times t_i$ (mm)	D_i/t_i	f_{syi} (MPa)			f'_{co} (MPa)	$P_{u,exp}$ (kN)	$P_{u,num}$ (kN)	
scbc1-1	1070	120 × 120 × 3	40	275.9	58 × 3	19.3	374.5	39.78	4	856	863	1.01	[12]
scbc1-2	1070	120 × 120 × 3	40	275.9	58 × 3	19.3	374.5	39.78	4	872	863	0.99	
scbc2-1	1070	120 × 120 × 3	40	275.9	58 × 3	19.3	374.5	39.78	14	667	704	1.06	
scbc2-2	1070	120 × 120 × 3	40	275.9	58 × 3	19.3	374.5	39.78	14	750	704	0.94	
scbc3-1	1070	120 × 120 × 3	40	275.9	58 × 3	19.3	374.5	39.78	45	480	438	0.91	
scbc3-2	1070	120 × 120 × 3	40	275.9	58 × 3	19.3	374.5	39.78	45	486	438	0.90	
scbc5-1	2136	120 × 120 × 3	40	275.9	58 × 3	19.3	374.5	39.78	15.5	596	555	0.93	
scbc5-2	2136	120 × 120 × 3	40	275.9	58 × 3	19.3	374.5	39.78	15.5	570	555	0.97	
scbc6-1	2136	120 × 120 × 3	40	275.9	58 × 3	19.3	374.5	39.78	45	380	354	0.93	
scbc6-2	2136	120 × 120 × 3	40	275.9	58 × 3	19.3	374.5	39.78	45	379	354	0.93	
Mean													0.96
Standard Deviation (SD)													0.05
Coefficients of Variance (COV)													0.05

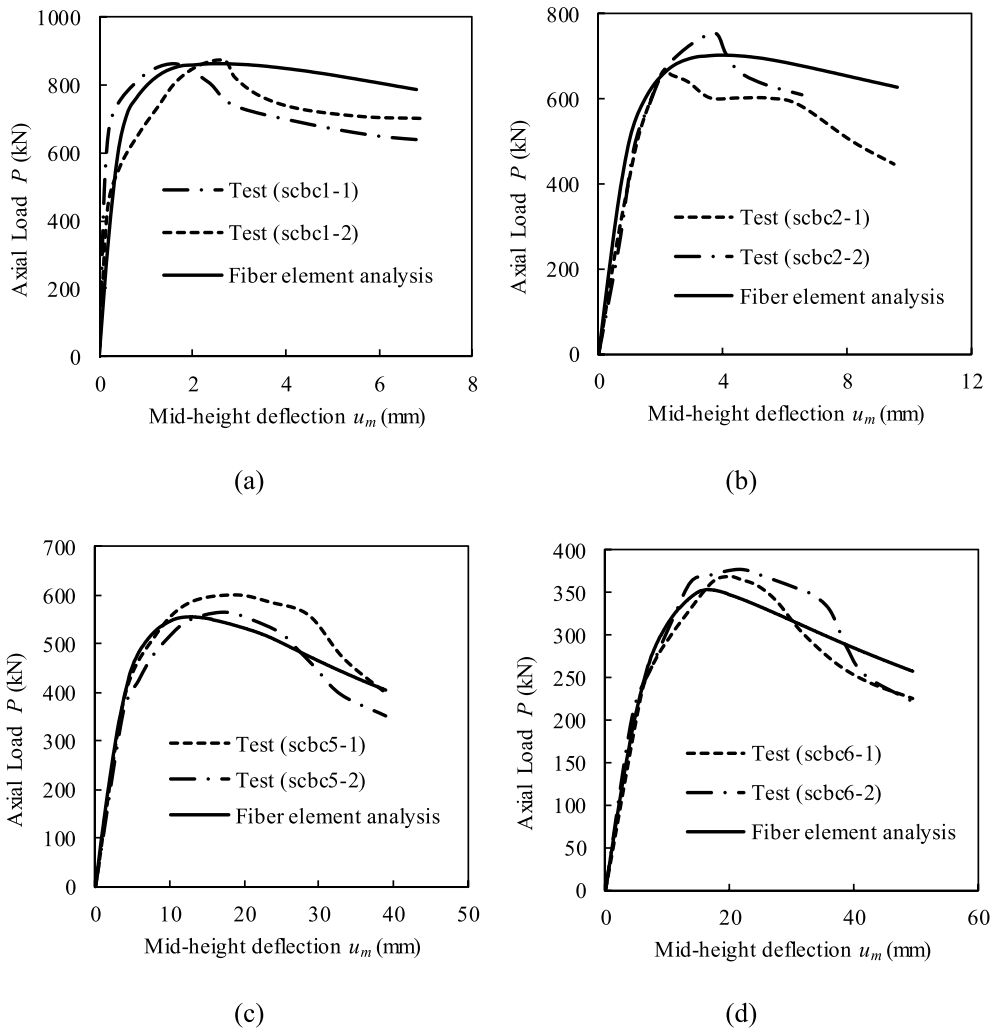


Fig. 10. Comparison of predicted and experimental axial load-deflection curves of square DCFST slender beam-columns tested by Han et al. [12].

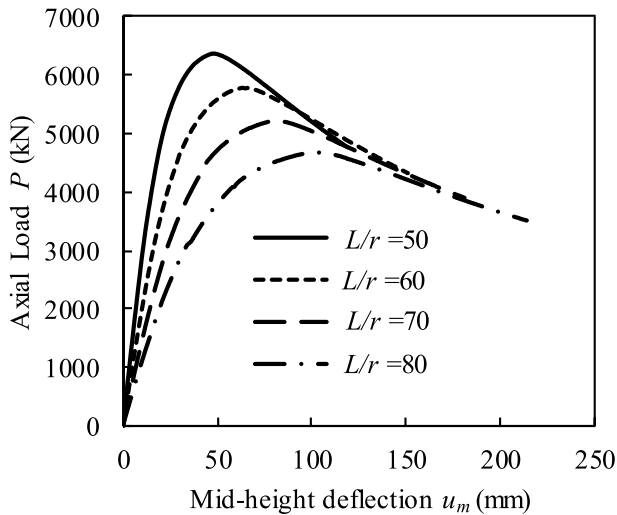


Fig. 11. Influences of L/r ratio on the axial load-deflection curves of square CFDST slender columns.

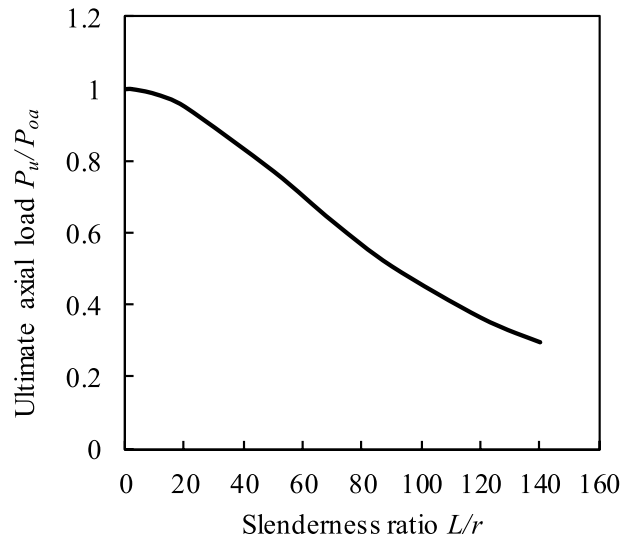


Fig. 12. The column strength curve of square CFDST columns.

remarkable reduction in the column ultimate load as well as its initial stiffness. The ultimate load of slender CFDST columns is reduced by 15.98%, 26.08% and 46.28%, respectively when increasing the B_o/t_o ratio from 40 to 60, 80 and 100. This is because increasing

the B_o/t_o ratio induces a reduction in the cross-sectional area of the steel tubes that are susceptible to local buckling so that the column ultimate load decreases remarkably. The effect of B_o/t_o ratio on the column-strength-curves are demonstrated in Fig. 14, where P_{0a} is the ultimate

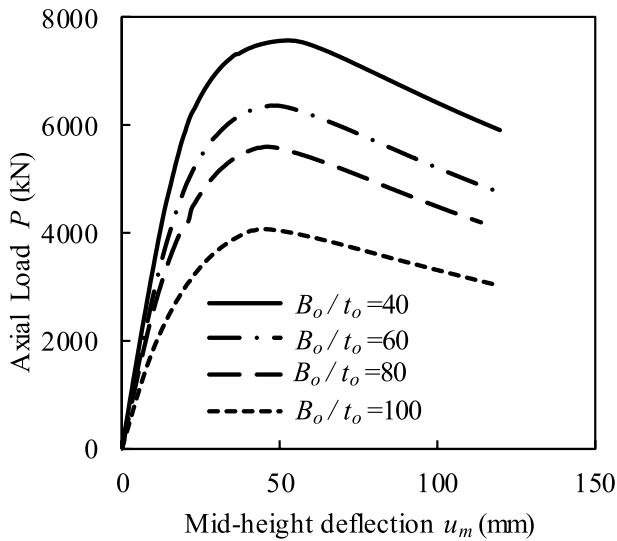


Fig. 13. Influences of B_o/t_o ratio on the axial load-deflection curves of square CFDST slender columns.

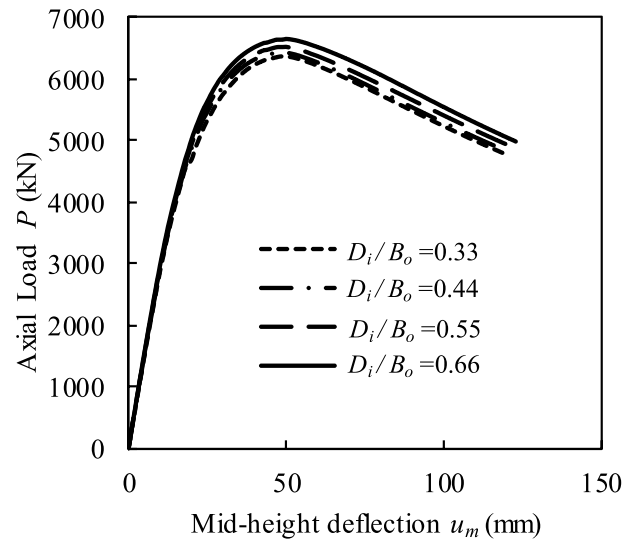


Fig. 15. Influences of D_i/B_o ratio on the axial load-deflection curves of square CFDST slender columns.

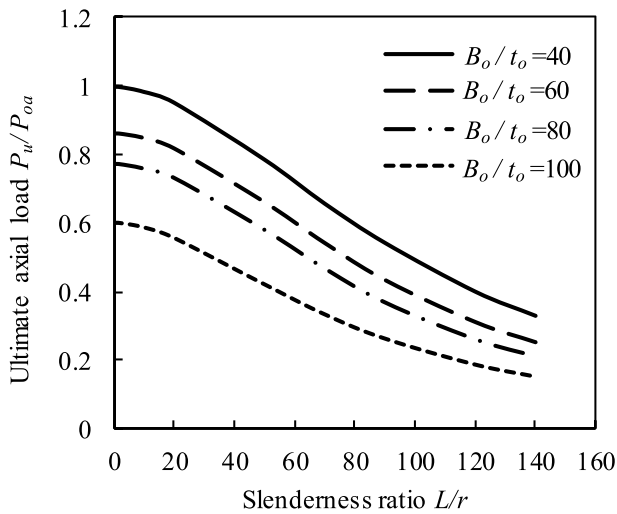


Fig. 14. Influences of B_o/t_o ratio on the column strength curves of square CFDST columns.

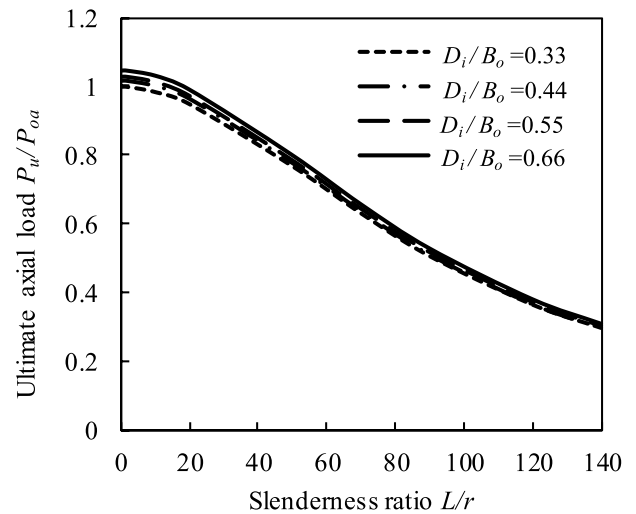


Fig. 16. Influences of D_i/B_o ratio on the column strength curves of square CFDST columns.

load of the eccentrically loaded column with the B_o/t_o ratio of 40 and the column slenderness ratio approaching zero. It is noted that the column ultimate load decreases substantially when increasing the B_o/t_o ratio for same the member slenderness. The effect of the B_o/t_o ratio on the section axial strength is the most pronounced but increasing the column slenderness decreases its effect. When changing the B_o/t_o ratio from 40 to 60, 80 and 100, the section axial load reduces by 14%, 22.5% and 39.8%, respectively.

6.3. Influences of D_i/B_o ratio

The computer program developed was utilized to study the responses of loaded CFDST slender columns to the changes of D_i/B_o ratios. The diameter of the inner circular tube was altered from 150 mm to 200 mm, 250 mm and 300 mm. The D_i/B_o ratios of these sections were calculated as 0.33, 0.44, 0.55 and 0.66, respectively. Fig. 15 presents the computed axial load-buckling displacement curves which are dependent on the D_i/B_o ratio. It is shown that the D_i/B_o ratio has only a minor influence on the column overall buckling behavior. The effect of D_i/B_o ratio on the strength curves for the columns is illustrated in Fig. 16, where P_{0a} is the ultimate load of the concentrically loaded column with

the D_i/B_o ratio of 0.33 and the column slenderness ratio approaching zero. The effect of D_i/B_o ratio is also insignificant. When the D_i/B_o ratio is changed from 0.33 to 0.66, the section axial load reduces by 5% while its column strength with $L/r = 140$ reduces only 4.5%.

6.4. Influences of e/B_o ratio

The investigation into the sensitivities of the interaction local-global buckling behavior of CFDST columns to the loading eccentricity ratio (e/B_o) was conducted by using the proposed computational model. The e/B_o ratios of 0.2, 0.25, 0.3 and 0.35 were considered in the investigation. It is seen from Fig. 17 that as a result of using a larger e/B_o ratio, a sustainable reduction in the column initial stiffness as well as its ultimate load is obtained. This is attributed to the increase in the second order effects of the column. The column ultimate strength is reduced by 35.3% by changing the e/B_o ratio from 0.2 to 0.35. The influences of e/B_o ratio on the ultimate strength of CFDST slender columns are illustrated in Fig. 18, where P_{0a} is the ultimate load of the concentrically loaded slender column. Increasing e/B_o ratio remarkably reduces the ultimate strength of the column. Fig. 19 gives the column strength curves of square CFDST columns with varying e/B_o ratios, in which P_{0a} is

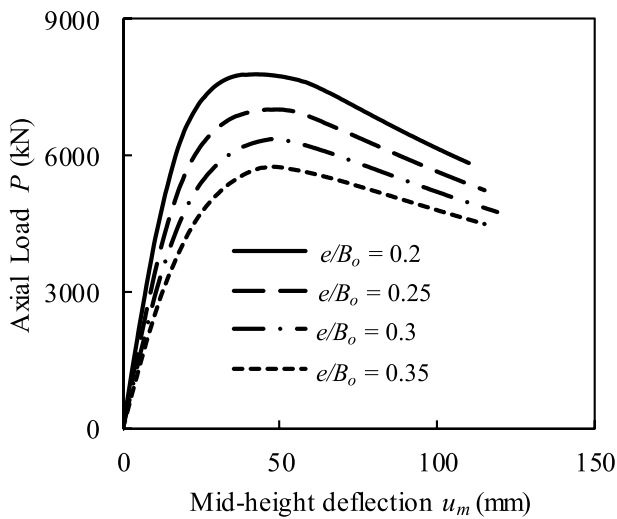


Fig. 17. Influences of e/B_o ratio on the axial load-deflection curves of square CFDST slender columns.

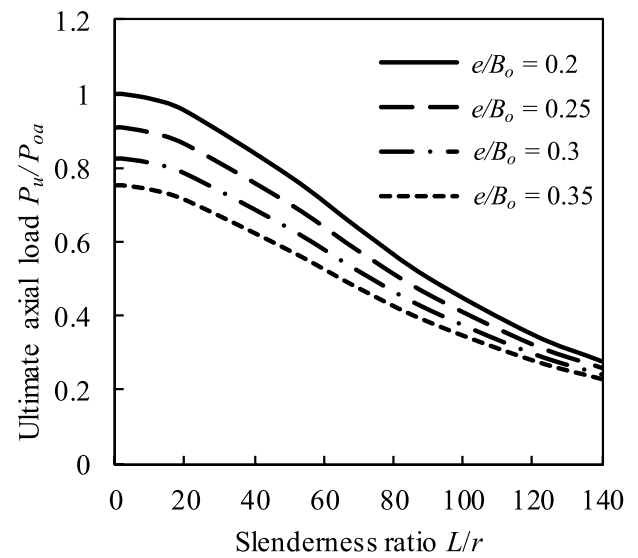


Fig. 19. Influences of e/B_o ratio on the column strength curves of square CFDST columns.

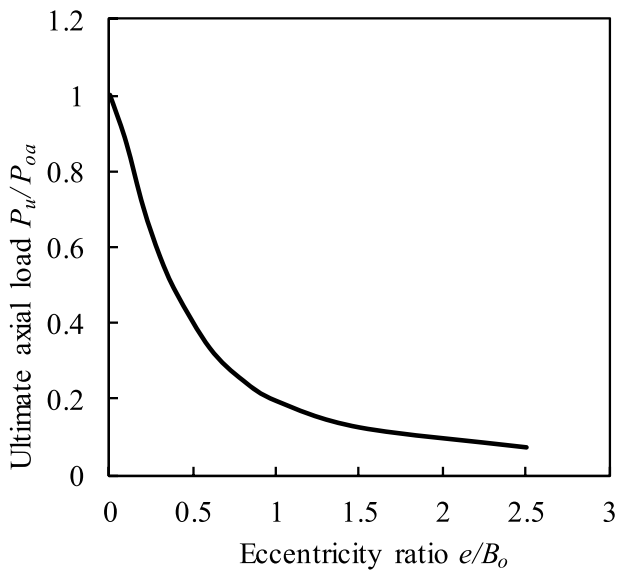


Fig. 18. Influences of e/B_o ratio on ultimate axial strengths of square CFDST slender columns.

taken as the ultimate load of the eccentrically loaded column with the e/B_o ratio of 0.2 and the column slenderness ratio approaching zero. It is evident that increasing the e/B_o ratio decreases the column ultimate strength regardless of the member slenderness.

6.5. Influences of D_i/t_i ratio

The influences of D_i/t_i ratio on the behavior of slender CFDST columns were examined by varying the D_i/t_i ratio from 20 to 50. The internal tube thickness was varied while the other parameters were unchanged. The local-global interaction buckling behavior of the slender columns is illustrated in Fig. 20. It is discovered that the complete curves of axial load-buckling displacement for the slender CFDST columns are not sensitive to the D_i/t_i ratio. The post-peak load-buckling displacement curves cannot be distinguished for different D_i/t_i ratios. By increasing D_i/t_i ratio from 20 to 50, the column ultimate load decreases by 1.25% only. The reason for this is that the global buckling of square CFDST slender columns mainly depends on the B_o/t_o ratio, member slenderness and e/B_o ratios. The column strength curves of square CFDST beam-columns with varying D_i/t_i ratios are given in Fig. 21, in

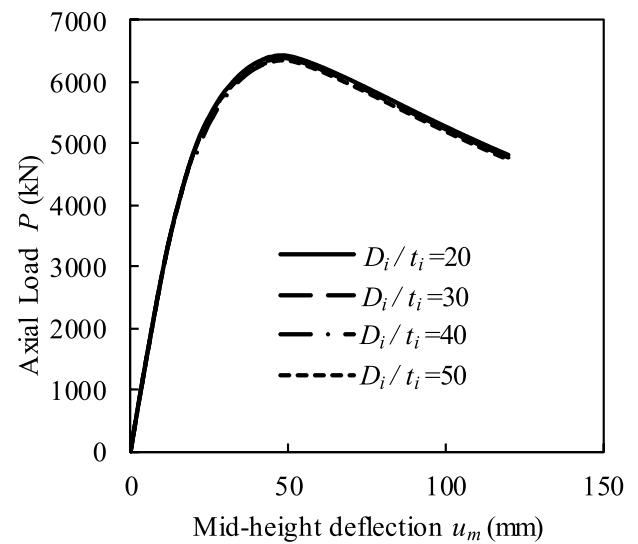


Fig. 20. Influences of D_i/t_i ratio on the axial load-deflection curves of square CFDST slender columns.

which P_{oa} is the ultimate load of the eccentrically loaded column with the D_i/t_i ratio of 20 and the column slenderness ratio approaching zero. It is obvious from Fig. 21 that D_i/t_i ratio has an insignificant effect on the column strength curves.

6.6. Influences of local buckling

The influence of the outward local-buckling of the outer tubes with square sections on the global buckling of CFDST slender columns under eccentric loading was investigated. The B_o/t_o and e/B_o ratios of the column were taken as 100 and of 0.5, respectively. As demonstrated in Fig. 22, the columns ultimate load is overestimated by 8.4% when the analysis ignored local buckling. The sensitivities of the column strength curve to the local buckling of the square section are shown in Fig. 23, in which P_{oa} is the ultimate load of the eccentrically loaded column with the column slenderness ratio approaching zero considering local buckling. Local buckling has the most prominent influence on the section axial-load capacity. However, its effect on the column strength decreases when the column slenderness increases. For very slender CFDST columns with a L/r ratio greater than 200, the local buckling

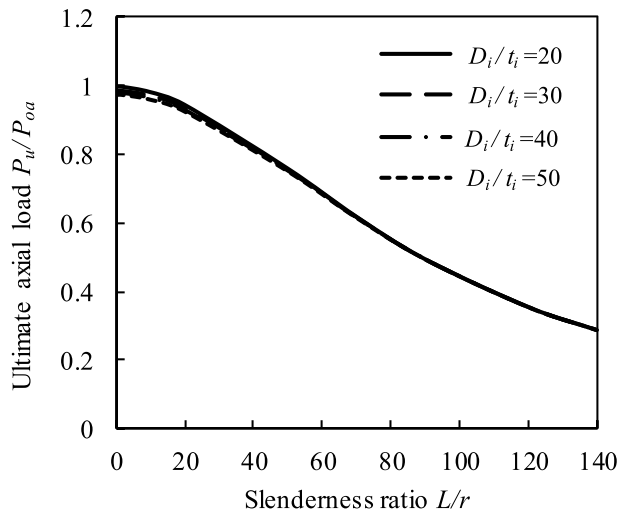


Fig. 21. Influences of D_i/t_i ratio on the column strength curves of square CFDST columns.

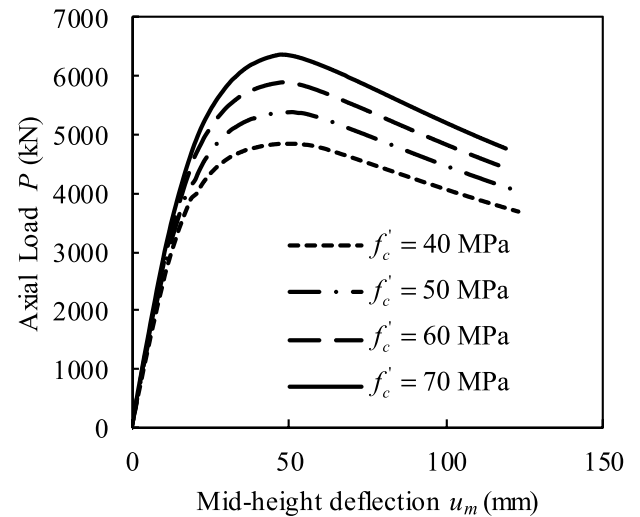


Fig. 24. Influences of concrete compressive strength on the axial load-deflection curves of square CFDST slender columns.

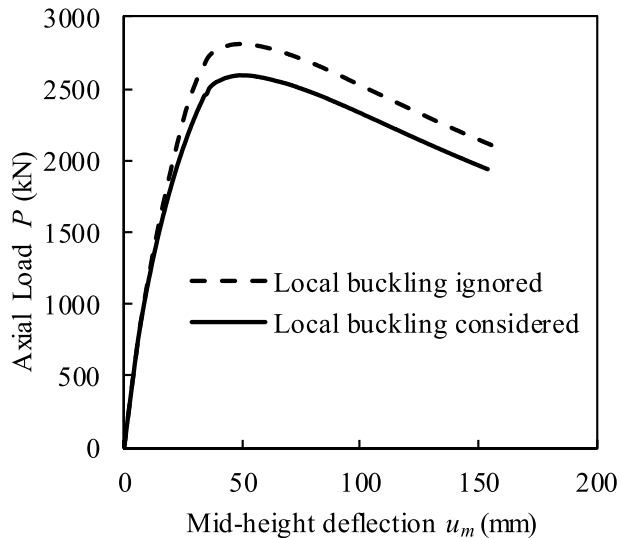


Fig. 22. Influences of the local buckling of outer steel tube on the axial load-deflection curve of square CFDST slender column.

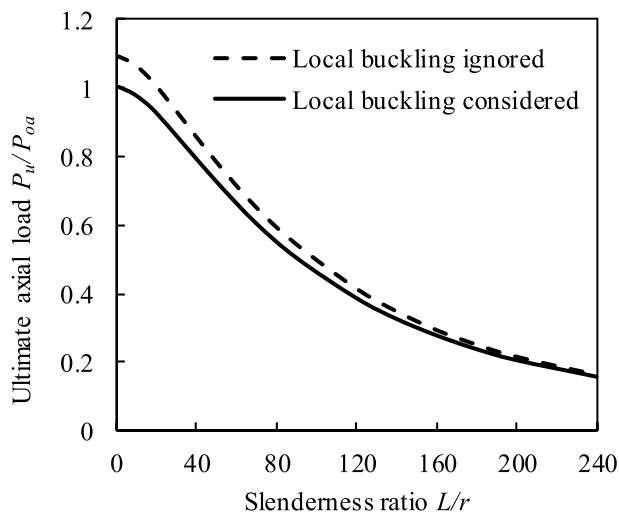


Fig. 23. Influences of the local buckling of outer steel tube on the column strength curves of square CFDST columns.

effect diminishes. This is because the ultimate strength of very slender columns is mainly governed by the global buckling and the strength reduction due to the local buckling can be ignored.

6.7. Influences of concrete strength

The concrete in square CFDST slender columns carries most of the compressive load. It is vital to understand the influences of high-strength concrete on the interaction local-global buckling responses of slender CFDST columns for the economical design of such columns. Three different scenarios were considered as follows: (1) the sandwiched-concrete and core-concrete had the same compressive strength; (2) the sandwiched-concrete strength was varied from 40 MPa to 70 MPa while the core-concrete strength was not changed; and (3) the sandwiched-concrete strength was not changed while the core-concrete strength was varied from 40 MPa to 70 MPa. For the first case, the axial load-buckling displacement curves of CFDST columns with different concrete strengths are given in Fig. 24. The column ultimate load is increased by 10.0%, 17.8% and 23.9%, respectively, by changing the concrete strength from 40 MPa to 50, 60 and 70 MPa. The column strength curves which are dependent on the concrete strengths are provided in Fig. 25, in which P_{oa} is the ultimate load of the eccentrically

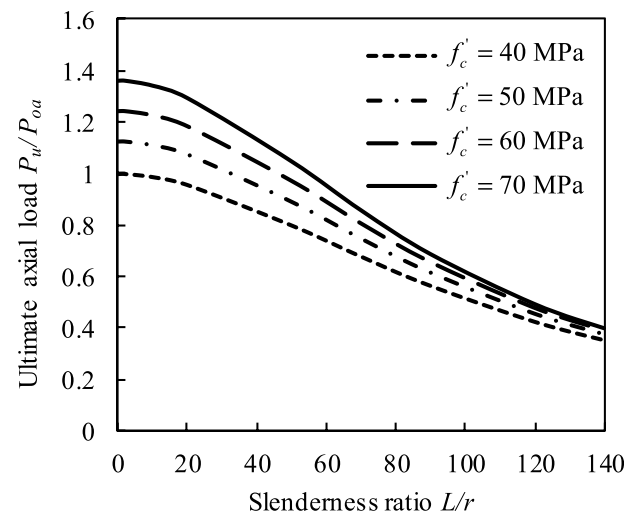


Fig. 25. Influences of concrete compressive strength on the column strength curves of square CFDST columns.

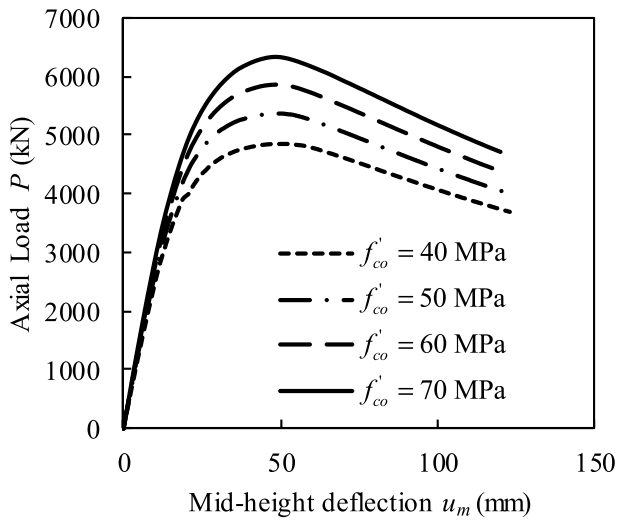


Fig. 26. Influences of sandwiched concrete strength on the axial load-deflection curves of square CFDST slender columns.

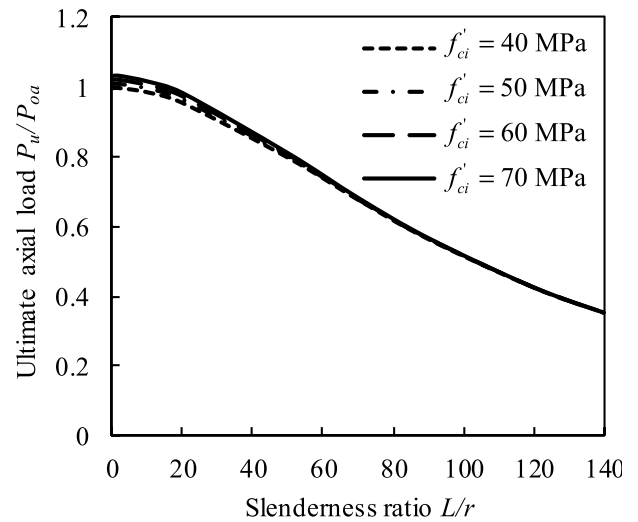


Fig. 29. Influences of core concrete strength on the column strength curves of square CFDST columns.

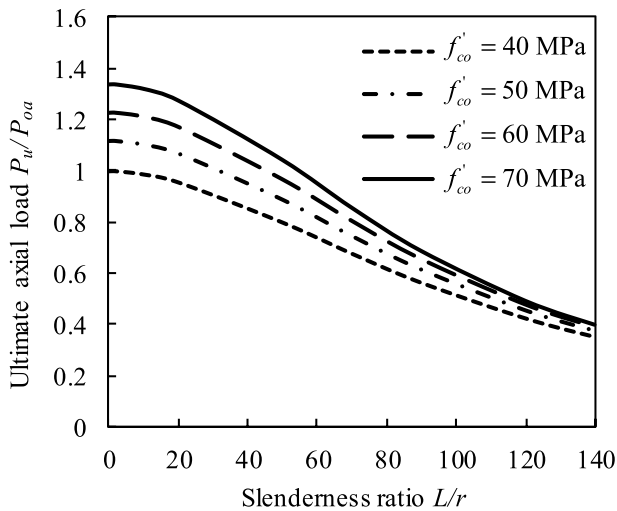


Fig. 27. Influences of sandwiched concrete strength on the column strength curves of square CFDST columns.

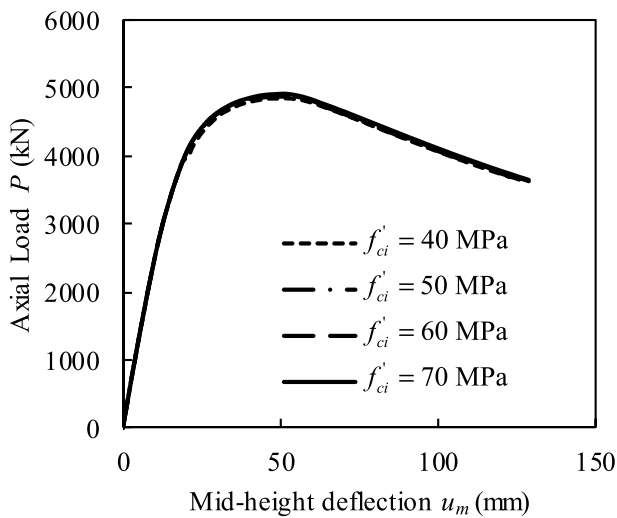


Fig. 28. Influences of core concrete strength on the axial load-deflection curves of square CFDST slender columns.

loaded column with $f'_c = 40$ MPa and the column slenderness ratio approaching zero. The use of higher strength concrete leads to a higher column ultimate load irrespective of its slenderness ratio. However, the concrete strength effect decreases as the column slenderness increases. When changing the concrete strength from 40 MPa to 70 MPa, the section axial capacity increases by 36% while its member axial strength with $L/r = 140$ increases by 13.5%. The influences of sandwiched-concrete strength on the load-deflection curves and column strength curves are illustrated in Fig. 26 and Fig. 27, respectively. In Fig. 27, P_{0a} is the ultimate load of the eccentrically loaded column with $f'_{co} = 40$ MPa and the column slenderness ratio approaching zero. The effects of the core-concrete strength on the structural behavior are presented in Fig. 28 and Fig. 29, in which P_{0a} is the ultimate load of the eccentrically loaded column with $f'_{ci} = 40$ MPa and the column slenderness ratio approaching zero. It can be seen that the sandwiched-concrete strength has a remarkable effect on the global buckling behavior of square slender CFDST columns but the influence of core-concrete strength is insignificant.

6.8. Influences of steel yield strength

The studies on the inelastic buckling behavior of slender square CFDST columns with various steel yield strengths were undertaken. Three cases were investigated. The first case was to change the yield stress of both external and inner steel tubes from 350 MPa to 450 MPa, 550 MPa, and 650 MPa. The interaction local-global buckling responses of CFDST columns that are a function of the steel yield stress are given in Fig. 30. The figure shows that the yield stress of both tubes does not affect the column initial stiffness, but remarkably increases the column axial capacity. As shown in Fig. 30, when the steel yield stress of the tubes is changed from 350 MPa to 650 MPa, the percentage increase in the column ultimate strength with a L/r ratio of 40 is 20.8%. The influences of steel yield strength on the column strength curves are shown in Fig. 31, in which P_{0a} is the ultimate load of the eccentrically loaded column with $f_{sy} = 350$ MPa and the column slenderness ratio approaching zero. The effect of the steel yield stress of both tubes on the column ultimate load decreases as the L/r ratio increases. The second case was to alter only the yield strength of the internal steel tube. As depicted in Figs. 32 and 33, the effect of internal steel tube yield stress on the load-buckling displacement responses and column strength curves is very minor and can be ignored. In Fig. 33, P_{0a} is the ultimate load of the eccentrically loaded column with $f_{syi} = 350$ MPa and the column slenderness ratio approaching zero. The third case was to vary the yield strength of the external steel tube only. It is seen from Figs. 34

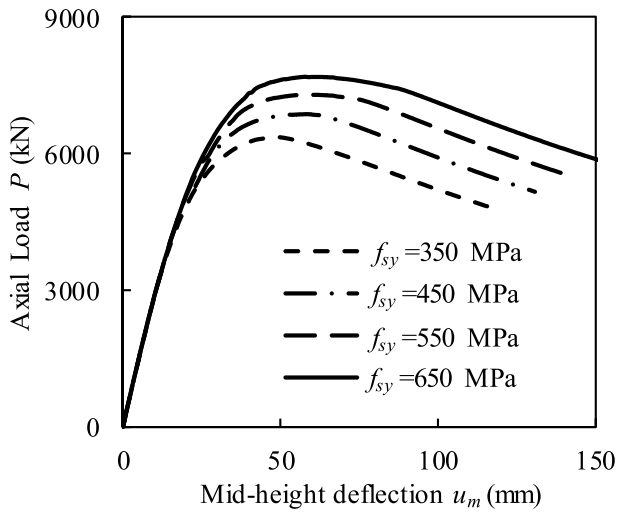


Fig. 30. Influences of steel yield strength on the axial load-deflection curves of square CFDST slender columns.

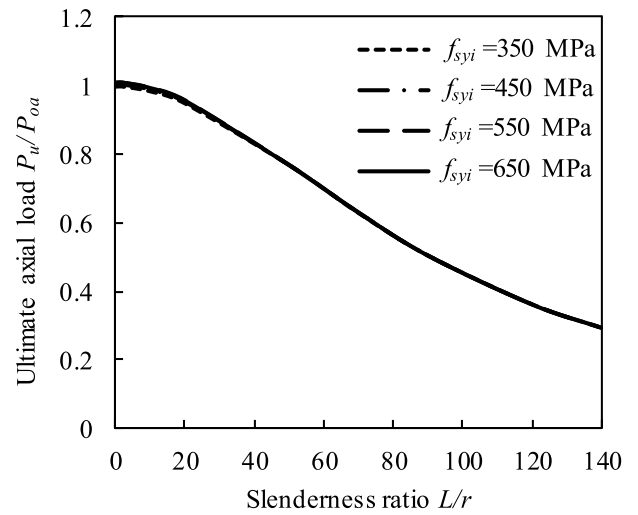


Fig. 33. Influences of steel yield strength of the inner steel tube on the column strength curves of square CFDST columns.

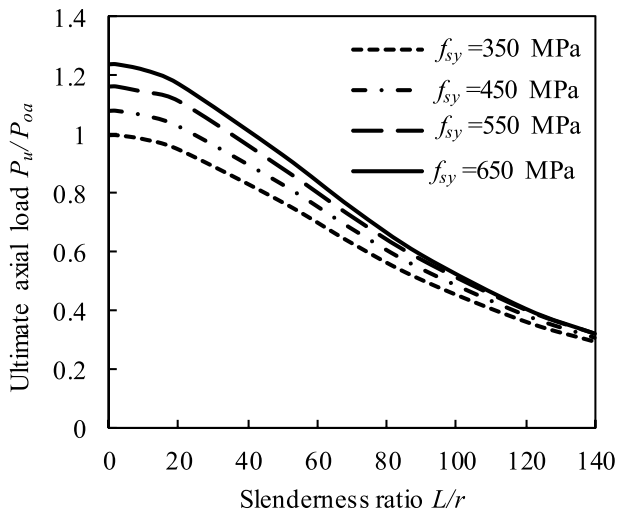


Fig. 31. Influences of steel yield strength on the column strength curves of square CFDST columns.

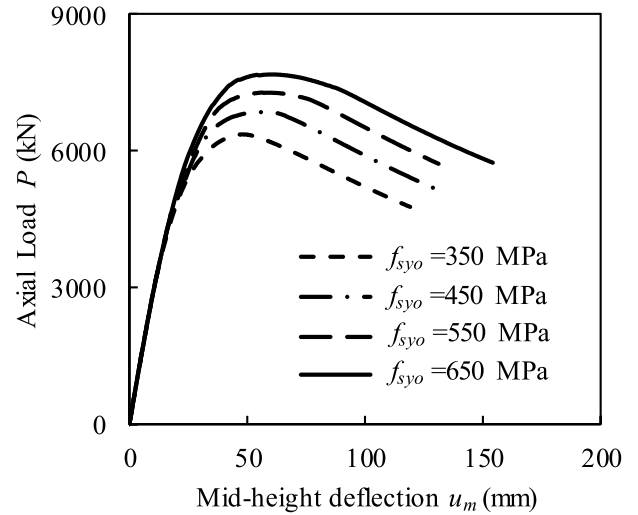


Fig. 34. Influences of steel yield strength of the outer steel tube on the axial load-deflection curves of square CFDST slender columns.

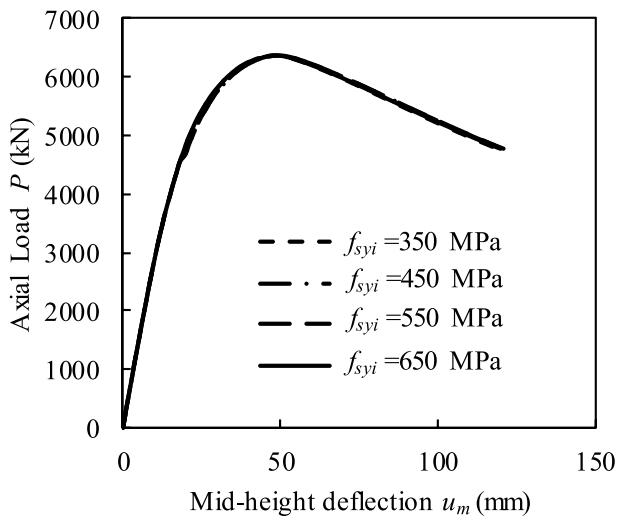


Fig. 32. Influences of steel yield strength of the inner steel tube on the axial load-deflection curves of square CFDST slender columns.

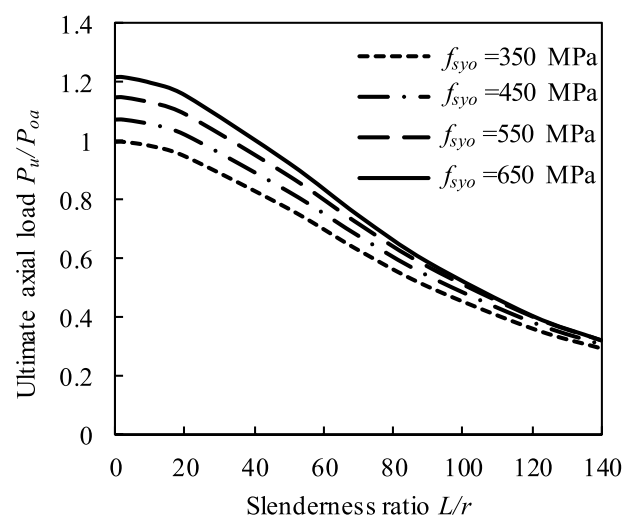


Fig. 35. Influences of steel yield strength of the outer steel tube on the column strength curves of square CFDST columns.

and 35 that the global buckling responses and the column strength curves are affected predominantly by the yield strength of the external steel tube. In Fig. 35, P_{oa} is the ultimate load of the eccentrically loaded column with $f_{syo} = 350$ MPa and the column slenderness ratio approaching zero. Thus, it is effective to use high strength external steel tube to improve the strength of CFDST columns with short and immediate lengths.

7. Proposed design models

7.1. CFDST slender columns under axial compression

The computational model developed in this study has been used to obtain the column strength curves for square CFDST columns under axial compression with a wide range of parameters and initial geometric imperfection of $L/1000$. Based on the numerical results and Eurocode 4 [42], a simple design model for calculating the ultimate strength of square slender CFDST columns loaded concentrically is proposed herein as:

$$P_{u,des} = \chi P_{uo} \tag{23}$$

where P_{uo} is the column section ultimate strength under axial compression and calculated as

$$P_{uo} = f_{syo} A_{soe} + f_{syt} A_{sti} + \gamma_{co} f'_{co} A_{co} + \gamma_{ci} f'_{ci} A_{ci} \tag{24}$$

where A_{soe} is the effective area of the outer tube conserving local buckling effects, A_{sti} the cross-sectional area of inner tube, A_{co} the cross-sectional area of sandwiched concrete, A_{ci} the cross-sectional area of core concrete, f'_{co} and f'_{ci} the compressive strength of sandwiched-concrete and core-concrete, respectively.

In Eq. (23), χ is the slenderness reduction factor. The original expression for χ suggested by Eurocode 4 is modified herein as:

$$\chi = \frac{1}{\varphi + \sqrt{\varphi^2 - \bar{\lambda}^2}} \leq 1.0 \tag{25}$$

$$\varphi = \frac{1.03 + 0.21(\bar{\lambda} - 0.2) + \bar{\lambda}^2}{2} \tag{26}$$

The relative slenderness ratio $\bar{\lambda}$ is expressed as

$$\bar{\lambda} = \sqrt{\frac{P_{uo}}{P_{cr}}} \tag{27}$$

in which P_{cr} is the Euler buckling load of CFDST columns and computed by

$$P_{cr} = \frac{\pi^2 (EI)_{eff}}{L^2} \tag{28}$$

in which $(EI)_{eff}$ is the effective flexural stiffness of the composite cross-section, expressed as

$$(EI)_{eff} = E_{s,so} I_{s,so} + 0.6 E_{cm,co} I_{c,co} + E_{s,si} I_{s,si} + 0.6 E_{cm,ci} I_{c,ci} \tag{29}$$

where E_s is the Young's modulus of steel, I_s the second moment of area of the steel tube, E_{cm} the Young's modulus of concrete, I_c the second moment of area of concrete. The subscripts *so*, *si*, *co* and *ci* define the outer steel tube, inner steel tube, sandwiched concrete and core concrete, respectively. The Young's modulus of concrete can be estimated by

$$E_{cm} = 22000 \left(\frac{f'_c + 8}{10} \right)^{1/3} \tag{30}$$

Fig. 36 presents the validation of the proposed design model. The column strength curve of the reference column given in Section 6 is compared with the one calculated using the design model. It is shown that the agreement between numerical predictions and design calculations is good. Therefore, the proposed design model can be used in the

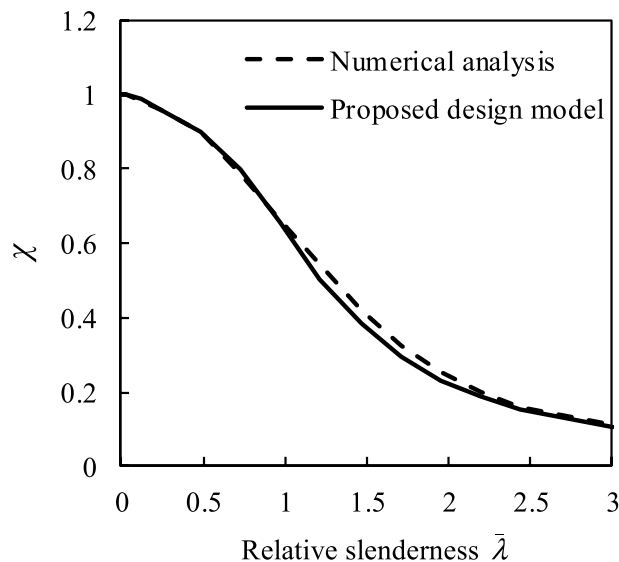


Fig. 36. Comparison of proposed design model with numerical analysis.

design of square CFDST slender columns loaded concentrically in practice.

7.2. CFDST slender columns under eccentric loading

The numerical models developed by Liang et al. [24] and in this paper were employed to generate the axial load-moment interaction diagrams of square CFDST slender columns considering local buckling. Based on the numerical studies, the nominal interaction equations for CFDST slender columns with non-compact or slender sections under eccentric loading are proposed as

$$M_u = 1.04 M_o \left[1 - \left(\frac{P_u}{P_o} \right)^{\alpha_m} \right] \quad \text{for } P_u \geq 0.2 P_o \tag{31}$$

$$M_u = M_o \left[1 - \frac{1}{10} \left(\frac{P_u}{P_o} \right)^{\alpha_n} \right] \quad \text{for } P_u < 0.2 P_o \tag{32}$$

where P_u is the axial load, M_u the corresponding ultimate bending resistance of the slender CFDST column, P_o the ultimate pure axial strength of the slender column without moment, M_o the column ultimate bending resistance without axial load, α_m and α_n the shape factors of the interaction curves depending on the L/r ratio of CFDST columns and are proposed as

$$\alpha_m = 2.44 - 0.012 \left(\frac{L}{r} \right) \quad (1.0 \leq \alpha_m \leq 2.0) \tag{33}$$

$$\alpha_n = \begin{cases} 2.668(L/r) - 2.496 & \text{for } 1.0 \leq \alpha_m \leq 1.5 \\ 1.5 & \text{for } 1.5 < \alpha_m \leq 2.0 \end{cases} \tag{34}$$

The comparison of the interaction curves for CFDST columns with various design parameters given in the parametric study obtained by the proposed equations and the numerical model is shown in Fig. 37. It is seen that the agreement between the proposed design equations and numerical results for a wide range of design parameters is good. The design interaction curves are also compared with those computed by the formulas given in AISC 360-16 [43]. The proposed design equations yield better results than those specified in AISC 360-16 as can be seen from Fig. 37.

8. Conclusions

This paper has reported on the development of a mathematical

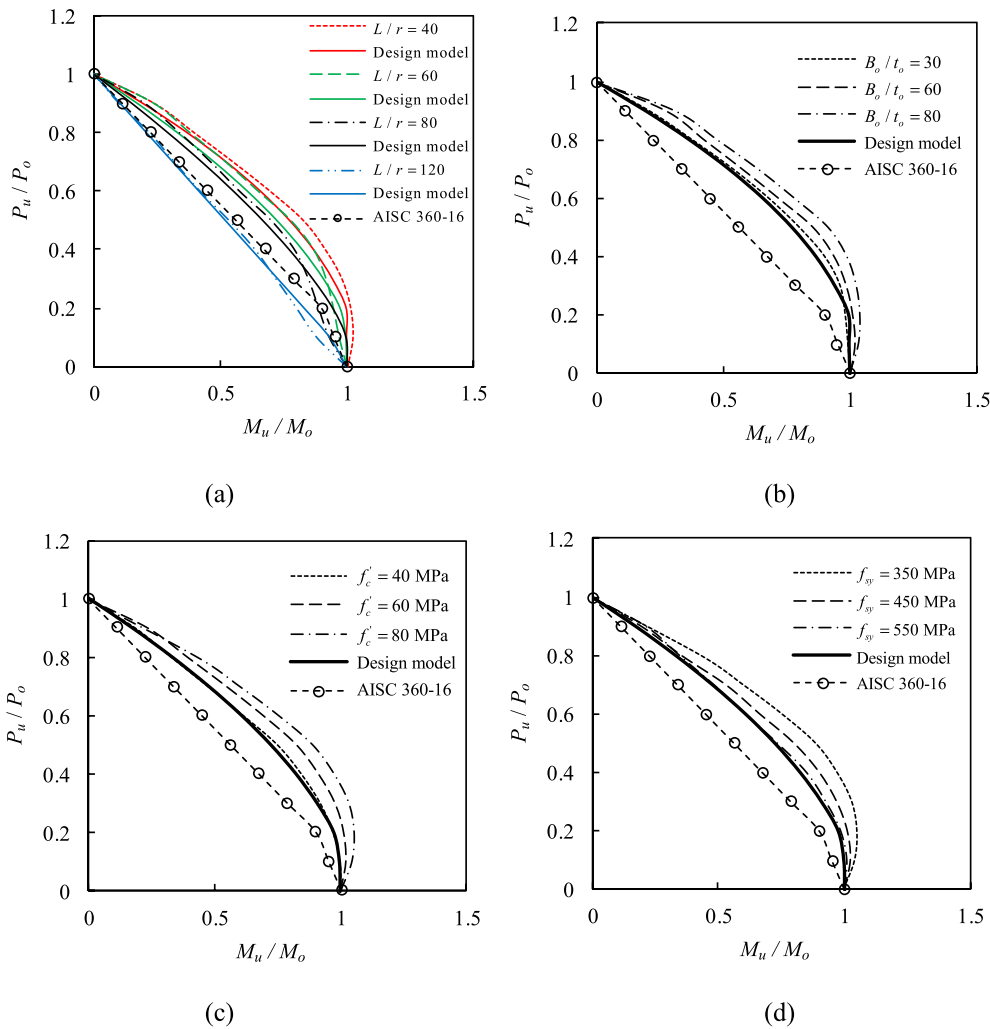


Fig. 37. Comparison of axial load-moment interaction curves for slender CFDST columns obtained by the proposed design equations and numerical model.

model incorporating the fiber approach for the simulation of the interaction local-global buckling responses of slender CFDST beam-columns with thin-walled square sections loaded eccentrically. Salient features associated with slender CFST square columns have been taken into consideration in the formulation of the mathematical model, including confinement, local-global interaction buckling, geometric imperfection, and second-order as well as high-strength materials. Efficient computational solution algorithms implementing the inverse quadratic method have been developed to obtain converged solutions to the nonlinear dynamic functions generated in the incremental-iterative analysis process for slender CFDST columns. The computational model has been verified by test data on CFST and DCFST columns and employed to determine the local-global interaction buckling behavior of CFDST columns with various important parameters. Design models have been developed for calculating the ultimate strengths of slender square CFDST columns subjected to axial compression and eccentric loading.

The concluding remarks are provided as follows:

- (1) Further tests on the behavior of slender square CFDST columns should be conducted to provide results that can be used to validate numerical models.
- (2) The initial stiffness and ultimate axial load of square CFDST columns are found to reduce significantly when increasing the column slenderness ratio.
- (3) The B_0/t_0 ratio has a remarkable effect on the strength and initial

stiffness of CFDST columns but its influence decreases with increasing the column slenderness.

- (4) The D_i/B_0 ratio has a minor influence on the global buckling behavior of CFDST columns.
- (5) Increasing the e/B_0 ratio results in marked reductions in the column initial stiffness and ultimate axial load.
- (6) The buckling behavior of slender CFDST columns is almost not affected by the D_i/t_i ratio.
- (7) The outward local buckling of the outer steel tube considerably reduces the ultimate load of CFDST square columns, but this effect decreases when the column slenderness increases.
- (8) Increasing the sandwiched-concrete strength substantially improves the column ultimate load. The influence of concrete strength, however, decreases with increasing the column slenderness ratio. The core-concrete strength has an insignificant influence on the column strength.
- (9) The ultimate strength of CFDST columns is shown to increase appreciably by using higher yield strength external steel tube. However, the column global buckling behavior is almost not affected by the yield stress of the inner steel Tube.
- (10) The proposed design models derived based on the numerical results predict well the ultimate strengths of square CFDST slender columns under axial compression and eccentric loading.

References

- [1] AS 3600-2009, Australian Standard for Concrete Structures, Standards Australia, Sydney, NSW, Australia, 2009.
- [2] A.H. Varma, J.M. Ricles, R. Sause, L.W. Lu, Experimental behavior of high strength square concrete-filled steel tube beam-columns, *J. Struc. Eng. ASCE* 128 (3) (2002) 309–318.
- [3] M. Mursi, B. Uy, Strength of concrete filled steel box columns incorporating interaction buckling, *J. Struc. Eng. ASCE* 129 (5) (2003) 626–639.
- [4] M. Mursi, B. Uy, Strength of slender concrete filled high strength steel box columns, *J. Constr. Steel Res.* 60 (12) (2004) 1825–1848.
- [5] D. Liu, Behaviour of high strength rectangular concrete-filled steel hollow section columns under eccentric loading, *Thin-Walled Struct.* 42 (12) (2004) 1631–1644.
- [6] Y. Du, Z. Chen, Y.B. Wang, J.Y.R. Liew, Ultimate resistance behavior of rectangular concrete-filled tubular beam-columns made of high-strength steel, *J. Constr. Steel Res.* 133 (2017) 418–433.
- [7] Y. Du, Z. Chen, J.Y.R. Liew, M.X. Xiong, Rectangular concrete-filled steel tubular beam-columns using high-strength steel: experiments and design, *J. Constr. Steel Res.* 131 (2017) 1–18.
- [8] Z. Tao, L.H. Han, Behaviour of concrete-filled double skin rectangular steel tubular beam-columns, *J. Constr. Steel Res.* 62 (7) (2006) 631–646.
- [9] Z. Tao, L.H. Han, X.L. Zhao, Behaviour of concrete-filled double skin (CHS inner and CHS outer) steel tubular stub columns and beam-columns, *J. Constr. Steel Res.* 60 (8) (2004) 1129–1158.
- [10] X.L. Zhao, R. Grzebieta, M. Elchalakani, Tests of concrete-filled double skin CHS composite stub columns, *Steel Compos. Struct.* 2 (2) (2002) 129–146.
- [11] X.L. Zhao, L.W. Tong, X.Y. Wang, CFDST stub columns subjected to large deformation axial loading, *Eng. Struct.* 32 (3) (2010) 692–703.
- [12] L.H. Han, Z. Tao, H. Huang, X.L. Zhao, Concrete-filled double skin (SHS outer and CHS inner) steel tubular beam-columns, *Thin-Walled Struct.* 42 (9) (2004) 1329–1355.
- [13] L.H. Han, H. Huang, Z. Tao, X.L. Zhao, Concrete-filled double skin steel tubular (CFDST) beam-columns subjected to cyclic bending, *Eng. Struct.* 28 (12) (2006) 1698–1714.
- [14] M.X. Xiong, D.X. Xiong, J.Y.R. Liew, Behaviour of steel tubular members infilled with ultra high strength concrete, *J. Constr. Steel Res.* 138 (2017) 168–183.
- [15] W.J. Pei, Research on Mechanical Performance of Multibarrel Tube-Confined Concrete Columns, ME Thesis, Chang'an Univ., Xian, China, 2005 (in Chinese).
- [16] J. Qian, N. Li, X. Ji, Z. Zhao, Experimental study on the seismic behavior of high strength concrete filled double-tube columns, *Earthq. Eng. Eng. Vib.* 13 (1) (2014) 47–57 (in Chinese).
- [17] J. Qian, Y. Zhang, X. Ji, W. Cao, Test and analysis of axial compressive behavior of short composite-sectioned high strength concrete filled steel tubular columns, *J. Build. Struct.* 32 (12) (2011) 162–169 (in Chinese).
- [18] J. Qian, Y. Zhang, W. Zhang, Eccentric compressive behavior of high strength concrete filled double-tube short columns, *J. Tsinghua Univ.* 55 (1) (2015) 1–7 (in Chinese).
- [19] M.X. Xiong, D.X. Xiong, J.Y.R. Liew, Axial performance of short concrete filled steel tubes with high-and ultra-high-strength materials, *Eng. Struct.* 136 (2017) 494–510.
- [20] Z.B. Wang, Z. Tao, Q. Yu, Axial compressive behaviour of concrete-filled double-tube stub columns with stiffeners, *Thin-Walled Struct.* 120 (2017) 91–104.
- [21] N.E. Shanmugam, B. Lakshmi, B. Uy, An analytical model for thin-walled steel box columns with concrete in-fill, *Eng. Struct.* 24 (6) (2002) 825–838.
- [22] Z. Vrcelj, B. Uy, Strength of slender concrete-filled steel box columns incorporating local buckling, *J. Constr. Steel Res.* 58 (2) (2002) 275–300.
- [23] V.I. Patel, Q.Q. Liang, M.N.S. Hadi, High strength thin-walled rectangular concrete-filled steel tubular slender beam-columns, Part I: Modeling, *J. Constr. Steel Res.* 70 (2012) 377–384.
- [24] Q.Q. Liang, V.I. Patel, M.N.S. Hadi, Biaxially loaded high-strength concrete-filled steel tubular slender beam-columns, Part I: multiscale simulation, *J. Constr. Steel Res.* 75 (2012) 64–71.
- [25] M. Ahmed, Q.Q. Liang, V.I. Patel, M.N.S. Hadi, Nonlinear analysis of rectangular concrete-filled double steel tubular short columns incorporating local buckling, *Eng. Struct.* 175 (2018) 13–26.
- [26] T.Q. Lü, G.F. Zhao, Numerical method for analysis of ultimate strength of concrete-filled square steel Tubular columns under eccentric compression reinforced by inner circular steel tube, *J. Dalian Univ. Technolgy* 41 (5) (2001) 612–616 (in Chinese).
- [27] Q.Q. Liang, Performance-based analysis of concrete-filled steel tubular beam-columns, Part I: theory and algorithms, *J. Constr. Steel Res.* 65 (2) (2009) 363–372.
- [28] Q.Q. Liang, Performance-based analysis of concrete-filled steel tubular beam-columns, Part II: verification and applications, *J. Constr. Steel Res.* 65 (2) (2009) 351–362.
- [29] Q.Q. Liang, Analysis and Design of Steel and Composite Structures, CRC Press, Taylor and Francis Group, Boca Raton and London, 2014.
- [30] V.I. Patel, Q.Q. Liang, M.N.S. Hadi, Concrete-filled Stainless Steel Tubular Columns, CRC Press, Taylor and Francis, Boca Raton and London, 2018.
- [31] P.O. Persson, G. Strang, A simple mesh generator in MATLAB, *SIAM Rev.* 46 (2) (2004) 329–345.
- [32] M. Ahmed, Q.Q. Liang, V.I. Patel, M.N.S. Hadi, Numerical analysis of axially loaded circular high strength concrete-filled double steel tubular short columns, *Thin-Walled Struct.* 138 (2019) 105–116.
- [33] Q.Q. Liang, B. Uy, J.Y.R. Liew, Local buckling of steel plates in concrete-filled thin-walled steel tubular beam-columns, *J. Constr. Steel Res.* 63 (3) (2007) 396–405.
- [34] Q.Q. Liang, High strength circular concrete-filled steel tubular slender beam-columns, Part I: numerical analysis, *J. Constr. Steel Res.* 67 (2) (2011) 164–171.
- [35] J.B. Mander, Seismic Design of Bridge Piers (Ph.D. Thesis), Depart. Of Civil Eng. Uni. of Canterbury, Christchurch, New Zealand, (1983).
- [36] J.B. Mander, M.J. Priestley, R. Park, Theoretical stress-strain model for confined concrete, *J. Struc. Eng. ASCE* 114 (8) (1988) 1804–1826.
- [37] J.C. Lim, T. Ozbakkaloglu, Stress-strain model for normal-and light-weight concretes under uniaxial and triaxial compression, *Constr. Build. Mater.* 71 (2014) 492–509.
- [38] Q.Q. Liang, S. Fragomeni, Nonlinear analysis of circular concrete-filled steel tubular short columns under axial loading, *J. Constr. Steel Res.* 65 (12) (2009) 2186–2196.
- [39] H.T. Hu, C.S. Huang, M.H. Wu, Y.M. Wu, Nonlinear analysis of axially loaded concrete-filled tube columns with confinement effect, *J. Struc. Eng. ASCE* 129 (10) (2003) 1322–1329.
- [40] J. Tang, S. Hino, I. Kuroda, T. Ohta, Modeling of stress-strain relationships for steel and concrete in concrete filled circular steel tubular columns, *Steel Constr. Eng. JSSC* 3 (11) (1996) 35–46.
- [41] D.J. Oehlers, M.A. Bradford, Elementary Behaviour of Composite Steel and Concrete Structural Members, Butterworth-Heinemann, Oxford U.K., 1999.
- [42] Eurocode 4, Design of Composite Steel and Concrete Structures-Part 1-1: General Rules and Rules for Buildings, European Committee for Standardization, CEN, Brussels, Belgium, 2004 EN 1994-1-1.
- [43] AISC 360-16, Specification for Structural Steel Buildings, American Institute of Steel Construction, Chicago (IL), 2016.

5.2 CONCLUDING REMARKS

A nonlinear fiber-element technique has been proposed in this chapter for predicting the load and deflection responses of eccentrically-loaded square slender CFDST beam-columns where the internal steel section is circular. The computational model has explicitly included the salient features observed in experiments, such as the interaction of local buckling of the external thin-walled steel section and global buckling, and the confinement provided by the internal tube on the core concrete. It has been shown that the computer model provides solutions which are in good agreement with experimentally measured results. The interaction buckling behavior of slender square CFDST columns with a wide range of design variables has been investigated by using the computer model developed. The design models proposed based on numerical results can be employed in designing slender square CFDST columns including local buckling.

Chapter 6

CIRCULAR CFDST SLENDER COLUMNS UNDER ECCENTRIC LOADING

6.1 INTRODUCTION

This chapter deals with the computational simulation and design of pin-ended circular CFDST slender columns composed of an inner circular steel tube subjected to eccentric loading. The computational model of nonlinear fiber analysis is developed for the simulation of load-deflection behavior and strength interaction diagrams of slender circular CFDST columns, including the effects of concrete confinement, imperfections, second-order, and geometric and material nonlinearities. Computer codes are written to implement the inverse quadratic method for numerically solving the incremental-iterative equilibrium functions of CFDST slender columns. The computational results are justified against the independent test results of slender CFDST and DCFST columns loaded eccentrically. The influences of important design parameters on the load distribution and behavior of slender CFDST columns are examined using the computer program developed. Design expressions are provided for the design of CFDST slender columns and compared with numerical results and codified design methods.

This chapter includes the following paper:

1. **Ahmed, M.**, Liang, Q. Q., Patel, V. I. and Hadi, M. N. S. (2020). Computational simulation of eccentrically-loaded circular thin-walled concrete-filled double steel tubular slender columns. *Engineering Structures*, 213, 110571.

OFFICE FOR RESEARCH TRAINING, QUALITY AND INTEGRITY

DECLARATION OF CO-AUTHORSHIP AND CO-CONTRIBUTION: PAPERS INCORPORATED IN THESIS

This declaration is to be completed for each conjointly authored publication and placed at the beginning of the thesis chapter in which the publication appears.

Title of
Paper/Journal/Book:

Ahmed, M., Liang, Q. Q., Patel, V. I. and Hadi, M. N. S. (2020).
Computational simulation of eccentrically-loaded circular thin-walled
concrete-filled double steel tubular slender columns. Engineering
Structures, (currently under review).

Surname:

Ahmed

First
name:

Mizan

Institute:

Institute for Sustainable Industries and Liveable Cities

Candidate's Contribution (%):

60

Status:

Accepted and in press:

Date:

Published:

Date:

2. CANDIDATE DECLARATION

I declare that the publication above meets the requirements to be included in the thesis as outlined in the HDR Policy and related Procedures – policy.vu.edu.au.

Mizan Ahmed

Digitally signed by Mizan Ahmed
Date: 2020.01.06 14:04:00 +11'00'

06-01-2020

Signature

Date

3. CO-AUTHOR(S) DECLARATION

In the case of the above publication, the following authors contributed to the work as follows:

The undersigned certify that:

1. They meet criteria for authorship in that they have participated in the conception, execution or interpretation of at least that part of the publication in their field of expertise;
2. They take public responsibility for their part of the publication, except for the responsible author who accepts overall responsibility for the publication;

3. There are no other authors of the publication according to these criteria;
4. Potential conflicts of interest have been disclosed to a) granting bodies, b) the editor or publisher of journals or other publications, and c) the head of the responsible academic unit; and
5. The original data will be held for at least five years from the date indicated below and is stored at the following **location(s)**:

R:\CFDST Columns

Name(s) of Co-Author(s)	Contribution (%)	Nature of Contribution	Signature	Date
Mizan Ahmed	60	Methodology, Software, Validation, Formal analysis, Investigation, Data curation, Writing–Original draft, Visualization.	Mizan Ahmed Digitally signed by Mizan Ahmed Date: 2020.01.06 14:04:13 +11'00'	06-01-2020
Qing Quan Liang	20	Conceptualization, Methodology, Software, Validation, Writing–Review and Editing, Supervision, Project administration.	Qing Quan Liang Digitally signed by Qing Quan Liang Date: 2020.01.06 14:38:55 +11'00'	06-01-2020
Vipulkumar I. Patel	10	Validation, Writing–Review and Editing, Supervision.	Vipul Patel Digitally signed by Vipul Patel Date: 2020.01.06 15:06:52 +11'00'	06-01-2020
Muhammad N.S. Hadi	10	Validation, Writing–Review and Editing, Supervision.	Muhammad Hadi Digitally signed by Muhammad Hadi cn=Muhammad Hadi, o=University of Wollongong, l=Wollongong, st=NSW, c=AU, email=mhadi@uow.edu.au Date: 2020.01.06 15:31:14 AEDT	06-01-2020

Computational simulation of eccentrically loaded circular thin-walled concrete-filled double steel tubular slender columns by M. Ahmed, Q.Q. Liang, V.I. Patel, and M.N.S. Hadi was published in the peer review journal, *Engineering Structures*, 213, 2020.

The full-text of this article is subject to copyright restrictions, and cannot be included in the online version of the thesis.

The published version is available from: <https://doi.org/10.1016/j.engstruct.2020.110571>

6.2 CONCLUDING REMARKS

The computer simulation and design of circular CFDST slender columns having an internal circular steel tube under eccentric loading have been presented in this chapter. The computational simulation technology developed has recognized the characteristics of circular CFDST slender columns, such as the confining stresses provided by both the steel tubes on the concrete, imperfections, second-order effects and inelastic material behavior. The modeling technology developed has been found to accurately simulate the load-deflection behavior, column strength curves, strength envelopes and load-distributions in the steel tubes and concrete of CFDST slender columns. Computational results obtained from the parametric studies have been used to develop design equations for designing slender CFDST columns loaded either concentrically or eccentrically. It has been shown that the proposed design equations generally provide more accurate strength predictions of CFDST columns than the codified methods and can be used in practice.

Chapter 7

CFDST SLENDER COLUMNS WITH PRELOAD EFFECTS

7.1 INTRODUCTION

In the composite construction of high-rise buildings, the hollow steel tubes are designed to support the permanent and construction loads of several upper floors before the concrete is filled into the steel tubes to form CFDST columns. The preloads result in the initial deformations and stresses in the hollow steel tubes and may reduce the performance of slender CFDST columns. This chapter presents nonlinear computational modeling, fundamental behavior and design of slender square and circular CFDST columns composed of an internal circular tube incorporating preload effects. The local buckling of the square outer steel section, the concrete confinement by the circular steel tube, imperfections, second-order effects, and geometric and material nonlinearities are taken into account in the computer model. The deformation caused by the preload is included in the column analysis as an additional geometric imperfection. Robust and computationally efficient algorithms are developed to obtain satisfactory solutions to the highly dynamic, nonlinear equilibrium functions of slender CFDST columns having preload effects. The computational results are verified with the experimental and FE results of CFST and DCFST columns subjected to preloads. The significance of preloads

and other important design variables on the behavior of slender CFDST columns is ascertained using the mathematical models developed. Design models are proposed for designing CFDST columns in which the steel tubes are under preloads.

This chapter includes the following papers:

1. **Ahmed, M.**, Liang, Q. Q., Patel, V. I. and Hadi, M. N. S. (2020). Nonlinear analysis of square concrete-filled double steel tubular slender columns incorporating preload effects. *Engineering Structures*, 207, 110272 (published on 15th March 2020).
2. **Ahmed, M.**, Liang, Q. Q., Patel, V. I. and Hadi, M. N. S. (2020). Behavior of circular concrete-filled double steel tubular slender beam-columns including preload effects. *Engineering Structures* (currently under review).

OFFICE FOR RESEARCH TRAINING, QUALITY AND INTEGRITY

DECLARATION OF CO-AUTHORSHIP AND CO-CONTRIBUTION: PAPERS INCORPORATED IN THESIS

This declaration is to be completed for each conjointly authored publication and placed at the beginning of the thesis chapter in which the publication appears.

Title of
Paper/Journal/Book:

Ahmed, M., Liang, Q. Q., Patel, V. I. and Hadi, M. N. S. (2020). Nonlinear analysis of square concrete-filled double steel tubular slender columns incorporating preload effects. Engineering Structures, (accepted).

Surname:

First
name:

Institute:

Candidate's Contribution (%):

Status:

Accepted and in press:

Date:

Published:

Date:

2. CANDIDATE DECLARATION

I declare that the publication above meets the requirements to be included in the thesis as outlined in the HDR Policy and related Procedures – policy.vu.edu.au.

Mizan Ahmed

Digitally signed by Mizan
Ahmed
Date: 2020.01.22 11:34:55
+11'00'

22-01-2020

Signature

Date

3. CO-AUTHOR(S) DECLARATION

In the case of the above publication, the following authors contributed to the work as follows:

The undersigned certify that:

1. They meet criteria for authorship in that they have participated in the conception, execution or interpretation of at least that part of the publication in their field of expertise;
2. They take public responsibility for their part of the publication, except for the responsible author who accepts overall responsibility for the publication;

3. There are no other authors of the publication according to these criteria;
4. Potential conflicts of interest have been disclosed to a) granting bodies, b) the editor or publisher of journals or other publications, and c) the head of the responsible academic unit; and
5. The original data will be held for at least five years from the date indicated below and is stored at the following **location(s)**:

R:\CFDST Columns

Name(s) of Co-Author(s)	Contribution (%)	Nature of Contribution	Signature	Date
Mizan Ahmed	60	Methodology, Software, Validation, Formal analysis, Investigation, Data curation, Writing–Original draft, Visualization.	Mizan Ahmed Digitally signed by Mizan Ahmed Date: 2020.01.22 11:35:10 +11'00'	22-01-2020
Qing Quan Liang	20	Conceptualization, Methodology, Software, Validation, Writing–Review and Editing, Supervision, Project administration.	Qing Quan Liang Digitally signed by Qing Quan Liang Date: 2020.01.22 12:33:04 +11'00'	22-01-2020
Vipulkumar I. Patel	10	Validation, Writing–Review and Editing, Supervision.	Vipul Patel Digitally signed by Vipul Patel Date: 2020.01.22 12:37:49 +11'00'	22-01-2020
Muhammad N.S. Hadi	10	Validation, Writing–Review and Editing, Supervision.	Muhammad Hadi Digitally signed by Muhammad Hadi DN: cn=Mohammad Hadi, o=University of Wollongong, ou=School of CME, email=mhadi@uow.edu.au, c=AU Date: 2020.01.22 13:07:27 +11'00'	22-01-2020

OFFICE FOR RESEARCH TRAINING, QUALITY AND INTEGRITY

DECLARATION OF CO-AUTHORSHIP AND CO-CONTRIBUTION: PAPERS INCORPORATED IN THESIS

This declaration is to be completed for each conjointly authored publication and placed at the beginning of the thesis chapter in which the publication appears.

Title of
Paper/Journal/Book:

Ahmed, M., Liang, Q. Q., Patel, V. I. and Hadi, M. N. S. (2020). Behavior of circular concrete-filled double steel tubular slender beam-columns including preload effects. Marine Structures, (currently under review).

Surname:

Ahmed

First
name:

Mizan

Institute:

Institute for Sustainable Industries and Liveable Cities

Candidate's Contribution (%):

60

Status:

Accepted and in press:

Date:

Published:

Date:

2. CANDIDATE DECLARATION

I declare that the publication above meets the requirements to be included in the thesis as outlined in the HDR Policy and related Procedures – policy.vu.edu.au.

Mizan Ahmed

Digitally signed by Mizan Ahmed
Date: 2020.01.13 05:52:31 +11'00'

Signature

13-01-2020

Date

3. CO-AUTHOR(S) DECLARATION

In the case of the above publication, the following authors contributed to the work as follows:

The undersigned certify that:

1. They meet criteria for authorship in that they have participated in the conception, execution or interpretation of at least that part of the publication in their field of expertise;
2. They take public responsibility for their part of the publication, except for the responsible author who accepts overall responsibility for the publication;

3. There are no other authors of the publication according to these criteria;
4. Potential conflicts of interest have been disclosed to a) granting bodies, b) the editor or publisher of journals or other publications, and c) the head of the responsible academic unit; and
5. The original data will be held for at least five years from the date indicated below and is stored at the following **location(s)**:

R:\CFDST Columns

Name(s) of Co-Author(s)	Contribution (%)	Nature of Contribution	Signature	Date
Mizan Ahmed	60	Methodology, Software, Validation, Formal analysis, Investigation, Data curation, Writing–Original draft, Visualization.	Mizan Ahmed Digitally signed by Mizan Ahmed Date: 2020.01.13 05:52:49 +11'00'	13-01-2020
Qing Quan Liang	20	Conceptualization, Methodology, Software, Validation, Writing–Review and Editing, Supervision, Project administration.	Qing Quan Liang Digitally signed by Qing Quan Liang Date: 2020.01.13 12:35:48 +11'00'	13-01-2020
Vipulkumar I. Patel	10	Validation, Writing–Review and Editing, Supervision.	Vipul Patel Digitally signed by Vipul Patel Date: 2020.01.13 12:38:51 +11'00'	13-01-2020
Muhammad N.S. Hadi	10	Validation, Writing–Review and Editing, Supervision.	Muhammad Hadi Digitally signed by Muhammad Hadi cn=Muhammad Hadi, o=University of Wollongong, ou=Wollongong, st=NSW, c=AU, email=mhadi@uow.edu.au Date: 2020.01.13 13:26:0 AEDT	13-01-2020

Nonlinear analysis of square concrete-filled double steel tubular slender columns incorporating preload effects by M. Ahmed, Q.Q. Liang, V.I. Patel, and M.N.S. Hadi was published in the peer review journal, *Engineering Structures*, 207, 2020.

The full-text of this article is subject to copyright restrictions, and cannot be included in the online version of the thesis.

The published version is available from: <https://doi.org/10.1016/j.engstruct.2020.110272>

Manuscript prepared for

Engineering Structures

January 2020

Behavior of circular concrete-filled double steel tubular slender beam-columns including preload effects

Mizan Ahmed^a, Qing Quan Liang^{a,*}, Vipulkumar Ishvarbhai Patel^b, Muhammad N. S. Hadi^c

^a College of Engineering and Science, Victoria University, PO Box 14428, Melbourne, VIC 8001, Australia

^b School of Engineering and Mathematical Sciences, La Trobe University, Bendigo, VIC 3552, Australia

^c School of Civil, Mining and Environmental Engineering, University of Wollongong, Wollongong, NSW 2522, Australia

Corresponding author:

Dr Qing Quan Liang
College of Engineering and Science
Victoria University
PO Box 14428
Melbourne VIC 8001
Australia
E-mail: Qing.Liang@vu.edu.au

Behavior of circular concrete-filled double steel tubular slender beam-columns including preload effects

Mizan Ahmed^a, Qing Quan Liang^{a,*}, Vipulkumar Ishvarbhai Patel^b, Muhammad N. S. Hadi^c

^a *College of Engineering and Science, Victoria University, PO Box 14428, Melbourne, VIC 8001, Australia*

^b *School of Engineering and Mathematical Sciences, La Trobe University, Bendigo, VIC 3552, Australia*

^c *School of Civil, Mining and Environmental Engineering, University of Wollongong, Wollongong, NSW 2522, Australia*

ABSTRACT

The hollow circular steel tubes support the permanent and construction loads of several upper platforms/floors during the construction of an offshore structure before the concrete is filled into the steel tubes to form circular concrete-filled double steel tubular (CFDST) columns. The preloads acting on the steel tubes may cause a marked reduction in the performance of slender CFDST columns. This paper presents a numerical modeling technique underlying the method of fiber elements for quantifying the behavior of circular slender CFDST beam-columns loaded eccentrically with preloads acting on the hollow steel tubes. The numerical model considers the concrete confinement, second-order effects, initial geometric imperfection, deformations induced by preloads as well as geometric and material nonlinearities. The dynamic nonlinear equilibrium functions are solved using efficient computational solution algorithms developed. The validation of the numerical modeling technique is made by comparing computations with existing results obtained by experiments and finite element analyses. The influences of preloads on the structural behavior of slender CFDST beam-columns with various important parameters are investigated by means of utilizing the developed computer model. It is shown that the

*Corresponding author.

E-mail address: Qing.Liang@vu.edu.au (Q. Q. Liang)

numerical modeling method is an efficient computational simulation and design tool for slender CFDST columns including preloads.

Keywords: Concrete-filled double steel tubes; nonlinear analysis; slender beam-columns; preload effects.

1. Introduction

Circular concrete-filled double steel tubular (CFDST) columns as shown in Fig. 1(a) have high ductility, stiffness, strength, and fire resistance because of the utilization of the internal circular steel tube filled with concrete. The common practice in the construction of an offshore structure or composite structure is to erect the hollow steel tubes that support several upper platforms or floors prior to filling the concrete into the steel tubes. The preloads acting on the steel hollow tubes may cause considerable reductions in the stiffness and strength of CFDST slender columns and affect the load distribution in concrete and steel components in the columns. Therefore, it is important to quantify the influences of preloads on the structural behavior of CFDST columns to achieve safe and effective designs. However, the experimental and computational studies of preload effects on the performance and load distribution in the components of CFDST columns are extremely rare. The objective of this paper is to ascertain the fundamental behavior of circular CFDST columns where the steel tubes are preloaded by using an efficient computational model, which is developed based on the theory of the nonlinear fiber analysis.

The structural performance of CFDST columns composed of circular sections without preload effects has been investigated experimentally by Peng et al. [1], Xiong et al. [2], Ekmekyapar

and Al-Eliwi [3], Chang et al. [4], Romero et al. [5], Ibañez et al. [6], Xiong et al. [7], and Ahmed et al. [8]. Ahmed et al. [8] undertook experiments to evaluate the significance of loading eccentricity on the behavior of CFDST short beam-columns. The beam-columns were constructed by cold-formed steel tubes that had yield stress up to 412 MPa and normal strength concrete. The eccentricity ratio (e/D_o) varied from 0.0 to 0.21. Like concrete-filled steel tubular (CFST) columns depicted in Fig. 1(b), the ultimate load of CFDST columns was discovered to be affected by the steel ratio and concrete area. However, the utilization of the circular inner tube improved the ductility and strength of such composite columns under eccentric loading. Romero et al. [9] and Ibañez et al. [6] examined the influences of different combinations of steel thickness and concrete strength on the responses of slender CFDST columns loaded either concentrically or eccentrically. The ultra-high-strength (UHS) concrete up to 150 MPa was used in the construction of these column specimens. The UHS concrete was found to have an insignificant effect on the strength of slender columns that were loaded eccentrically as the failure of slender columns was mainly caused by the global buckling. Tao et al. [10] undertook tests on double-skin CFST columns where the e/D_o ratios of the columns varied from 0.0 to 0.4. The columns failed in a ductile manner due to the composite action. A theoretical model was presented for the response analysis of such composite columns and a design model was also proposed by Tao et al. [10].

Tests on steel-concrete composite columns subjected to preloads have been very limited [11-16]. Han and Yao [13] performed tests on square CFST columns where the steel tubes were subjected to initial stresses that were applied by using the pre-stressing bars. The slenderness of the column specimens varied from 10 to 40. It was observed that due to the initial stress acting on the steel tube, the strength of CFST columns was reduced by up to 20%. The significance of initial stresses on the behavior of CFST columns of circular sections with the

preload ratio (β_a) ranged from 0.0 to 0.4 were ascertained experimentally by Liew and Xiong [14]. Test results showed that the preload effect was insignificant when the β_a ratio was less than 0.2. However, when the β_a ratio was greater than 0.6, the reduction in the column strength was about 20%. Huang et al. [15] examined the sensitivities of the ultimate load of CFST columns to preloads. It was found that the preload effect increased with increasing the member slenderness and a significant preload remarkably reduced the strength of slender columns.

Numerical models have been developed and employed to numerically determine the structural performance of CFST columns under preloads by Han and Yao [13], Liew and Xiong [14], Xiong and Zha [17], Patel et al. [18], Patel et al. [19] and Huang et al. [15]. Patel et al. [18] developed a mathematical model that considered the influences of concrete confinement, second-order, and geometric and material nonlinearities. The significance of preloads on the responses of double-skin DCFST columns as shown in Fig. 1(c) was studied by Li et al. [20] using the finite element (FE) software Abaqus. The initial stresses on either outer steel tube or both tubes were considered. Numerical models for circular CFDST columns without preloads were previously developed by researchers [4, 8, 21-27]. Ahmed et al. [27] investigated the significance of material properties in addition to geometry on the global buckling of CFDST columns by means of using a mathematical modeling approach. From the load distribution of CFDST columns, it was discovered that the sandwiched-concrete carried most of the load and the load carried by the external tube was reduced remarkably by increasing the e/D_o ratio.

No experimental and computational investigations on the behavior of slender CFDST circular beam-columns having preloads acting on the hollow steel tubes have been reported. This paper describes a numerical modeling approach for ascertaining the behavior of eccentrically loaded CFDST slender beam-columns where the steel tubes are preloaded. The numerical model

explicitly considers the effects of concrete confinement, second-order, geometric and material nonlinearities and deformations induced by preloads. The computational procedure and the validation of the model are presented. The influences of preloads and important design parameters on the structural behavior of slender CFDST circular beam-columns loaded eccentrically are studied.

2. Nonlinear inelastic fiber element simulation

2.1. General

The numerical modeling technique utilizes the concept of fiber analysis to divide the cross-section of a CFDST beam-column as shown in Fig. 2. The fiber analysis approach assumes that no slippage in the longitudinal direction between the concrete infill and steel tubes occurs. The strain in the cross-sectional depth is linearly distributed as shown in Fig. 2. The fiber strains are determined from the curvature (ϕ) and plastic neutral axis depth (d_n) of the cross-section under axial compression in addition to uniaxial bending. The ratio of preload is defined as $\beta_a = P_{pre} / P_{us}$, where P_{pre} denotes the preload acting on the hollow steel tubes and P_{us} the ultimate axial load of the hollow steel tubes. The fiber stress is calculated from the fiber strain using the material models of steel and concrete. The internal axial force (P) and moment (M) are calculated by stress integration [28].

2.2. Constitutive model for steel material

The steel tubes of a CFDST beam-column composed of circular sections offer confinement to the filled concrete. Both steel tubes of a CFDST beam-column are subjected to hoop tension

owing to the concrete expansion. This confinement effect decreases the steel yield stress in the longitudinal direction, which is taken into account in the constitutive model for steel material in CFDST columns using a reduction factor of 0.9. The elastic-plastic stress-strain curve with strain hardening presented by Ahmed et al. [26] is adopted in the present model. The stress in the strain range of $0.9\varepsilon_{sy} < \varepsilon_s \leq \varepsilon_{st}$ and strain hardening is calculated using the expressions suggested by Liang [28] and Mander [29]. The strain at the start of strain-hardening (ε_{st}) is assumed to be 0.005 while the ultimate strain (ε_{su}) of 0.2 is used.

2.3. Constitutive model for concrete material

The stress-strain curves for confined and unconfined concrete are illustrated in Fig. 3. In a circular CFDST column, the sandwiched-concrete is mainly confined by the external tube while the core-concrete is confined by both the external and internal tubes [26]. The stress-strain curve for confined compressive concrete consists of ascending and descending portions. The ascending portion of the stress-strain curve is expressed as [30]:

$$\sigma_c = \frac{f'_{cc}(\varepsilon_c / \varepsilon'_{cc})^\lambda}{(\varepsilon_c / \varepsilon'_{cc})^\lambda + \lambda - 1} \quad \text{for } 0 \leq \varepsilon_c \leq \varepsilon'_{cc} \quad (1)$$

in which σ_c and ε_c are the concrete stress and corresponding strain, respectively. In Eq. (1), λ is given by

$$\lambda = \frac{E_c \varepsilon'_{cc}}{E_c \varepsilon'_{cc} - f'_{cc}} \quad (2)$$

The concrete modulus of elasticity (E_c) is estimated by the expressions given by Lim and Ozbakkaloglu [31] after considering the column size effect on the concrete compressive strength using the reduction factor $\gamma_c = 1.85 D_c^{-0.135}$, which was originally proposed by Liang [28] and $D_c = (D - 2t)$.

The equations presented by Mander et al. [30] are used to compute the compressive strength (f'_{cc}) and the corresponding strain (ϵ'_{cc}) of confined concrete, expressed as

$$f'_{cc} = \gamma_c f'_c + 4.1 f_{rp} \quad (3)$$

$$\epsilon'_{cc} = \epsilon'_c + \frac{20.5 f_{rp} \epsilon'_c}{\gamma_c f'_c} \quad (4)$$

The strain of unconfined concrete (ϵ'_c) in compression is estimated by the expressions suggested by De Nicolo et al. [32]. The lateral pressure (f_{rp}) improves the strength of concrete in circular CFDST columns. The lateral pressure on the sandwiched-concrete is quantified using the formulas derived by Hu et al. [33]. An equation for calculating the lateral pressure acting on the core-concrete (f_{rpi}) was proposed by Ahmed et al. [26] as

$$f_{rpi} = 2.2897 + 0.0066 \frac{D_o}{t_o} - 0.1918 \frac{D_i}{t_i} - \left(0.0585 \frac{D_o}{t_o} - 0.3801 \frac{D_i}{t_i} \right) \zeta^{-1} \quad (f_{rpi} \geq 0) \quad (5)$$

where ζ is the confinement factor given by

$$\zeta = \frac{A_{so} f_{syo} + A_{si} f_{syi}}{A_{sc} \gamma_c f'_{sc} + A_{cc} \gamma_c f'_{cc}} \quad (6)$$

in which A is the cross-sectional area of the components of the CFDST column; the subscripts so , si , sc and cc represent the outer steel tube, inner steel tube, sandwiched-concrete and core-concrete, respectively; f'_{sc} and f'_{cc} the compressive strengths of the sandwiched and core-concrete, respectively; and f_{syo} , f_{syi} the steel yield stresses of the outer and inner steel tubes, respectively.

The descending portion of stress-strain curve is described by the formula given by Lim and Ozbakkaloglu [31] as

$$\sigma_c = f'_{cc} - \frac{f'_{cc} - f_{cr}}{1 + \left(\frac{\varepsilon_c - \varepsilon'_{cc}}{\varepsilon_{ci} - \varepsilon'_{cc}} \right)^{-2}} \quad \text{for } \varepsilon'_{cc} < \varepsilon_c \quad (7)$$

The residual concrete strength (f_{cr}) proposed by Ahmed et al. [26] is determined by

$$\frac{f_{cr}}{f'_{cc}} = 1.2420 - 0.0029 \left(\frac{D}{t} \right) - 0.0044 \gamma_c f'_c \quad \left(0 \leq \frac{f_{cr}}{f'_{cc}} \leq 1.0 \right) \quad (8)$$

The strain at the inflection point ε_{ci} in Eq. (7) defining the shape of the post-peak stress-strain curve is computed after modifying the original expression suggested by Lim and Ozbakkaloglu [31] as

$$\varepsilon_{ci} = 2.8 \varepsilon'_{cc} \left(\frac{f_{cr}}{f'_{cc}} \right) (\gamma_c f'_c)^{-0.12} + 10 \varepsilon'_{cc} \left(1 - \frac{f_{cr}}{f'_{cc}} \right) (\gamma_c f'_c)^{-0.47} \quad (9)$$

The concrete in tension displaces strain-softening as well as tension stiffening characteristics after the concrete cracks. According to the constitutive law of concrete under tension presented in Fig. 3, the concrete stress increases proportionately with the increase of axial strain until the concrete cracks. The concrete tensile stress is then linearly reduced to zero. The ultimate concrete tensile strain (ε_u) is taken as 10 times of the concrete cracking strain (ε_{tc}). The ultimate tensile strength (f_{ct}) of concrete is specified as $0.6\sqrt{\gamma_c f'_c}$.

2.4. Column analysis

For the global analysis of the slender CFDST beam-column where the steel tubes are preloaded, it is assumed that the beam-column is pin-ended under the same loading eccentricity (e) at both ends and subjected to single curvature bending. The initial geometric imperfection (u_o) and second-order effects (u_m) are included in the mathematical formulation. The lateral displacement (u_{mo}) due to the preload on the steel tubes is considered as a geometric imperfection and determined using a load-control analysis procedure [18, 19]. The deformations of the beam-column are represented by a part-sine displacement function from which the mid-height curvature of the column (ϕ_m) is determined as [34]:

$$\phi_m = u_m \left(\frac{\pi}{L} \right)^2 \quad (10)$$

The external moment occurring at the beam-column mid-height is

$$M_e = P(e + u_o + u_{mo} + u_m) \quad (11)$$

A displacement-control method is employed in the global response analysis of CFDST slender beam-columns incorporating preload effects. The column mid-height deflection (u_m) is increased gradually under an eccentricity (e) and the corresponding internal axial force (P) and moment (M) are determined [34]. The external moment (M_{me}) and internal moment (M_{mi}) at the column mid-height must be equal to satisfy the equilibrium condition. To achieve this condition, efficient solution algorithms that implement the inverse quadratic method have been programmed to iteratively calculate the plastic neutral axis depth of the circular slender CFDST column. The computational method is expressed by

$$d_{n,j+3} = d_{n,j+1} - r_{p,j+1} \left(\frac{A}{C} \right) \quad (12)$$

$$A = (r_{p,j})^2 (d_{n,j+2} - d_{n,j+1}) + r_{p,j} r_{p,j+1} (d_{n,j+1} - d_{n,j+2}) + (r_{p,j+1} - r_{p,j+2}) r_{p,j+2} (d_{n,j} - d_{n,j+1}) \quad (13)$$

$$C = (r_{p,j+1} - r_{p,j})(r_{p,j+2} - r_{p,j})(r_{p,j+2} - r_{p,j+1}) \quad (14)$$

in which j stands for the number of iteration and r_p the residual moment, which is expressed as

$$r_p = P(e + u_o + u_{mo} + u_m) - M_{mi} \quad (15)$$

A computer program has been developed to iteratively adjust the plastic neutral axis depth in the nonlinear analysis. Three initial values are required to start the computational process of the plastic neutral axis depth and are taken as $d_{n1} = D_0$, $d_{n2} = D_0 / 2$ and $d_{n3} = (d_{n1} + d_{n2}) / 2$. The analysis of tracing the plastic neutral axis depth continues until the convergence criterion

$|r_p| \leq \varepsilon_k$ is met, where the convergence tolerance ε_k is taken as 10^{-4} . The proposed incremental-iterative computational procedure that computes the complete axial load-deflection curve for the slender CFDST column including preload effects is given as:

- (1) Input the material and geometric properties of the CFDST column.
- (2) Mesh the cross-section of the column with fine fibers.
- (3) Calculate the lateral displacement (u_{mo}) of the hollow steel tubes under preload.
- (4) Set $u_o = u_o + u_{mo}$.
- (5) Initialize the lateral displacement as $u_m = \Delta u_m$.
- (6) Determine the curvature (ϕ_m) at the column mid-height.
- (7) Compute the true plastic neutral axis depth by the numerical solution program.
- (8) Calculate the internal force P and moment M by stress integrations.
- (9) Compute the residual moments (r_p).
- (10) Repeat Steps (7)-(9) until $|r_p| \leq 10^{-4}$.
- (11) Increase the lateral deflection by $u_m = u_m + \Delta u_m$.
- (12) Repeat Steps (6)-(12) until $P_u < 0.5P_{\max}$ (where P_{\max} is the maximum load on the axial load-deflection curve) or the specified displacement limit is exceeded.
- (13) Plot the axial load-lateral deflection curve.

3. Comparisons with test and finite element results

Since no experimental and numerical works have been undertaken on CFDST slender beam-columns where the steel tubes are preloaded, the verification of the numerical modeling method is made by comparisons of computations with the test and finite element results of CFST

columns having preloads on the steel tubes reported by Zha [11], Zhang et al. [12], Liew and Xiong [14] and Huang et al. [15]. The details of the tested columns are given in Table 1, in which the predicted ultimate axial load ($P_{u,num}$) and the experimentally measured ultimate load ($P_{u,exp}$) are also included. The comparison of the test and computational results indicates that the numerical modeling method can predict reasonably well the ultimate strengths of CFST columns with preloads. The mean value of $P_{u,num} / P_{u,exp}$ is 0.95 with a standard deviation of 0.08. The simulated and experimental load-deflection curves are presented in Fig. 4. Reasonable agreement between numerical predictions and test results is obtained. The discrepancy between the test and predicted stiffness of the tested Columns B122 and B124 are due to the slip occurred during the experiment which was ignored in the mathematical modeling.

The computer model is further validated against the FE results on DCFST beam-columns with preload effects provided by Li et al. [20]. The comparison of the FE analysis and numerical results obtained from this study is given in Table 2, where $k_{p,FE} = P_{up} / P_{wp}$ is the strength index, in which P_{up} and P_{wp} are the ultimate axial strength of DCFST columns with and without preload effects, respectively. Good accuracy is observed between the FE and numerical results.

4. Behavior of CFDST slender beam-columns with preload effects

The effects of preload and important parameters on the behavior of CFDST columns were studied by employing the numerical modeling method developed. The details of the reference column utilized for the parameter study are: $D_o = 600$ mm, $t_o = 10$ mm, $D_i = 200$ mm, $t_i = 10$ mm, $f_{syo} = f_{syi} = 350$ MPa, $E_s = 200$ GPa, $f'_{co} = f'_{ci} = 60$ MPa, $L/r = 50$, $e/D_o = 0.3$ and $\beta_a = 0.6$.

4.1. Effects of preload ratio

The ratio of preload (β_a) was varied from 0.0 to 0.8 to examine the significance of preloads on the deflection responses and load-distributions of CFDST columns. It can be observed from Fig. 5 that the column ultimate load reduces by 3.0%, 6.2% and 8.7%, respectively when β_a is increased from 0.0 to 0.3, 0.6 and 0.8. This can be explained by the fact that the preload causes initial stresses and deformations in the steel tubes, which reduce the load-carrying capacity of the columns. From the load-distributions of the components of CFDST columns with various β_a ratios shown in Fig. 6, it is found that the β_a ratio has a considerable impact on the deflections of the components of CFDST columns. The load carried by the outer tube, the inner tube and the core-concrete decreases by 13%, 16.4% and 15.6%, respectively when the β_a ratio increases from 0.0 to 0.3, 0.6 and 0.8. However, the load carried by the sandwiched-concrete reduces by only about 2.9%. Furthermore, regardless of the β_a ratio, the sandwiched concrete carries most of the ultimate load as illustrated in Fig. 6. However, increasing β_a ratio from 0.0 to 0.8, the contribution of the sandwiched concrete to the ultimate load increases from 91.7% to 94.6%.

4.2. Effects of preload and e/D_o ratios

The influences of preloads and e/D_o ratio on the deflection and load-distributions of CFDST columns were examined by altering the e/D_o ratio from 0.1 to 0.4 as well as the β_a ratio from 0.0 to 0.6. Figure 7 demonstrates that increasing the e/D_o ratio remarkably reduces the strength and stiffness of CFDST columns. This is because increasing the e/D_o ratio increases the

moment on the column, which decreases the column ultimate load. The reduction in the column ultimate load was estimated as 24.8%, 42% and 53.4%, respectively by changing the e/D_o ratio from 0.1 to 0.2, 0.3 and 0.4. However, the displacement ductility of the columns improves as the e/D_o ratio increases. The effects of the e/D_o ratio on the relationships between load and deflection of the components of CFDST columns under preloads are given in Fig. 8. It is demonstrated that changing the e/D_o ratio from 0.1 to 0.2, 0.3 and 0.4 reduces the load carried by the outer tube, inner tube, sandwiched-concrete and core-concrete at the ultimate strength limit state by 68.3%, 72.9%, 30.4% and 73%, respectively. While increasing e/D_o ratio from 0.1 to 0.4 reduces the load contribution rate of outer steel tube at the ultimate load from 19.7% to 8.6%, the increase in the contribution rate of sandwiched concrete was calculated as 59.5% to 79.1% at the same time as can be seen in Fig. 9. The influences of β_a and e/D_o ratios on the ultimate axial loads are presented in Fig. 10. When the e/D_o ratio is greater than 1.0, the influence of the β_a ratio on the column-strength curve can be ignored.

4.3. Effects of preload and L/r ratios

To examine the influences of preload and L/r ratios on the deflection curves and load-distributions of CFDST columns, the L/r ratios of CFDST columns were varied from 22 to 90 while the β_a ratios were from 0.0 to 0.4 and 0.8. The load-deflection responses of columns that have various L/r ratios and the β_a ratio of 0.6 are depicted in Fig. 11. It is noted that increasing the L/r ratio leads to a remarkable reduction in the ultimate strength of CFDST beam-columns, but increases their deflections and the displacement ductility. This reduction in strength is due to the applied axial load which induces bending actions and lateral deflections in the beam-column with initial geometric imperfections. The bending actions and lateral

deflections increase with an increase in the column slenderness, which results in a reduction in the strength of the beam-column [36]. The column ultimate strength is reduced by 54.9% when increasing the L/r ratio from 22 to 90. Figure 12 gives the load-deflection responses of concrete and steel components in CFDST columns. As the L/r ratio increases, the resultant tensile force in the external and internal steel tubes also increases. Altering the L/r ratio from 22 to 90 decreases the load carried by the outer tube, inner tube, sandwiched-concrete and core-concrete by 50.2%, 76%, 35.4% and 81.5%, respectively. The influences of the β_a and L/r ratios on the column-strength curves are illustrated in Fig. 13. It is seen that for CFDST columns that have the L/r ratio less than 20, the effect of preloads can be neglected.

4.4. Effects of preloads and D_i/D_o ratios

The effects of the preload β_a and D_i/D_o ratios on the structural behavior of CFDST columns were ascertained by changing the D_i/D_o ratios from 0.33 to 0.66 and the β_a ratios from 0.0 to 0.6. It should be noted that only D_i was changed to give different D_i/D_o ratios. The load-displacement curves shown in Fig. 14 illustrate that the ratio of D_i/D_o has a moderate influence on the bending stiffness and ultimate strength of the columns. The column ultimate load increases by 18.7% when the D_i/D_o ratio is changed from 0.33 to 0.66. The influence of the D_i/D_o ratio on the column strength curves are provided in Fig. 15. It is shown that the ratio of D_i/D_o has the most prominent influence on the section capacity as D_i is a sectional dimension. However, its effect decreases with an increase in the member slenderness as the strength of more slenderness columns is governed by the member slenderness rather than the section property. The effects of the β_a and D_i/D_o ratios on the ultimate loads are demonstrated in Fig. 16. Increasing the β_a ratio reduces the column ultimate load regardless of the D_i/D_o

ratio. When the D_i/D_o ratio is 0.33, changing the β_a ratio from 0.0 to 0.8 causes 8.7% reduction in the ultimate load.

4.5. Effects of preload and D_o/t_o ratios

The D_o/t_o ratios of CFDST columns subjected to preloads were ranged from 20 to 80 by altering the thickness of the outer tube to examine their influences on the performance of columns. The predicted load-deflection responses of CFDST columns having various D_o/t_o ratios are given in Fig. 17. Significant reductions in the column ultimate load and flexural stiffness are observed by increasing the ratio of D_o/t_o . The ultimate load of the CFDST columns is reduced by 53.4% by changing the D_o/t_o ratio from 20 to 80. The strength curves of CFDST columns as a function of D_o/t_o ratios are shown in Fig. 18. The figure demonstrates that the D_o/t_o ratio has the most prominent effect on the section capacity and its influence become less significant as the L/r ratio increases. In addition, increasing the β_a ratio further reduces the column ultimate load as depicted in Fig. 19. When the D_o/t_o ratio is 80 and changing the β_a ratio from 0.0 to 0.8, the column ultimate load decreases by 9.8%.

4.6. Effects of preload and D_i/t_i ratios

The influences of D_i/t_i ratios, which were ranged from 20 to 50 by altering the thickness of the internal steel tube, on the structural responses of CFDST columns were studied by the computer model. The results shown in Fig. 20 indicate that the ratio of D_i/t_i does not have a significant impact on the load-deflection curves of the CFDST columns. Changing the D_i/t_i

ratio from 20 to 30, 40 and 50 leads to minor reductions in the ultimate load by 0.8%, 1.2% and 1.4%, respectively. This is because reducing the thickness of the inner tube decreases the steel area and concrete confinement but slightly increases the area of core-concrete, which decreases the column strength. The significance of the β_a and D_i / t_i ratios on the column axial strength is demonstrated in Fig. 21. The column ultimate strength slightly decreases by increasing the β_a ratio. The reductions in the column ultimate axial load with D_i / t_i ratios of 20, 30, 40 and 50 are about 8.8%, 8.1%, 7.8% and 7.6%, respectively if the β_a ratio increases from 0.0 to 0.8.

4.7. Effects of preload ratio and concrete strength

The sensitivities of the strengths of CFDST columns to the β_a ratio and concrete compressive strength were examined by means of utilizing the computational model. The computed load-deflection curves and column strength curves of CFDST columns with different concrete strengths are depicted in Figs. 22 and 23, respectively. Figure 22 indicates that using higher strength concrete leads to a marked improvement in the stiffness and ultimate strength of the columns. This is because increasing the concrete strength increases both the concrete modulus and sectional capacity of the column. It is expected that the ultimate load of the CFDST column would have a 35.7% increase by altering the concrete strength from 40 MPa to 100 MPa. However, the displacement ductility is shown to reduce as the concrete strength increases. The column strength curves presented in Fig. 23 demonstrate that the section axial strength of CFDST columns is improved by 44% due to the increase in the concrete strength from 40 MPa to 100 MPa. The influences of β_a ratio and concrete strength on the column axial strength are presented in Fig. 24. It is found that changing the β_a ratio from 0.0 to 0.8 results in 9.7% reduction in the column axial load with concrete strength of 100 MPa.

4.8. Effects of preload ratio and steel yield strength

The β_a ratio and steel yield stress were varied to ascertain their effects on the performance of CFDST columns. The load-deflection responses of the columns made of steel tubes that had different yield strengths are shown in Fig. 25. It is noted that the steel yield stress does not have an effect on the initial bending stiffness of the columns. However, the use of higher strength steel tube remarkably improves the column ultimate load as the strength of the column depends on the material strength. Changing the steel yield stress from 250 MPa to 550 MPa causes a 41.8% increase in the column ultimate strength. However, this effect decreases with increasing the member slenderness as depicted in Fig. 26. The figure demonstrates that the section capacity is increased up to 54% by using 550 MPa steel tube instead of 250 MPa one. The effects of preload and steel yield stress on the ultimate axial load of CFDST columns are shown in Fig. 27. It indicates that increasing the β_a ratio decreases the column strength, but the reduction is higher for the columns with higher steel yield stress.

4.9. Effects of preload ratio and concrete confinement

The influences of concrete confinement and preloads were investigated using the computer program. The L/r and e/D_o ratios of the reference column were taken as 40 and 0.1, respectively. The effects of concrete confinement on the load-displacement curves and column strength curves are presented in Figs. 28 and 29, respectively. Figure 28 indicates that the ultimate axial strength of the CFDST column is underestimated by 7% if the concrete confinement was not considered in the analysis. It would appear from Fig. 29 that ignoring the influence of concrete confinement results in the underestimation of the section capacity of the

column by 8.3%. However, the confinement effect decreases as the member slenderness ratio increases and can be ignored for the columns with L/r ratio greater than 60.

5. Conclusions

The influences of preloads on the structural behavior of CFDST slender columns composed of circular sections loaded eccentrically have been investigated in this paper. A computational method utilizing the fiber approach has been developed for this purpose that considers the effects of concrete confinement, second-order, geometric and material nonlinearities, and deflections caused by preloads. Efficient solution algorithms have been developed to solve the nonlinear equilibrium functions during the entire loading history. The accuracy of the computer modeling technique has been verified by comparing computations against existing experimental results as well as FE results. The model has been employed to study the significance of preloads and several design parameters on the behavior of slender CFDST circular columns loaded eccentrically.

Numerical results obtained have shown that significant preloads have remarkable influences on the ultimate loads and deflection responses of slender circular CFDST columns loaded eccentrically. Increasing the e/D_o , L/r or D_o/t_o ratio considerably reduces the ultimate load of CFDST columns where the preloads are applied to the steel tubes. However, these effects become less pronounced as the slenderness of the column increases. Furthermore, the D_i/t_i ratio has a negligible impact on the performance of CFDST columns with the presence of preloads. Ignoring concrete confinement considerably underestimates the performance of CFDST columns where the steel tubes are preloaded at the construction stages.

References

- [1] Peng YY, Tan KF, Yao Y. Mechanical properties of duplex steel tube high-strength concrete short columns under axial compression. *J. Wuhan Univ. Techn.* 2011; 33 (2): 105-109 (In Chinese).
- [2] Xiong MX, Xiong DX, Liew JYR. Axial performance of short concrete filled steel tubes with high-and ultra-high-strength materials. *Eng. Struct.* 2017; 136: 494-510.
- [3] Ekmekyapar T, Al-Eliwi BJ. Concrete filled double circular steel tube (CFDCST) stub columns. *Eng. Struct.* 2017; 135: 68-80.
- [4] Chang X, Ru ZL, Zhou W, Zhang YB. Study on concrete-filled stainless steel-carbon steel tubular (CFSCST) stub columns under compression. *Thin-Walled Struct.* 2013; 63: 125-133.
- [5] Romero ML, Ibañez C, Espinós A, Portolés J, Hospitaler A. Influence of ultra-high strength concrete on circular concrete-filled dual steel columns. *Struct.* 2017; 9: 13-20.
- [6] Ibañez C, Romero ML, Espinós A, Portolés JM, Albero V. Ultra-high strength concrete on eccentrically loaded slender circular concrete-filled dual steel columns. *Struct.* 2017; 12: 64-74.
- [7] Xiong MX, Xiong DX, Liew JYR. Behaviour of steel tubular members infilled with ultra high strength concrete. *J. Constr. Steel Res.* 2017; 138: 168-183.
- [8] Ahmed M, Liang QQ, Patel VI, Hadi MNS. Behavior of eccentrically loaded double circular steel tubular short columns filled with concrete. *Eng. Struct.* 2019; 201:109790.
- [9] Romero ML, Espinós A, Portolés J, Hospitaler A, Ibañez C. Slender double-tube ultra-high strength concrete-filled tubular columns under ambient temperature and fire. *Eng. Struct.* 2015; 99: 536-545.

- [10] Tao Z, Han LH, Zhao XL. Behaviour of concrete-filled double skin (CHS inner and CHS outer) steel tubular stub columns and beam-columns. *J. Constr. Steel Res.* 2004; 60 (8): 1129-1158.
- [11] Zha XX. Investigation on the behavior of concrete filled steel tubular compression-bending-torsion members under the initial stress. China, Harbin University; 1996. PhD Thesis.
- [12] Zhang XQ, Zhong ST, Yan SZ, Lin Wei Cao HL. Experimental study about the effect of initial stress on bearing capacity of concrete-filled steel tubular members under eccentric compression. *J. Harbin Univ. Civil Eng. Arch.* 1997; 30 (1): 50-56 (in Chinese).
- [13] Han LH, Yao GH. Behaviour of concrete-filled hollow structural steel (HSS) columns with pre-load on the steel tubes. *J. Constr. Steel Res.* 2003; 59 (12): 1455-1475.
- [14] Liew JYR, Xiong DX. Effect of preload on the axial capacity of concrete-filled composite columns. *J. Constr. Steel Res.* 2009; 65 (3): 709-722.
- [15] Huang F, Yu X, Chen B, Li J. Study on preloading reduction of ultimate load of circular concrete-filled steel tubular columns. *Thin-Walled Struct.* 2016; 98: 454-464.
- [16] Li Y, Li G, Hou C, Zhang W-J. Long-term experimental behavior of concrete-encased CFST with preload on the inner CFST. *J. Constr. Steel Res.* 2019; 155: 355-369.
- [17] Xiong DX, Zha XX. A numerical investigation on the behaviour of concrete-filled steel tubular columns under initial stresses. *J. Constr. Steel Res.* 2007; 63 (5): 599-611.
- [18] Patel VI, Liang QQ, Hadi MNS. Numerical analysis of circular concrete-filled steel tubular slender beam-columns with preload effects. *Int. J. Struc. Stab. Dyn.* 2013; 13 (03): 1250065.
- [19] Patel VI, Liang QQ, Hadi MNS. Behavior of biaxially-loaded rectangular concrete-filled steel tubular slender beam-columns with preload effects. *Thin-Walled Struct.* 2014; 79: 166-177.

- [20] Li W, Han LH, Zhao XL. Axial strength of concrete-filled double skin steel tubular (CFDST) columns with preload on steel tubes. *Thin-Walled Struct.* 2012; 56: 9-20.
- [21] Hassanein MF, Kharoob OF, Liang QQ. Behaviour of circular concrete-filled lean duplex stainless steel-carbon steel tubular short columns. *Eng. Struct.* 2013; 56: 83-94.
- [22] Wan CY, Zha XX. Nonlinear analysis and design of concrete-filled dual steel tubular columns under axial loading. *Steel Compo. Struc.* 2016; 20 (3): 571-597.
- [23] Hassanein MF, Elchalakani M, Patel VI. Overall buckling behaviour of circular concrete-filled dual steel tubular columns with stainless steel external tubes. *Thin-Walled Struct.* 2017; 115: 336-348.
- [24] Pons D, Espinos A, Albero V, Romero ML. Numerical study on axially loaded ultra-high strength concrete-filled dual steel columns. *Steel Compo. Struc.* 2018; 26 (6): 705-717.
- [25] Zheng Y, Tao Z. Compressive strength and stiffness of concrete-filled double-tube columns. *Thin-Walled Struct.* 2019; 134: 174-188.
- [26] Ahmed M, Liang QQ, Patel VI, Hadi MNS. Numerical analysis of axially loaded circular high strength concrete-filled double steel tubular short columns. *Thin-Walled Struct.* 2019; 138: 105-116.
- [27] Ahmed M, Liang QQ, Patel VI, Hadi MNS. Nonlinear analysis of circular concrete-filled double steel tubular slender columns under eccentric-loading. *J. Constr. Steel Res.* 2019 (under review).
- [28] Liang QQ. Performance-based analysis of concrete-filled steel tubular beam-columns, Part I: Theory and algorithms. *J. Constr. Steel Res.* 2009; 65 (2): 363-372.
- [29] Mander JB. Seismic design of bridge piers. Christchurch, New Zealand, Department of Civil Engineering, University of Canterbury; 1983. PhD Thesis.
- [30] Mander JB, Priestley MJ, Park R. Theoretical stress-strain model for confined concrete. *J. Struc. Eng.* 1988; 114 (8): 1804-1826.

- [31] Lim JC, Ozbakkaloglu T. Stress–strain model for normal-and light-weight concretes under uniaxial and triaxial compression. *Const. Build. Mat.* 2014; 71: 492-509.
- [32] De Nicolo B, Pani L, Pozzo E. Strain of concrete at peak compressive stress for a wide range of compressive strengths. *Mat. Struc.* 1994; 27 (4): 206-210.
- [33] Hu HT, Huang CS, Wu MH, Wu YM. Nonlinear analysis of axially loaded concrete-filled tube columns with confinement effect. *J. Struc. Eng.* 2003; 129 (10): 1322-1329.
- [34] Liang QQ. High strength circular concrete-filled steel tubular slender beam–columns, Part I: Numerical analysis. *J. Constr. Steel Res.* 2011; 67 (2): 164-171.
- [35] Diniz SM, Frangopol DM. Strength and ductility simulation of high-strength concrete columns. *J. Struc. Eng.* 1997; 123 (10): 1365-1374.
- [36] Liang QQ. *Analysis and Design of Steel and Composite Structures*. CRC Press, Taylor and Francis Group, Boca Raton and London, 2014.

Figures and tables

Table 1 Comparisons of predicted and experimental ultimate axial loads of circular CFST slender columns with preload effects.

Column	Length L (mm)	$D \times t$ (mm)	f_{sy} (MPa)	f'_c (MPa)	e (mm)	β_a	$P_{u,exp}$ (kN)	$P_{u,num}$ (kN)	$\frac{P_{u,num}}{P_{u,exp}}$	Ref.
ZI1-1	1862	133×4.5	325	35.9	0	0	895	889	0.99	[11]
ZI1-2	1862	133×4.5	325	35.9	0	0	872	889	1.02	
ZI2	1862	133×4.5	325	35.9	0	0.305	882	882	1.00	
ZI3	1862	133×4.5	325	35.9	0	0.436	715	853	1.19	
ZL1-1	2793	133×4.5	325	35.9	0	0	743	729	0.98	
ZL1-2	2793	133×4.5	325	35.9	0	0	682	729	1.07	
ZL2	2793	133×4.5	325	35.9	0	0.311	748	706	0.94	
ZL3	2793	133×4.5	325	35.9	0	0.498	800	682.9	0.85	
A120	1670	133×4.3	325	35.9	50	0	438	407	0.93	[12]
A122	1670	133×4.3	325	35.9	50	0.22	430	398	0.92	
A124	1670	133×4.3	325	35.9	50	0.42	416	389	0.93	
A126	1670	133×4.3	325	35.9	50	0.58	412	370	0.90	
B122	1670	133×4.3	325	35.9	60	0.23	347	351	1.01	
B124	1670	133×4.3	325	35.9	50	0.42	335	344	1.03	
A200	2730	133×4.3	325	35.9	60	0	306	279	0.91	
A202	2730	133×4.3	325	35.9	60	0.22	293	267	0.95	
A204	2730	133×4.3	325	35.9	60	0.41	282	285	1.01	[14]
A206	2730	133×4.3	325	35.9	60	0.59	268	253	0.94	
CFT-S-40-30P	708	219×6.3	300	37	0	0.252	3677	3152	0.86	
CFT-S-100-0P	708	219×6.3	300	108	0	0	5410	4799	0.89	
CFT-S-100-30P	708	219×6.3	300	107	0	0.252	4667	4761	1.02	
CFT-I-40-30P	1728	219×6.3	405	44	0	0.299	3648	3230	0.89	
CFT-I-100-0P	1728	219×6.3	405	99	0	0	4977	4805	0.97	
CFT-I-100-30P	1728	219×6.3	405	113	0	0.305	5278	5108	0.97	
CFT-I-130-40P	1728	219×6.3	405	139	0	0.38	5437	5848	1.08	[15]
CFT-L-40-30P	3078	219×6.3	393	49	0	0.306	3610	2858	0.79	
CFT-L-100-0P	3078	219×6.3	393	100	0	0	4204	3680	0.88	
CFT-L-100-30P	3078	219×6.3	393	111	0	0.31	4580	3875	0.85	
CFT-L-130-40P	3078	219×6.3	393	125	0	0.399	4827	4303	0.89	
I-0	1296	108×4	336	46.7	0	0	792	786	0.99	
I-1	1296	108×4	336	46.7	0	0.25	804	774	0.96	
I-2	1296	108×4	336	46.7	0	0.50	729	761	1.04	
L-0	1944	108×4	336	46.7	0	0	734	659	0.90	
L-1	1944	108×4	336	46.7	0	0.24	731	642	0.88	
L-2	1944	108×4	336	46.7	0	0.48	702	631	0.90	
Mean									0.95	
Standard Deviation (SD)									0.08	
Coefficients of Variance (COV)									0.08	

Table 2 Comparisons of strength indices of circular slender DCFST columns with preload effects.

Column	$D_o \times t_o$ (mm)	$D_i \times t_i$ (mm)	L (mm)	β_a	$k_{p,FE}$	$k_{p,num}$	$\frac{k_{p,num}}{k_{p,FE}}$
C1	400×9.3	191×6	2190	0	1.000	1.000	1.000
C2	400×9.3	191×6	2190	0.2	0.982	0.986	1.004
C3	400×9.3	191×6	2190	0.4	0.974	0.961	0.987
C4	400×9.3	191×6	2190	0.6	0.966	0.950	0.983
C5	400×9.3	191×6	2190	0.8	0.963	0.941	0.977
C6	400×9.3	191×6	4380	0	1.000	1.000	1.000
C7	400×9.3	191×6	4380	0.2	0.964	0.975	1.011
C8	400×9.3	191×6	4380	0.4	0.935	0.949	1.015
C9	400×9.3	191×6	4380	0.6	0.904	0.929	1.028
C10	400×9.3	191×6	4380	0.8	0.873	0.901	1.032
C11	400×9.3	191×6	6570	0	1.000	1.000	1.000
C12	400×9.3	191×6	6570	0.2	0.970	0.968	0.998
C13	400×9.3	191×6	6570	0.4	0.915	0.938	1.025
C14	400×9.3	191×6	6570	0.6	0.868	0.904	1.041
C15	400×9.3	191×6	6570	0.8	0.814	0.860	1.057
C16	400×17.4	191×6	4380	0	1.000	1.000	1.000
C17	400×17.4	191×6	4380	0.2	0.978	0.978	1.000
C18	400×17.4	191×6	4380	0.4	0.965	0.952	0.987
C19	400×17.4	191×6	4380	0.6	0.932	0.927	0.995
C20	400×17.4	191×6	4380	0.8	0.911	0.914	1.003
C21	400×9.3	191×6	4380	0	1.000	1.000	1.000
C22	400×9.3	191×6	4380	0.2	0.972	0.974	1.002
C23	400×9.3	191×6	4380	0.4	0.946	0.948	1.002
C24	400×9.3	191×6	4380	0.6	0.921	0.924	1.003
C25	400×9.3	191×6	4380	0.8	0.896	0.912	1.018
C26	400×9.3	95.5×6	4380	0	1.000	1.000	1.000
C27	400×9.3	95.5×6	4380	0.2	0.965	0.985	1.021
C28	400×9.3	95.5×6	4380	0.4	0.947	0.964	1.018
C29	400×9.3	95.5×6	4380	0.6	0.931	0.949	1.019
C30	400×9.3	95.5×6	4380	0.8	0.919	0.937	1.020
C31	400×9.3	286×6	4380	0	1.000	1.000	1.000
C32	400×9.3	286×6	4380	0.2	0.983	0.988	1.005
C33	400×9.3	286×6	4380	0.4	0.963	0.966	1.003
C34	400×9.3	286×6	4380	0.6	0.941	0.946	1.005
C35	400×9.3	286×6	4380	0.8	0.922	0.937	1.016
Mean							1.008
Standard Deviation (SD)							0.016
Coefficients of Variance (COV)							0.016

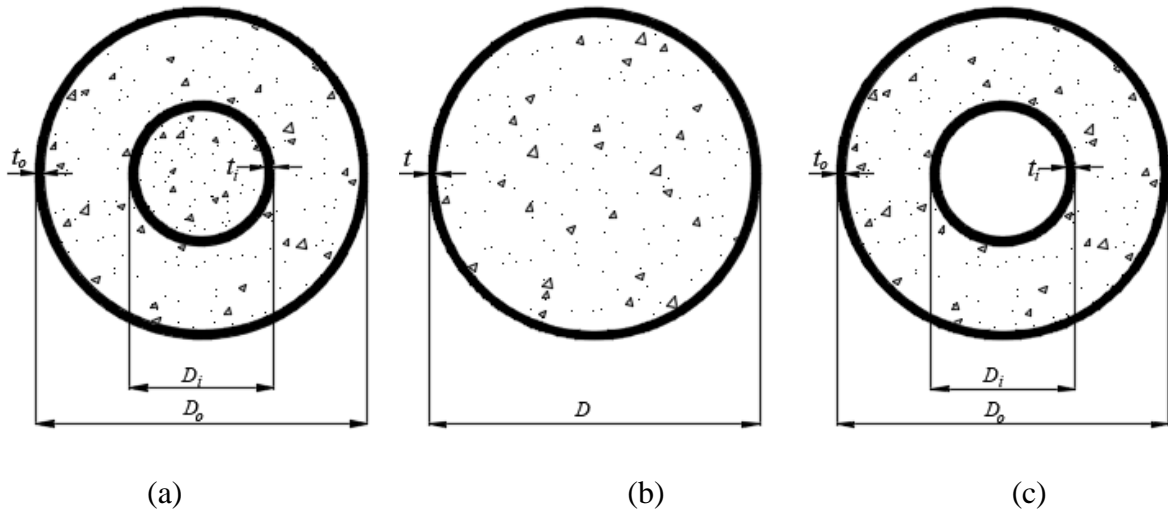


Fig. 1. Cross-section of circular concrete-filled steel tubular columns: (a) CFDST column, (b) CFST column and (c) DCFST column.

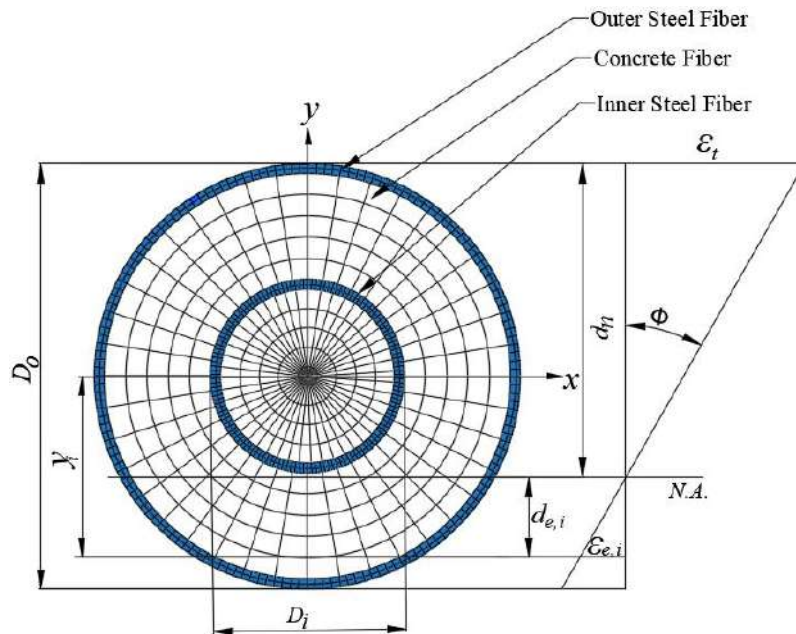


Fig. 2. Typical discretization and strain distribution of circular CFDST beam-column.

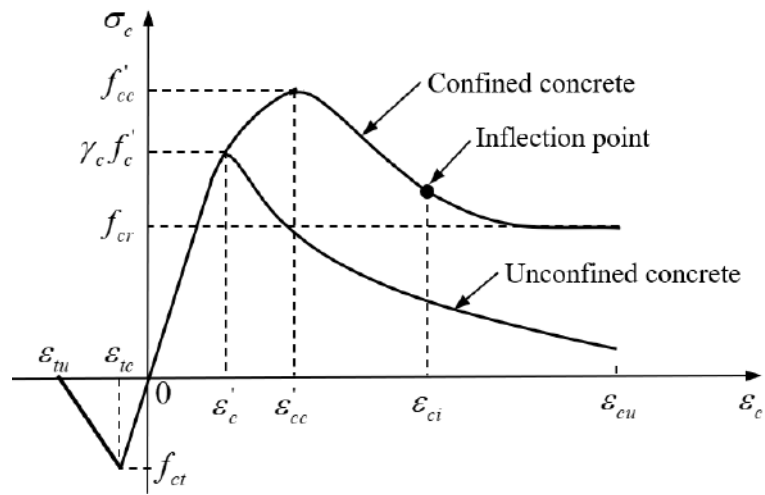
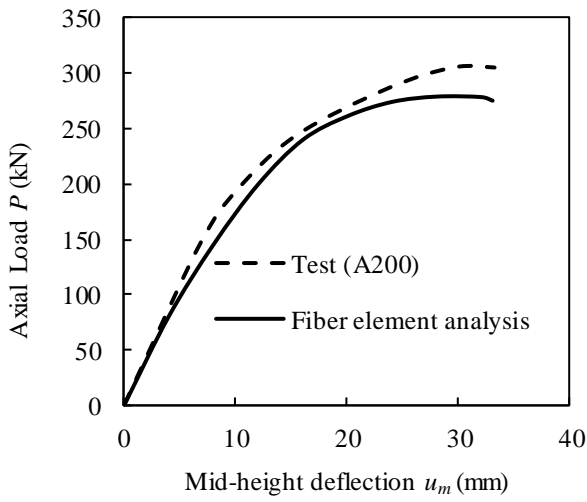
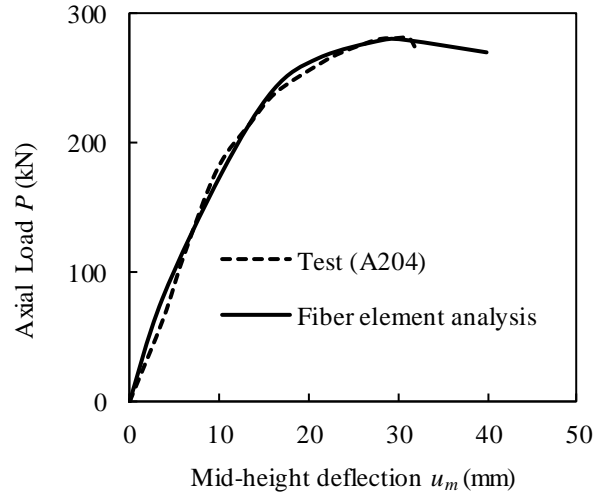


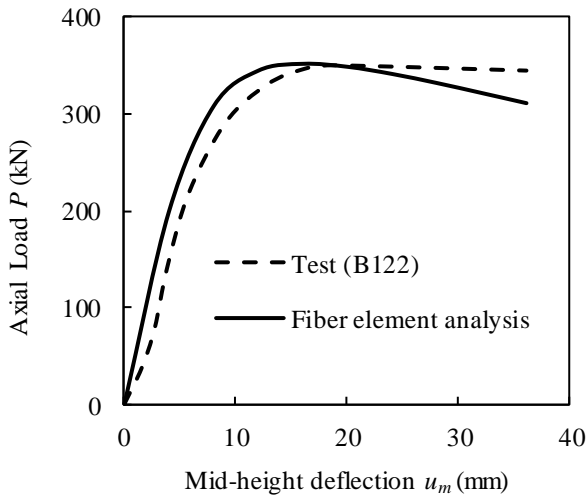
Fig. 3. Typical stress-strain curves for confined and unconfined concrete.



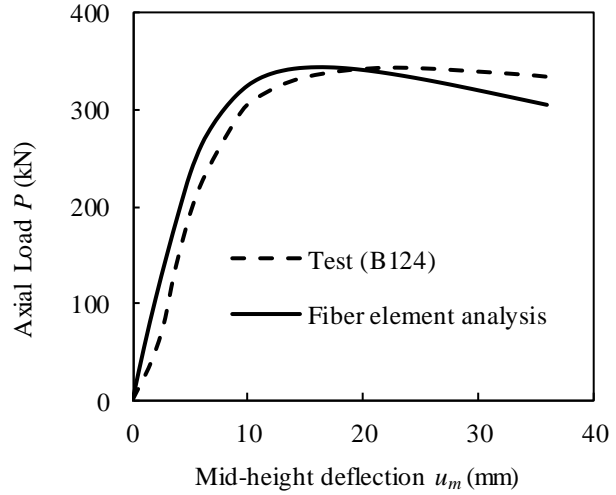
(a)



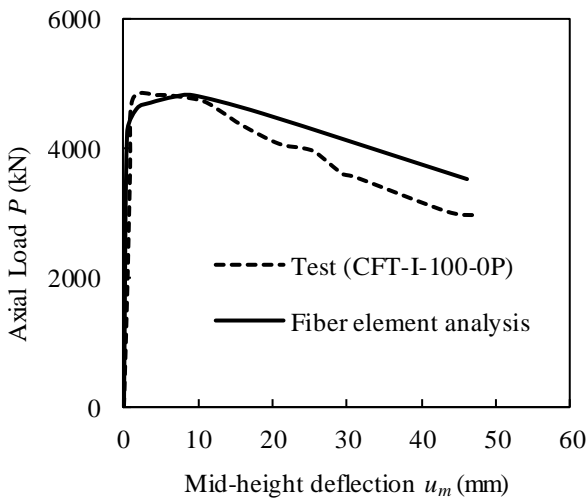
(b)



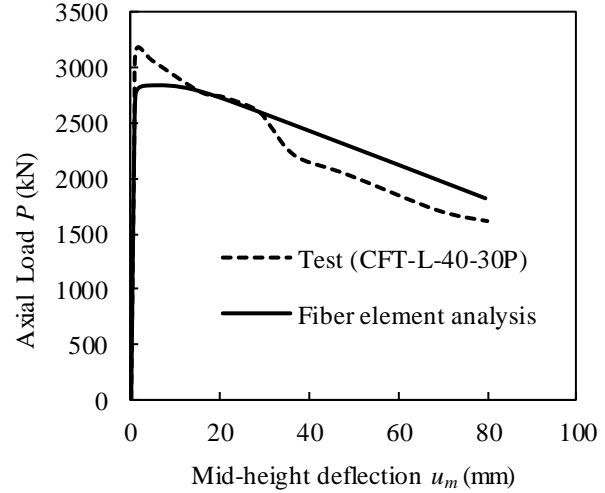
(c)



(d)



(e)



(f)

Fig. 4. Comparison of computational and experimental axial load-displacement curves for CFST slender beam-columns with preload effects.

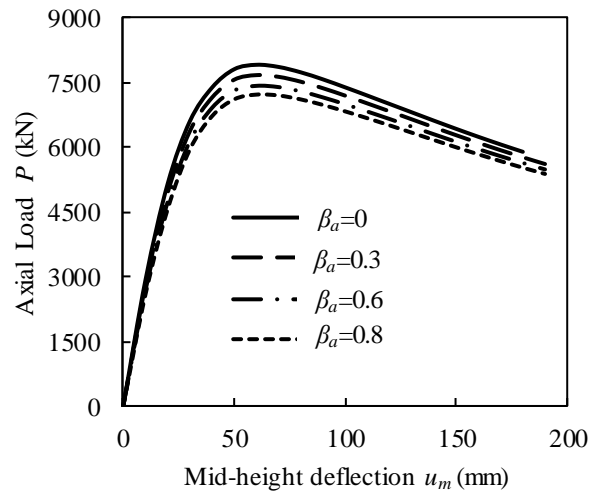


Fig. 5. Effects of preload ratio on the axial load-displacement curves of circular CFDST slender columns.

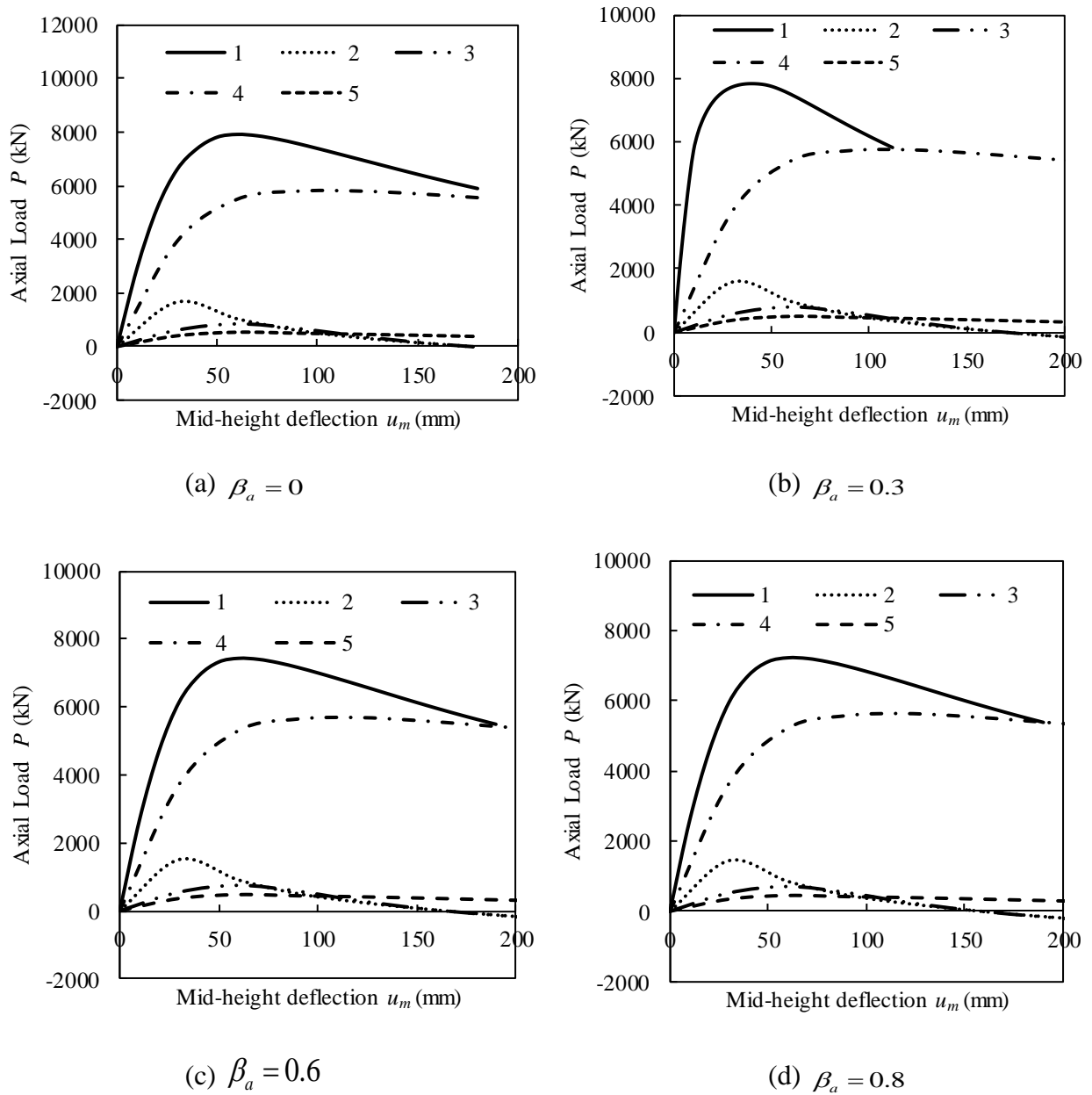


Fig. 6. Load-distributions in circular CFDST slender beam-columns with various preload ratios. (1- CFDST column, 2- Outer steel tube, 3- Inner steel tube, 4- Sandwiched concrete and 5- Core concrete)

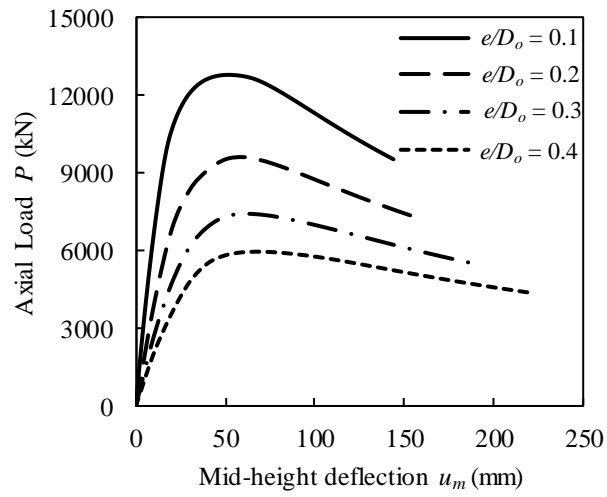


Fig. 7. Effects of e/D_o ratio on the load-deflection curves of circular CFDST slender columns with preloads on steel tubes.

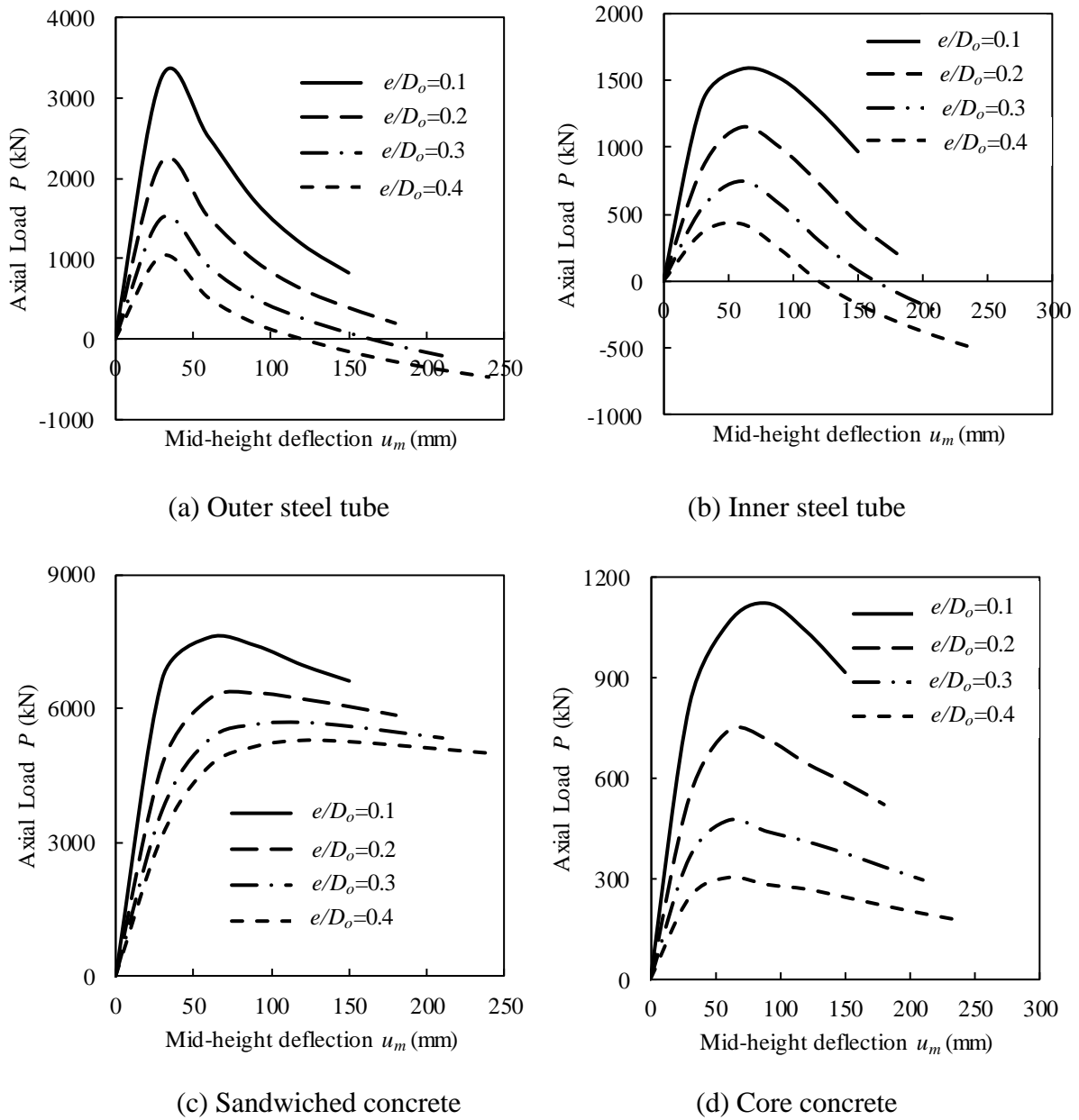


Fig. 8. Influences of e/D_o ratio on the load-deflection responses of components in circular CFDST slender beam-columns.

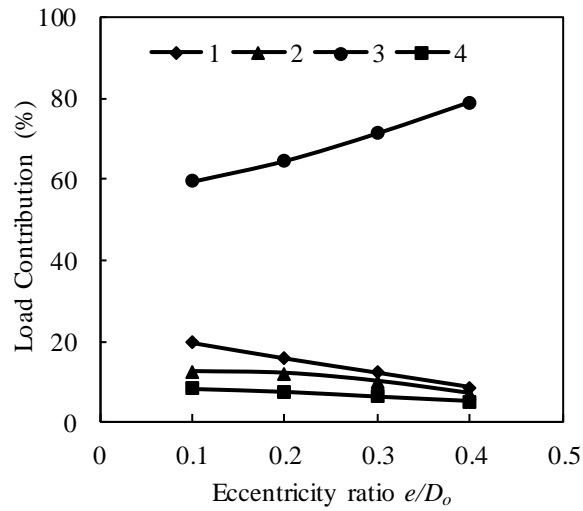


Fig. 9. Load contribution rate of the components in circular CFDST columns with various e/D_o ratios (1- Outer steel tube, 2- Inner steel tube, 3- Sandwiched concrete and 4- Core concrete).

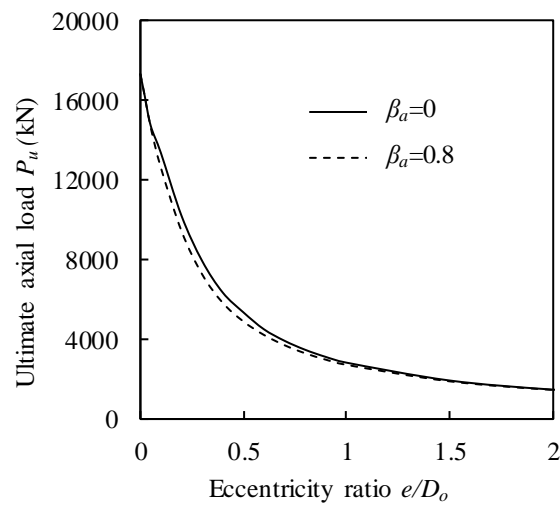


Fig. 10. Effects of e/D_o and preload ratios on the ultimate axial loads of circular CFDST slender columns.

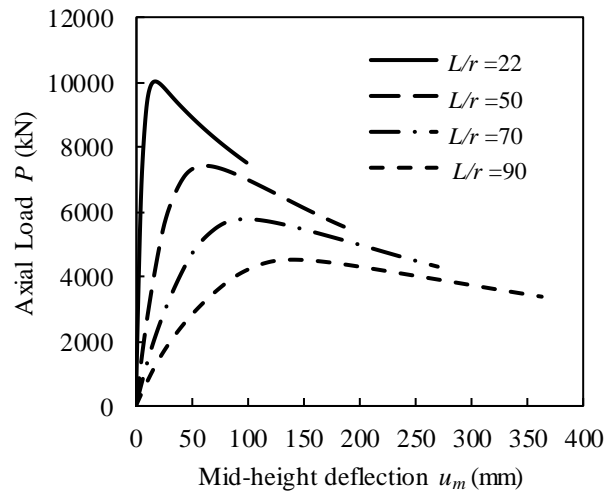
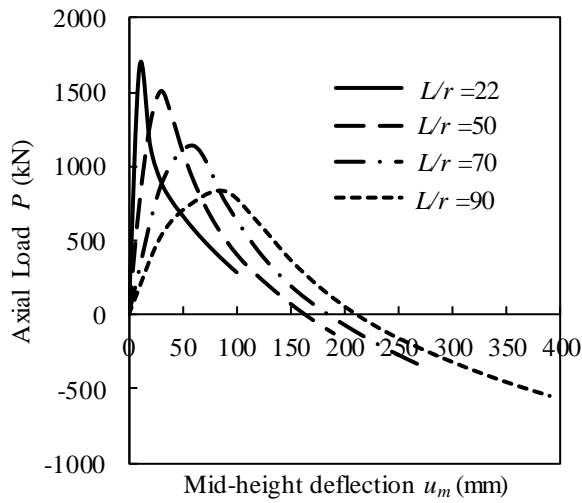
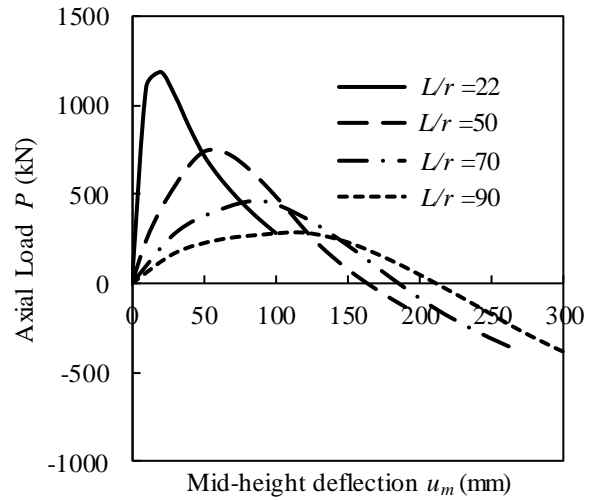


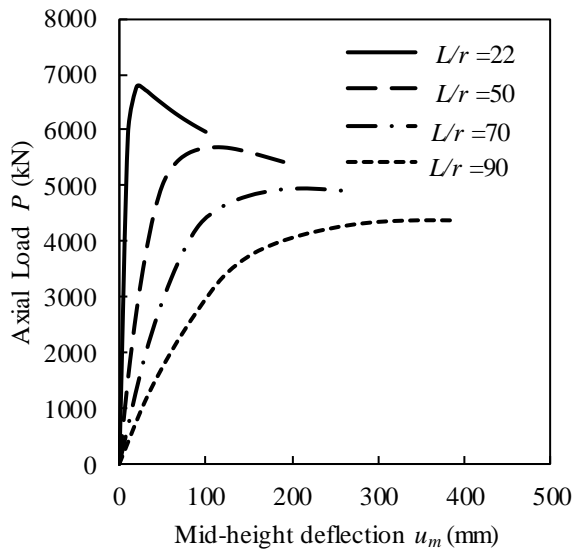
Fig. 11. Effects of L/r ratio on the load-deflection curves of circular CFDST slender columns with preloads on the steel tubes.



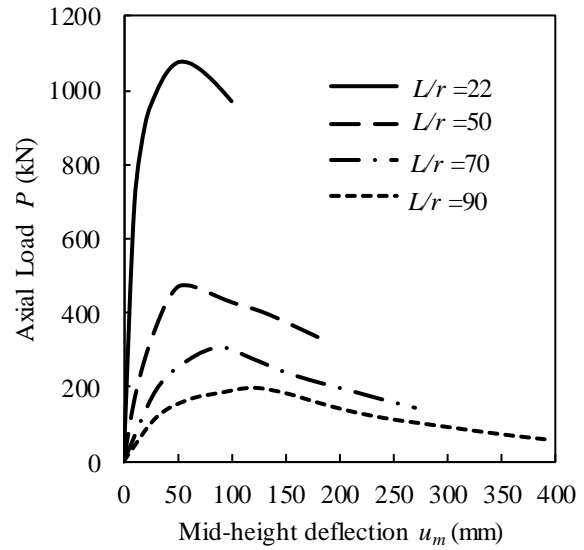
(a) Outer steel tube



(b) Inner steel tube



(c) Sandwiched concrete



(d) Core concrete

Fig. 12. Influences of L/r ratio on the load-deflection responses of components in circular CFDST slender beam-columns.

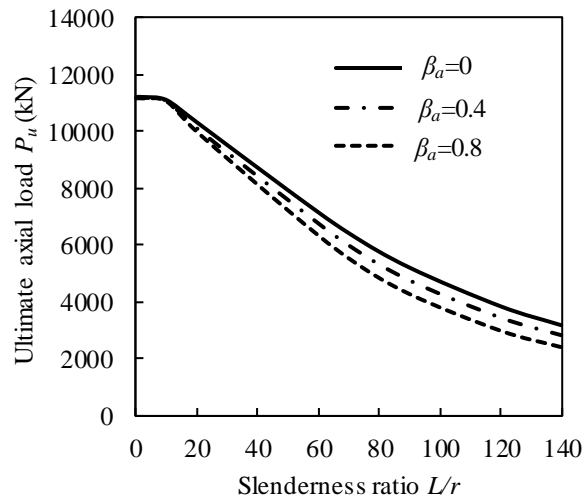


Fig. 13. Effects of L/r and preload ratios on the column strength curves of circular CFDST columns.

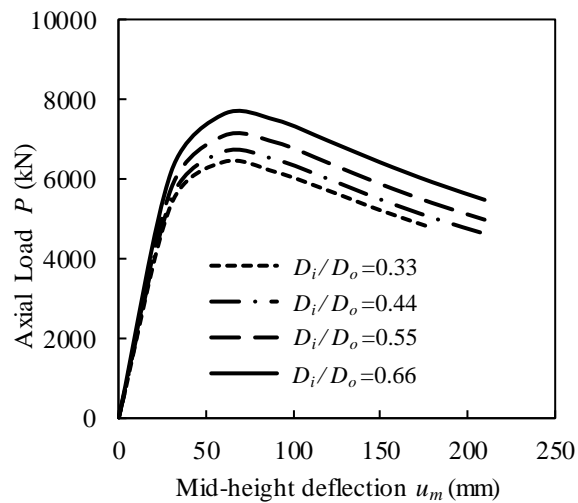


Fig. 14. Effects of D_i/D_o ratio on the load-deflection curves of circular CFDST slender columns with preloads on the steel tubes.

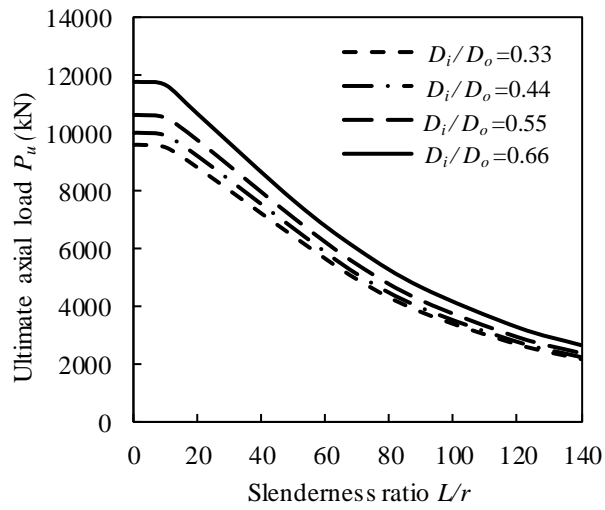


Fig. 15. Effects of D_i/D_o ratio on the strength curves of circular CFDST columns with preloads on the steel tubes.

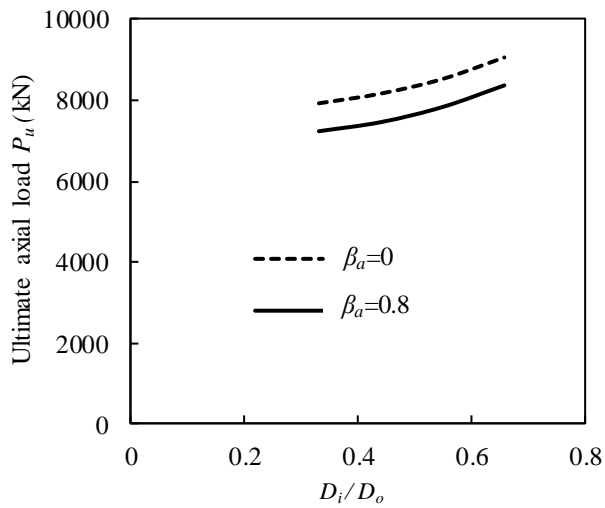


Fig. 16. Effects of D_i/D_o and preload ratios on the strength curves of circular CFDST slender columns.

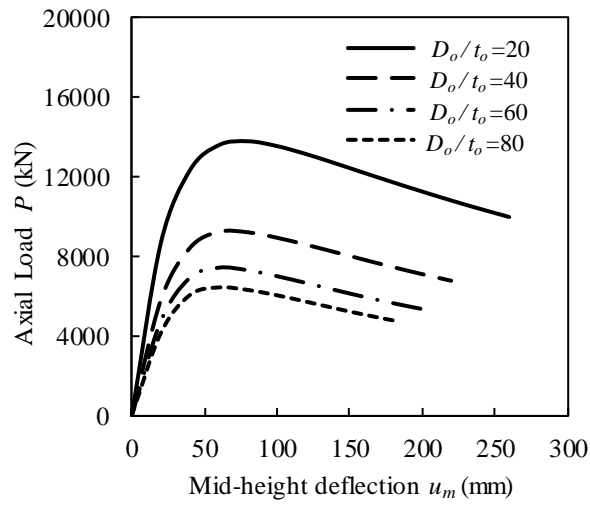


Fig. 17. Effects of D_o/t_o ratio on the load-deflection curves of circular CFDST slender columns with preloads on the steel tubes.

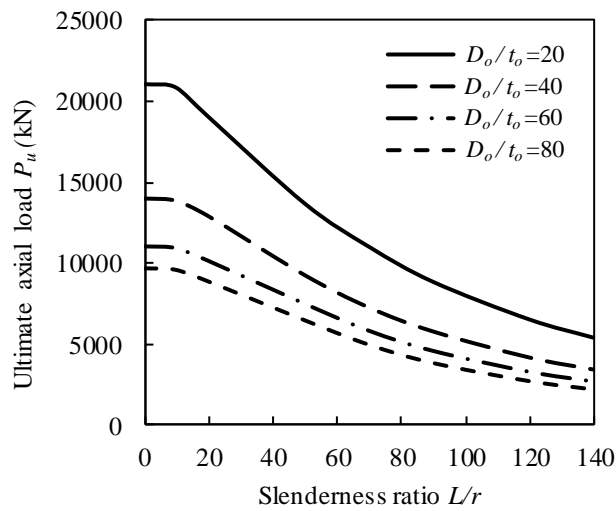


Fig. 18. Effects of D_o/t_o ratio the strength curves of circular CFDST columns with preloads on the steel tubes.

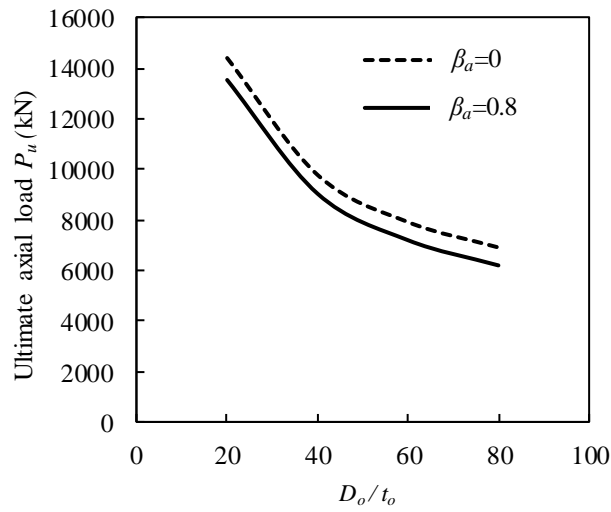


Fig. 19. Effects of D_o/t_o and preload ratios on the strengths of circular CFDST slender columns.

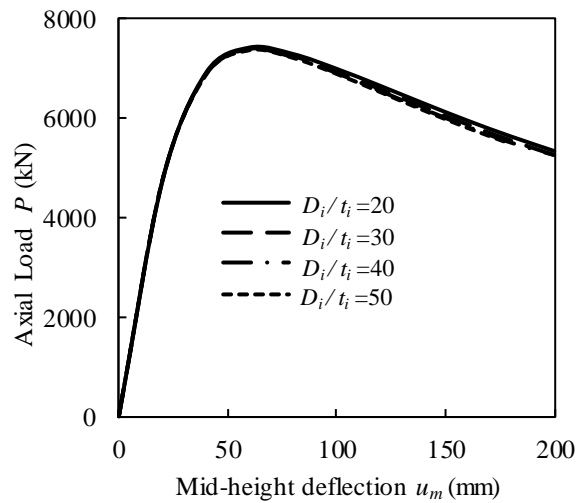


Fig. 20. Effects of D_i/t_i ratio on the load-deflection curves of circular CFDST slender columns with preloads on the steel tubes.

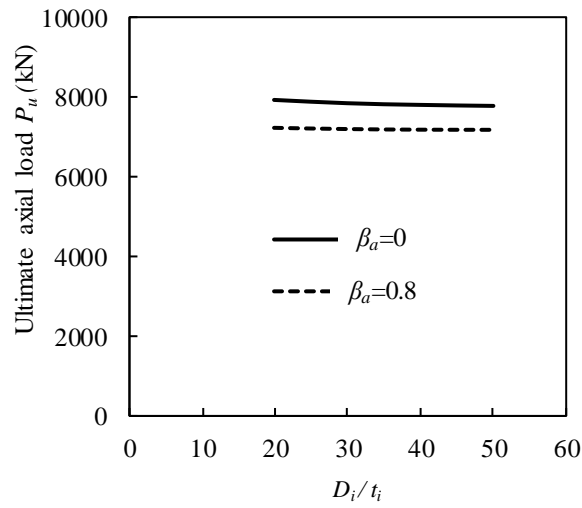


Fig. 21. Effects of D_i / t_i and preload ratios on the strengths of circular CFDST slender columns.

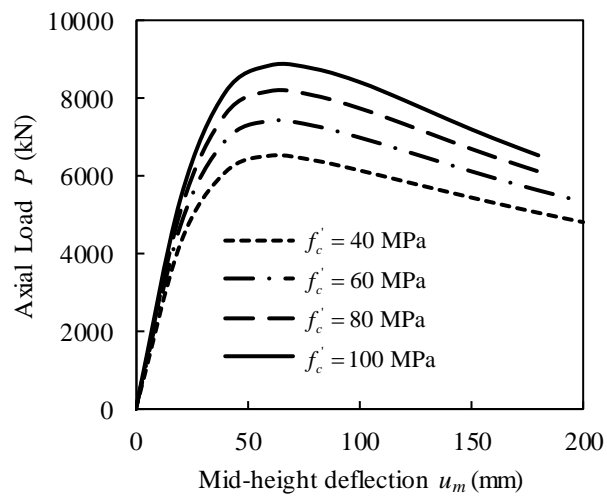


Fig. 22. Effects of concrete compressive strength on the load-deflection curves of circular CFDST slender columns with preloads on the steel tubes.

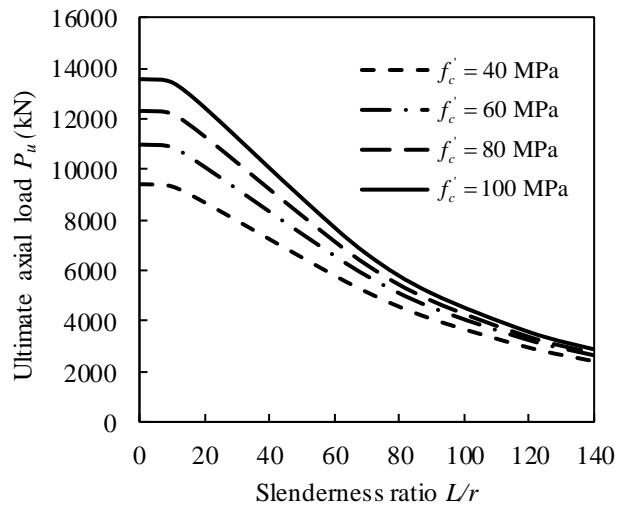


Fig. 23. Effects of concrete compressive strength on the strength curves of circular CFDST columns with preloads on the steel tubes.

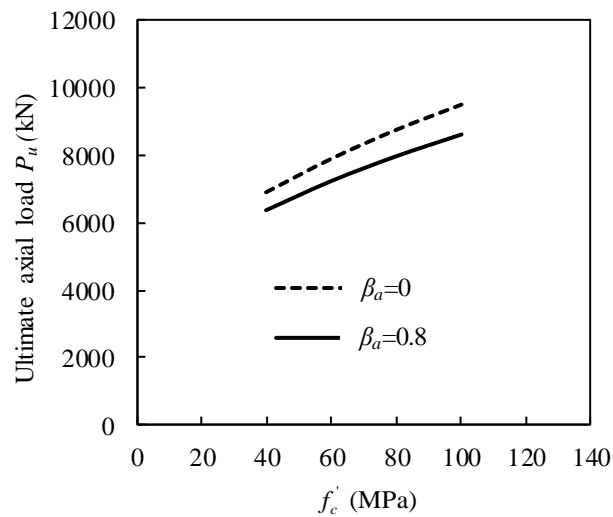


Fig. 24. Effects of concrete compressive strength and preloads on the strengths of circular CFDST slender columns.

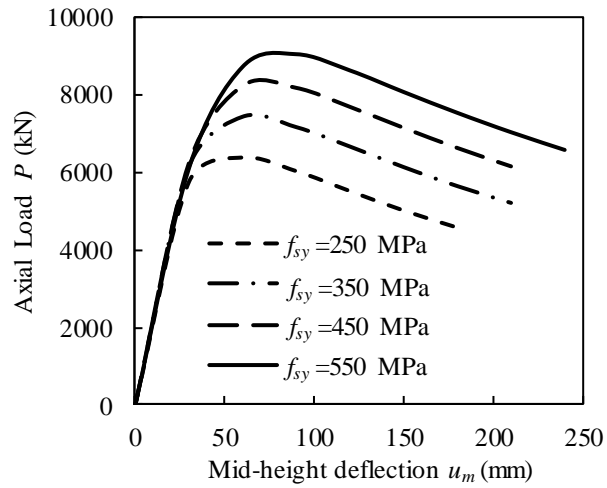


Fig. 25. Effects of steel yield strength on the load-deflection curves of circular CFDST slender columns with preloads on the steel tubes.

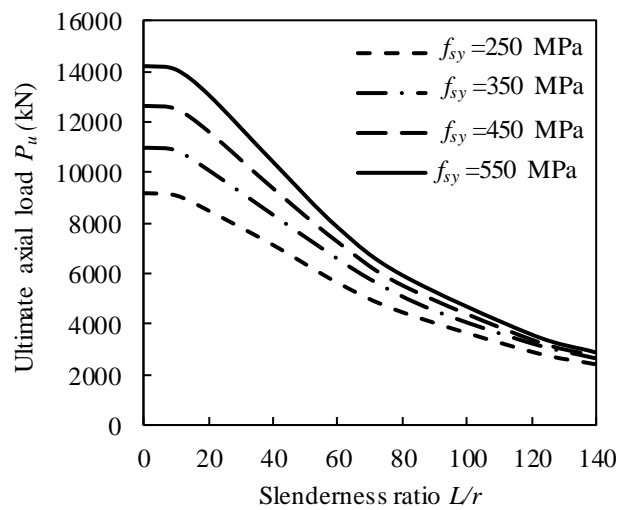


Fig. 26. Effects of steel yield strength on the strength curves of circular CFDST columns with preloads on the steel tubes.

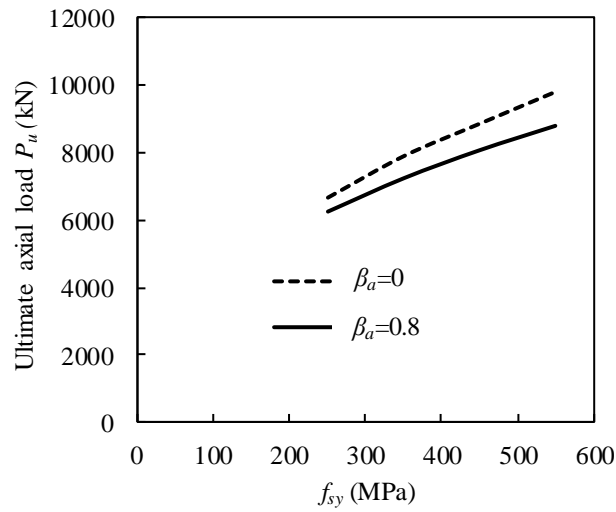


Fig. 27. Effects of steel yield strength and preloads on the strengths of circular CFDST slender columns.

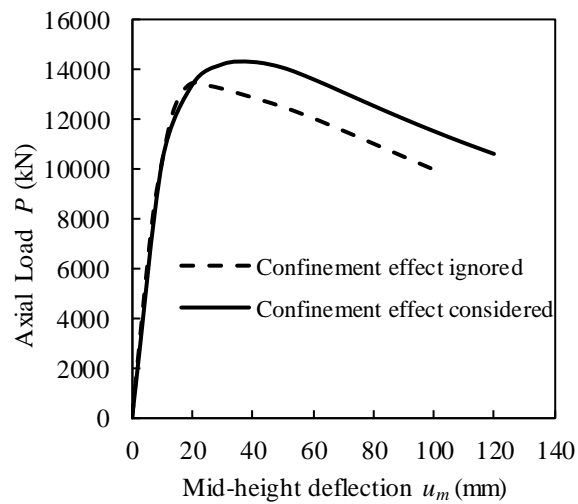


Fig. 28. Effects of concrete confinement on the load-deflection curves of circular CFDST slender column with preloads on the steel tubes.

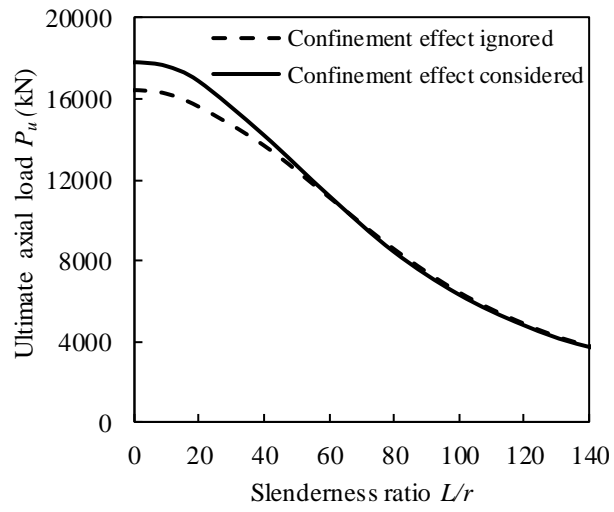


Fig. 29. Effects of concrete confinement on the strength curves of circular CFDST columns with preloads on the steel tubes.

7.2 CONCLUDING REMARKS

This chapter has described the computer modeling, performance and structural design of slender square and circular CFST columns composed of an internal circular steel tube where the steel tubes are preloaded before concrete filling. The mathematical models have considered the interaction of local and global buckling in square CFDST columns, deformation induced by the preload, concrete confinement by the circular steel tube, geometric imperfections, and material nonlinearities. The computer modeling techniques developed have been demonstrated to accurately capture the experimentally measured load-deflection responses, and to efficiently generate the column strength curves and load distributions in concrete and steel components of slender CFDST columns having preloads. Computational results obtained from the parametric studies have indicated that significant preloads may remarkably reduce the performance of slender CFDST columns and must be accounted for in the nonlinear modeling and design of such composite columns. Design equations proposed have shown to yield good strength estimations of concentrically loaded CFDST slender columns subjected to preloads on the steel tubes.

Chapter 8

CONCLUSIONS

8.1 SUMMARY

This thesis has presented experimental and numerical investigations on the behavior of rectangular and circular CFDST columns composed of either a rectangular inner steel tube or a circular inner steel tube. Experimental programs on axially and eccentrically loaded CFDST short columns have been conducted to investigate the influences of the application of loading (axial or eccentric), cross-sections, geometric properties and loading eccentricity on the failure patterns, ultimate strengths, strain distributions and axial and lateral responses of CFDST columns. Computational models underlying the theory of fiber elements have been developed for the response analysis of CFDST short and slender columns under various loading conditions, incorporating the effects of concrete confinement, local buckling of the rectangular outer tube, second-order, geometric and material nonlinearities and preloads on the steel tubes. Based on the existing test results, new lateral pressure models and strength degradation parameters for the confined concrete have been derived and incorporated in the computational models. New efficient computational algorithms underlying the inverse quadratic method have also been developed to solve the dynamic nonlinear equilibrium functions of short and slender CFDST columns loaded eccentrically. The computational modeling methods have

been validated against the test data. The verified mathematical models have been utilized to investigate the responses of short and slender CFDST columns. Design models have been proposed for determining the ultimate strengths of CFDST short and slender columns under various loading conditions.

8.2 ACHIEVEMENTS

This research project has made significant contributions to the field of CFDST columns. The significant research achievements of this research work are summarized as follows:

1. The presented experimental results on circular, square and rectangular CFDST short columns under concentric and eccentric loading provide useful insights into the understanding of the structural behavior of such columns. The test data obtained can be used by other researchers to validate their numerical models of CFDST columns.
2. Proposed new confinement models and strength degradation factors for core concrete in circular CFDST columns as well as for core concrete in square CFDST columns with an inner circular tube. The confinement models proposed yield more accurate results than existing models which were modified from those proposed for conventional CFST columns.
3. Developed fiber-based numerical models for circular, square and rectangular CFDST short columns under concentric and eccentric loading. The numerical models developed incorporate the local buckling of the outer steel tube, concrete confinement, and material nonlinearities. The fiber models developed are accurate and cost-effective design tools for design engineers.

4. Developed computational models for circular and square CFDST slender beam-columns under axial load and bending considering the influences of confinement, the interaction of local-global buckling and second-order. Efficient solution algorithms were developed to solve nonlinear equilibrium functions. The accuracy of the computational models was validated against the independent test results.
5. Developed mathematical models for eccentrically loaded square and circular CFDST slender columns incorporating preload effects, the local buckling of the outer steel tube and confinement provided by the steel tube.
6. Proposed a set of design models for the design of CFDST short and slender columns. The design models for conventional CFST short columns originally proposed by Liang and Fragomeni (2009) were modified for the design of CFDST columns composed of circular and square cross-sections whereas design equations given by Eurocode 4 (2004) were modified to propose the design models for CFDST slender columns under axial loading. These design models can be used by practicing design engineers in the design of CFDST columns.

8.3 FURTHER RESEARCH

This thesis focuses on experimental and numerical studies on the fundamental behavior of CFDST short and slender columns under various loads, including axial compression, eccentric loading and preloads. However, further tests are still required to fully understand their behavior and numerical models should be developed for CFDST

columns under other loading conditions. The following research studies on CFDST columns are recommended:

1. Tests on eccentrically loaded slender circular and rectangular CFDST columns are very limited. Therefore, further tests on slender CFDST columns that are loaded eccentrically should be carried out to investigate their behavior.
2. Tests on slender CFDST columns having preloads are absent in the literature. Hence, the experimental program should be carried out to examine the structural performance of eccentrically loaded CFDST slender columns with preload effects.
3. Tests on CFDST short and slender columns under dynamic loading (e.g. cyclic, impact loading) have not been performed. However, CFDST columns may be subjected to cyclic loading in the seismic active regions or subjected to impact loading caused by the vehicle collision or terrorist attacks or by the flying debris from the nearby explosions. Therefore, influences of dynamic loadings on the responses of such columns should be experimentally investigated.
4. Fiber-based numerical models for eccentrically loaded CFDST slender columns under cyclic or impact loading have not been developed. Therefore, further research should be conducted to extend the developed numerical models to CFDST columns under cyclic and impact loading considering the influences of concrete confinement, geometric imperfection, and local buckling.
5. The numerical models developed in this research project are only applicable to CFDST columns made of carbon steel. The behavior of stainless-steel is different from that of carbon steel owing to the distinguished strain-hardening

characteristics of stainless steel. Therefore, further research should be performed on CFDST columns made of stainless steel.

6. The CFDST columns used in high-rise composite buildings are likely exposed to fire. Therefore, further experimental and numerical studies on CFDST columns at elevated temperatures should be conducted.

REFERENCES

Abdella, K., Tahannon, R. A., Mehri, A. I. and Alshaikh, F. A. (2011). "Inversion of three-stage stress–strain relation for stainless steel in tension and compression."

Journal of Constructional Steel Research, **67**(5), 826-832.

ACI 318-02. (2002). *Building Code Requirements for Structural Concrete and Commentary*. Detroit, MI, USA: American Concrete Institute.

ACI 318-05. (2005). *Building Code Requirements for Structural Concrete and Commentary*. Detroit, MI, USA: American Concrete Institute.

AISC 360-05. (2005). *Specification for Structural Steel Buildings*. Chicago, IL, USA: American Institution of Steel Construction.

AISC 360-16. (2016). *Specification for Structural Steel Buildings*. Chicago, IL, USA: American Institution of Steel Construction.

AS 3600. (1994). *Australian Standard for Concrete Structures*. Sydney, New South Wales, Australia: Standards Australia..

AS 3600. (2009). *Australian Standard for Concrete Structures*. Sydney, New South Wales, Australia: Standards Australia.

AS/NZS 2327:2017. (2017). *Australian/New Zealand Standard for Composite Structures- Composite Steel-Concrete Construction in Buildings*. Sydney, New South Wales, Australia: Standards Australia and Standards New Zealand.

Azhari, M. and Bradford, M. A. (1991). "Buckling modes using a complex finite strip method." School of Civil Engineering, University of New South Wales, Sydney, Australia, Research Report No. R291.

Bedair, O. (2009). "Analytical effective width equations for limit state design of thin plates under non-homogeneous in-plane loading." *Archive of Applied Mechanics*, **79**(12), 1173-1189.

Bedair, O. (2010). "Stability analysis of plates with partial restraints using unconstrained optimization techniques." *International Journal of Structural Stability and Dynamics*, **10**(03), 571-587.

Bradford, M. A. (1985a). "Local and post-local buckling of fabricated box members." *Civil Engineering Transactions*, Institution of Engineers Australia, **27** (4): 391-6.

Bradford, M. A. (1985b). "Distortional buckling of monosymmetric I-beams." *Journal of Constructional Steel Research*, **5**(2), 123-136.

Bradford, M. A. and Cuk, P. E. (1988). "Elastic buckling of tapered monosymmetric I-beams." *Journal of Structural Engineering, ASCE*, **114**(5), 977-996.

- Bradford, M. A. and Hancock, G. J. (1984). "Elastic interaction of local and lateral buckling in beams." *Thin-Walled Structures*, **2**(1), 1-25.
- Bradford, M. A. and Wong, T. (1991). "Local buckling of composite box girders under negative bending". School of Civil Engineering, University of New South Wales, Sydney, Australia, Research Report No. R292.
- Bridge, R. Q. (1976). Concrete filled steel tubular columns. School of Civil Engineering, The University of Sydney, Sydney, Australia. Research Report No. R283.
- Bridge, R. Q. and O'Shea, M. D. (1998). "Behaviour of thin-walled steel box sections with or without internal restraint." *Journal of Constructional Steel Research*, **47**(1), 73-91.
- Bryan, G. H. (1890). "On the stability of a plane plate under thrusts in its own plane, with applications to the buckling of the sides of a ship." *Proceedings of the London Mathematical Society*, **1**(1), 54-67.
- BS 5400 (1979). *British Standard for Steel, Concrete and Composite Bridges: Part: 5 Code of Practice For Design of Composite Bridges*. London, United Kingdom, British Standards Institution.
- Bulson, P. S. (1969). *The Stability of Flat Plates*. Netherland, Elsevier.

- Chang, X., Ru, Z. L., Zhou, W. and Zhang, Y. B. (2013). "Study on concrete-filled stainless steel–carbon steel tubular (CFSCST) stub columns under compression." *Thin-Walled Structures*, **63**, 125-133.
- Chilver, A. (1953). "A generalised approach to the local instability of certain thin-walled struts." *The Aeronautical Quarterly*, **4**(3), 245-260.
- Couto, C., Real, P. V., Lopes, N. and Zhao, B. (2014). "Effective width method to account for the local buckling of steel thin plates at elevated temperatures." *Thin-Walled Structures*, **84**, 134-149.
- DBJ/T 13-51. (2010). *Technical Specification for Concrete-filled Steel Tubular Structures*. Fuzhou, China, The Department of Housing and Urban–Rural Development of Fujian Province (in Chinese).
- Ekmekyapar, T. and Al-Eliwi, B. J. (2017). "Concrete filled double circular steel tube (CFDCST) stub columns." *Engineering Structures*, **135**, 68-80.
- Elchalakani, M., Zhao, X.-L. and Grzebieta, R. (2002). "Tests on concrete filled double-skin (CHS outer and SHS inner) composite short columns under axial compression." *Thin-Walled Structures*, **40**(5), 415-441.

Ellobody, E., Young, B. and Lam, D. (2006). "Behaviour of normal and high strength concrete-filled compact steel tube circular stub columns." *Journal of Constructional Steel Research*, **62**(7), 706-715.

Eurocode 4 (1994). *Design of Composite Steel and Concrete Structures, Part 1.1 General Rules and Rules for Buildings*. European Committee for Standardization, CEN, London, UK.

Eurocode 4 (2004). *Design of Composite Steel and Concrete Structures, Part 1.1 General Rules and Rules for Buildings*. European Committee for Standardization, CEN, Brussels, Belgium.

Fujimoto, T., Mukai, A., Nishiyama, I. and Sakino, K. (2004). "Behavior of eccentrically loaded concrete-filled steel tubular columns." *Journal of Structural Engineering, ASCE*, **130**(2), 203-212.

Furlong, R. W. (1967). "Strength of steel-encased concrete beam columns." *Journal of the Structural Division, ASCE*, **93**(5), 113-124.

Gerard, G. and Becker, H. (1957). *Handbook of Structural Stability: Failure of Plates and Composite Elements*, National Advisory Committee for Aeronautics.

Giakoumelis, G. and Lam, D. (2004). "Axial capacity of circular concrete-filled tube columns." *Journal of Constructional Steel Research*, **60**(7), 1049-1068.

- Han, L. H. (2002). "Tests on stub columns of concrete-filled RHS sections." *Journal of Constructional Steel Research*, **58**(3), 353-372.
- Han, L. H. (2007). *Concrete Filled Steel Tube Structures-Theory and Application*. Beijing, China, Science Press.
- Han, L.-H. and Huo, J.-S. (2003). "Concrete-filled hollow structural steel columns after exposure to ISO-834 fire standard." *Journal of Structural Engineering, ASCE*, **129**(1), 68-78.
- Han, L.-H., Lam, D. and Nethercot, D. A. (2018). *Design Guide for Concrete-filled Double Skin Steel Tubular Structures*. London, UK, CRC Press, Taylor and Francis Group.
- Han, L. H., Ren, Q. X. and Li, W. (2011). "Tests on stub stainless steel–concrete–carbon steel double-skin tubular (DST) columns." *Journal of Constructional Steel Research*, **67**(3), 437-452.
- Han, L.-H. and Yao, G.-H. (2003). "Behaviour of concrete-filled hollow structural steel (HSS) columns with pre-load on the steel tubes." *Journal of Constructional Steel Research*, **59**(12), 1455-1475.

- Han, L.-H., Zhao, X.-L. and Tao, Z. (2001). "Tests and mechanics model for concrete-filled SHS stub columns, columns and beam-columns." *Steel and Composite Structures*, **1**(1), 51-74.
- Hassanein, M., Elchalakani, M., Karrech, A., Patel, V. and Yang, B. (2018). "Behaviour of concrete-filled double-skin short columns under compression through finite element modelling: Shs outer and shs inner tubes." *Structures*, **14**, 358-375.
- Hassanein, M. F. and Kharoob, O. F. (2014). "Compressive strength of circular concrete-filled double skin tubular short columns." *Thin-Walled Structures*, **77**, 165-173.
- Hassanein, M. F., Kharoob, O. F. and Gardner, L. (2015). "Behaviour and design of square concrete-filled double skin tubular columns with inner circular tubes." *Engineering Structures*, **100**, 410-424.
- Hassanein, M. F., Kharoob, O. F. and Liang, Q. Q. (2013a). "Behaviour of circular concrete-filled lean duplex stainless steel–carbon steel tubular short columns." *Engineering Structures*, **56**, 83-94.
- Hassanein, M. F., Kharoob, O. F. and Liang, Q. Q. (2013b). "Circular concrete-filled double skin tubular short columns with external stainless steel tubes under axial compression." *Thin-Walled Structures*, **73**, 252-263.

- Heidarpour, A. and Bradford, M. A. (2007). "Local buckling and slenderness limits for flange outstands at elevated temperatures." *Journal of Constructional Steel Research*, **63**(5), 591-598.
- Heidarpour, A. and Bradford, M. A. (2008). "Local buckling and slenderness limits for steel webs under combined bending, compression and shear at elevated temperatures." *Thin-Walled Structures*, **46**(2), 128-146.
- Hu, H.-T., Huang, C.-S., Wu, M.-H. and Wu, Y.-M. (2003). "Nonlinear analysis of axially loaded concrete-filled tube columns with confinement effect." *Journal of Structural Engineering, ASCE*, **129**(10), 1322-1329.
- Hu, H.-T. and Su, F.-C. (2011). "Nonlinear analysis of short concrete-filled double skin tube columns subjected to axial compressive forces." *Marine Structures*, **24**(4), 319-337.
- Huang, H., Han, L. H., Tao, Z. and Zhao, X. L. (2010). "Analytical behaviour of concrete-filled double skin steel tubular (CFDST) stub columns." *Journal of Constructional Steel Research*, **66**(4), 542-555.
- Huang, Z., Li, D., Uy, B., Thai, H.-T. and Hou, C. (2019). "Local and post-local buckling of fabricated high-strength steel and composite columns." *Journal of Constructional Steel Research*, **154**, 235-249.

- Huang, F., Yu, X., Chen, B. and Li, J. (2016). "Study on preloading reduction of ultimate load of circular concrete-filled steel tubular columns." *Thin-Walled Structures*, **98**, 454-464.
- Kapur, K. K. and Hartz, B. J. (1966). "Stability of plates using the finite element method." *Journal of the Engineering Mechanics Division*, **92**(2), 177-196.
- Katwal, U., Tao, Z., Hassan Md, K. and Wang, W.-D. (2017). "Simplified Numerical Modeling of Axially Loaded Circular Concrete-Filled Steel Stub Columns." *Journal of Structural Engineering, ASCE*, **143**(12), 04017169.
- KBCS (2009). *Korean Building Code- Structure*. Seoul, Korea: Architectural Institute of Korea.
- Kloppel, V. and Goder, W. (1957). "An investigation of the load carrying capacity of concrete-filled steel tubes and development of design formula." *Der Stahlbau*, **26**(2), 44-50.
- Knobloch, M. and Fontana, M. (2006). "Strain-based approach to local buckling of steel sections subjected to fire." *Journal of Constructional Steel Research*, **62**(1-2), 44-67.
- Knowles, R. B. and Park, R. (1969). "Strength of concrete filled steel columns." *Journal of the Structural Division, ASCE*, **95**(12), 2565-2587.

- Knowles, R. B. and Park, R. (1970). "Axial load design for concrete filled steel tubes." *Journal of the Structural Division, ASCE*, **96**(10), 2125-2153.
- Lee, S.-H., Uy, B., Kim, S.-H., Choi, Y.-H. and Choi, S.-M. (2011). "Behavior of high-strength circular concrete-filled steel tubular (CFST) column under eccentric loading." *Journal of Constructional Steel Research*, **67**(1), 1-13.
- Li, W., Han, L. H. and Chan, T. M. (2014). "Tensile behaviour of concrete-filled double-skin steel tubular members." *Journal of Constructional Steel Research*, **99**, 35-46.
- Li, W., Han, L.-H. and Zhao, X.-L. (2012). "Axial strength of concrete-filled double skin steel tubular (CFDST) columns with preload on steel tubes." *Thin-Walled Structures*, **56**, 9-20.
- Li, Y., Li, G., Hou, C. and Zhang, W.-J. (2019). "Long-term experimental behavior of concrete-encased CFST with preload on the inner CFST." *Journal of Constructional Steel Research*, **155**, 355-369.
- Liang, Q. Q. (2009a). "Performance-based analysis of concrete-filled steel tubular beam-columns, Part I: Theory and algorithms." *Journal of Constructional Steel Research*, **65**(2), 363-372.

- Liang, Q. Q. (2009b). "Performance-based analysis of concrete-filled steel tubular beam–columns, Part II: Verification and applications." *Journal of Constructional Steel Research*, **65**(2), 351-362.
- Liang, Q. Q. (2011a). "High strength circular concrete-filled steel tubular slender beam–columns, Part I: Numerical analysis." *Journal of Constructional Steel Research*, **67**(2), 164-171.
- Liang, Q. Q. (2011b). "High strength circular concrete-filled steel tubular slender beam–columns, Part II: Fundamental behavior." *Journal of Constructional Steel Research*, **67**(2), 172-180.
- Liang, Q. Q. (2014). *Analysis and Design of Steel and Composite Structures*. Boca Raton FL, USA and London, UK, CRC Press, Taylor and Francis Group.
- Liang, Q. Q. (2017). "Nonlinear analysis of circular double-skin concrete-filled steel tubular columns under axial compression." *Engineering Structures*, **131**, 639-650.
- Liang, Q. Q. (2018). "Numerical simulation of high strength circular double-skin concrete-filled steel tubular slender columns." *Engineering Structures*, **168**, 205-217.

- Liang, Q. Q. and Fragomeni, S. (2009). "Nonlinear analysis of circular concrete-filled steel tubular short columns under axial loading." *Journal of Constructional Steel Research*, **65**(12), 2186-2196.
- Liang, Q. Q. and Fragomeni, S. (2010). "Nonlinear analysis of circular concrete-filled steel tubular short columns under eccentric loading." *Journal of Constructional Steel Research*, **66**(2), 159-169.
- Liang, Q. Q., Patel, V. I. and Hadi, M. N. S. (2012). "Biaxially loaded high-strength concrete-filled steel tubular slender beam-columns, Part I: Multiscale simulation." *Journal of Constructional Steel Research*, **75**, 64-71.
- Liang, Q. Q. and Uy, B. (1998). "Parametric study on the structural behaviour of steel plates in concrete-filled fabricated thin-walled box columns." *Advances in Structural Engineering*, **2**(1), 57-71.
- Liang, Q. Q. and Uy, B. (2000). "Theoretical study on the post-local buckling of steel plates in concrete-filled box columns." *Computers & Structures*, **75**(5), 479-490.
- Liang, Q. Q., Uy, B. and Liew, J. R. (2006). "Nonlinear analysis of concrete-filled thin-walled steel box columns with local buckling effects." *Journal of Constructional Steel Research*, **62**(6), 581-591.

- Liang, Q. Q., Uy, B. and Liew, J. Y. R. (2007). "Local buckling of steel plates in concrete-filled thin-walled steel tubular beam–columns." *Journal of Constructional Steel Research*, **63**(3), 396-405.
- Liang, Q. Q., Uy, B., Wright, H. D. and Bradford, M. A. (2003). "Local and post-local buckling of double skin composite panels." *Structures and Buildings, Proceedings of the Institution of Civil Engineers*, **156**(2), 111-119.
- Liang, Q. Q., Uy, B., Wright, H. D. and Bradford, M. A. (2004). "Local buckling of steel plates in double skin composite panels under biaxial compression and shear." *Journal of Structural Engineering, ASCE*, **130**(3), 443-451.
- Liew, J. Y. R. and Xiong, D. X. (2009). "Effect of preload on the axial capacity of concrete-filled composite columns." *Journal of Constructional Steel Research*, **65**(3), 709-722.
- Lundquist, E. and Stowell, E. (1939). "Local instability of columns with I, Z, channel and rectangular tube sections." Langley Memorial Aeronautical Laboratory. Research Report No. NACA TN, 722.
- Lundquist, E. E., Stowell, E. Z. and Schuette, E. H. (1943). "Principles of moment distribution applied to stability of structures composed of bars or plates." National Advisory Committee for Aeronautics.

- Maas, C. J. V. D. (1954). "Charts for the calculation of the critical compressive stress for local instability of columns with hat sections." *Journal of the Aeronautical Sciences*, **21**(6), 399-403.
- Marguerre K. (1938). Zur Theorie der gekrummten Platte grosser Formänderung, In Proceedings of the fifth international congress for applied mechanics, pp. 93–101.
- Mursi, M. and Uy, B. (2003). "Strength of concrete filled steel box columns incorporating interaction buckling." *Journal of Structural Engineering, ASCE*, **129**(5), 626-639.
- Mursi, M. and Uy, B. (2004). "Strength of slender concrete filled high strength steel box columns." *Journal of Constructional Steel Research*, **60**(12), 1825-1848.
- Oehlers, D. J. and Bradford, M. A. (1999). *Elementary Behaviour of Composite Steel and Concrete Structural Members*. Oxford, London, UK, Butterworth-Heinemann.
- O'Shea, M. D. and Bridge, R. Q. (2000). "Design of circular thin-walled concrete filled steel tubes." *Journal of Structural Engineering, ASCE*, **126**(11), 1295-1303.
- Pagoulatou, M., Sheehan, T., Dai, X. and Lam, D. (2014). "Finite element analysis on the capacity of circular concrete-filled double-skin steel tubular (CFDST) stub columns." *Engineering Structures*, **72**, 102-112.

- Patel, V. I., Liang, Q. Q. and Hadi, M. N. S (2013). "Numerical analysis of circular concrete-filled steel tubular slender beam-columns with preload effects." *International Journal of Structural Stability and Dynamics*, **13**(03), 1250065.
- Patel, V. I., Liang, Q. Q. and Hadi, M. N. S (2014). "Behavior of biaxially-loaded rectangular concrete-filled steel tubular slender beam-columns with preload effects." *Thin-Walled Structures*, **79**, 166-177.
- Patel, V. I., Liang, Q. Q. and Hadi, M. N. S. (2015a). *Nonlinear Analysis of Concrete-filled Steel Tubular Columns*, Germany, Scholar's Press.
- Patel, V. I., Liang, Q. Q. and Hadi, M. N. S. (2015b). "Biaxially loaded high-strength concrete-filled steel tubular slender beam-columns, Part II: Parametric study." *Journal of Constructional Steel Research*, **110**, 200-207.
- Patel, V. I., Liang, Q. Q. and Hadi, M. N. S. (2017a). "Nonlinear analysis of circular high strength concrete-filled stainless steel tubular slender beam-columns." *Engineering Structures*, **130**, 1-13.
- Patel, V. I., Liang, Q. Q. and Hadi, M. N. S. (2017b). "Nonlinear analysis of biaxially loaded rectangular concrete-filled stainless steel tubular slender beam-columns." *Engineering Structures*, **140**, 120-133.

Patel, V. I., Liang, Q. Q. and Hadi, M. N. S. (2018). *Concrete-filled Stainless Steel Tubular Columns*. Boca Raton FL, USA and London, UK, CRC Press, Taylor and Francis Group.

Patel, V. I., Liang, Q. Q. and Hadi, M. N. S. (2020). "Numerical simulations of circular high strength concrete-filled aluminum tubular short columns incorporating new concrete confinement model." *Thin-Walled Structures*, **147**, 106492.

Pei, W. J. (2005). *Research on Mechanical Performance of Multibarrel Tube-confined Concrete Columns*. ME Thesis, Chang'an University, China (in Chinese).

Peng, Y. Y., Tan, K. F. and Yao, Y. (2011). "Mechanical properties of duplex steel tube high- strength concrete short columns under axial compression." *Journal of Wuhan University of Technology*, **33**(2), 105-109 (In Chinese).

Portolés, J. M., Romero, M. L., Bonet, J. L. and Filippou, F. C. (2011). "Experimental study of high strength concrete-filled circular tubular columns under eccentric loading." *Journal of Constructional Steel Research*, **67**(4), 623-633.

Przemieniecki, J. S. (1963). "Matrix structural analysis of substructures." *AIAA Journal*, **1**(1), 138-147.

Przemieniecki, J. S. (1968). "Discrete-element methods for stability analysis of complex structures." *The Aeronautical Journal*, **72**(696), 1077-1086.

- Qian, J., Li, N., Ji, X. and Zhao, Z. (2014). "Experimental study on the seismic behavior of high strength concrete filled double-tube columns." *Earthquake Engineering and Engineering Vibration*, **13**(1), 47-57 (in Chinese).
- Qian, J., Zhang, Y., Ji, X. and Cao, W. (2011). "Test and analysis of axial compressive behavior of short composite-sectioned high strength concrete filled steel tubular columns." *Journal of Building Structures*, **32**(12), 162-169 (in Chinese).
- Quach, W., Teng, J. G. and Chung, K. (2008). "Three-stage full-range stress-strain model for stainless steels." *Journal of Structural Engineering, ASCE*, **134**(9), 1518-1527.
- Quiel, S. E. and Garlock, M. E. (2010). "Calculating the buckling strength of steel plates exposed to fire." *Thin-Walled Structures*, **48**(9), 684-695.
- Ragheb, W. F. (2015). "Local buckling of welded steel I-beams considering flange–web interaction." *Thin-Walled Structures*, **97**, 241-249.
- Ragheb, W. F. (2016). "Estimating the local buckling capacity of structural steel I-section columns at elevated temperatures." *Thin-Walled Structures*, **107**, 18-27.
- Ritz, W. (1909). "Über eine neue Methode zur Lösung gewisser Variationsprobleme der mathematischen Physik." *Journal Für Die Reine und Angewandte Mathematik*, **1909**, 135, 1-61.

- Romero, M. L., Espinós, A., Portolés, J., Hospitaler, A. and Ibañez, C. (2015). "Slender double-tube ultra-high strength concrete-filled tubular columns under ambient temperature and fire." *Engineering Structures*, **99**, 536-545.
- Sakino, K., Nakahara, H., Morino, S. and Nishiyama, I. (2004). "Behavior of centrally loaded concrete-filled steel-tube short columns." *Journal of Structural Engineering, ASCE*, **130**(2), 180-188.
- Schneider, S. P. (1998). "Axially loaded concrete-filled steel tubes." *Journal of Structural Engineering, ASCE*, **124**(10), 1125-1138.
- Shakir-Khalil, H. and Mouli, M. (1990). "Further tests on concrete-filled rectangular hollow-section columns." *The Structural Engineer*, **68**, 405-13.
- Shakir Khalil, H. and Zeghiche, J. (1989). "Experimental behaviour of concrete-filled rolled rectangular hollow-section columns." *The Structural Engineer*, **67**, 346-53.
- Tao, Z. and Han, L.-H. (2006). "Behaviour of concrete-filled double skin rectangular steel tubular beam–columns." *Journal of Constructional Steel Research*, **62**(7), 631-646.
- Tao, Z., Han, L.-H. and Zhao, X.-L. (2004a). "Behaviour of concrete-filled double skin (CHS inner and CHS outer) steel tubular stub columns and beam-columns." *Journal of Constructional Steel Research*, **60**(8), 1129-1158.

- Tao, Z., Han, L. H. and Zhao, X. L. (2004b). "Behaviour of concrete-filled double skin (CHS inner and CHS outer) steel tubular stub columns and beam-columns." *Journal of Constructional Steel Research*, **60**(8), 1129-1158.
- Tao, Z., Wang, Z.-B. and Yu, Q. (2013). "Finite element modelling of concrete-filled steel stub columns under axial compression." *Journal of Constructional Steel Research*, **89**, 121-131.
- Timoshenko, S. P. and Gere, J. M. (1961). *Theory of Elastic Stability*. New York, USA, McGraw-Hill.
- Uenaka, K., Kitoh, H. and Sonoda, K. (2010). "Concrete filled double skin circular stub columns under compression." *Thin-Walled Structures*, **48**(1), 19-24.
- Usami, T. (1982). "Post-buckling of plates in compression and bending." *Journal of the Structural Division, ASCE*, **108**(3), 591-609.
- Usami, T. and Fukumoto, Y. (1982). "Local and overall buckling of welded box columns." *Journal of the Structural Division, ASCE*, **108**(3), 525-542.
- Usami, T. and Fukumoto, Y. (1984). "Welded box compression members." *Journal of Structural Engineering, ASCE*, **110**(10), 2457-2470.

- Uy, B. (2000). "Strength of concrete filled steel box columns incorporating local buckling." *Journal of Structural Engineering, ASCE*, **126**(3), 341-352.
- Uy, B. (2001). "Strength of short concrete filled high strength steel box columns." *Journal of Constructional Steel Research*, **57**(2), 113-134.
- Uy, B. and Bradford, M. A. (1995). "Local buckling of cold formed steel in composite structural elements at elevated temperatures." *Journal of Constructional Steel Research*, **34**(1), 53-73.
- Uy, B. and Bradford, M. A. (1996). "Elastic local buckling of steel plates in composite steel-concrete members." *Engineering Structures*, **18**(3), 193-200.
- Uy, B., Tao, Z. and Han, L.-H. (2011). "Behaviour of short and slender concrete-filled stainless steel tubular columns." *Journal of Constructional Steel Research*, **67**(3), 360-378.
- Vrcelj, Z. and Uy, B. (2002). "Strength of slender concrete-filled steel box columns incorporating local buckling." *Journal of Constructional Steel Research*, **58**(2), 275-300.
- Wan, C. Y. and Zha, X. X. (2016). "Nonlinear analysis and design of concrete-filled dual steel tubular columns under axial loading." *Steel and Composite Structures*, **20**(3), 571-597.

- Wang, Z. B., Tao, Z. and Yu, Q. (2017). "Axial compressive behaviour of concrete-filled double-tube stub columns with stiffeners." *Thin-Walled Structures*, **120**, 91-104.
- Wei, S., Mau, S., Vipulanandan, C. and Mantrala, S. (1995). "Performance of new sandwich tube under axial loading: experiment." *Journal of Structural Engineering, ASCE*, **121**(12), 1806-1814.
- Williams, F. and Wittrick, W. (1969). "Computational procedures for a matrix analysis of the stability and vibration of thin flat-walled structures in compression." *International Journal of Mechanical Sciences*, **11**(12), 979-998.
- Williams, F. and Wittrick, W. (1972). "Numerical results for the initial buckling of some stiffened panels in compression." *The Aeronautical Quarterly*, **23**(1), 24-40.
- Wittrick, W. (1968). "A unified approach to the initial buckling of stiffened panels in compression." *The Aeronautical Quarterly*, **19**(3), 265-283.
- Wittrick, W. and Curzon, P. (1968). "Stability functions for the local buckling of thin flat-walled structures with the walls in combined shear and compression." *The Aeronautical Quarterly*, **19**(4), 327-351.
- Wright, H. D. (1993). "Buckling of plates in contact with a rigid medium." *The Structural Engineer*, **71**(12), 209-15.

- Wright, H. D. (1995). "Local stability of filled and encased steel sections." *Journal of Structural Engineering, ASCE*, **121**(10), 1382-1388.
- Yaghoubshahi, M., Alinia, M., Testa, G. and Bonora, N. (2015). "On the postbuckling of flawed shear panels considering crack growth effect." *Thin-Walled Structures*, **97**, 186-198.
- Zhang, X. Q., Zhong, S. T., Yan, S. Z. and Lin Wei Cao, H. L. (1997). "Experimental study about the effect of initial stress on bearing capacity of concrete-filled steel tubular members under eccentric compression." *Journal of Harbin University of Civil Engineering and Architecture*, **30**(1), 50-56 (in Chinese).
- Zhao, X.-L., Han, L.-H. and Lu, H. (2010a). *Concrete-filled Tubular Members and Connections*. London, UK, CRC Press, Taylor and Francis Group.
- Zhao, X.-L., Tong, L.-W. and Wang, X.-Y. (2010b). "CFDST stub columns subjected to large deformation axial loading." *Engineering Structures*, **32**(3), 692-703.
- Zheng, Y. and Tao, Z. (2019). "Compressive strength and stiffness of concrete-filled double-tube columns." *Thin-Walled Structures*, **134**, 174-188.